DETECTION OF COOLANT BOILING BY ACOUSTIC NOISE METHOD(Dissertation_全文)

AUTHOR(S):

Nishihara, Hideaki

DETECTION OF COOLANT BOILING BY ACOUSTIC NOISE METHOD

HIDEAKI NISHIHARA

DETECTION OF COOLANT BOILING BY ACOUSTIC NOISE METHOD

Hideaki Nishihara

1973

ACKNOWLEDGEMENT

This investigation was performed at the University of Florida while the author was on leave from Kyoto University under the Japan-U.S. Scientists Exchange Program sponsored by the Japan Society for the Promotion of Science during the year 1972-1973. Cooperation of the personnel at the Oak Ridge National Laboratory was made possible through the Oak Ridge Associated Universities, Inc. The author is grateful to these organizations that made it possible for him to devote a full-time effort to research activities during this period.

This investigation could not have been carried out without the help of many people. In particular, the author wishes to express his appreciation to the following persons: Dr. R.E. Uhrig, Dean, College of Engineering, University of Florida, for extending an invitation to the author to pursue research in the field in which Dr. Uhrig is one of the pioneers of world-recognition, and for his continued interest and encouragement in this investigation; Dr. M.J. Ohanian, Chairman of the Department of Nuclear Engineering Sciences, University of Florida, and the Councilor of the Oak Ridge Associated Universities, for his administrative assistance while the author was a visiting faculty of the Department, and for his valuable advice and suggestions during this research; M.J. Dunn who with Dr. M.J. Ohanian initiated the boiling acoustic detection research at the University of Florida and offered the author to make use of the experimental facility; Dr. D. Roux, Instrumentation and Controls Division, the Oak Ridge National Laboratory,

who in cooperation with Dr. Ohanian made it possible for the author to work as a participant of the Laboratory; Dr. D.N. Fry of the Oak Ridge National Laboratory whose interest and discussions concerning the research subject were most valuable in performing this investigation, and who assisted the author in the analyses of cross-correlation functions by the digital Fourier analyzer at the Laboratory.

The author is also thankful to the following persons of the Department of Nuclear Engineering Sciences, University of Florida, for their technical assistance: K.L. Fawcett for the proficiency and ingenuity he displayed as instrumentation technician; J. Mueler and R.H. Jones for their assistance in fabricating the heater elements and rod bundle facility; C. Lynne Day for her skillful typing of the manuscript.

The author would also like to express his gratitude to Dr. I. Michiyoshi, Professor of the Department of Nuclear Engineering, Kyoto University, for his interest and encouragement given to the author during this investigation. He also assumed some of the author's duties at the Kyoto University while he was granted a leave for this investigation.

ABSTRACT

Characteristics of acoustic noise generated by nucleate boiling have been studied experimentally. The primary objective of the present investigation was to obtain fundamental information on the properties of boiling acoustic noise found in reactor systems with direct interest of applying the noise analysis technique to unambiguously detect and locate the coolant boiling in such systems. Early detection of anomalous coolant boiling is essential for the safe operation of nuclear reactors, especially of LMFBR's.

The boiling was produced in a steel water tank on a segment of zircalloy tube that was directly heated by applying low voltage, high current A. C. electric power. The boiling acoustic signals were detected by two hydrophones suspended in the water. The detected signals were analyzed in frequency spectra and in cross-correlation functions.

Spectral densities indicated the existence of acoustic signals up to 50 kHz. Spectral peaks were found near 2 kHz, which were identified by cross-correlation analysis as stemming from the container resonances. Use of signals beyond the resonance range could successfully triangulate the boiling

sites. The boiling acoustic noise was found to emanate from the vicinity of the heater surface. Reflected acoustic waves in a cylindrical vessel are strongly focused producing superfluous peaks in cross-correlation functions. A further study is needed in order to improve the triangulation method. Statistical testing used in pattern recognition studies should be incorporated into the detection system. Also the use of multi-sensor correlation will be found useful especially when strong reflected waves are present.

TABLE OF CONTENTS

LIST OF TABLES

LIST OF FIGURES

CHAPTER I

INTRODUCTION

Pressurized water reactors (PWR's) and liquid metal cooled fast breeder reactors (LMFBR's) are designed to operate under such conditions that the bulk boiling of the coolant should not be encountered. Especially in LMFBR's, coolant boiling should be avoided for two reasons. The first is the possibility of fuel burnout due to the sodium-vapor blanketing on fuel pin surfaces. The second is the possibility of introducing positive reactivity to the reactor through void-reactivity coefficient which may be locally positive depending upon the configurations of the core. The interplay of these two causes may aggravate the undesired situation.

Partial or total blockage of a coolant channel is a major cause of coolant boiling anomalies. Therefore coolant channel blockage or any effects directly related to the blockage should be detected at an early stage to control such anomalies. The effects directly related to the core blockage include decrease in the coolant flow rate or rise in the coolant temperature.

A number of instrumentation systems have been proposed for protection against local core anomalies in LMFBR's. Most of these systems are based on subassembly sensors. Protection systems against LMFBR local core anomalies based on subassembly sensors result in large numbers of reactor-trip channels. For a large LMFBR of approximately 1,000 MW(e) power output, this could be as many as between 250 and 300 channels [1].

Use of so many channels may be technically feasible but may not be practical. It is desirable, therefore, that anomalies in the reactor core could be detected by as small a number of sensing channels as possible but with a desired high accuracy. Moreover, it is hoped that the detection of anomalies should not disturb the normal operation of the reactor. This is accomplished by applying a technique normally known as reactor noise analysis [2,3]. Reactor noises are the fluctuating reactor-associated quantities that are generated by various different causes. For example, neutron flux may fluctuate because of reactivity fluctuation or because of the very stochastic nature of fission processes. Coolant temperature may fluctuate because of coolant flow rate fluctuations or because of fluctuations in the thermal power output.

Coolant boiling anomalies could be detected by reactor noise techniques. The following reactor noises are used for the detection of coolant boiling:

(1) Neutron and gamma noises

(2) Acoustic noises (including ultrasonic frequency region)

(3) Temperature noises.

In most cases these reactor noises are inherent to the reactor under investigation and generated during the normal or abnormal operations. In some cases, however, they are artificially brought into the reactor for the diagnostic purposes. Examples of the latter category are the measurement of the decrease in the strength of acoustic noise signals through two-phase medium, and external pressure modulation in the reactor vessel. When the vessel pressure is modulated, boiling vapor

bubbles are forced to fluctuate in volume and the resulting variations in reactivity cause the reactor power to fluctuate through void-reactivity relationship.

To date, acoustic detection of boiling appears to be the most feasible technique for use in nuclear reactors. A few detectors placed in strategic locations surrounding the reactor core (or placed outside the reactor vessel and coupled to the core by means of acoustic waveguides) can provide continuous and global detection; the primary requirement is that the boiling noise must be distinguishable from background noises such as pump and cavitation noises. Background noises, especially those due to cavitation bubbles, often have frequency spectra that extend and cover the same frequency range as the boiling noise. In fact, cavitation bubbles and boiling bubbles are indistinguishable after their formation; only the processes of formation are different. Therefore, as these bubbles collapse in the media some acoustic waves are expected to be generated characteristic only to their radii. Since the collapsing process of bubbles is considered as the major mechanism that contributes to the generation of acoustic waves in boiling, presence of cavitation in the liquid makes the boiling detection difficult in the frequency domain unless the signal to noise ratio is considerably high.

Detecting boiling sites is also an important aspect of the reactor diagnostics. Local core damage, if it occurs, is difficult to evaluate unless a search is made thoroughly to identify the failed location. Any anomalies leading to the core failure should be detected and removed. Local core boiling is the earliest indication of the major cause of the local core failure, i.e., the coolant flow blockage by foreign

substances such as debris from broken parts. Identification of the location of the boiling, therefore, is important, and such mission needs to be accomplished in the shortest period of time.

The primary objective of the present study is to investigate various fundamental aspects of cross-correlation techniques for the purpose of triangulating boiling sites in reactor coolant contained in vessel. Some of the important unknowns are: (1) effects of reflections from the container wall for the assessment of proper detector positions and for the interpretation of the cross-correlation functions, (2) strength and duration of signals necessary for the identification of boiling locations, (3) location of the boiling acoustic noise source relative to the heat transfer surface, (4) transmission characteristics of boiling acoustic noise signals through a medium composed of rod bundles and liquid. In addition, frequency characteristics of boiling acoustic noise need to be known as a prerequisite for pursuing these items.

In the next chapter, some of the previous works concerning coolant boiling detection by various noise methods are reviewed. Chapter III describes the experimental set-up and instrumentations used in the study. Frequency characteristics of the boiling acoustic noise measured by this facility are discribed in Chapter IV. In Chapter V methodology of triangulation technique using cross-correlation functions is discussed, and procedure of data processing is described. Chapter VI is devoted to the description of cross-correlation experiments and their results with interpretations. In Chapter VII discussions on the results obtained in this study are presented. Recommendations for further study are also included in the concluding chapter.

CHAPTER II

LITERATURE SURVEY

Neutronic Noise Measurements

Fluctuations in neutron flux density have been used for the detection of coolant boiling. The neutronic variations associated with boiling may be caused by three components [4]: (1) local thermal effects, (2) formation of coolant void by bubbles, and (3) vibration of fuel pins due to bubble growth and collapse.

Boyd [5] measured neutron flux fluctuations in thermal test reactor caused by boiling. He wound nichrome ribbon heater around an ion chamber and generated steam bubbles by electrically heating the heater element. The resulted power spectral density (PSD) showed a mild peak below 100 Hz, and the amplitude of the PSD increased with the heater current.

Colomb and Binford [6] performed a similar experiment with the Oak Ridge Research Reactor (ORR). A minor fuel-meltdown accident actually occurred in this reactor in 1963, caused by a coolant channel blockage by a broken gasket [7]. Severe neutron fluctuations were observed at that incident.

Colomb and Binford used an electrically heated bubble generator in their reactor and investigated the relationship between the coolant (water) boiling and the neutronic PSD as well as the acoustic PSD. The acoustic PSD showed a peak associated with the coolant boiling, but the effect of boiling on the reactor power fluctuation was not clear.

Later Binford measured the PSD of neutronic fluctuations caused by boiling by partly blocking the fuel channel with an orifice. A large peak was found in PSD at approximately 2 kHz. This peak was not caused by subcooled nucleate boiling, but it was estimated that 7.7% of the active region of the subassembly was voided and bulk boiling, with chugging and flow-reversal, had occurred. His results were reported by Tabor and Hurt [8].

Following the recommendation of Colomb and Binford for further studies on boiling detection by noise technique. Fry et al. continued the measurements on ORR. They measured PSD at various power levels to see if nucleate boiling affected the PSD [9]. They had to conclude, however, that if nucleate boiling did occur, it was not possible to detect it by the neutronic noise analysis.

In an experiment using a CP-5 reactor at the Pennsylvania State University, Schultz [10] was also unable to detect the onset of boiling based on neutronic noise analysis. He commented that peaks may have existed outside the frequency range covered by the measurement, i.e., below 1/30 Hz or in the kHz range.

Jordan [11] also used an orificed fuel subassembly to simulate channel blockage--coolant boiling abnormality. He used an instrumented fuel element of the Ground Test Reactor whose power output was 3MW. It was estimated that boiling should start at 2.2 MW. Thermocouples and an ion chamber indicated the onset of boiling at 2.35 MW. The response had a hysterisis, and it showed the same condition at a lower power level of 1.62 MW. The PSD of the neutronic noise did not change between power levels of 1.75 MW and 1.95 MW; it had seven or eight peaks between 0.2 Hz and 3 Hz which were reported to have vanished at a decreased power level of 1.65 MW.

Saxe et al.[12] performed boiling noise experiments with a 10 kW North Carolina State University swimming pool-type reactor. They used an electric heater under the reactor core to generate steam bubbles, and compared relative sensitivities of neutronic and acoustic noise methods for the detection of boiling. The PSD of the neutron noise was not affected by the steam bubbles ejected into the core; the PSD of the acoustic noise was more sensitive to the boiling. Their work on the acoustic detection will be mentioned later in this review.

Zwingelstein [13] performed a similar experiment on a swimming pool-type reactor SILOETTE. He found a peak around 1~2 Hz of the neutronic PSD, which he concluded was due to the coolant boiling.

Rajagopal et al.[14] conducted noise analysis of a 20 MW(th) PWR, the Saxton reactor. They found a peak around 16 Hz with the half width at half maximum of approximately 2 Hz. After observing this peak under various operating conditions they concluded that the peak was associated with the coolant boiling. Besides the Saxton reactor, Rajagopal [15,16] reported the results of noise measurements of the Carolinas-Virginia Tube Reactor (CVTR) (65 MW(th)), the Yankee (600 MW(th)) and Trino (280 MW(e)) power reactors. In all cases he found peaks in the PSD that were related to the nucleate boiling.

Izumi et al. [17] investigated the boiling neutronics noise on Japan Material Testing Reactor (JMTR). They compared the PSD's of the JMTR neutronics noise under the P-mode (PWR mode) and B-mode (BWR-mode) operation. Assuming B-mode with coolant boiling as the abnormal condition and choosing the probability of success of diagnosis to 0.9, they could identify the operational mode completely from the differences in

PSD's below 5 Hz. This result should be interpreted with caution since other effects besides "boiling" and "non-boiling" might have been involved with the differences in operational modes.

Robinson and Fry [18] obtained the volume of the dissolved helium gas in the Molten Salt Reactor Experiment (MSRE). The gas was entrained in the molten salt from the cover gas. They modulated the pressure of the primary fuel pump bowl by a saw-tooth type signal (period = 41 sec) and applied the usual noise analysis technique to the output of the neutron flux. The void quantity obtained by this method was 0.61 ± 0.04 % which compared well with 0.6 ± 0.1% obtained by a more laborious method based on the mass balance and the reactivity balance.

Fry et al. [19] conducted experiments on the detection of boiling in the High Flux Isotope Reactor (HFIR), a 100 MW(th) PWR constructed for the production of isotopes. The life cycle of HFIR is 3 weeks and it can repeat many fuel loading cycles in a relatively short period of time. This feature makes it suited for the study of malfunction diagnostics. They replaced the target fuel rod with a stainless steel rod, and heated it by radiation to generate boiling. The coolant flow rate was reduced from the rated 22 gpm to 0.56 gpm. The rod was instrumented with thermocouples to detect boiling by thermal measurements. The neutron fluctuation was measured by an ion-chamber placed outside the pressure vessel, and the acoustic noise was measured by a hydrophone placed in the reactor pool which was also outside the vessel.

The level of the neutronic noise signal was low compared with the background level; it was not possible to detect boiling from the neutronic

noise signature. Calculation showed the amount of void necessary to detect the boiling was 10 in^3, which was at least 10^3 times of the quantity of void present. The pressure modulation technique utilized in the MSRE experiment was also applied. The neutron flux fluctuated at the modulation frequency (0.1 Hz) when there was no conceivable coolant boiling. This was caused by the density variation of the water. The maximum void volume was only 1/7 of the volume necessary to produce significant information on the existence of boiling.

Instead of depending on the PSD signatures for boiling detection, Albrecht [20,21] proposed the use of signal coherence for detecting boiling anomalies, and applied the method to the University of Washington Nuclear Reactor (a 100-kW Argonaut). The essential difference of the coherence method is in the use of two detectors instead of one for generating the signature. The coherence function is given by the ratio of cross-power spectral density to the auto-power spectral density when the identical signal is measured by two detectors. The two-detector method was first used by Nomura et al. [22] and Seifritz et al. [23] independently to investigate reactor parameters, such as subcriticality. This method is superior to the conventional one-detector method also in anomaly detections. When the signal content in the fluctuations associated with an anomaly is small, it does not change the PSD; the same anomaly may change the coherence function measured by two detectors.

Albrecht used ^3He neutron detectors placed about 3 ft from the core in two opposite beam tubes. A simulated anomaly was produced by passing air through a container of water placed in the center core

region. The detected neutron fluctuation signals were conditioned by band limiting filters and hard limiters, and then multiplied to compute the coherence. In a recent experiment, the smallest observable rms reactivity perturbation due to the bubbler was determined to be 3.8×10^{-3} ¢. This is about an order of magnitude smaller than the rms bubble reactivity fluctuation (4.5×10^{-2} ¢) that was reported necessary for the unambiguous boiling detection by PSD signature analysis for the North Carolina State University reactor [12].

Acoustic Noise Measurements

General Remarks

As stated earlier, two types of acoustic noise methods have been proposed for use to detect anomalous coolant boiling. The one is the active method in which ultrasonic waves are aritifically introduced into the boiling medium and subsequently measured. This category includes the measurement of attenuation of ultrasonic signals in the two-phase medium, and the measurement of acoustic velocity variations in such a medium.

The other is a passive "listening" of the sound generated by boiling bubbles. Generation of acoustic noise by boiling liquid is well recognized, and the detection of coolant boiling by simply listening to this signal has been considered as an effective method from the early stages of liquid cooled reactor technology. Acoustic signals generated by boiling often exceed the audible frequency range and extend well into the mega-hertz range. For this reason the usual classification of ultrasonic and acoustic detection of boiling [24] will not be adopted here. Instead, the terms "active" and "passive" will be used. So far all the acoustic boiling detections actually used in reactors are by the passive method. This method seems to be a straightforward technique, but there still remain a number of problems to be solved before the method becomes a practical tool in power reactor technology. In the following examples of the acoustic method attempted to detect boiling acoustically in reactors will be reviewed.

Acoustic Boiling Detection in Reactors

Early work on acoustic boiling detection performed for water.

reactors encountered excessive system noise. Hogan and Boyd [25] attempted the detection of boiling by employing hydrophones and accelerometers. They were unable to obtain good results because of the background noise. In an out-of-pile boiling experiment, Boyd and Cummerow [26] were able to find a broad peak in PSD around 2 kHz.

Colomb and Binford [6] used neutronic and acoustic noise methods in ORR. They were able to detect the occurrence of boiling with the acoustic method; they could not, however, detect it when the coolant pump was in operation. The background noise was then higher than the boiling noise by 10 dB.

After the unsuccessful attempt of Colomb and Binford, Saxe [27] pursued acoustic boiling detection in ORR. He used a metallic pipe as an acoustic waveguide. The use of waveguides and ex-core detectors attached to the guides alleviates the difficulty of fabricating in-core detectors to be used in hostile environments. A crystal contact-microphone was attached to one end of the waveguide, and the other end was placed slightly above the water level inside the reactor vessel. It was reported that the boiling was hardly detected because of the high level of the background noise. Boiling detection in the HFIR was also attempted, but the result was similar. [28]

At the Argonne National Laboratory, measurements of the background acoustic noise of the Experimental Breeder Reactor No. 2 (EBR II) were performed [29]. The sodium cooled experimental reactor has a nominal power density of approximately 1 MW/ℓ, and a slight decrease of the coolant flow from the steady state (20 ft/sec) may bring the coolant to boiling. The reactor vessel is placed on the bottom of the

primary container filled with sodium. In the primary container two sodium pumps (total capacity of 9000 gpm), the primary heat exchanger, and the fuel exchange mechanism are placed. The cover of the reactor vessel is held down by three "holddowns". These holddowns played the roles of acoustic waveguides in the acoustic noise detection. An accelerometer was attached to the tie rod (7.6 cm diameter by 7.6 m length) of the holddown. As the coolant flow rate was reduced the amplitude of the PSD also reduced but its shape remained unchanged. On the other hand, acoustic noise from the detector attached to the motor of the pump showed a shift in the position of peaks of the PSD. It was evident that the motor noise was due to the bearings.

Saxe et al. [12] measured acoustic noise of the North Carolina State University swimming pool reactor. Acoustic noise was detected by a hydrophone placed in the water pool. The PSD had a similar shape under the boiling and non-boiling conditions, but the amplitude was large under the boiling condition. When the pump was at halt the background non-boiling noise was negligible. But the boiling noise level was large and detected up to close to 20 kHz.

Acoustic boiling noise was also measured in the Dounreay Fast Reactor (DFR) [30]. The general practice in England seems to have been the use of acoustic waveguide. In DFR, stainless steel tube filled with borated graphite was used as the waveguide. It is reported that the noise of the collapse of sodium bubbles in subcooled sodium was measured in DFR [31], but no detailed results have been published.

It is also reported by C.D. Swanson [32], who made a trip to European reactor installations and support facilities in 1969, that

the British attempted successfully to locate boiling sites in DFR by cross-correlating acoustic signals detected by waveguides and attached sensors. The details of this experiment have not been published by the original investigators, however.

Active Methods of Acoustic Boiling Detection

One of the most direct methods of detecting the incipience of coolant boiling is the measurement of degree of subcooling. De Prisco et al.[33] investigated a method of measuring the degree of subcooling of coolant by introducing high frequency acoustic waves in the medium and detecting the induced cavitation noise. Under atmospheric pressure, acoustic energy required to produce cavitation tripled when the water temperature was decreased from 100°C to 35°C. This detection method is also considered to have a potential usage in applied heat transfer studies and mock-ups for high-performance high-specific-power reactors [34]. This method was also reported by Kartluke et al. [5], and investigated by Aerojets, Inc. [36]. The drawback of this method is its inability of global detection; many detection channels are required for the purpose of reactor diagnostics.

Bonnet and Osborn proposed a new technique to monitor nucleate boiling in water-cooled [37] and Na-cooled [38] reactors. The proposed technique is based on the introduction of a standing acoustic wave in the core and measuring the deviations in the neutron density or gamma-ray population as boiling initiates. The change in the coolant density, $\Delta\rho$, is related to the acoustic pressure variations, Δp, and to the sound velocity, c, according to $\Delta\rho = \Delta p/c^2$. The resulting density variations change the neutron density, which is subsequently measured

by the standard technique of neutron noise analysis. This method may be thought of as a hybrid method of acoustic and neutronic noise measurement.

Spectral Aspects of Boiling Acoustic Noise

Understanding the frequency dependence of boiling acoustic noise is essential in applying the noise technique to the detection of coolant boiling in reactor systems. Early works on nucleate boiling acoustic noise have been reviewed previously by T.T. Anderson [39], and will be covered here only briefly.

As early as in 1917, Lord Rayleigh [40] analyzed the propagation of pressure pulse generated in liquid when a spherical void is collapsed in the medium. M.F.M. Osborne [41] measured pressure pulses generated by collapsing voids in water. Because of the existence of resolved air in water, cavities in water did not disappear instantly, but re-appeared two or three times before disappearing completely. The frequency of re-appearance was expressed by the following equation:

$$f = \frac{5}{R} p^{1/2} \qquad (2\text{-}1)$$

where

f = frequency (kHz)

R = radius of cavity (mm)

p = pressure (atm)

Pleset [42] obtained PSD's of pressure fluctuations associated with cavities that are generated when the liquid is depressurized and collapsed when pressurized. When the pressure field is uniform, Pleset's expression coincides with that of Rayleigh's.

Knapp and Hollander [43] used experimentally obtained values for the pressure field to the Pleset's equation, and numerically evaluated the growth-collapse curves for the cavity. The curves agreed very well with the experimental results. It was also shown that the results differed little if the cavity was considered to contain only steam vapor.

Rayleigh's analysis depends on the assumption that cavity collapses in liquid because of the inertial force. When the cavity is filled with vapor, the condensation of vapor inside the cavity due to heat transfer mechanism also plays a role in the collapse. Florschuetz and Chao [44] performed experiments using a free-fall, gravity free equipment. The collapse of vapor void was slow and no shock wave was observed. This indicated effects of heat transfer on the motion of boiling bubbles.

Forster and Zuber [45], and Plessel and Zwick [46] both treated a similar but reverse phenomenon of bubble formation in superheated liquids. Their analytical results agreed well with the experimental results of Dergarabedian [47].

Besides formation and collapse of bubbles, bubble oscillations are also considered to be one of the mechanisms of acoustic noise generation. Minnaert [48] derived the following relationship of the vibrational frequency of bubbles oscillating in volume by assuming that the kinetic energy and potential energy of the bubble are equal. His result is

$$f = \frac{1}{2\pi R}\sqrt{\frac{3\gamma p}{\rho}} \qquad (2\text{-}2)$$

where p is the system pressure, ρ is the density of the liquid, and γ

is the ratio of specific heats. Substitution of the values of subcooled water at 1 atm yields fR = 3.28 kHz - mm.

Recently Bree [49] also analyzed the motion of bubbles, and showed the results in the form of PSD. The maximum value of PSD occurred when fR = 2.1 kHz - mm for water and 0.3 kHz - mm for Na. The value for Na is smaller due to a larger heat conductivity.

Another mode of oscillation is the shape oscillation that does not involve variations in volume. The effect of the shape oscillation for the acoustic noise generation may be neglected since their contribution to the pressure pulse is six orders of magnitudes less than that of the volume oscillations [50].

All the works described above considered motion or oscillation of individual bubbles, and contained the radius of bubbles as a parameter. Thus the knowledge of bubble radii is essential in assessing the spectral dependence of boiling acoustic noise. The radius of bubbles is generally distributed, and depends on many parameters such as the roughness of the heat transfer surface.

Il'ichev and Lesonovskii [51] studied the spectral dependence of boiling acoustic noise by a stochastic approach. They assumed that the individual acoustic emission from bubbles is a quasi-delta-function of random amplitude and occurring randomly in time. They concluded that the PSD would be constant, or white, up to a high frequency and then would decrease as $1/\omega^2$ above that frequency.

In an attempt to explain the results obtained in a boiling acoustic measurement, Meier [52] postulated that the pressure signal from boiling bubbles is composed of random pulses of varied strengths and

intervals, each pulse decaying exponentially with a variable time constant. He was able to fit the model to the broad resonance that he observed in the low kilohertz range.

Container configuration is another factor that determined the PSD's of boiling acoustic noise. Anderson et al. [39] compared acoustic spectra of boiling water in various container geometries reported by several authors. If the boiling noise is white in an infinite body of fluid, the PSD obtained from boiling liquid contained in a finite dimension would show peaks at the resonance frequencies of the fluid contained in finite geometry. General tendencies of the shift in PSD peaks to the higher frequency domain are observed from the results of the reviewed works. They thus concluded that the acoustic emissions from boiling are composed of characteristic frequency spectra corresponding to bubble-volume resonances and the resonances of the fluid contained in finite geometry.

Triangulation of Acoustic Noise Source in Related Areas

Triangulation technique for determining the acoustic noise source has been applied in locating leakages in coolant loops. In the summer of 1967, leakage of NaK was detected from the primary loop of DFR [53]. The position of the leak was finally determined by injecting inert gas into the leak jacket, and by detecting the acoustic noise generated from the leak by using two microphones. Difference in the arrival time of the two signals determined the location of the leak.

In the following year, a crack developed in the primary coolant system of the Elk River Reactor. A similar technique used in the Dounreay incident was applied to locate the position of the anomaly [54].

Cash and Sweetin [55] advocated the use of an "active" acoustic

method for locating failed fuel elements. They used Outlet Region Feature Model (ORFM) to simulate a portion of the Fast Flux Test Facility (FFTF). Bubbles were introduced into the system to simulate the emission of fission gas, and the three outlet nozzles were placed under ultrasonic surveillance. Simultaneous measurements were made with lead-zirconate-titanate transducers on each of the three outlet nozzles. The volume of gas passing each transducer was proportional to the measured attenuation of the reflected signal. Triangulation of the ultrasonic attenuation in each outlet predicted a source position within a small zone of subassemblies and the arrival time data showed the source to be within one to two core lattice spaces.

Acoustic noise method is utilized in materials surveillance in many fields of engineering [56], and becoming to draw a vast interest in nuclear reactor pressure vessel surveillance programs [57-59]. When the strain energy stored in the material is suddenly released through a deformation process, acoustic wave pulses are generated. Detection method of flaws of materials by listening to these noises is referred to as "stress wave emission (SWE)" method, or "acoustic emission technique (AET)" in materials sciences. By using detector pairs, signal transmission delay times are measured, and the location of the emission site is determined by triangulation technique. Cross, et al. [60] reported several schemes of AET triangulation technique.

Relevant to the detection of acoustic noise source in liquid body is the vast field of underwater acoustics. The field has been developed primarily as a war-time effort to detect underwater vessels. The underwater sound detection technique uses an array of detectors, or

hydrophones, and a decision is made whether a seemingly random noise is common to these detectors. When the distances between the source and the detectors are equal, the common signal is the strongest, whereby making it possible to detect the location of the source. The process of detection involves some kind of correlation technique. An essential feature of the underwater sound detection process is the weakness of the signal compared with the background noises. Recently, outstanding papers on the subject were combined in a volume and reprinted [61].

A scheme similar to the underwater sound source detection was applied by D.A. Gilbrech and R.C. Binder for the detection of noise sounds in mechanical equipments [62]. They built a portable direction finder utilizing the correlation between signals received by the two microphones of a directional array. They found that the characteristics of this equipment were very much dependent on the noise source and on the geometry of the microphone system.

Temperature Noise Measurements

Temperatures inside a reactor are fluctuating even at the "steady state" like all other physical quantities. The cause of temperature fluctuation is manyfold and detailed account of this phenomenon is beyond the scope of this literature survey. In a very heuristic manner, it may be explained by the following equation [63].

$$\delta T \sim \delta\left(\frac{\text{power}}{\text{flow}}\right) = \frac{\text{power}}{\text{flow}}\left(\frac{\delta\ \text{power}}{\text{power}} - \frac{\delta\ \text{flow}}{\text{flow}}\right) \qquad (2\text{-}3)$$

where δ refers to random fluctuations about average values. Therefore, whenever either power or flow fluctuates coolant temperature also fluctuates.

In case of coolant channel blockage, coolant temperature may exhibit a different fluctuation pattern due to the decreased flow rate. Once boiling is initiated a large temperature fluctuation is expected. Then the partially superheated liquid is agitated by vapor bubbles and temperature fluctuations are enhanced.

Jiji et al. [64] measured temperature fluctuations of boiling water in a forced convection test loop. Considerable fluctuations in temperature within the single-phase core as well as the bubble boundary layer were indicated on oscillograph traces of traversing thermocouple signals. The frequency of oscillation was estimated to be 20 Hz throughout the single-phase core as well as in the bubble boundary layer. The amplitude of temperature fluctuations near the heat transfer surface decreased as the distance from the leading edge was increased. The recorded peak-to-peak amplitude of the temperature fluctuation was as large as 60°F.

In 1959, fuel-rod meltdown incident occurred in the Sodium Reactor Experiment (SRE). Thirteen of the 43 fuel elements were found severely damaged [65]. This incident was caused by coolant channel blockage for a considerable length along the channel. The boiling aggravated the blockage which resulted in oscillations of flow rate and temperature. A strip chart recording showed that the fuel temperature fluctuated as much as 100°C, and the coolant channel outlet temperature fluctuated more than 20°C.

Coolant temperature in the Prototype Fast Reactor (PFR) was measured to detect coolant channel blockage by using three instrumentation channels [66]. Two of the three channels were used to measure average temperatures, but the remaining channel was used to detect temperature fluctuation at the channel outlet. When the coolant channel was blocked, spatial temperature distribution at the channel outlet changed causing temperature fluctuation.

As mentioned previously, Fry et al. [19] investigated the possibility of boiling detection in HFIR by modulating the vessel pressure. Temperature fluctuations measured by a thermocouple attached to the cladding surface showed a peak in PSD at the modulation frequency of 0.1 Hz at reactor power levels above 44 MW. The incipience of boiling was not clear at 44 MW from the boiling curve. They concluded that the appearance of peak in PSD was an indication of boiling, and stated that the temperature noise could detect boiling more sensitively than the average temperature.

Tsunoda et al. [67] measured temperature fluctuations in a water loop. The heater was a bundle of seven rods (6.3 mm diameter by

60 cm length) simulating a fuel subassembly of Joyo. Temperature fluctuations were detected by a thermocouple placed at the channel outlet. Temperature fluctuation was four-fold when void generation was noticed.

Seifritz [68] reported a concept of a new temperature sensor (thermocouple) that can detect the boiling voids in liquid metal medium as well as the temperature. This may have a potential usage in detecting coolant boiling.

Nishihara et al. [69] measured radiation heating effect on a thermocouple immersed in water-air two-phase, and reported that the heating effect may be used to advantage in measuring temperature fluctuation associated with boiling.

CHAPTER III

EXPERIMENTAL EQUIPMENT

This chapter describes the construction of the water tank, the heater element and its power supply, the rod bundle lattice, the hydrophone acoustic detectors, the data processing equipments, and auxiliary equipments.

Water Tank System

Construction of Water Tank

A cylindrical steel tank, 50.5 cm I.D. by 94 cm height, was used as the water container in which the measurements were performed. Figure 1 schematically shows the water tank, the heater element and its power supply, and other equipments. The inner surface of the tank was lined with foam rubber of 2.5 cm thick to reduce the acoustic reflections from the wall. The tank is equipped with a removable lid which is bolted to the main body of the tank for pressurized experiments. Figure 2 is a photograph of the tank.

A coolant channel was constructed in the tank to facilitate experiments with water flow. The flow velocity could be changed by selecting the diameter of a lucite discharge nozzle. The tank can also be equipped with simulated fuel rods to be used in cross-correlation studies. When the rod bundle is in use, the flow channel should be removed from the tank.

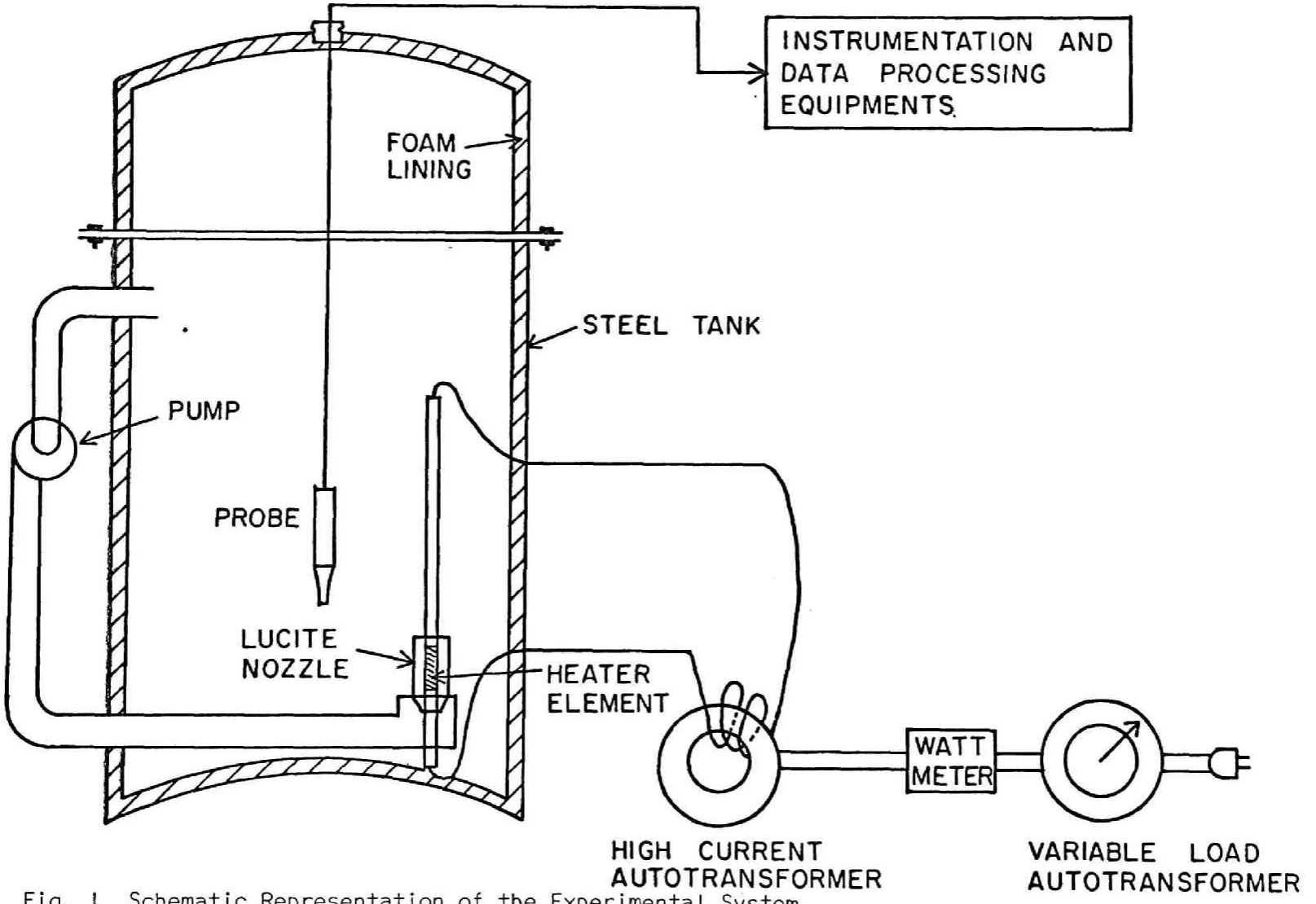

Fig. 1 Schematic Representation of the Experimental System

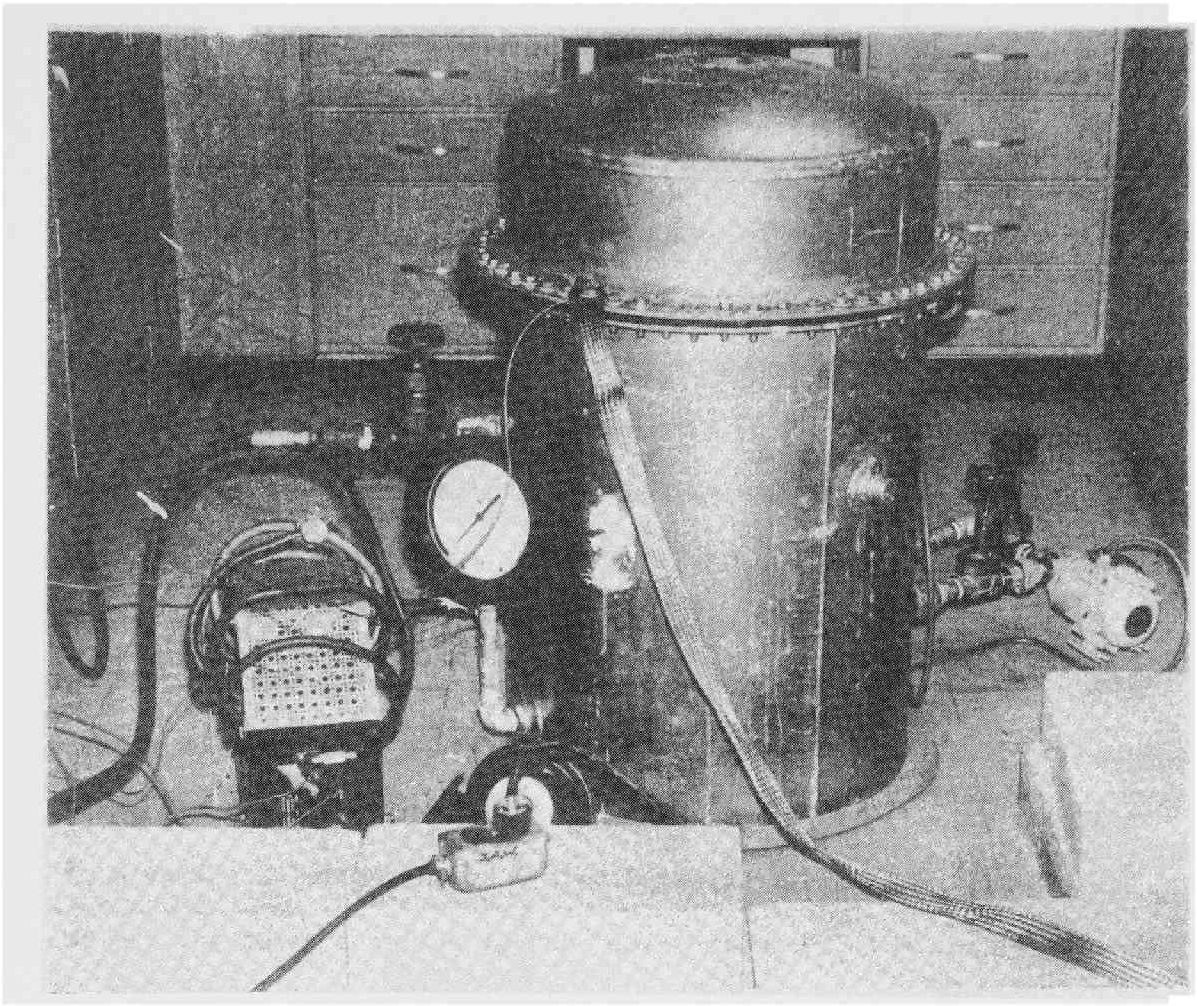

Fig. 2 Water Tank and [illegible] Power Supply

Heater Element and Power Supply

In order to simulate nucleate boiling on the surface of fuel pin cladding surfaces, sections of zirconium fuel tube (zircalloy-4) were machined to form cylindrical heater elements. Figure 3 shows the dimensions of the two heater elements used in the experiment. Two solid copper connectors, each approximately 1 cm in diameter and 1.2 cm long were press fit into the zircalloy heater. Threaded holes were machined into the copper connectors so that solid No. 4* copper wire (5.19 mm diam.) could be screwed into the copper connectors. Two ceramic discs were machined and epoxied to the copper connectors and finally zircalloy tube epoxied to the ceramic discs so that the copper wires were inside the hollow zircalloy tubes. Figure 4 is a drawing of the assembled heater pin.

Due to the difficulties associated with assembling a D.C. power supply to resistance heat the zircalloy tube, an A.C. supply was designed. Power was drawn from a 220 V A.C. line. The power line was connected to a variac autotransformer (rated capacity: 7.8 kW) which was used to adjust the power supplied to the heater element. The autotransformer was connected through a wattmeter to a second autotransformer (also rated at 7.8 kW). The second autotransformer was set at 100 percent load and No. 1 stranded copper wire (cross-section 42.4 mm^2) was wound in a coil around it to construct a high current, low voltage transformer. The No. 1 stranded copper wire was connected to the No. 4 solid copper wire.

Independent measurements of current and voltage across the heater

*American Wire Gauge number.

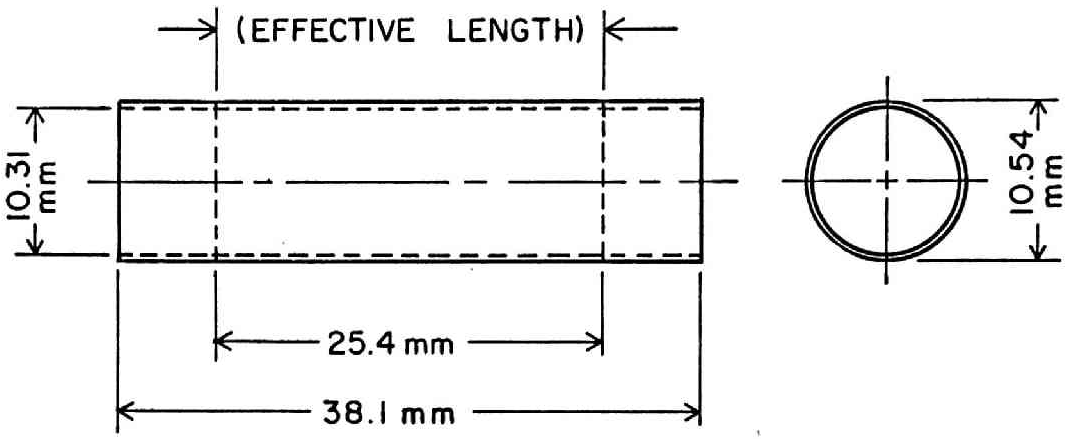

(a) TYPE A ELEMENT

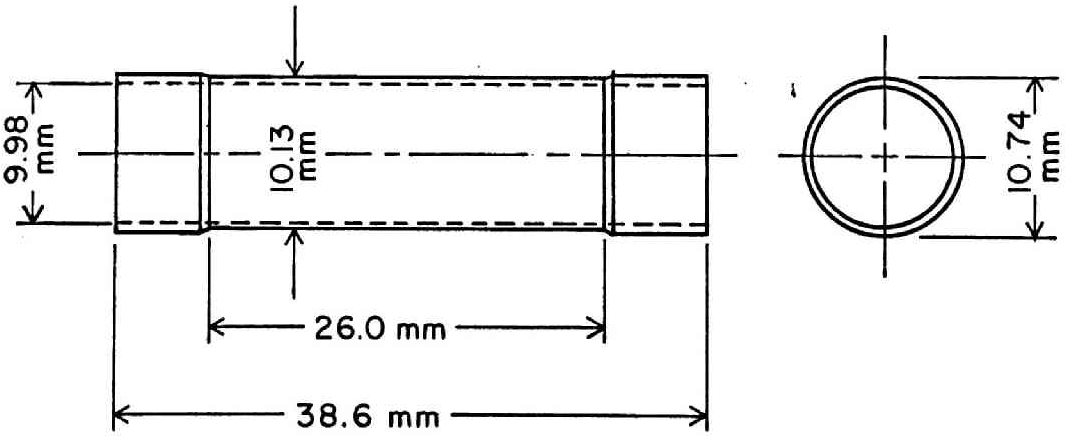

(b) TYPE B ELEMENT

Fig. 3 Zircaloy Heater Elements

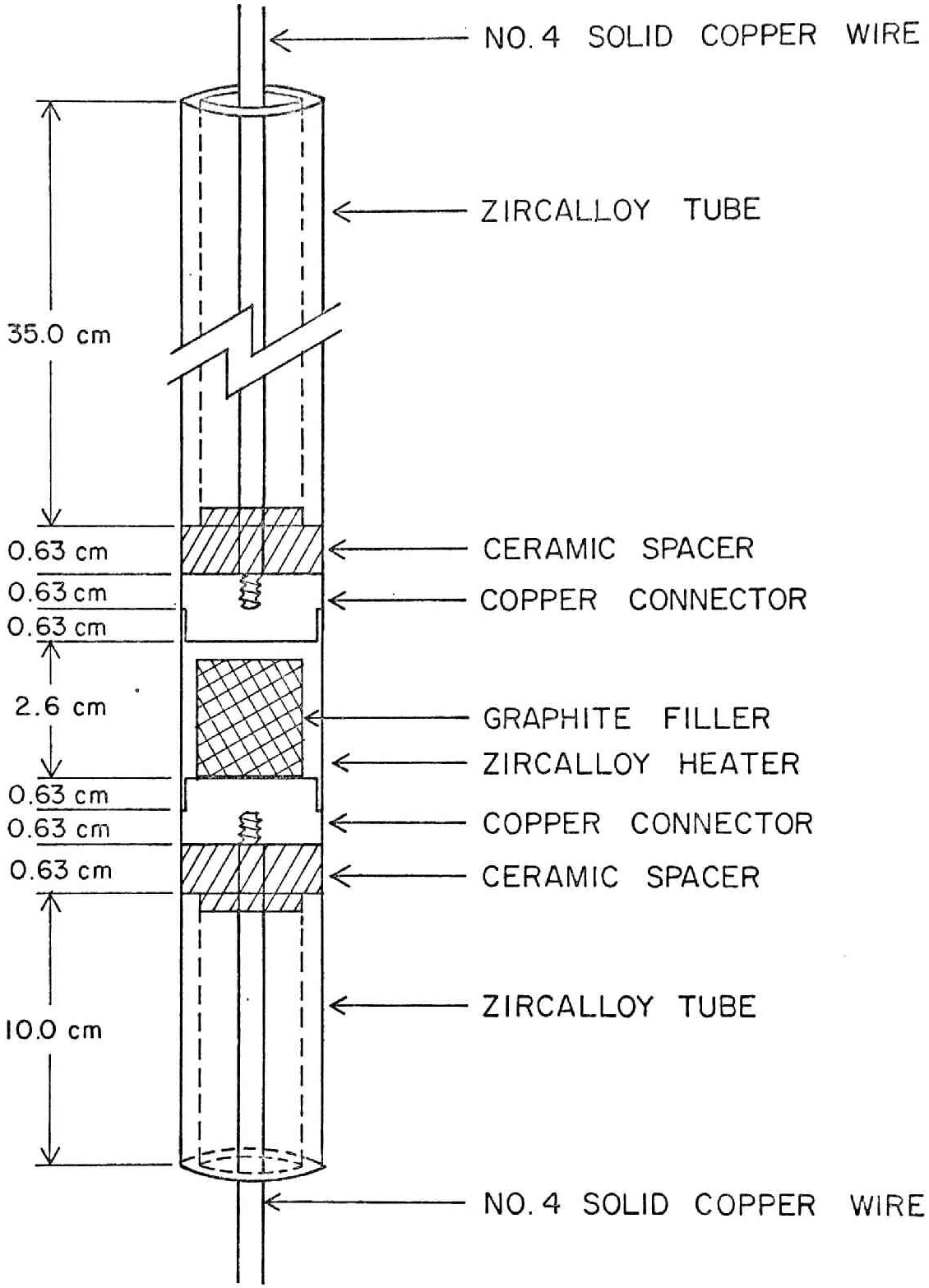

Fig. 4 Schematic of Heater Pin

were made to establish the relationship between the reading of the wattmeter and the true heating power. The efficiency, or the ratio of the power dissipated in the heater to the power measured by the wattmeter, was 63 percent for Type A and 57 percent for Type B heater element, respectively, and was constant for the range of power used in the present experiment. An electric blower was used to force air over the wires of the second autotransformer to prevent overheating and melting of the insulation.

Rod Bundle Lattice

In order to provide more realistic acoustic transmission paths, provision was made to assemble a rod bundle in the tank for cross-correlation studies. Aluminum rods, 1.27 cm in diameter and 61 cm long, could be arranged in a triangular lattice with a pitch of 1.905 cm. Holes were drilled in two Plexiglas plates, 1.27 cm thick, to form upper and lower grid plates which supported the rods vertically in the tank. When the bundle was in use, the heater element occupied one of the rod locations and was surrounded by a bundle of rods of various configurations.

Instrumentation and Data Processing

A system of instrumentation and data processing was assembled for detecting, conditioning, recording, and analyzing the acoustic signals generated by boiling. Figure 5 shows the schematic diagram of the system.

For the spectrum measurements, the boiling acoustic noise is detected by one hydrophone, Model 706, and analyzed on-line by the spectrum analyzer system. Two hydrophone systems are used in measuring cross-correlation functions. In the latter measurements the detected signals are conditioned by filters and amplifiers, and recorded on an F.M. tape recorder for further data processing.

The recorded signals are played back with a speed change, and fed into either an IBM-1800/AD-80 hybrid computer system, or to a Hewlett Packard Model 5451A Fourier analyzer. The detected noise signals are displayed on a dual oscilloscope during the measurement for monitoring purposes.

The Model 5451A digital Fourier analyzer was made available at the Division of Instrumentation and Controls of the Oak Ridge National Laboratory. The tape recorder was transported to the laboratory for processing the pre-recorded signals with this equipment.

Hydrophone Acoustic Detectors

Two hydrophone probes were available for the present study. Both of these were designed and constructed by Marine Resources, Inc. Table I shows some of the physical characteristics of the hydrophones. The Model 706 hydrophone had a flat response to 800 kHz, and this high cut-off frequency made it an especially delicate instrument.

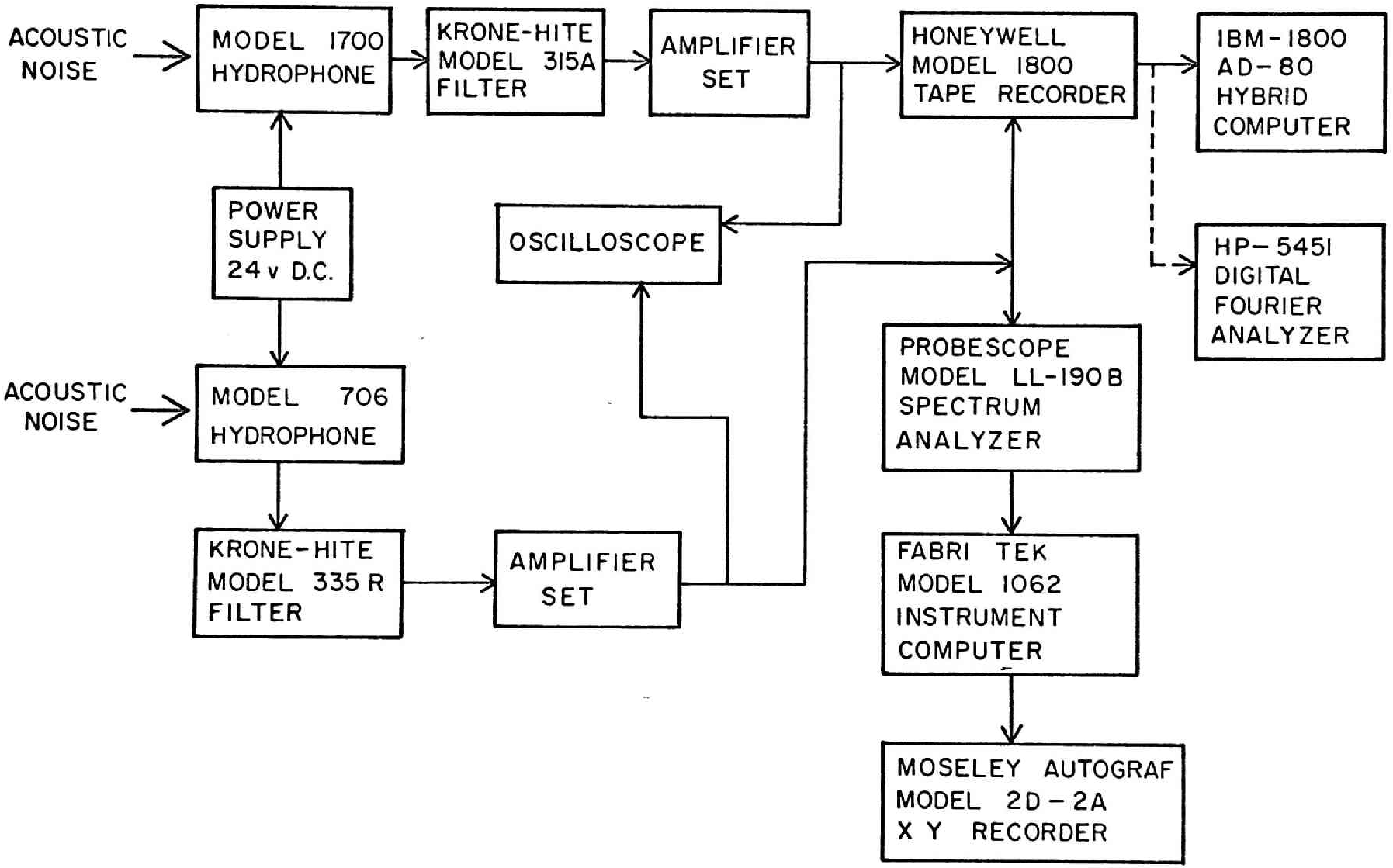

Fig. 5 Instrumentation and Data Processing System

TABLE I

Properties of Hydrophones

	Model 706	Model 1700
Frequency Response	Flat to 800 kHz	Flat to 120 kHz
Temperature Limit	< 35°C	< 80°C
Pressure Limit	< 65 psia*	---
Directionality	Omnidirectional up to 100 kHz	Omnidirectional up to 120 kHz
Crystals	Lead zirconate titanate, 0.157 cm diam. x 0.127 cm H cylinder	Lead zirconate titanate, 1.25 cm sphere

*Limit imposed on the preamplifier casing.

Figure 6 shows the frequency responses of the detectors. These curves include preamplifier gains. The preamplifiers are low noise units with a gain of 10 dB for the Model 706 and a gain of 30 dB for the Model 1700. The difference is due to the availability of the later stage amplifiers.

The overall views of the probes and the amplifiers are shown in the photographs of Figures 7 and 8. As shown the Model 706 comes with a preamplifier in the same brass casing with the ceramic crystal, whereas the Model 1700 has a preamplifier separated by a coaxial cable. Ceramic crystals of the two detectors are cast in plastic resin.

A solid state D.C. 24 V power supply unit was used for the hydrophone preamplifiers.

Filters and Amplifiers

The preamplified acoustic signals are further conditioned by filters and amplifiers. Two bandpass filters, a Krohn-Hite Model 335R unit and a Krohn-Hite Model 315A unit were available for the present experiment. Both of these filters could be used as either low-pass, high-pass, or band-pass filters. The Model 355R unit had a signal amplification capability of 20 dB gain. The lack of amplification factor in the Model 315A was fulfilled by building an additional gain in the Model 1700 hydrophone preamplifier.

High-pass filtering at a minimum frequency of 200 Hz was required to reject low frequency extraneous signals associated with the A.C. resistance heating mainly at 60 and 120 Hz.

The amplifiers used were low noise oscilloscope preamplifiers, Tektronix Type L and Type B plug-in units, mounted in Tektronix Type

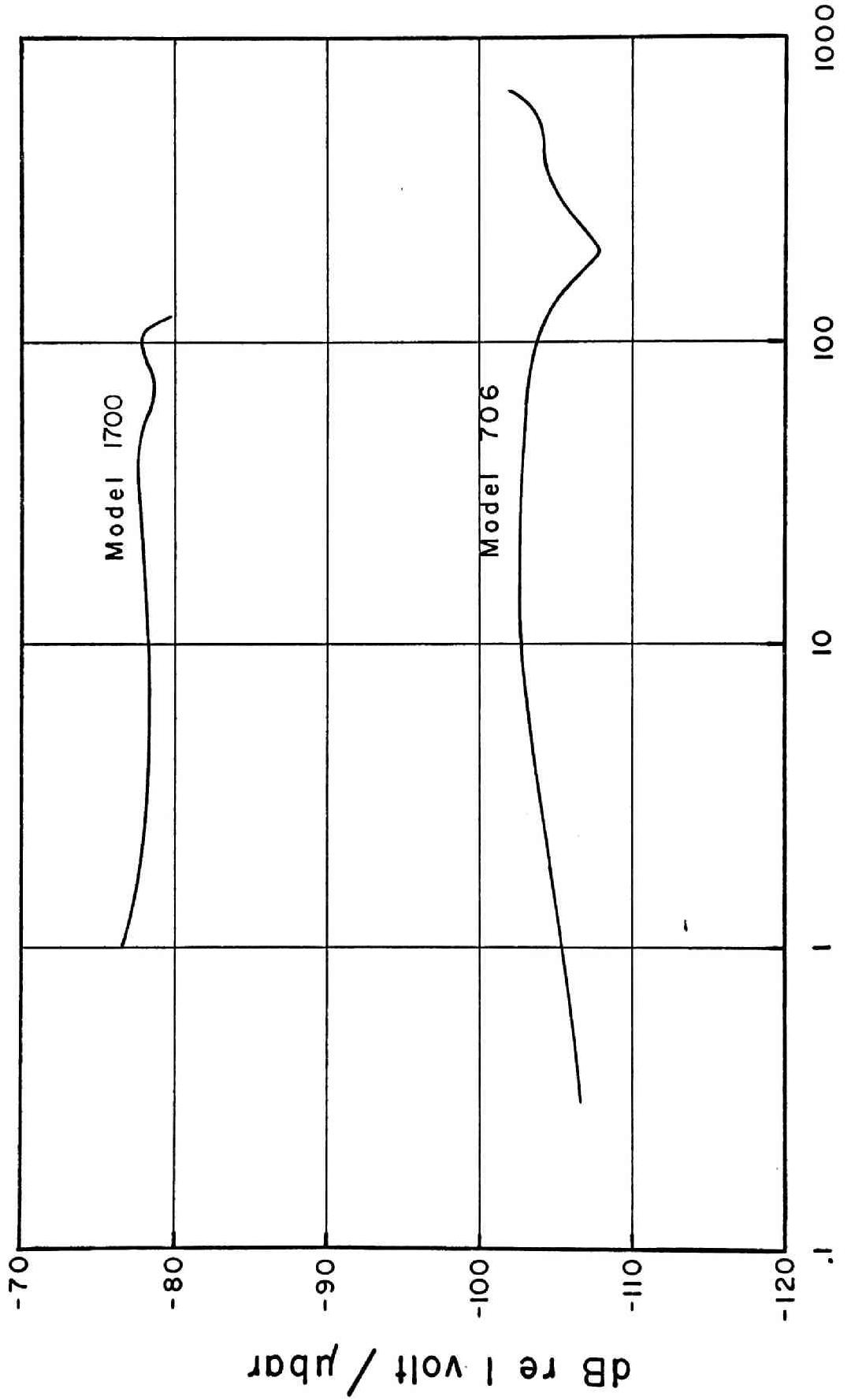

Fig. 6 Frequency Response of Hydrophones

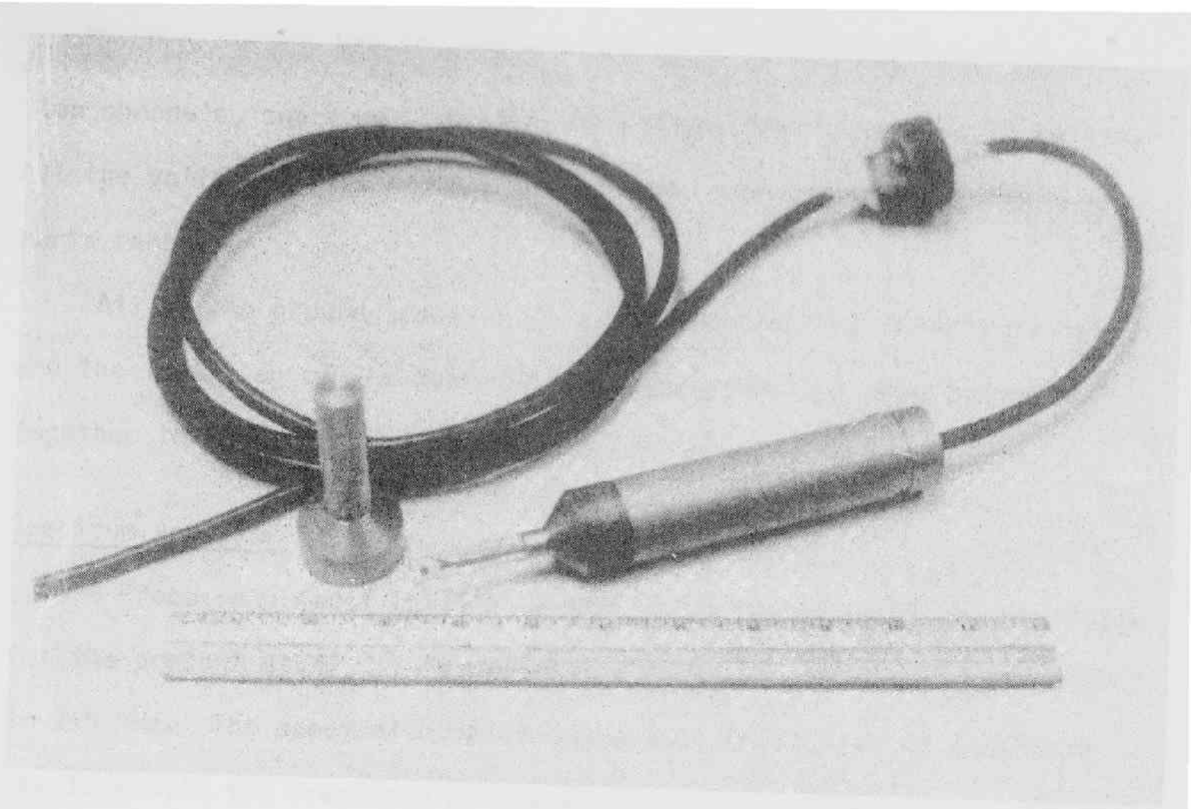

Fig. 7 Model 706 Hydrophone

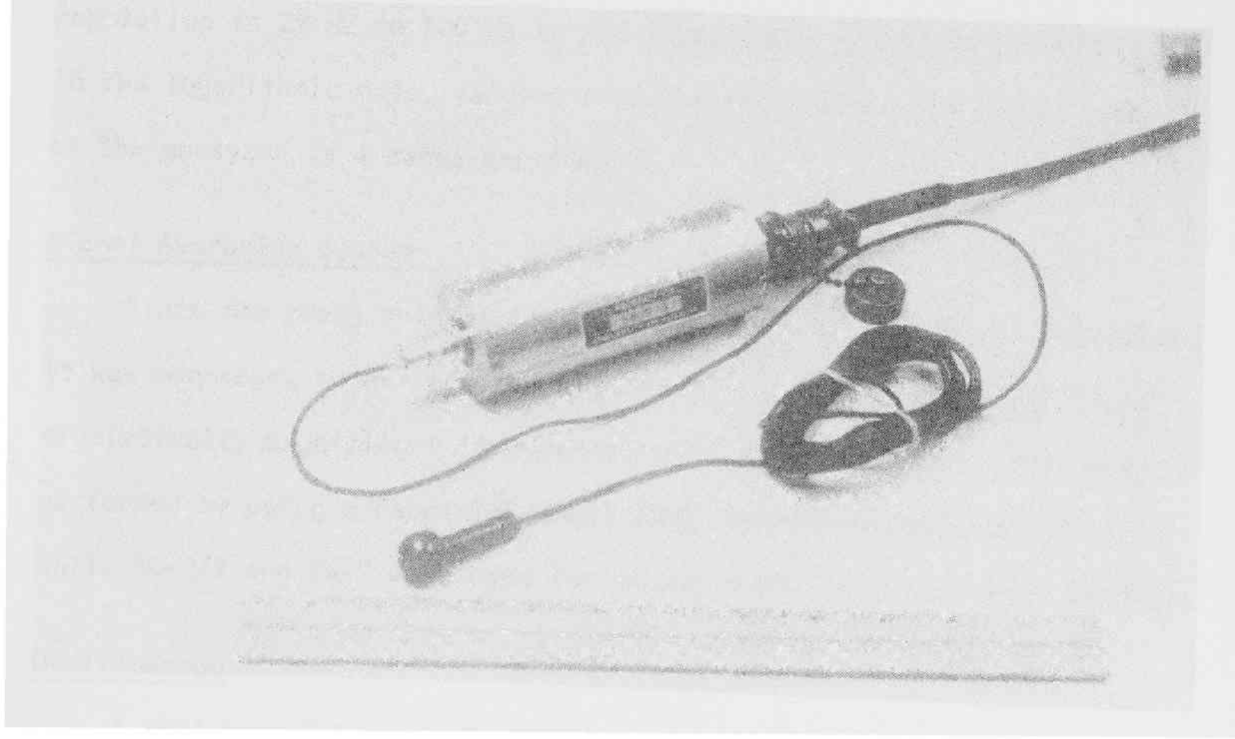

Preamplifier Power Supply units. For each of the two instrumentation channels, one Type L and one Type B amplifier was used in series. All the units had flat frequency responses extending beyond the megahertz range.

All of the ground levels of the instruments, the water tank wall, and the lower leg of the heater power supply bus bar were connected together to the ground by a heavy braided wire.

Spectrum Analyzer

A Probescope Model LL-190B on-line spectrum analyzer was available for the present study. This unit has a frequency range from 350 Hz to 215 kHz. The spectral display appears on the screen of a cathode ray tube with the frequency of the applied signal displayed on the horizontal axis, while the amplitude of the signal is displayed on the vertical axis. The frequency display is either linear or logarithmic. The resolution is 25 Hz to 500 Hz in the linear mode and 75 Hz to 5kHz in the logarithmic mode, varying with the frequency. The sweep rate of the analyzer is 1 sweep per second.

Signal Averaging System

Since the sweep rate of the spectrum analyzer was only 1 sweep/sec, it was necessary to average the signals for repeated sweeps to obtain statistically significant information for each data point. This was performed by using a Fabri-Tek Model 1062 Instrument Computer. Plug-in units SD-2/2 and SW-2 were used for signal digitizing and sweep control.

Oscilloscope

A dual-beam Tektronix Type 585A oscilloscope was available for the

on-line visual monitoring of the signals generated by boiling in the tank and detected by the hydrophones. The visual monitoring of the signals made it possible to select optimal gain factors for signals to be recorded on the magnetic tape.

Magnetic Tape Recording System

A four-channel Honeywell Model 1800 F.M. magnetic tape recorder was used for data recording, storage, and playback of the boiling acoustic noise signals detected by the two hydrophones. Table 2 lists some of the specifications of the equipment. The maximum frequency bandwidth attainable with the maximum tape speed of 30 ips controlled the maximum frequency range of the experiment with the tape recorder.

Figure 9 shows the measured frequency response of the instrument for the recording speed of 30 ips and the playback speed of 3.75 ips. These speeds were used for the entire experiment.

Hybrid Data Processor

An analog-digital hybrid computer system was used for most of the off-line computation of cross-correlation functions. The hybrid computer consists of an AD-80 analog computer interfaced to an IBM-1800 digital computer. A Datawest 370 Interface System, an analog-to-digital converter (ADC)., was a part of the system.

The Datawest is a 16 channel 12 bit machine. A full scale analog voltage of +102.4 volts is converted into the integer +2048. To obtain the maximum efficiency of the ADC, the recorded signals were conditioned as they were fed into amplifiers of the analog computer to give a maximum value of 100 volts. The two amplified signals were fed into

TABLE 2

Tape Recorder Characteristics

Tape Speed (ips)	Center Frequency (kHz)	Data Bandwidth (kHz)	S/N Ratio (dB)	Recording Level	Output Level
30	54	0-10	45	±2V peak minimum	±2V peak maximum
15	27	0-5	45		
3 3/4	6.75	0-1.25	42		
1 7/8	3.375	0-0.625	42		

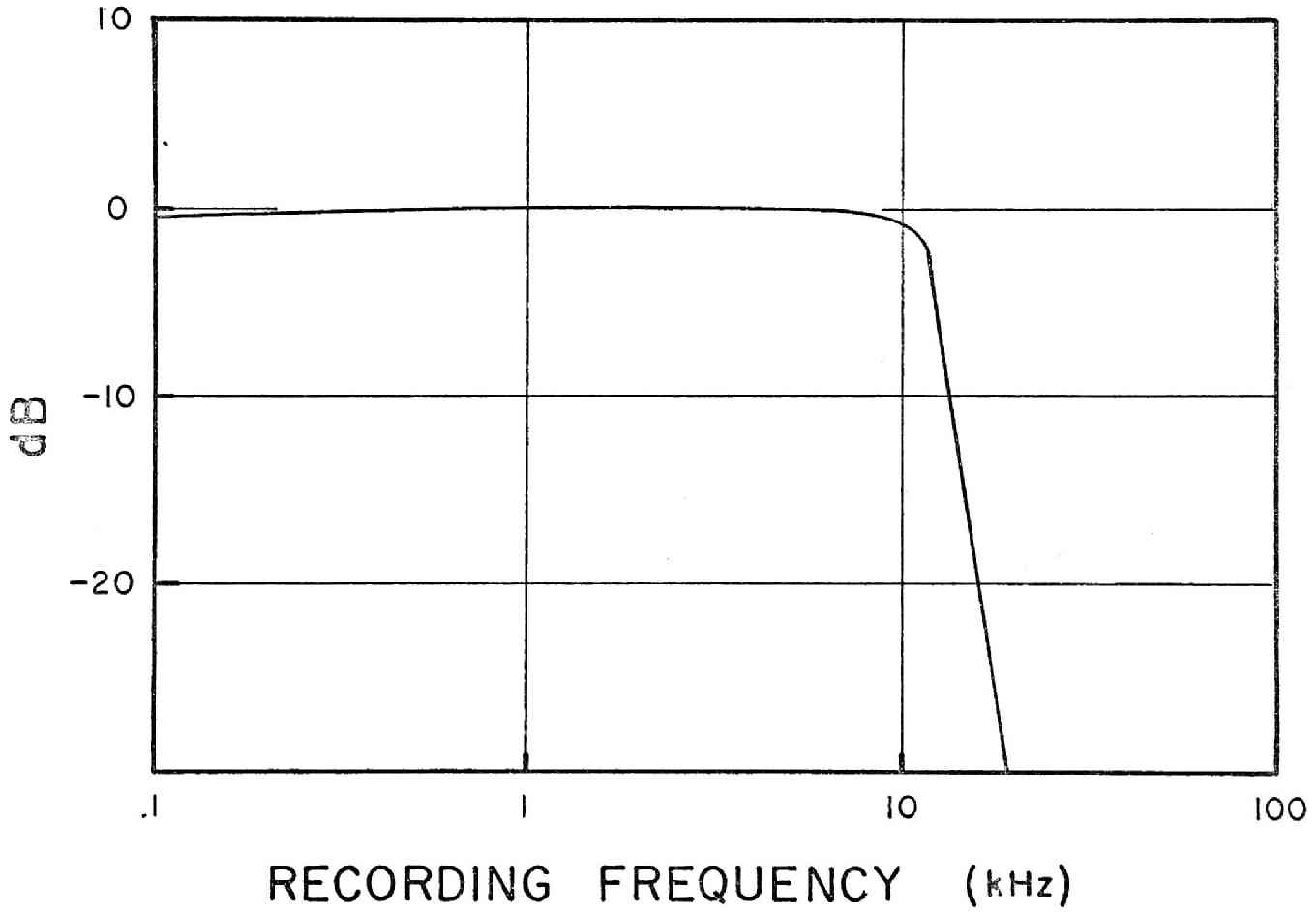

Fig. 9 Frequency Response of Tape Recorder

the ADC, which on the command of the IBM-1800 digitized the signals at a prescribed rate and stored the values on the disc memory.

An ADC subroutine was available at the user's level. This subroutine, ANLQK, returned a maximum of 254 data points at a nominal sampling speed of 31 μsec per data point plus an overhead time of 200 μsec. With the speed change capability of the tape recorder, this sampling rate provided a sufficient rapidness for processing the data.

Digital Fourier Analyzer

The Model 5451A Digital Fourier Analyzer is an integrated system which includes an ADC, display unit, digital processor, complete software package, and a user-oriented keyboard, and can process signals from D.C. to 100 kHz. The system employs mathematical techniques such as the Fourier transform and statistical averaging to calculate transfer function, coherence function, auto-power spectrum, cross-power spectrum, auto- and cross-correlation function, etc.

Signal Generator

In order to provide signals of known frequency and amplitude, a Krohn-Hite Model 440AR oscillator was used. This model is capable of generating sine and square waves in the frequency range of 0.01 Hz to 100 kHz. It was used to calibrate (1) the frequency axis of the spectrum analyzer readout, (2) frequency and amplitude of the cross-correlation data processing systems, (3) band-pass filter dial settings, and (4) amplifier gains.

CHAPTER IV

FREQUENCY SPECTRUM OF BOILING ACOUSTIC NOISE

General Remarks

Before applying the two-detector cross-correlation method for the triangulation of boiling sites, the frequency dependence of the boiling acoustic noise in the described facility is needed for proper planning of the triangulation method. Extensive measurements of frequency spectra of boiling noise were performed by M.J. Dunn [70] under varying experimental conditions.

Early measurements of the frequency spectrum showed that nucleate pool boiling at atmospheric pressure produced a large peak in the low kilohertz range and then was constant at a low level to near 50 kHz. Based on this observation two sets of measurements were made. The first set consisted of examining the spectral density from 400 Hz to 20 kHz. The second set examined the spectral density from 20 to 100 kHz.

In the subsequent triangulation studies, only the low frequency components of less than 10 kHz were used due to the equipmental capabilities, and the high frequency components were discarded. However, the high frequency components play important roles in identifying the boiling noise against the background, and will be reported in this chapter.

All the frequency spectrum measurements were performed using Model

706 hydrophone because of its sensitivity that extended into the megahertz frequency range. The detector location relative to the heater element is shown in Figure 10. The location of the detector was chosen so that the amplitude of the detected acoustic signal is the largest in that location. The lid of the tank was bolted to the tank main, and the tank was made water-tight for pressurized experiments. All the frequency measurements were taken with the Type A heater element.

In all cases except for measurements with a heat flux of 10.0×10^5 Btu/hr-ft^2 (2.71×10^6 k cal/hr m^2) the spectrum obtained was an average of 128 sweeps of the spectrum analyzer. For the cases where the heat flux was 10.0×10^5 Btu/hr-ft^2 64 sweeps were averaged. This change was made because use of the heater at this heat flux in excess of 1.5 minutes caused overheating of the power supply.

For the entire set of measurements only relative variations in the frequency spectrum are reported.

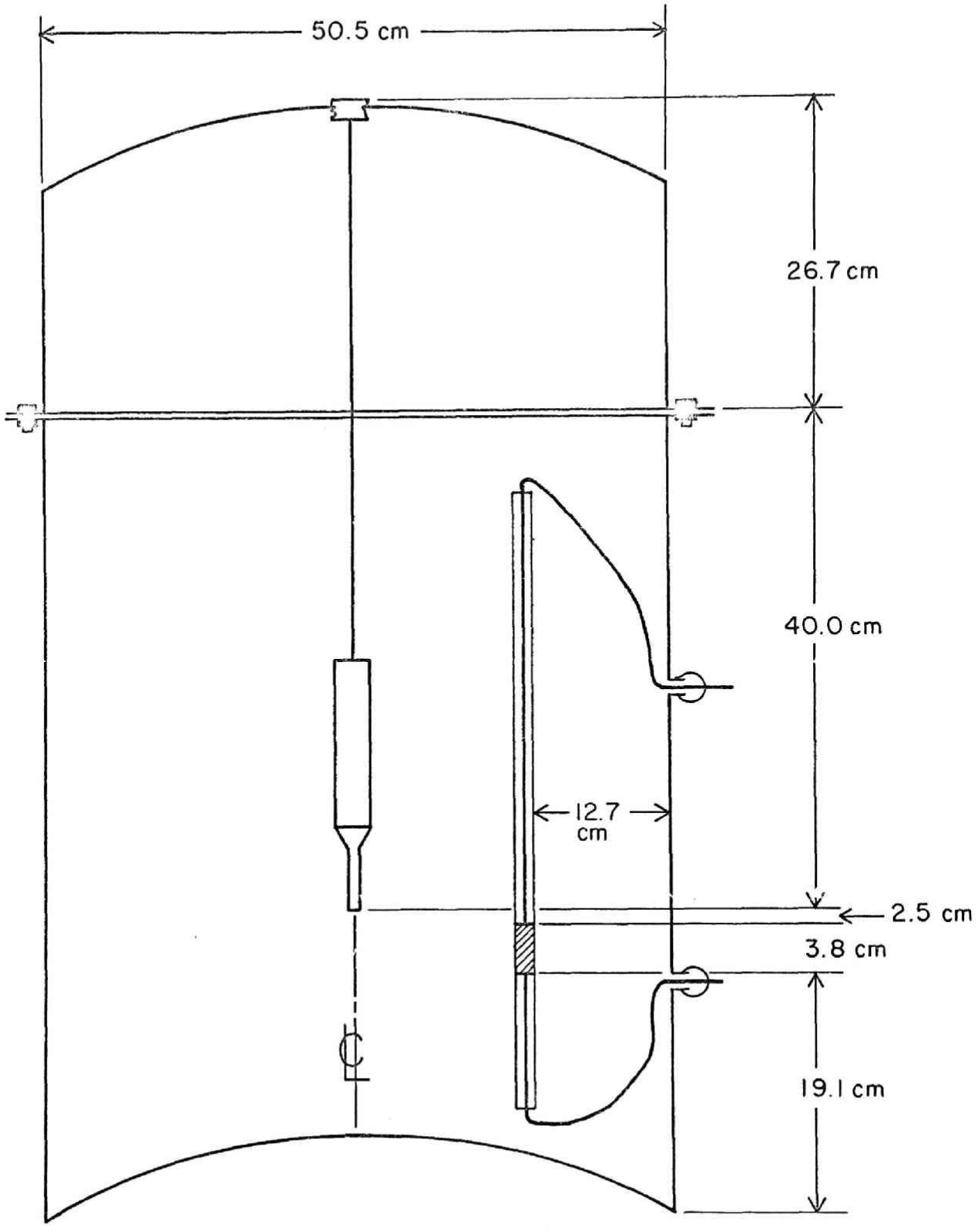

Fig. 10 Schematic of Tank Defining Probe Placement for Spectrum Measurements

Low Frequency Measurements

Measurements below 20 kHz were made for atmospheric pressure, no coolant flow, constant subcooling at the bulk water temperature of 27°C, and heat fluxes of 0.0, 1.5, 2.0, and 2.5 x 10^5 Btu/hr-ft^2. Figures 11 through 14 show the spectral densities measured for heat fluxes of 0, 1.5, 2.0 and 2.5 x 10^5 Btu/hr-ft^2. Resonance peaks are displayed near 2 kHz.

Most of the detected resonance peaks in the low frequency measurements may be identified as characteristics of the fluid contained in finite geometry. The solution of the acoustic pressure equation

$$c^2\nabla^2 p = \frac{\partial^2 p}{\partial t^2} \tag{4-1}$$

in cylindrical coordinates (r,Φ,z) is [71]

$$p = \begin{matrix}\cos\\ \sin\end{matrix} (m\Phi)\, \cos\left(\frac{\omega_z z}{c}\right)\, J_m\left(\frac{\omega_r r}{c}\right) e^{-2\pi i \nu t} \tag{4-2}$$

with

$$\nu = 1/2\pi\sqrt{\omega_z^2 + \omega_r^2}, \tag{4-3}$$

where

c = sound velocity

p = pressure

t = time.

At one of the end walls, or at the bottom of the cylinder, z = 0. The pertinent boundary conditions are satisfied at the other end wall, or the top of the cylinder, z = ℓ and at cylinder walls, at r = a, for the following characteristic values:

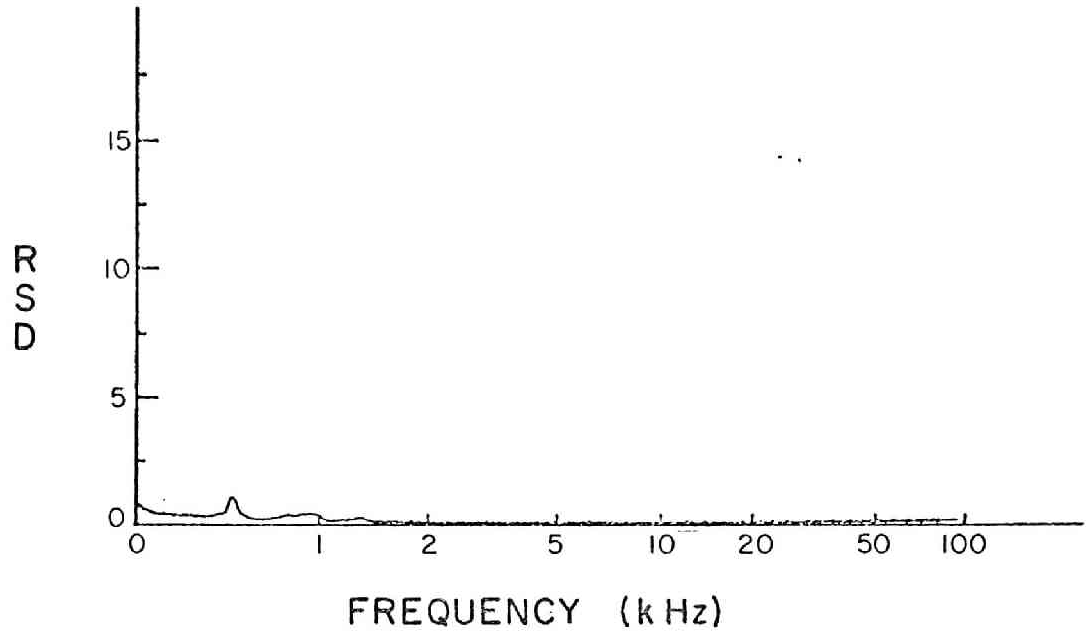

Fig. 11 Relative Spectral Density (RSD) for Q = 0.0 x 10^5 Btu/hr-ft^2, Pressure = 15 psia, and Flow Velocity = 0 fps. Low Frequency Range

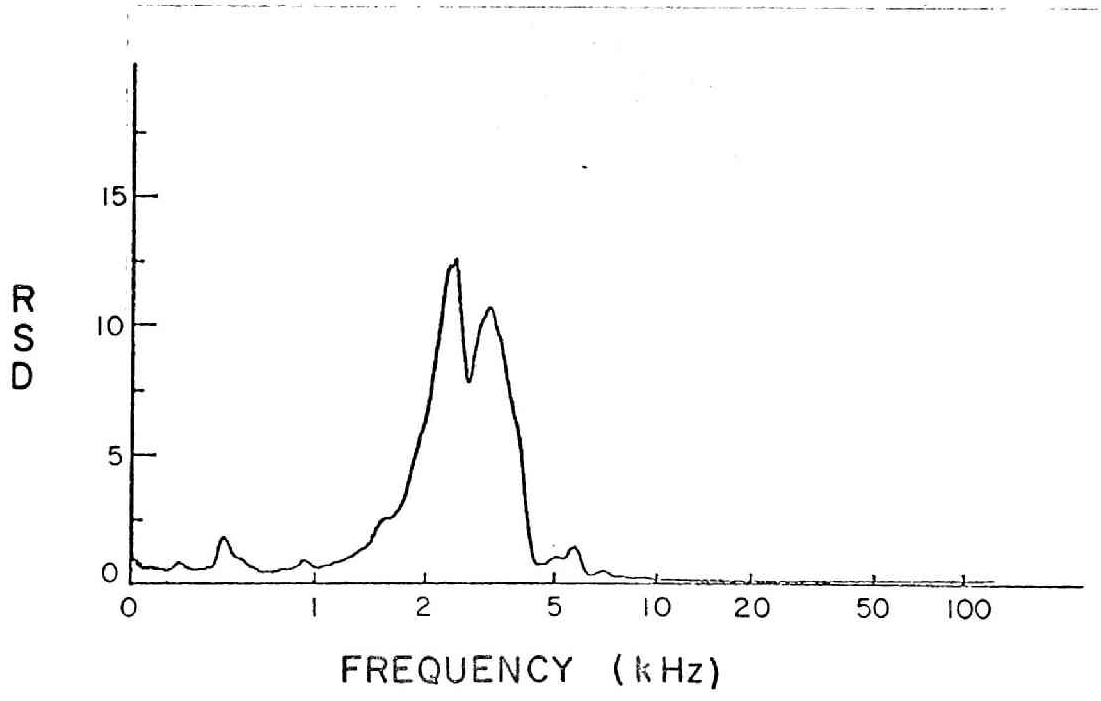

Fig. 12 Relative Spectral Density (RSD) for Q = 1.5 x 10^5 Btu/hr-ft^2, Pressure = 15 psia, and Flow Velocity = 0 fps. Low Frequency Range

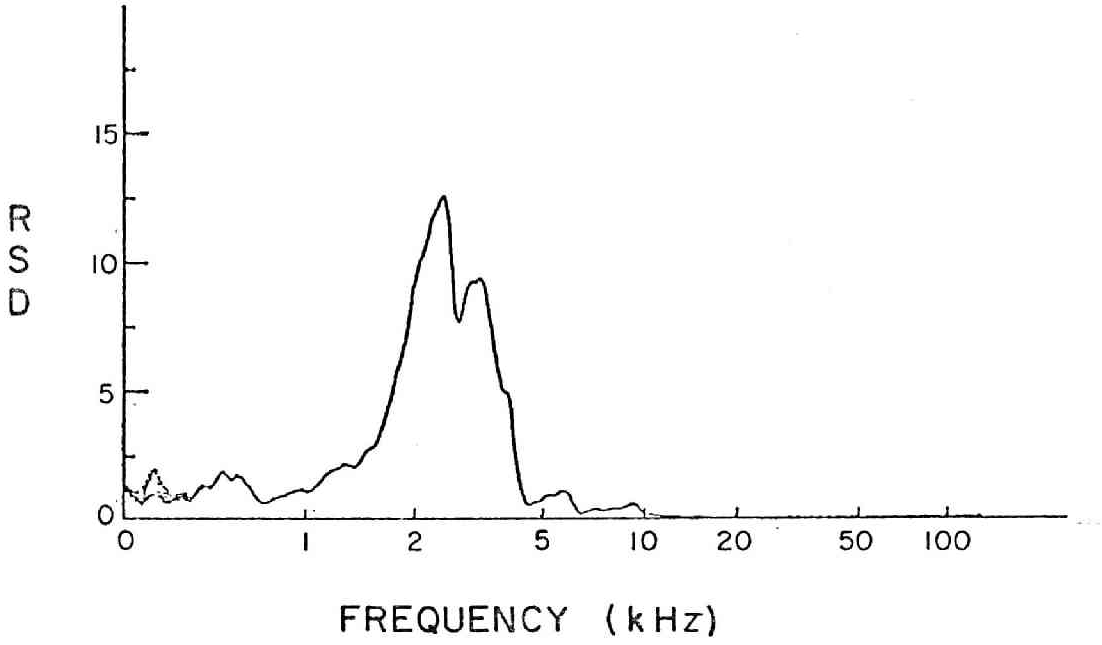

Fig. 13 Relative Spectral Density (RSD) for Q = 2.0×10^5 Btu/hr-ft^2, Pressure = 15 psia, and Flow Velocity = 0 fps. Low Frequency Range

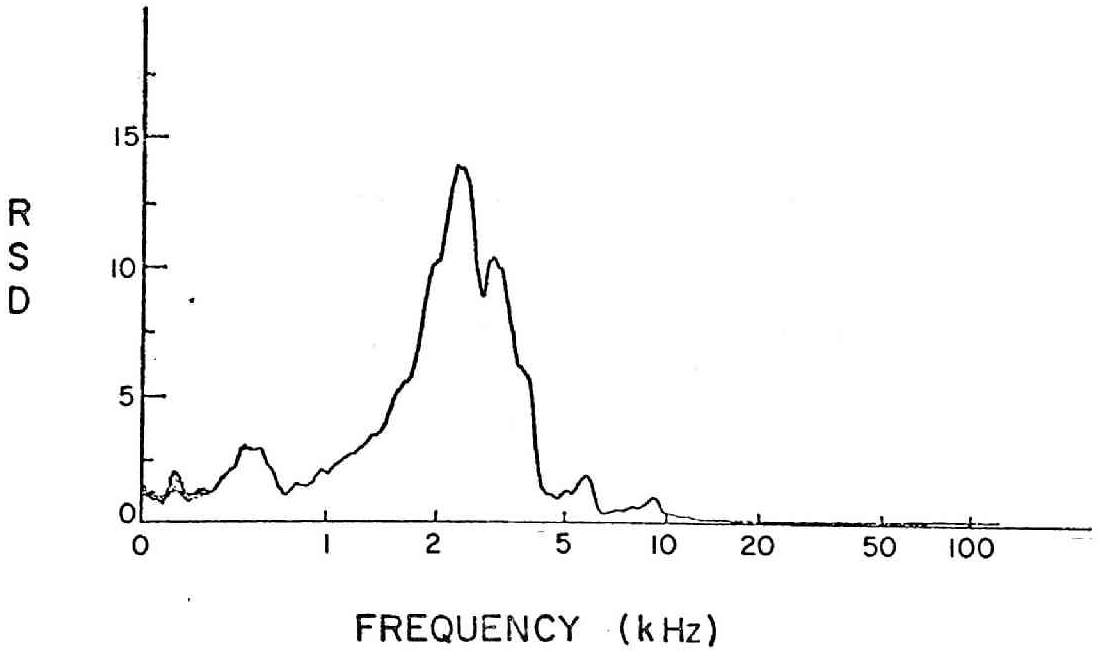

Fig. 14 Relative Spectral Density (RSD) for Q = 2.5×10^5 Btu/hr-ft^2, Pressure = 15 psia, and Flow Velocity = 0 fps. Low Frequency Range

$$\omega_z = \left(\frac{\pi n_z c}{\ell}\right) \qquad (n_z = 0,1,2,\ldots) \qquad (4\text{-}4)$$

$$\omega_r = \left(\frac{\pi \alpha_{mn} c}{a}\right) \qquad (4\text{-}5)$$

Thus

$$\nu = \frac{c}{2}\sqrt{\left(\frac{n_z}{\ell}\right)^2 + \left(\frac{\alpha_{mn}}{a}\right)^2} \qquad (4\text{-}6)$$

where α_{mn} is a solution of the equation

$$\frac{d}{d\alpha} J_m(\pi\alpha) = 0 \qquad (4\text{-}7)$$

Table 3 lists the calculated resonance frequencies for the tank geometry in which the spectrum measurements were taken. It is seen that the measured peaks in the frequency spectra agree well with some of the initial resonance modes.

TABLE 3

Resonance Frequencies for Some Initial Modes (kHz)

$n_z = 0$

m \ n	0	1	2
0	0.0000	3.6590	6.6992
1	1.7583	5.0909	9.1419
2	2.9165	6.4037	9.5201
3	4.0118	7.6538	10.8344

$n_z = 1$

m \ n	0	1	2
0	0.9375	3.7772	6.7645
1	1.9926	5.1765	8.1957
2	3.0635	6.4720	9.5662
3	4.1199	7.7110	10.8749

$n_z = 2$

m \ n	0	1	2
0	1.8750	4.1115	6.9567
1	2.5704	5.4253	8.3551
2	3.4673	6.6726	9.7030
3	4.4284	7.8802	10.9955

High Frequency Measurements

The high frequency measurements were performed to determine if acoustic noise, characteristic of nucleate boiling, was present at frequencies significantly above 20 kHz and to investigate the behavior of this boiling noise as a function of the heat flux, pressure and coolant flow. The 20 kHz cut-off frequency was selected because, in a nuclear reactor, differentiation of boiling noise from cavitation and pump noises is very difficult at lower frequencies.

By high-pass filtering the signal at 20 kHz a resonance shaped peak was forced into the relative spectral density data, with a low frequency cut-off near 15 kHz (due to filtering) and a naturally occurring high frequency cut-off beyond 50 kHz.

Figures 15 and 16 are examples of resonance shaped peaks. The change in the peak value of the relative spectral density, and in the naturally occurring high frequency cut-off due to the variations in the experimental parameters have been throughly studied [24,70]. In the following results of these studies are summarized. The results agree with intuitive picture of the phenomenon, and indicate that the detected high frequency acoustic signals were indeed generated by the nucleate boiling process.

1) The effect of increasing heat flux at constant system pressure and coolant flow velocity is to increase the peak value of the spectral density. This is expected since, once nucleate boiling has begun, increase in the heat flux increases the quantity of bubbles and therefore the noise level.

2) The effect of increasing system pressure at constant heat flux

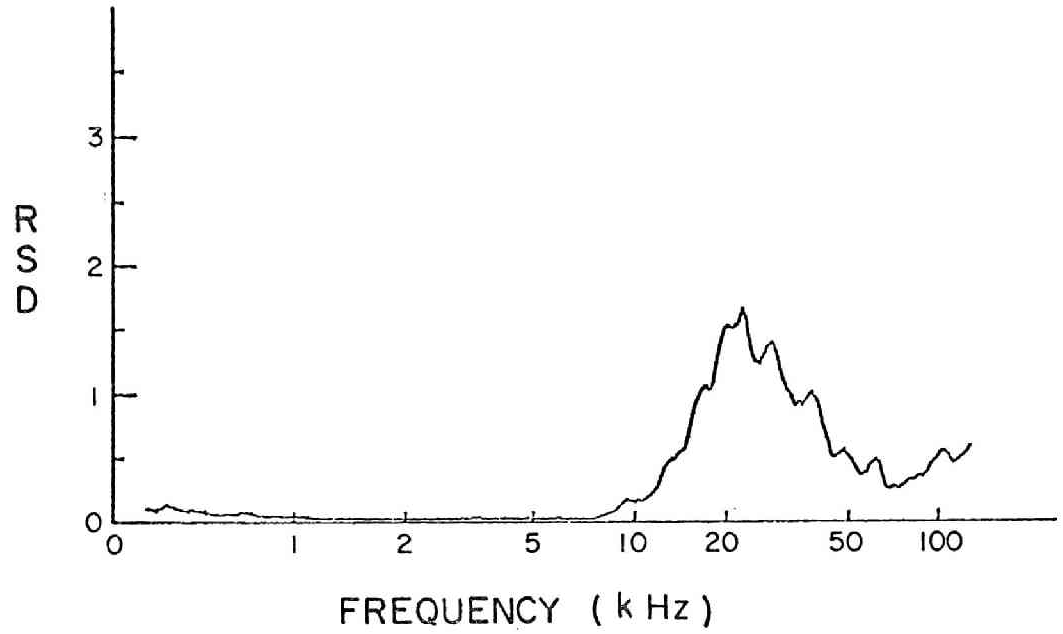

Fig. 15 Relative Spectral Density (RSD) for Q = 2.5 x 10^5 Btu/hr-ft^2, Pressure = 15 psia, and Flow Velocity = 0 fps. High Frequency Range

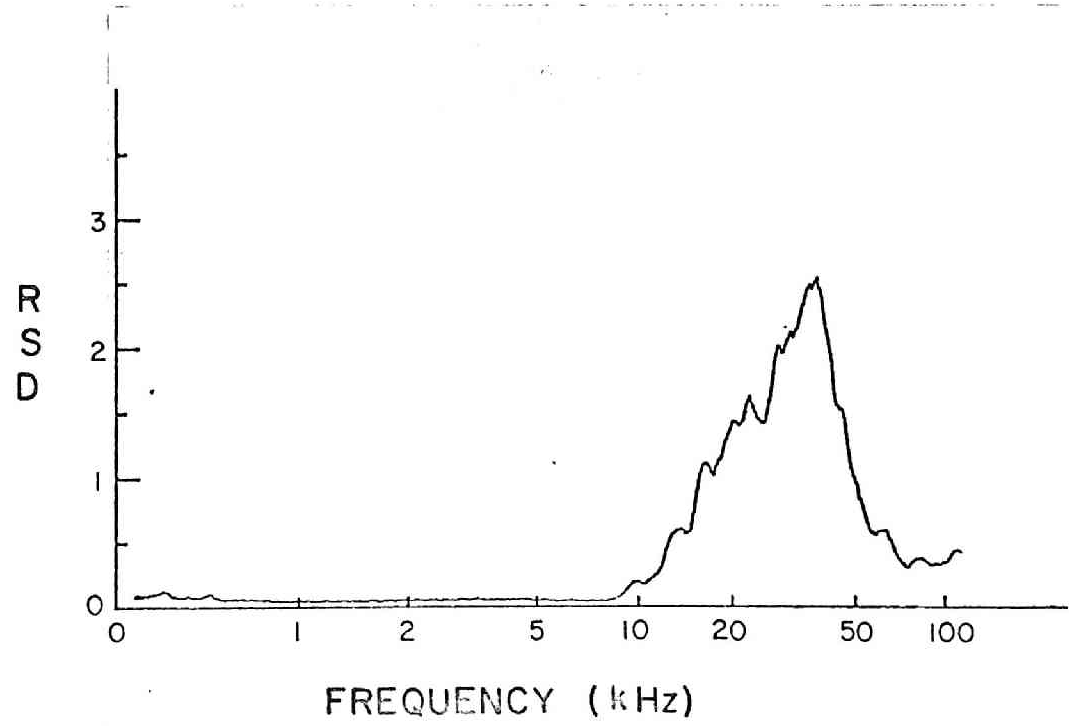

Fig. 16 Relative Spectral Density (RSD) for Q = 2.5 x 10^5 Btu/hr-ft^2, Pressure = 30 psia, and Flow Velocity = 0 fps. High Frequency Range

and coolant flow velocity is to increase the peak value of the spectral density and the high frequency cutoff for heat fluxes sufficiently above the threshold heat flux for nucleate boiling. For heat fluxes near the threshold value, the effect of increasing pressure is to decrease the peak value of the spectral density.

3) The effect of increasing the coolant flow velocity at constant heat flux and system pressure is to increase the peak value of the spectral density and the high frequency cutoff for heat fluxes sufficiently above the threshold heat flux. For heat fluxes near the threshold value, the effect of increasing coolant flow velocity is to decrease the peak value of the spectral density.

CHAPTER V

CROSS-CORRELATION FUNCTIONS AND TRIANGULATION TECHNIQUE

General Remarks

When a random signal is passing through a linear system, its transit time between two points along the path, or between the input and output, may be obtained by a cross-correlation measurement. The signal transit velocity is obtained if the time delay is measured between two points of a known separation distance. As the output from the system is displaced in time relative to the input, the cross-correlation function will peak at that time displacement equal to the time required for the signal to pass through the system.

A typical example of the use of the cross-correlation technique in nuclear reactors may be found in the transit-time flow-meter [72]. This technique is based on the detection of thermal eddies at two points separated a known distance in a flowing stream and determination of the average transit time of the fluid between the sensors by cross-correlation functions.

If the transmission velocity or the path through the system is sensitive to frequency, this technique may not be practical. In case of acoustic wave transmission in liquid, however, the sound velocity is independent of frequency but the problem of the variation of transmission path due to reflection and refraction may have to be considered carefully.

Cross-Correlation Functions

The cross-correlation function of two random functions $x(t)$ and $y(t)$ is defined as

$$R_{xy}(\tau) = \lim_{T\to\infty} \frac{1}{T} \int_0^T x(t)y(t+\tau)dt \qquad (5\text{-}1)$$

where

T = total observation time

τ = delay time

t = instantaneous time.

The definition of cross-correlation functions includes the auto-correlation function as a special case when the two random functions are equal. Properties of auto- and cross-correlation functions are discussed in many references [3,73-75] on noise analysis. When mean values are subtracted from the variables before multiplication, the resulting correlation functions are sometimes referred to as covariance functions. In the present study, correlation functions are used in the sense of covariance functions.

In practice total observation time is finite, and consequently only an estimate for the correlation function is obtained by taking the average over that finite period.

Recent practices for computing correlation functions are carried out on digital correlators in which random variables are treated as sets of random numbers rather than continuous variables. If the random variables are sampled at every time interval Δ, the correlation function is computed by using the following approximate formula.

$$R_{xy}(\tau) = \frac{1}{N} \sum_{t=1}^{N} \zeta_t^{x} \zeta_{t+\tau}^{y} \qquad (5\text{-}2)$$

where

$$\zeta_t^{x} = x(t\Delta)$$

$$\zeta_t^{y} = y(t\Delta)$$

and t is now a positive integral-valued index, and N is the number of data pairs. The sampling time or the fundamental time increment Δ needs to be less than the Nyquist interval. The Nyquist interval is reciprocal to the Nyquist frequency which is two times the frequency beyond which no signal component exists.

As an alternative to the cross-correlation function, polarity-coincidence correlation (PCC) function is sometimes used in application when such a computational scheme produces sufficient results. This is usually accomplished by strong clipping of the input signals by hard limiter circuits prior to the multiplication. It has been reported [76-79] that the performance of the PCC scheme is slightly inferior to the ordinary correlation scheme when the noise is Gaussian and stationary. However, it is superior when the noise is non-stationary, and the degree of superiority depends on the characteristics of the noise [80-82].

The PCC is calculated by the following formula:

$$R_{xy}(\tau) = \frac{1}{N} \sum_{t=1}^{N} \operatorname{sgn}(\zeta_t^{x}) \operatorname{sgn}(\zeta_{t+\tau}^{y}) \qquad (5\text{-}3)$$

where $\operatorname{sgn}(\cdot)$ is the sign function defined as

$$\operatorname{sgn}(u) = \begin{cases} 1 & u > 0 \\ 0 & u = 0 \\ -1 & u < 0 \end{cases} \qquad (5\text{-}4)$$

PCC scheme has been widely used in SONAR and RADAR systems, and was also applied in reactor noise applications. As mentioned previously Albrecht [20,21] investigated the possibility of detecting coolant boiling anomaly by analyzing the coherence function of neutron noise by PCC technique.

Triangulation Techniques

It was seen that cross-correlation functions of noise signals detected by two sensors placed in two locations along the signal path can assess the propagation velocity of the signal. If the two detectors are not on the same transmission path but receiving signals generated by the same source, the obtained time lags for the maximum peak positions in the cross-correlation functions yield the relative difference in the distance from the source to the detectors provided the transmission velocity of the signal is known.

The source location is found on a hypaboloid of revolution whose axis of revolution passes through the two detector positions. The positions of the two detectors form a set of focii of the hypaboloid. The choise of one of the two hypaboloid surfaces is determined by the sign of delay times for the arrival of signals, i.e., by the closeness to the source of either one of the two detectors. Other schemes of triangulation technique are reported by Cross et al. [60].

The terminology "triangulation" suggests the detection of the source on a plane. Three detectors can form sets of two detector pairs, and can pin-point the source location on the plane which these detectors determine. Likewise three detector pairs placed not on the same plane can detect the source location in a three dimensional space. Obviously only one pair is sufficient to locate the source on a line, or in one dimensional geometry. We shall use this terminology rather loosely here to imply detection schemes of locating the source position by using

pair(s) of detectors. The method of determining differences in the distance does not have to be through correlation functions. Other delayed-coincidence techniques could be used depending on the nature of the noise signal.

Computer Programs

Most of the cross-correlation functions of the measured boiling acoustic noise were calculated by the hybrid computer at the University of Florida. Some of them were obtained by the digital Fourier analyzer at the Oak Ridge National Laboratory. Descriptions of these equipments are found in Chapter III. In this section some features of the computer programs developed for use with the hybrid computer system will be described. The programs are listed in Appendix I.

The main program controls the ADC to perform the conversion on a batch of data. Under the control of the IBM-1800, the ADC or the Datawest 370 Interface System can sample $2^8-2 = 254$ data points at a time at a fixed interval of 31 μsec in series, thus provides a set of 127 data points per each of the two data channels. The sampling sequence of the ADC is shown in Figure 17. Since the two channels are not sampled at the same time, one of the sample pair lags behind the other by 31 μsec. This discrepancy of the sampling time is corrected by the computer program when the results are displayed on the plotter.

In order to improve the statistics of correlation function calculation, up to 100 data sets, each comprising 127 data pairs, are stored on the magnetic disc to be processed in cross-correlation functions set by set.

Cross-correlation functions are computed by calling a subprogram CROSS supplied by the manufacturer of the digital computer [83] and modified to include the option of calculating PCC functions. The number of lags used for the present study was set at 30, but this can be modified easily. This number approximately corresponds to the maximum

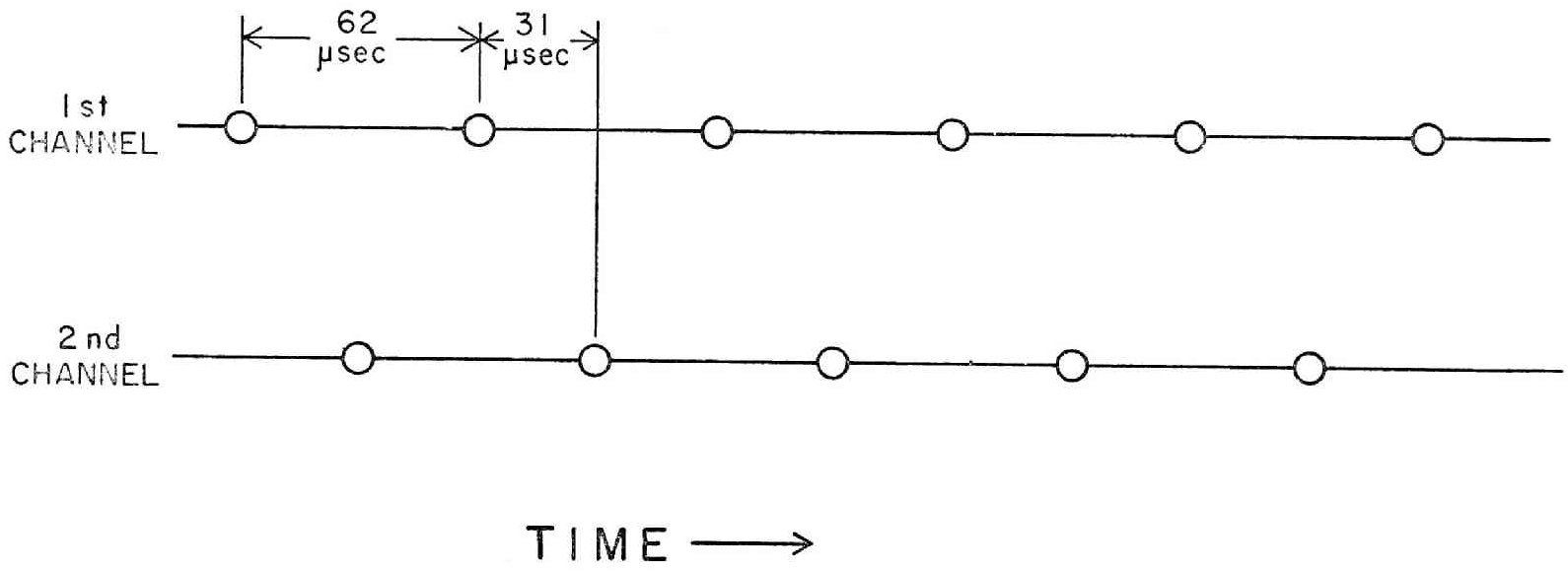

Fig. 17 Sampling Sequence of Datawest 370 Interface System

separation distance of the two detectors used for the measurements. Any peaks in cross-correlation functions outside this range are considered superfluous, having been produced by irrelavant reflections of acoustic waves in the container.

When the calculation of the cross-correlation function of a set of data pairs is completed, the results are stored in the core memory and the process is repeated. When cross-correlation functions for all the data sets are accumulated they are averaged and plotted on the curve plotter of the system. Subroutine FIGR plots the results. In addition, one segment of the raw data recorded on the disc may be plotted by the plotter. This is accomplished by a subprogram NOISE.

The sampling time per data pair is 62 μsec, but can be made shorter or longer in practice by changing the ratio of recording and playback speed of the tape recorder. By recording at a speed of 30 ips and reproducing at a slower speed of 3.75 ips, the normal unit lag time of 62 μsec is reduced to 7.75 μsec real time, or conversely to 0.129 lag channel/μsec.

The lag time at the peak location of the cross-correlation function is converted to the difference in the distances from the boiling site to the two detectors by multiplying it by the sound speed in water which is dependent on temperature. Figure 18 shows the temperature dependence of sound speed in pure water [84].

Pre-recorded 8.0 kHz sinusoidal signals were used to calibrate the time scale as well as the amplitude. A signal level of 4 volts at the recording stage was amplified by operational amplifiers of the AD-80 analog computer to 80 volts. When converted, this voltage is equivalent to a digital number of 1600.

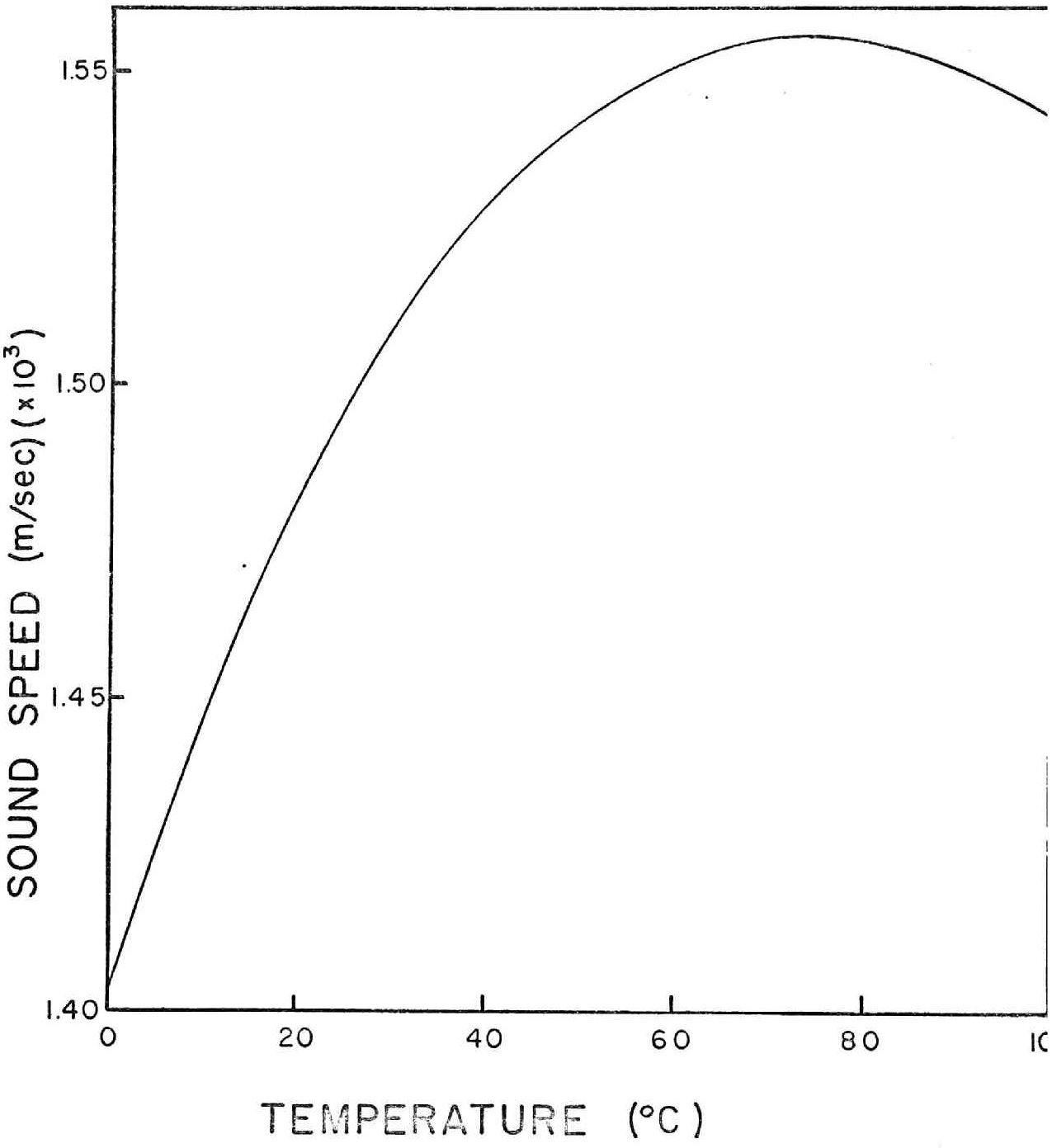

Fig. 18 Speed of Sound in Pure Water

The computer time for 10 sets of 127 data pairs for the maximum lag of 30 is approximately 5 minutes excluding the time required for plotting the output curves. Normally 30 to 50 sets are used for processing the measured data.

CHAPTER VI

MEASUREMENTS OF CROSS-CORRELATION FUNCTIONS

General Procedure

Measurements of cross-correlation functions of the boiling acoustic noise signals detected by the two hydrophones were performed subsequent to those of the frequency spectra. In order to facilitate the placement of two detectors in the tank, the lid of the tank was removed and the measurements were taken in the open tank system. The flow nozzle was also removed from the system. All the measurements were taken under quiescent conditions.

The single heater pin was placed in the same location as in the spectral measurements. Type B heater element (Figure 3(b))was used throughout the cross-correlation measurements. The placement of the heater rod in an eccentric position facilitated to incorporate various values of the difference in the distance from the boiling site to the two detectors, thus simulating the in-core boiling in an unspecified fuel channel.

In a later series of experiments, a bundle of cylindrical aluminum rods were placed surrounding the heater rod to simulate a more realistic configuration. Aluminum rods, 1.27 cm in diameter and 61 cm long, were arranged in a triangular array of 1.905 cm pitch. The solid-liquid volume ratio of the lattice was 1.963. The rods were supported vertically by two plastic grid plates, 1.27 cm thick, placed on the bottom and on the top flange of the tank.

The two hydrophones were suspended in the water from the rim of the tank. Type 1700 hydrophone was mounted on an aluminum rod of 1.27 cm in diameter since the coaxial cable attached to the hydrophone was so flexible that the reinforcement was needed for the exact positioning of this hydrophone.

Hydrophone Locations

The hydrophones were placed along the tank wall for most of the measurements. Most probably detectors will be placed in similar locations when this technique is implemented in reactors. In one series of experiments, they were positioned diametrically across the tank. Figure 19 shows horizontal locations of the hydrophone placement. In most cases the two hydrophones were placed at a same height for one set of measurements. On one occasion they were separated vertically on a line parallel to the tank axis. The vertical locations will be designated by distances from the location of the center of the heater element. Thus, for example, level 10 will mean that the hydrophone is located on a horizontal plane 10 cm above the center of the heater element.

Experimental Procedure

Preceeding each day's measurements the tank water was replaced with fresh distilled water to avoid contamination from corrosion of the tank. In all of the measurements water was filled to the rim of the tank. Calibrations of amplifiers, filters and the tape recorder were also checked every time the measurements were taken.

Most of the measurements were performed with maximum gain settings

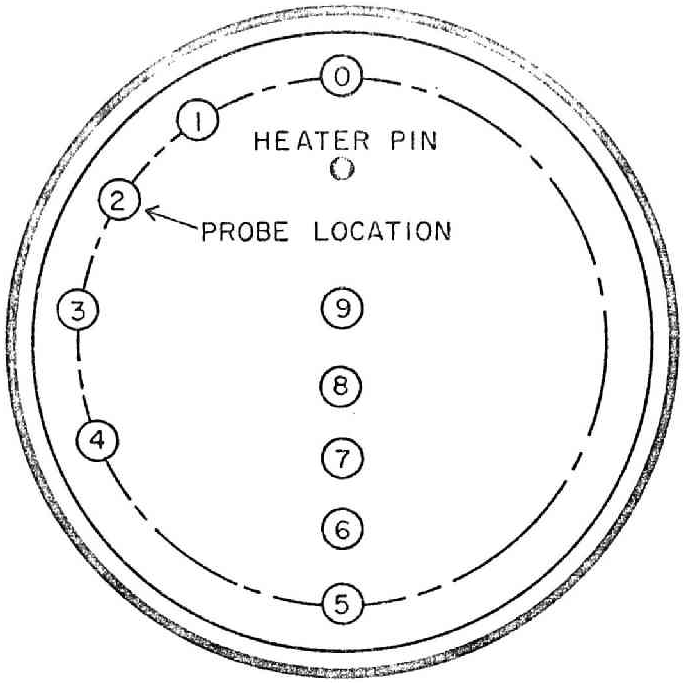

DISTANCE FROM HEATER PIN TO PROBE (cm)

0 8.5	3 7 23.5
1 9 13.5	4 6 28.5
2 8 18.5	5 33.5

Fig. 19 Designation of Horizontal Probe Locations for Cross-correlation Measurements

on the amplifiers. The amplifier gains were measured by introducing small sinusoidal signals of known intensity in the interested range of frequency into each amplifier set, and by measuring the output signal intensities on the oscilloscope. The amplifier gains were determined to be 200 and 160, respectively for the sets used with Type 706 and Type 1700 hydrophones, with the error bounds of ±10 percent. By using these values and the sensitivity curves of the hydrophones provided by the manufacturer (Figure 6), the overall sensitivity of the instrumentation was determined to be 1.46×10^{-2} rms v/μbar and 1.92×10^{-2} rms v/μbar for channels with Type 706 and Type 1700 hydrophones, respectively. These gain settings produced signals with sufficiently large amplitude to be recorded on magnetic tape for later processing.

Three frequency pass bands were chosen to use selectively various frequency components of the boiling acoustic noise signals. These are

(1) 400 Hz to 10 kHz

(2) 400 Hz to 5 kHz

(3) 5 kHz to 10 kHz.

The lower break frequency of 400 Hz was chosen to eliminate significant low frequency components due primarily to the power line induced noise. The upper break frequency of 10 kHz is the maximum frequency limited by the capability of the magnetic tape recorder used. The mid-frequency of 5 kHz was chosen since large peaks were previously found below this frequency (see Chapter IV), and the effects of these

low-frequency components on the cross-correlation functions were to be investigated.

The band-pass filters may introduce errors in phase relationships of the two signals and consequently in the difference of the signal arrival times unless they are accurately turned in at the same frequency settings. Careful settings of the break frequencies were accomplished and checked by feeding sine waves to the units and observing the outputs from the two sets of amplifiers.

The tape recorder was calibrated for recording and playback as specified in the manual. The maximum input signal level was set at the suggested 2 volts peak-to-peak value. Signals from the two detectors were recorded on tape at the speed of 30 ips. They were played back at a reduced speed of 3.75 ips for analysis. The change of speed enabled to reduce the sampling time interval of the ADC by a factor of 8. For calibration purposes, a sine wave of 8 kHz, 4V peak-to-peak, was recorded on the two channels of the tape recorder for each series of measurement. At the playback stage, the calibration signal produced sinusoidal signals of 1 kHz.

The power input to the heater was chosen at a value of 1000 W at the wattmeter, or 2.2×10^5 Btu/ft^2-hr (5.97×10^5 kcal/hr-m^2) on the heater element surface for most of the experiment. This heat flux gave sufficiently large levels of boiling acoustic noise to be detected and processed by the equipments used in the present study, but was low enough not to overheat the power supply system and the heater element. Occasionally, however, 1.36 kW (or 3.0×10^5 Btu/ft^2-hr = 8.14×10^5 kcal/hr-m^2) was supplied to enhance the acoustic noise signals.

The bulk water temperature was measured by a mercury thermometer suspended in the tank.

Results and Interpretations

Results of the cross-correlation functions calculated by the hybrid computer are contained in Appendix II. These are direct reproductions of the computer plotter outputs showing cross-correlation functions as functions of lag channels. The number of lag channels may be converted into time lag by using the cross-correlation functions of the sinusoidal calibration signals recorded preceeding series of experiments. It may be further converted into distance by multiplying it by the sound speed in water at the temperature at which the measurement was taken.

Strength of Acoustic Noise Signal and Background Noise

Figure 20 shows examples of boiling acoustic noise signals detected by the hydrophones. As observed from these traces, the boiling acoustic noise showed pressure fluctuations of the order of 1 m bar, or 1000 dynes/cm^2. This is in agreement with the results of other investigators [29]. In Figure 20, an example of the background noise trace is also shown. The background trace was taken with a heating power of 200 W at the wattmeter. At this power level only very small number of bubbles were visually observed near the heating surface. The cross-correlation function of this background noise is also included in Appendix II (see Figure 38). Clearly the background signals detected by the two detectors are uncorrelated. This indicates that the hydrophones did not pick up common mode noise from the A.C. power line.

The background noise was mainly due to the instrumentation noise, and the signal to noise ratio was in the range of 25 to 30 dB.

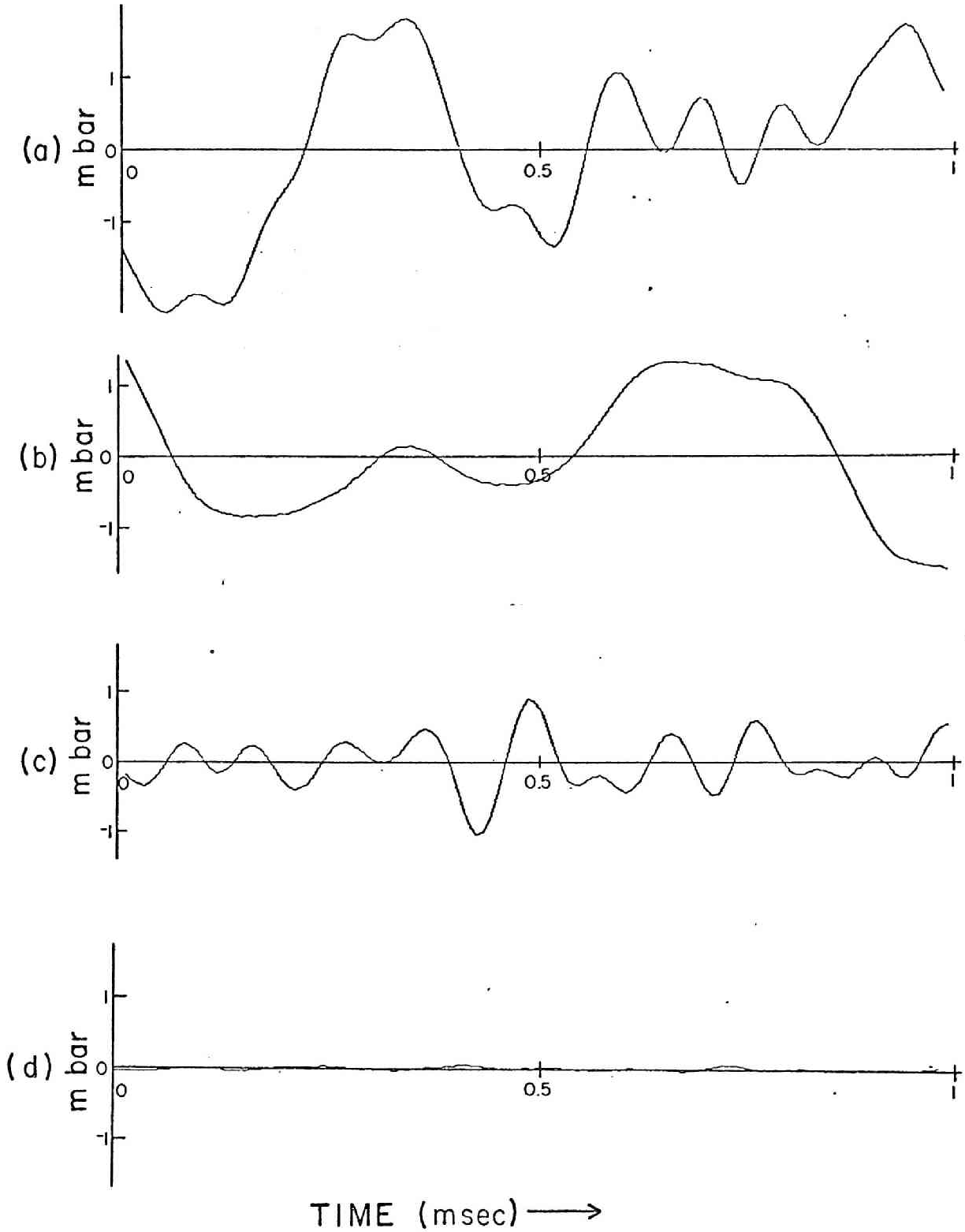

Fig. 20 Examples of Boiling Acoustic Noise Signals. (a) 400 Hz - 10 kHz Pass-band, (b) 400 Hz - 5 kHz Pass-band, (c) 5 kHz - 10 kHz Pass-band, (d) Background. Hydrophone at Location 0, Level 0

Effects of Frequency Passbands

As stated previously, large peaks were found in the frequency range of less than approximately 5 kHz in the frequency spectrum measurements. If these large peaks are due to the acoustic noise generated by boiling process itself and not related with the resonance of the fluid contained in finite geometry, signals in this frequency range could be used most effectively for the triangulation of boiling sites. For this reason the band-pass filters were first set for the frequency range of 400 Hz to 5 kHz.

Figure 21 shows normalized peaks of the cross-correlation functions. In these runs hydrophones were placed at the same height as the center of the heater element, or at level 0, in a horizontal array. Each of the curves was obtained by correlating 2910 to 3810 data pairs, or from 30 sets of 127 data pairs, with the maximum displacement of 30 lag channels.

Contrary to the assumption, the peak locations all fell near the zero-lag position. This result indicates the existence of a strong common mode fluctuation. In other words, the acoustic waves were coming from all directions showing characteristics of the system resonance [71]. Thus, though a large amplitude is detected in this frequency range, it is of no value to the evaluation of boiling sites by the triangulation technique. Similar experiments were carried out at other detector levels at 10 and 20 cm above the heater level. These measurements also gave similar results.

Eliminating this frequency range, data were taken in the upper

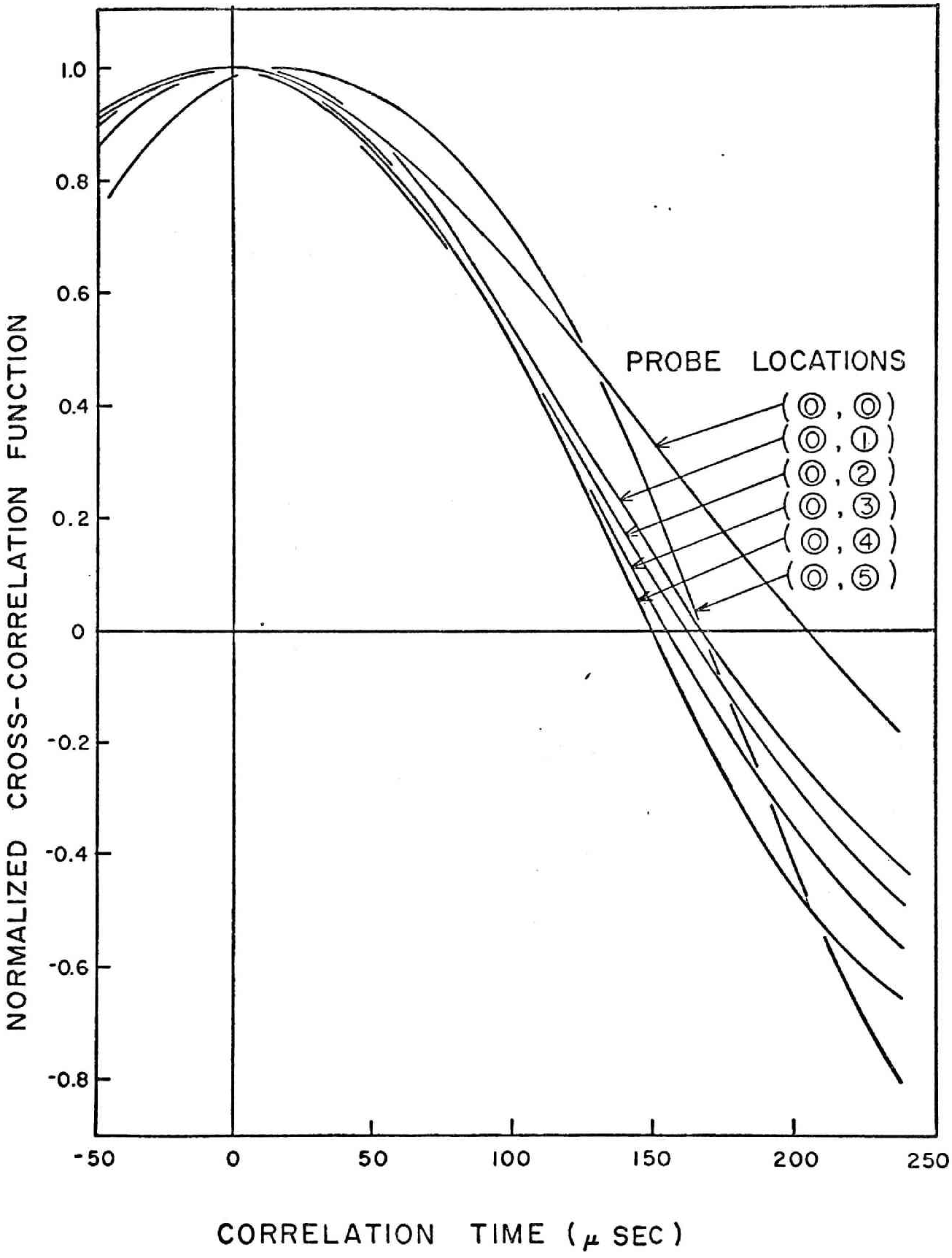

Fig. 21 Cross-correlation Functions in the 400 Hz - 5 kHz Frequency Range. Hydrophones at Level 0

frequency range of 5 to 10 kHz. Figure 22 is the result of these runs. The hydrophones were again at level 0. The figure shows the largest peaks in the cross-correlation functions detected within the range of 30 lag channels. Definite shifts in the positions of the peak are noticed in this frequency range. The peak locations agree very well with the predicted values which are based on the speed of sound in water and on the differences in distances between the heater and the probes.

Measurements with probes placed at a level 10 cm higher than the heater location, or level 10, produced similar results. Figure 23 shows the measured and the theretical distances for the two levels of the hydrophone array. The agreement of the two distances are clearly illustrated.

Comparison of these two series of experiments reveals that the low frequency resonance is indeed the system resonance and that in cross-correlation boiling acoustic signals for triangulation purposes the resonating signals should be removed before processing the detected signals.

Cross-correlation functions in the frequency passband of 400 Hz to 10 kHz naturally contain informations of the resonating low frequency signals and of the high frequency signals that arrive at the hydrophones at distinct times. Correlation peaks of Figures 51 through 56 in Appendix II show this mixed property.

Since it is only the high frequency information beyond the system resonance frequency domain that contributes to the triangulation of the boiling site, only the cross-correlation functions in the 5 kHz to 10 kHz passband will be treated in the remainder of this chapter.

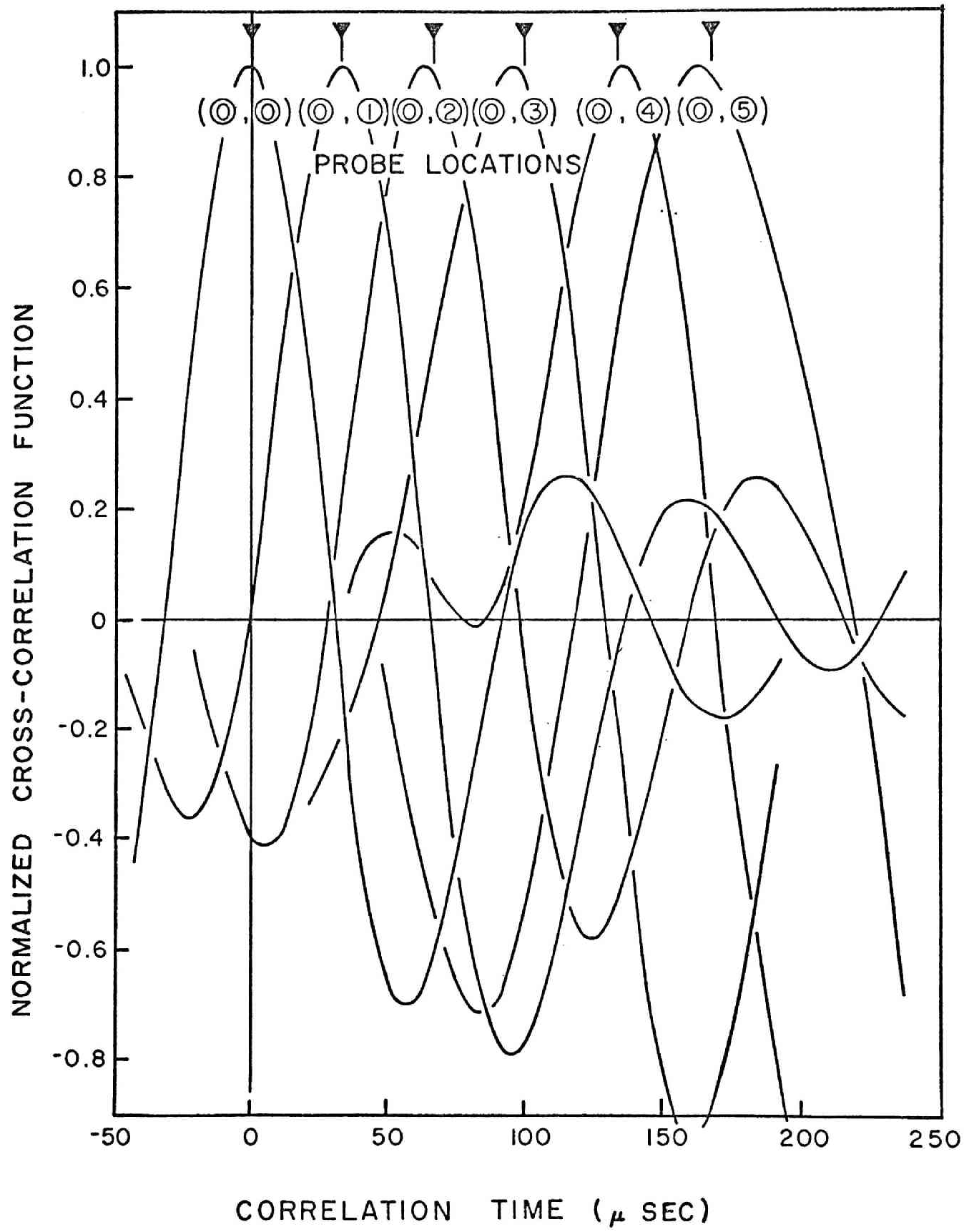

Fig. 22 Cross-correlation Functions in the 5 kHz - 10 kHz Frequency Range. Hydrophones at Level 0

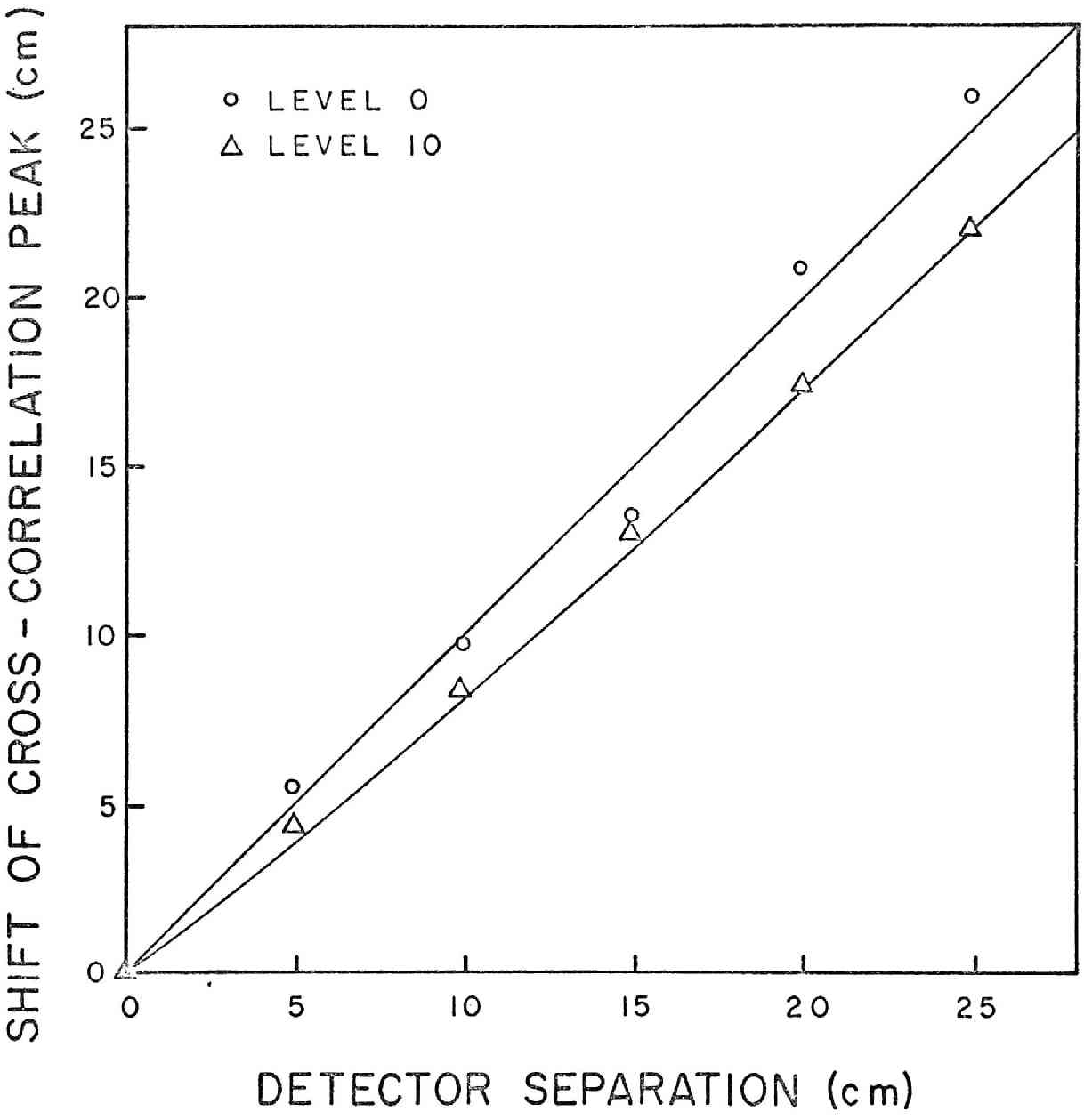

Fig. 23 Peak Locations of Cross-correlation Functions at Level 0 and Level 10

Effects of Container Wall Reflections

Contrary to the triangulation method in the flaw detection in steel slabs or in a vast quantity of liquid, triangulation in a relatively small quantity of liquid contained in a small tank made of reflecting walls presents an annoying problem of reflected waves. This phenomena is observed in the present experiment at (0.4) and (0.5) locations when the hydrophones were located at levels 0 and 10.

Figure 24 shows cross-correlation functions measured at level 0. These curves were taken at the Oak Ridge National Laboratory by using the digital Fourier analyzer. This equipment is superior to the hybrid computer system in its versatility in changing the sampling time, the scope of the time lag, and the size of the raw data points.

The peak marked "direct" is the one produced by the acoustic wave arriving at different times to the detectors directly; the peaks marked "reflected" are identified as the peaks due to the correlated signals in the direct wave and the wave that is scattered back from the wall directly behind the other detector. The amount of the peak shift agrees with the time of travel of the acoustic wave front across the diameter of the tank.

In these detector locations the two hydrophones were facing the opposite sides of the heater element, and a strong correlation is expected between a direct signal from one side of the heater element and the reflection of this signal to the other detector which faces the other side of the heater element. The latter detector is in the "shadow" of the heater element with respect to the "direct" signal.

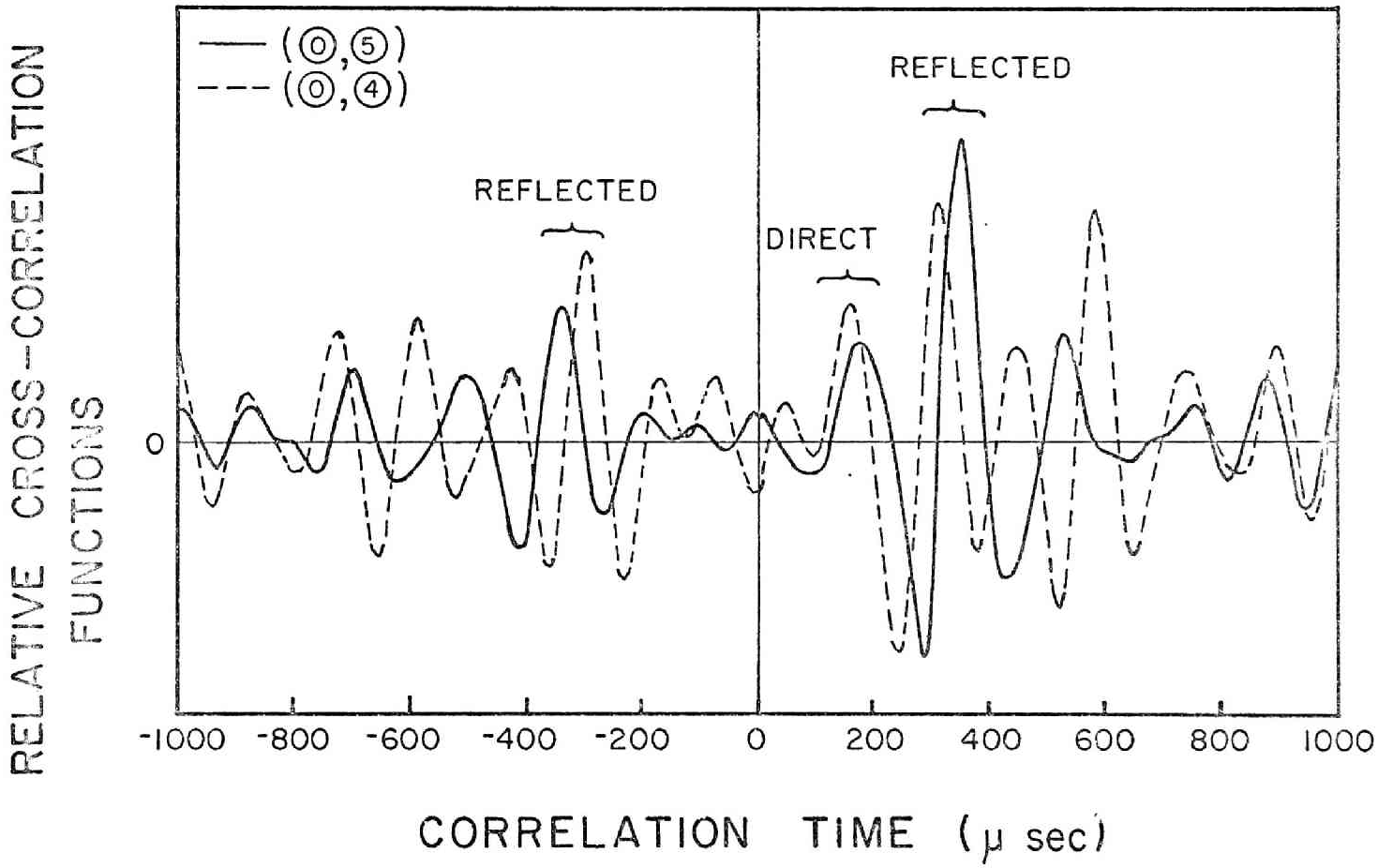

Fig. 24 Correlation Peaks due to the Direct and Reflected Wavefronts

When waves are reflected on a concave surface the reflected wave fronts are intensified due to the focusing effect. This is also true for acoustic waves. Figure 25 is a ray-wavefront diagram for the present arrangement obtained on the IBM-1800 plotter. Appendix IV lists the computer program that produced this figure. From the ray-wavefront curves it is seen that the reflected waves are intensified along the diameter of the symmetric axis.

The ratio of the sound energy reflected back into medium 1 after striking medium 2 is given by

$$P_R = \frac{Z_2 - Z_1}{Z_1 + Z_2} \tag{6-1}$$

where Z_1 and Z_2 are the acoustic impedances of the medium 1 and 2 respectively [39]. In the present case medium 1 is water and 2 is the composite of the foam rubber lining and the steel wall whose acoustic characteristics are not known.

The relative strength of the acoustic energy of the reflected wave is represented by the divergence factor of the reflected wave [85]. We denote the strengths of the incident and reflected acoustic shock waves by $P_0^{(i)}$ and $P_0^{(r)}$, and let $\underline{x}$ be a point on a reflected ray which issues from the point $\underline{x}_0$ of the reflector surface R. Let also σ be the distance of $\underline{x}_0$ from $\underline{x}$ and F_1, F_2 be the principal radii of curvature of the reflected front at $\underline{x}_0$. Then

$$P_0^{(r)}(\underline{x}) = AP_0^{(i)}(\underline{x}_0), \tag{6-2}$$

where

$$A = \left\{ \frac{F_1 F_2}{(F_1+\sigma)(F_2+\sigma)} \right\}^{1/2} \tag{6-3}$$

is the divergence factor of the reflected rays normalized so that its value on R is unity.

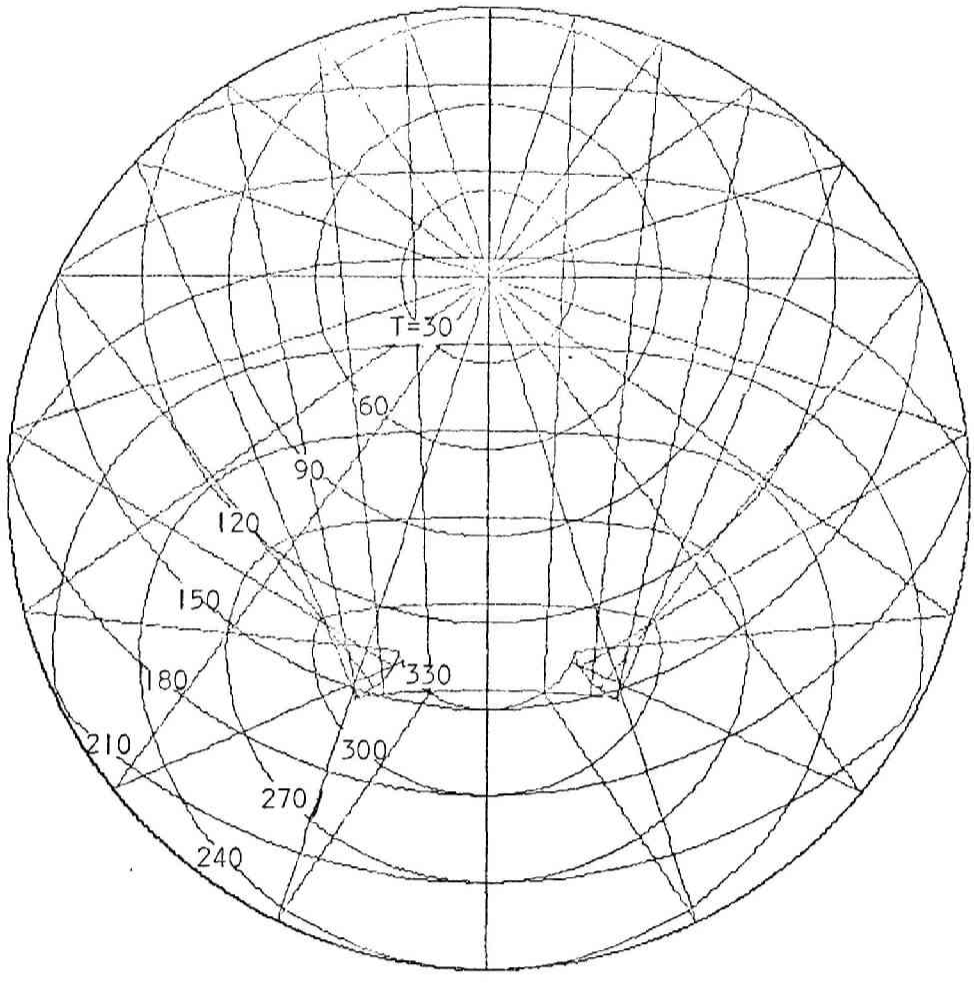

Fig. 25 Ray-Wavefront Diagram at Level 0. (T in μsec)

A general formula for the strength of an acoustic shock wave due to the reflection of a spherical shock at an arbitrary surface has been obtained by J.B. Keller and H.B. Keller [86]. Assuming that the reflector is an infinite circular cylinder for the present geometry, the divergence factor was calculated. Figure 26 shows the computer output for the standard location of the heater element. The computer program is also listed in Appendix III.

In Figure 26 (a), contours for constant divergence factors for the incident wave fronts are shown, while those of the reflected waves are shown in Figure 26 (b). The divergence factor is normalized to unity at the instant of first contact of the acoustic wave with the wall. Clearly the reflected wave is intensified due to focusing effect near the detector location 5.

In interpreting peaks in cross-correlation functions, those peaks found at time lags greater than the acoustic transmission time between the two detectors should be rejected as stemming from the coherent but reflected waves. Since the intensities of the reflected waves are strongly focused in the semi-circular domain not containing the heater rod, cross-correlation functions obtained from the signals detected by hydrophone pairs located in this domain do not provide good results for triangulating the boiling sites. Figure 27 shows the results when detectors are placed along the diameter containing the heater rod. In this arrangement both of the hydrophones are strongly affected by the reflected waves. Compared with the results of Figure 23, the agreement of the measured and the true separation distance is poor showing the effects of reflection.

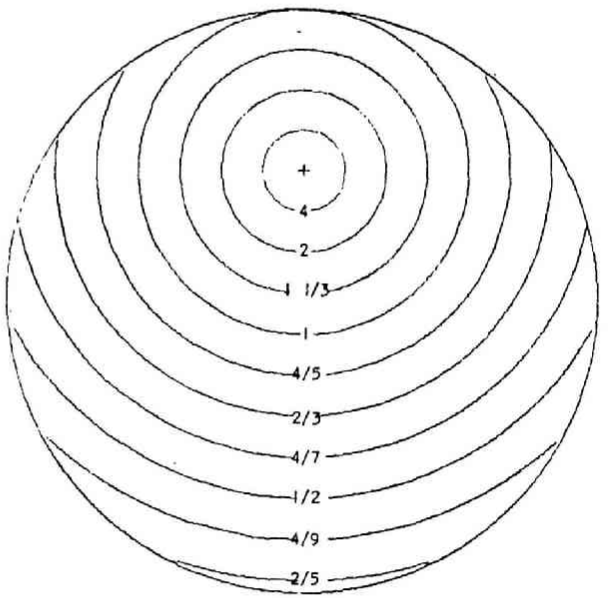

(a) Direct Wave

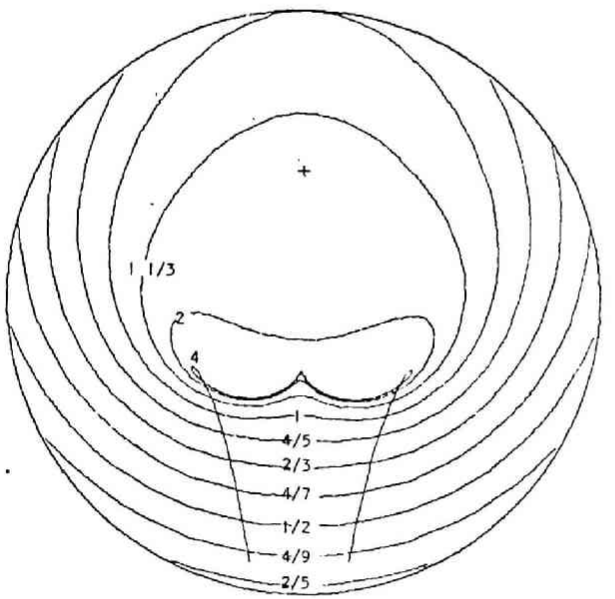

(b) Reflected Wave

Fig. 26 Divergence Factor Contours

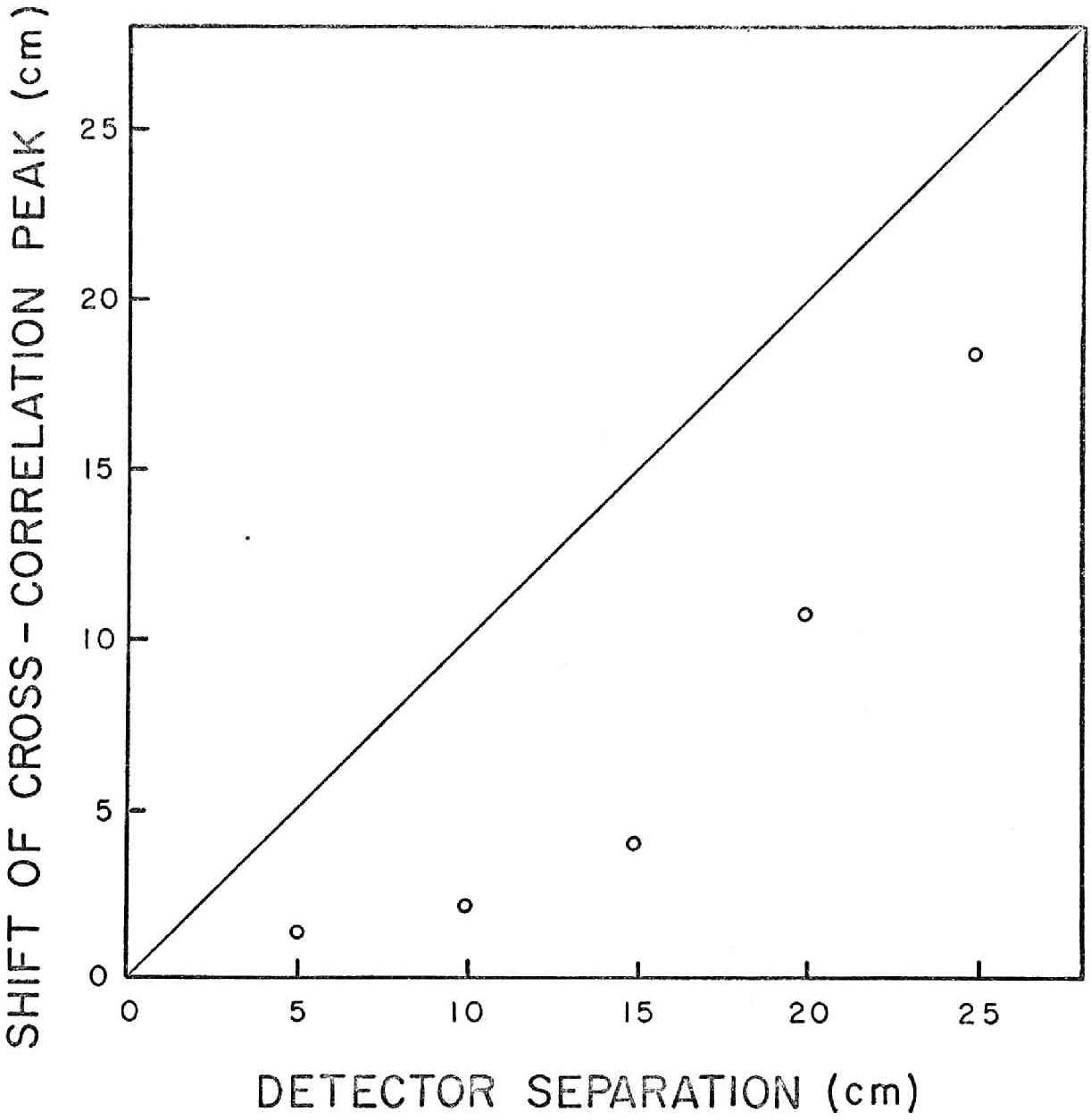

Fig. 27 Peak Locations of Cross-correlation Functions with Hydrophones Placed Diametrically Across the Tank at Level 0

Figure 28 shows the results obtained with hydrophone pairs at level 0, but placed at locations little affected by reflections. A good agreement is clearly shown in this figure.

Effects of Detector Levels

In the preceeding sections only the results of the measurements taken by hydrophone pairs located at level 0 and 10 were presented for the frequency passband of 5-10 kHz. Cross-correlation functions taken by detector arrays at level 20, however, were difficult to interpret (Figures 77 through 82 in Appendix II). Measurements and analysis were repeated, but the results were similar. One noticeable effect was the shift of the cross-correlation peak toward the wrong direction when one hydrophone was placed at position 0 and the other was moved to 1 and 2. The hydrophone placed at position 0 closer to the heater was receiving signals at a later time than the other placed at a farther distance from the heater.

Various attempts were made in order to explain this puzzling phenomenon. It was not possible to attribute it mainly to the effect of the reflections of the acoustic signal from the confining walls and the air-water boundary. One possibility was the smallness of the angle between the vertical heater pin surface and the signal path to the detector at position 0. Inhomogeneity of the water density and hence the variation of sound speed due to temperature gradient along the transmission path was suspected to have created this inability of triangulation. Also the angle between the transmission path and the vertical wall surface was small (approximately 23° at position 0, level 20), which may have produced some acoustic paths by bouncing

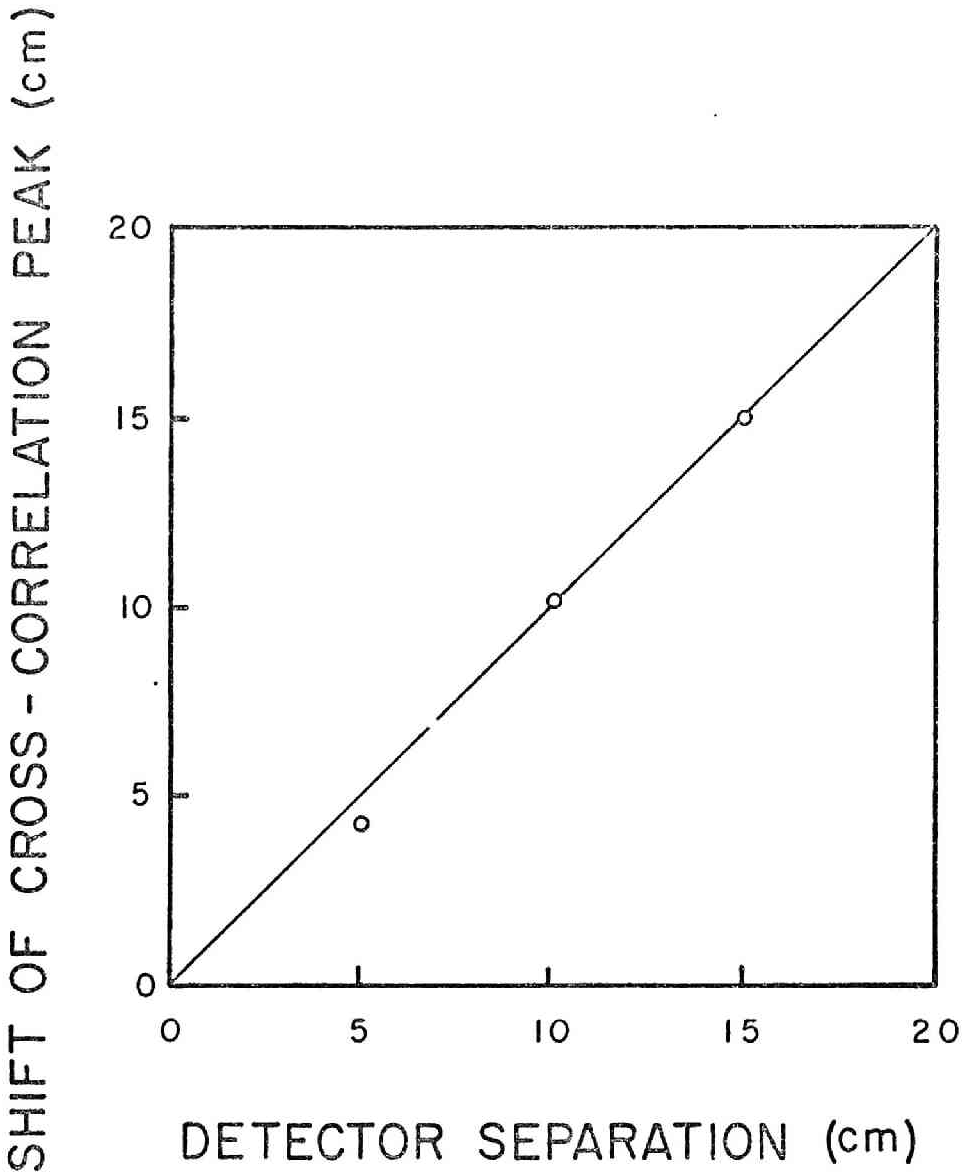

Fig. 28 Peak Locations of Cross-correlations Functions with the Fixed Hydrophone at Location 3 at Level 0

the wave pulses by the composite wall in some complex manner.

In order to circumvent the situation, measurements were taken with the fixed detector at position 3, and placing the other detector at 3, 2, 1, and 0. Figure 29 shows the result. The agreement between the measured and the expected peak locations is generally good but the discrepancy is apparent. The result did not change very much when the heat flux was increased to 1360 W, or 3.0×10^5 Btu/ft^2-hr ($=8.14 \times 10^5$ k cal/hr-m^2). At the higher heat flux the detected signals were quite large, but the increase in the signal level did not have any effect on the resulting cross-correlation functions.

In the next series of experiments hydrophones were placed in a vertical array at position 0, one being fixed at level 0 and the other at a progressively elevated level. Two sets of measurements were taken with this detector arrangement. One was taken in water at a temperature approximately 35°C, and the other has taken at a temperature near freezing. The low temperature was realized by adding a large amoung of finely crushed ice to the water. The latter case was intended to enhance the temperature gradient along the transmission path of the acoustic signals to the hydrophone placed at an elevated location.

Figure 30 shows the results. At the higher temperature the measured values tend to divert from the predicted values when the hydrophone displacement exceeded 15 cm. Cross-correlation functions at these detector locations indicated the existence of the persistent sine wave-like fluctuations which interfered with the coherent signal. Measurements in the cold medium resulted in a better agreement with the predicted values denying the adverse effect of temperature gradient.

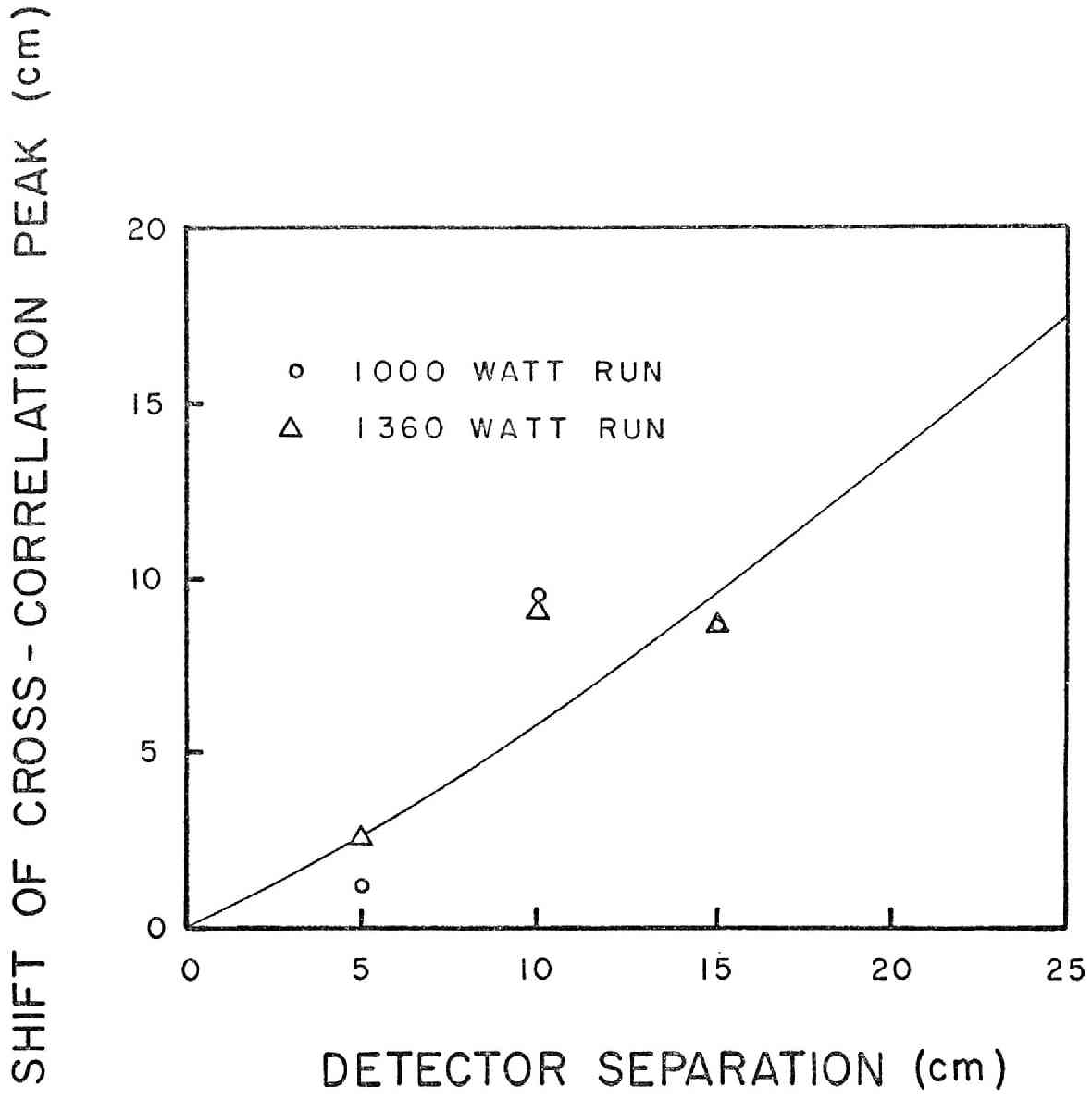

Fig. 29 Peak Locations of Cross-correlation Functions with the Fixed Hydrophone at Location 3 at Level 20

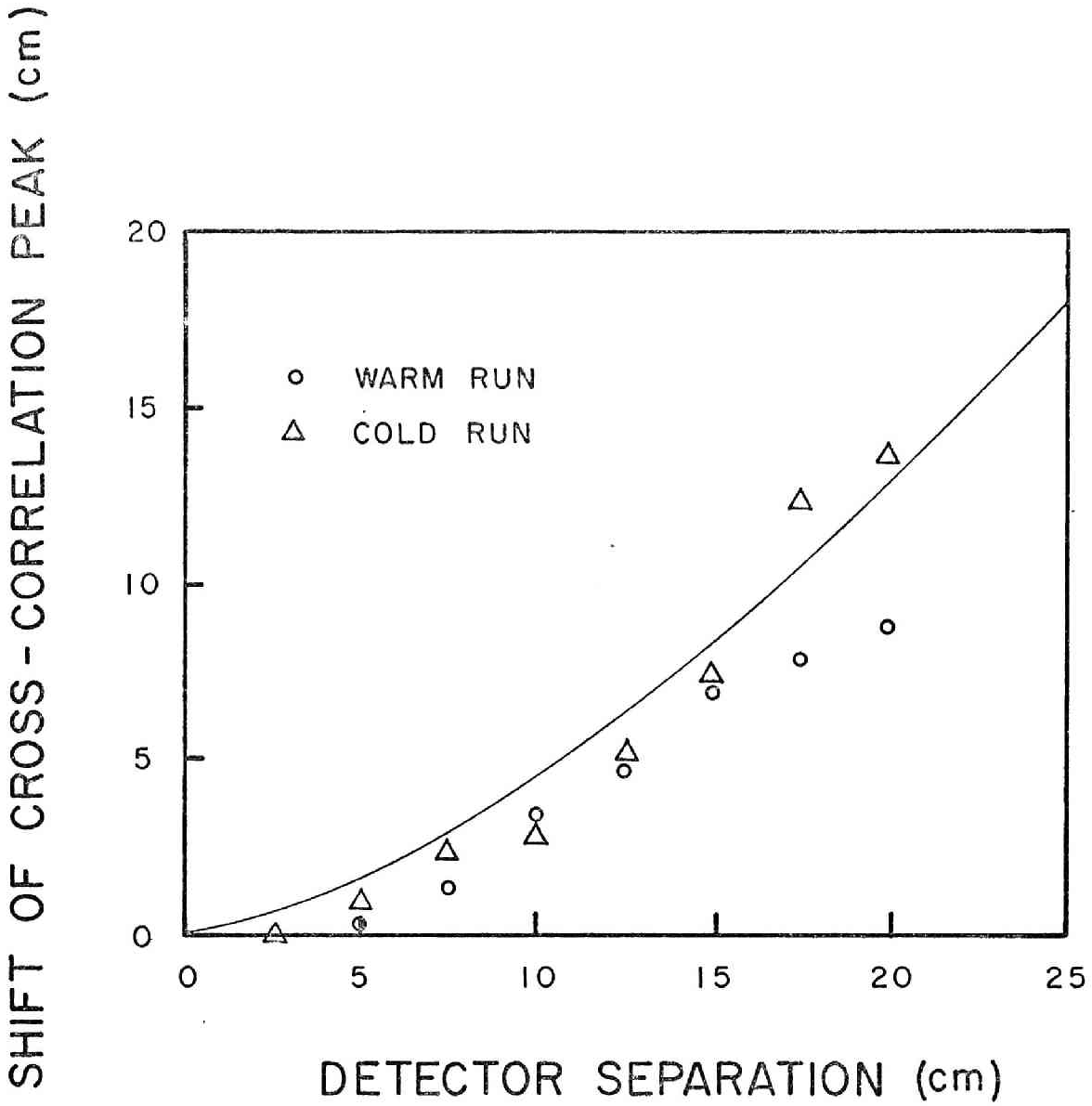

Fig. 30 Peak Locations of Cross-correlation Functions with Vertical Hydrophone Array at Location 0

In these measurements cross-correlation functions did not show oscillatory behavior as observed in some of the warm water experiments. Also the intensity of acoustic noise received by the two hydrophones was much larger in cold water runs than in warm water runs.

Experiments were repeated with horizontal array of detectors at level 20, but this time in cold water. Figure 31 shows this result. Initially the peak moved slightly to the wrong direction again showing the same tendency as before. Gradually the peak shifted toward the expected direction. The agreement is not very good, but the general trend was consistent with the expectation.

Several reasons for the improvement of the results in cold runs are postulated. Increased signal level may have been caused by more vigorous collapse of bubbles in more subcooled medium. The detector sensitivity may be dependent on the temperature. The latter assumption was discarded when the detectors alone were immersed in cold water contained in a thin plastic bag in the tank with the bulk water at higher temperature, but no noticeable change was observed on the detected signals. Also the data provided by the manufacturer showed little temperature effect on the sensitivity at this temperature. Even if the detectors were sensitive to temperature change, the change in the signal intensity should have no effect on the location of the cross-correlation peaks. Large subcooling may have changed the mode of bubble collapse and excited some resonance mode.

The puzzling phenomenan may be best explained by the existence of more bubbles in warmer medium along the signal transmission path. At an elevated detector location, especially when the angle between the transmission path and the heater rod is small, the acoustic signal must

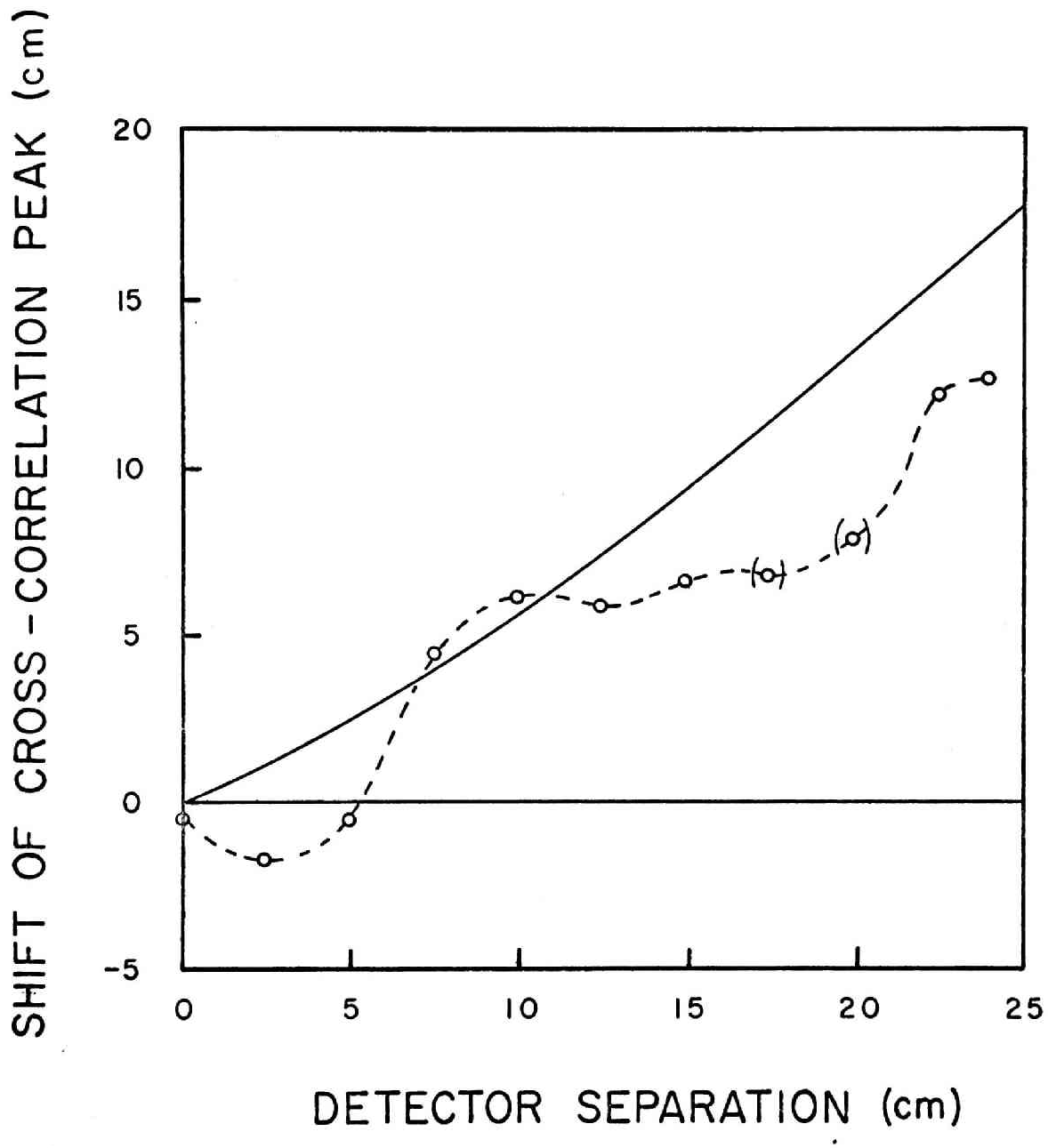

N.B. Data points in parentheses represent the shifts of the secondary peaks.

Fig. 31 Peak Locations of Cross-correlation Functions Measured in Cold Water at Level 20

travel in a path with more vapor bubbles delaying the arrival time and losing intensity. This reduces the amount of coherent acoustic signals reaching the hydrophone directly and results in the increase in the background noise comprising reflected waves. This also explains why the more closely located detector was receiving the signal at a later time in the warm water experiment. When the medium is highly subcooled, bubbles are collapsed near the heater surface and only small number of bubbles interfere with the signal transmission.

In order to prove this hypothesis, experiments were performed with reversed locations of the heater and the horizontal hydrophone array. The hydrophones were placed at the same horizontal level 20, but the heater element was moved to a higher level, corresponding to level 40, while maintaining the same radial location. In this arrangement the upper connector of the heater element was only 1 cm below the water level. The transmission path of the acoustic signal is now downward and the bubbles should have little effect on the acoustic transmission.

Figure 32 compares this result with that of the normal position. In this figure data points enclosed in parentheses are not the largest peaks in the respective cross-correlation functions. Some improvements are observed especially when the detector separations are small. With this geometric arrangement warm water layer is formed near the surface of the water during the measurement and the bubbles are seen spreading along the water surface. Further investigations are needed in a larger facility to prove this hypothesis conclusively.

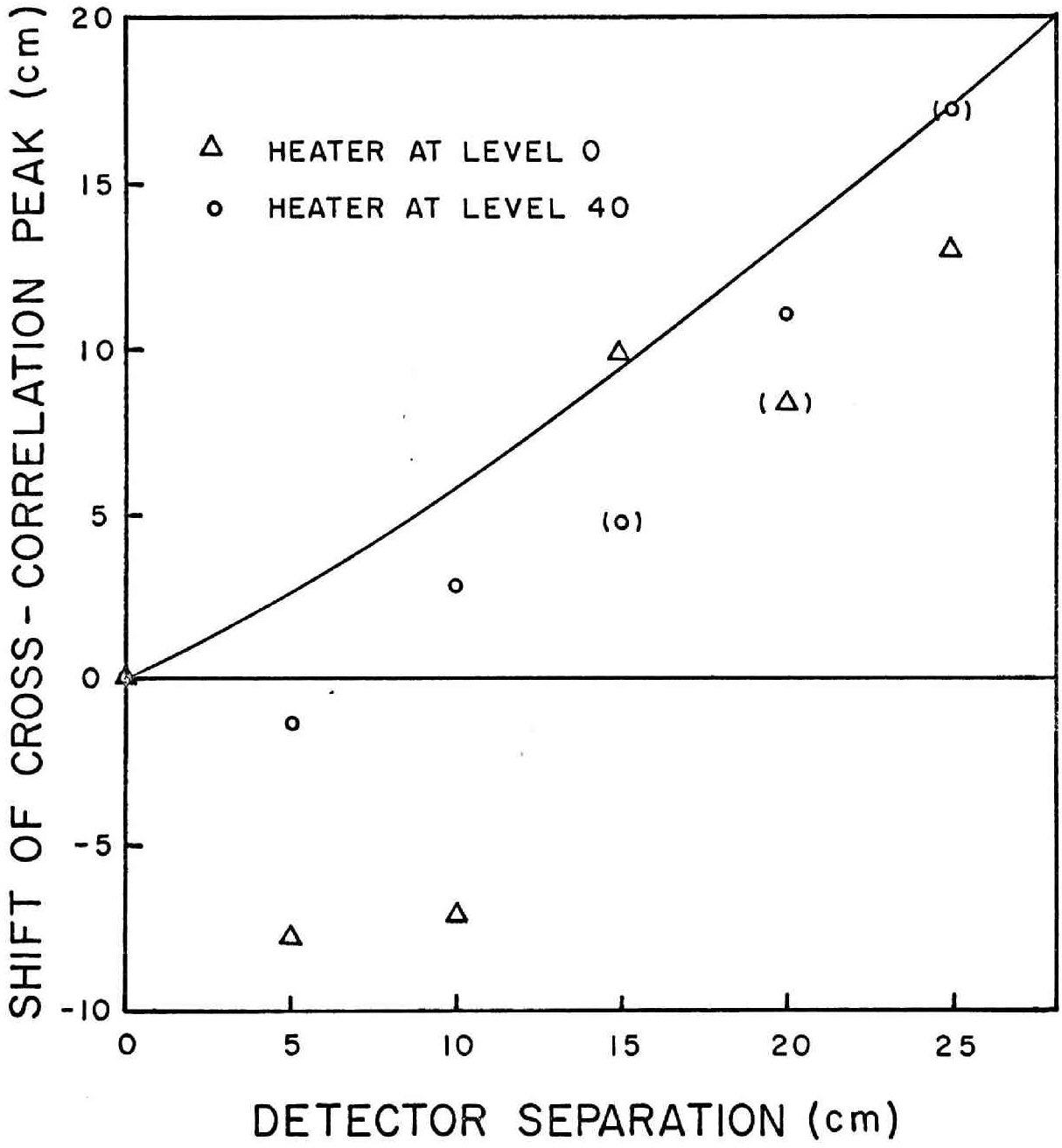

N.B. Data points in parentheses represent the shifts of the secondary peaks.

Fig. 32 Peak Locations of Cross-correlation Functions with Horizontal Hydrophone Array at Level 20

Effects of Rod Bundles

So far all the measurements were taken under the idealized condition of a single heater pin in the tank water. In reality boiling acoustic noise must travel through a heterogeneous medium composed of fuel rods and the liquid coolant. In order to verify the feasibility of the acoustic triangulation technique in heterogeneous media, it is desired to pursue the experiment in real reactor systems or in mock-up systems that are capable to simulate the transmission behavior of acoustic waves in reactors. Since these were not readily available, aluminum rod bundle was built into the water tank as described previously.

Figure 33 is a horizontal view of a 37-rod bundle with the heater pin placed in the center of the bundle. In the experiments with rod bundles it was not possible to place the heater pin at an arbitrary position, but it had to be placed at one of the rod locations determined by the lattice structure. With the arrangement of Figure 33, the closest hydrophone location was 10.0 cm apart from the heater pin, instead of 8.5 cm as was the case in the one-rod experiments (Figure 19). The other hydrophone was moved along the wall as in the previous experiments.

Peak locations of the cross-correlation functions measured by the horizontal array of hydrophones at level 0 in the heterogeneous medium of 37 rods are plotted in Figure 34. Agreement with the predicted values based on the speed of sound in pure water is evident. The heterogeneity due to the bundle of rods had no effect on the arrival time of acoustic noise signals. Apparently the acoustic waves traveled through the water medium in between the aluminum rods.

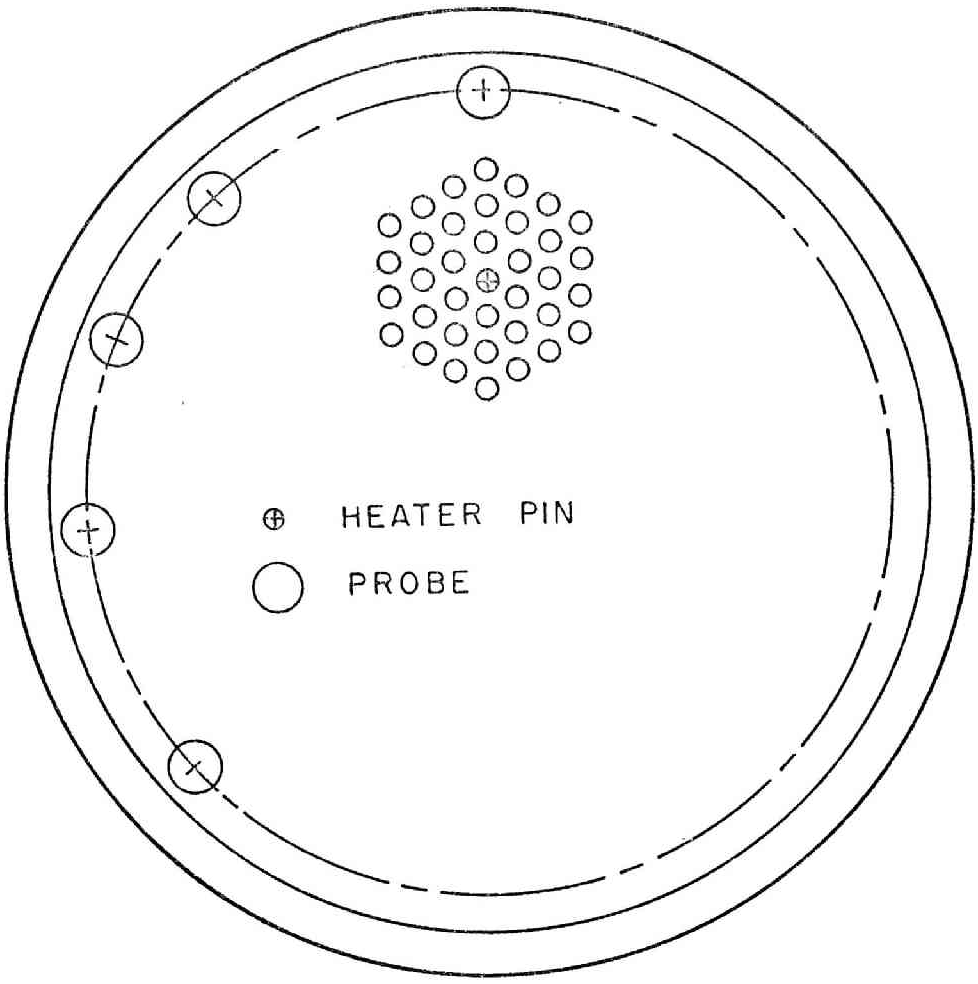

Fig. 33 Horizontal View of 37-Rod Bundle Arrangement

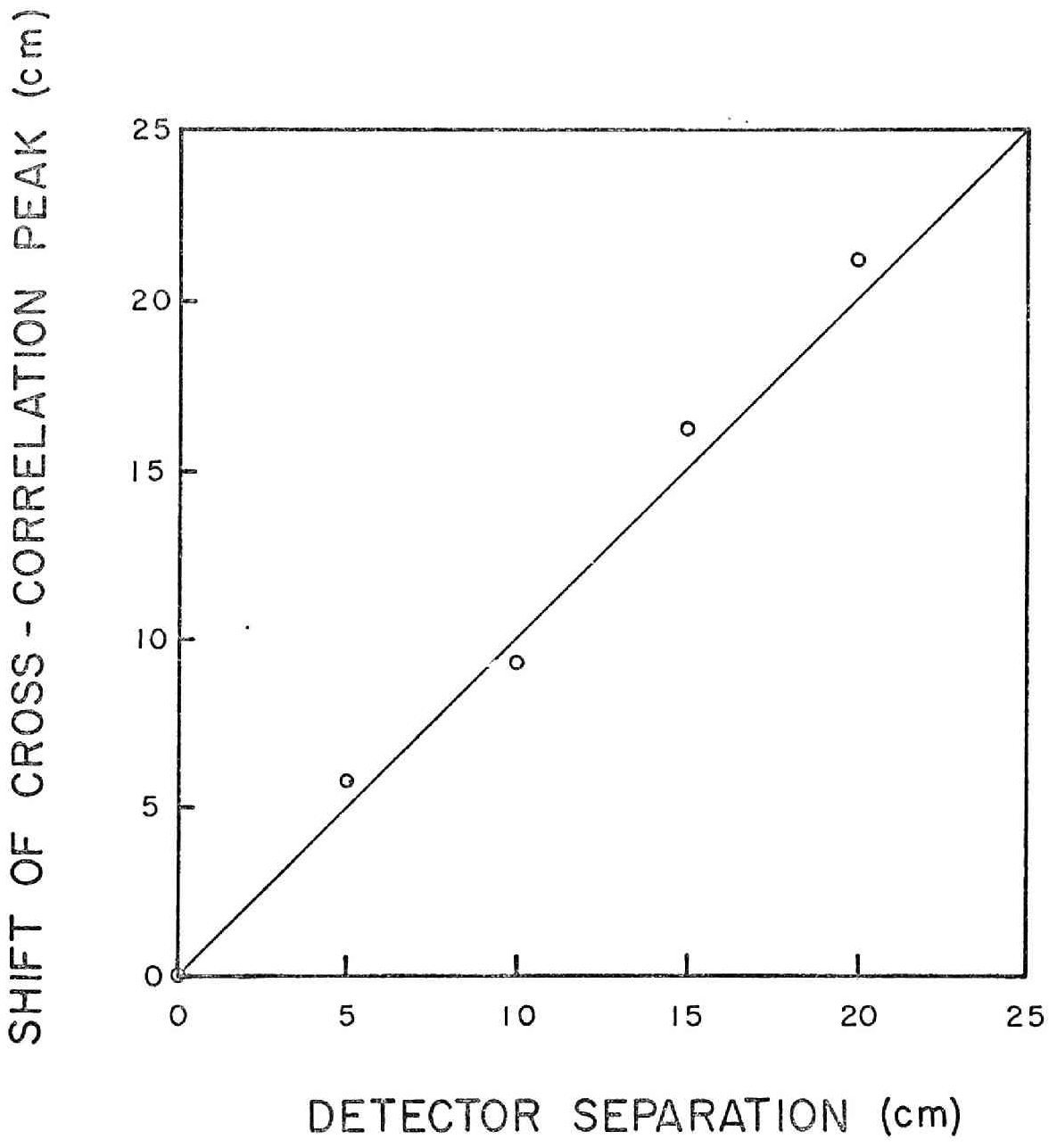

Fig. 34 Peak Locations of Cross-correlation Functions Measured with 37-Rod Bundle Arrangement by Horizontal Hydrophone Array at Level 0

When the number of rods was increased, the agreement between the measured and the predicted peak locations of the cross-correlation functions was again remarkable. Figure 35 shows the tank almost two thirds filled with aluminum rods. The remaining open space was reserved for wiring the heater power supply. Figure 36 shows the result in this rod bundle arrangement with horizontal hydrophone pairs again at level 0. Measurements with hydrophones at the elevated level of 20 were also taken with the rod bundle arrangement of Figure 33. Results were similar to the measurements with single rod arrangment previously described.

Effects of Computation Modes

Most of the cross-correlation functions reported in this chapter were calculated from 3810 to 6350 sample pairs (30 to 50 segments of 127 data pairs) and produced well defined correlation peaks. These numbers of the sample pairs correspond to the measuring time of approximately 30 to 50 msec (real time), which are relatively short durations of time.

After the advent of recent development in digital computation machinery, on-line processing of noise signals sampled at time intervals considerably shorter than the present sampling time is possible by using equipments commercially available on the market at costs not inaccessible for research and developmental purposes.

A simpler way of obtaining cross-correlation functions is to use a simplified computational mode of PCC. The calculation of PCC requires much simpler machinery compared with the calculation of regular cross-correlation functions. For this reason, the effect of the PCC computational mode for triangulation purposes was examined.

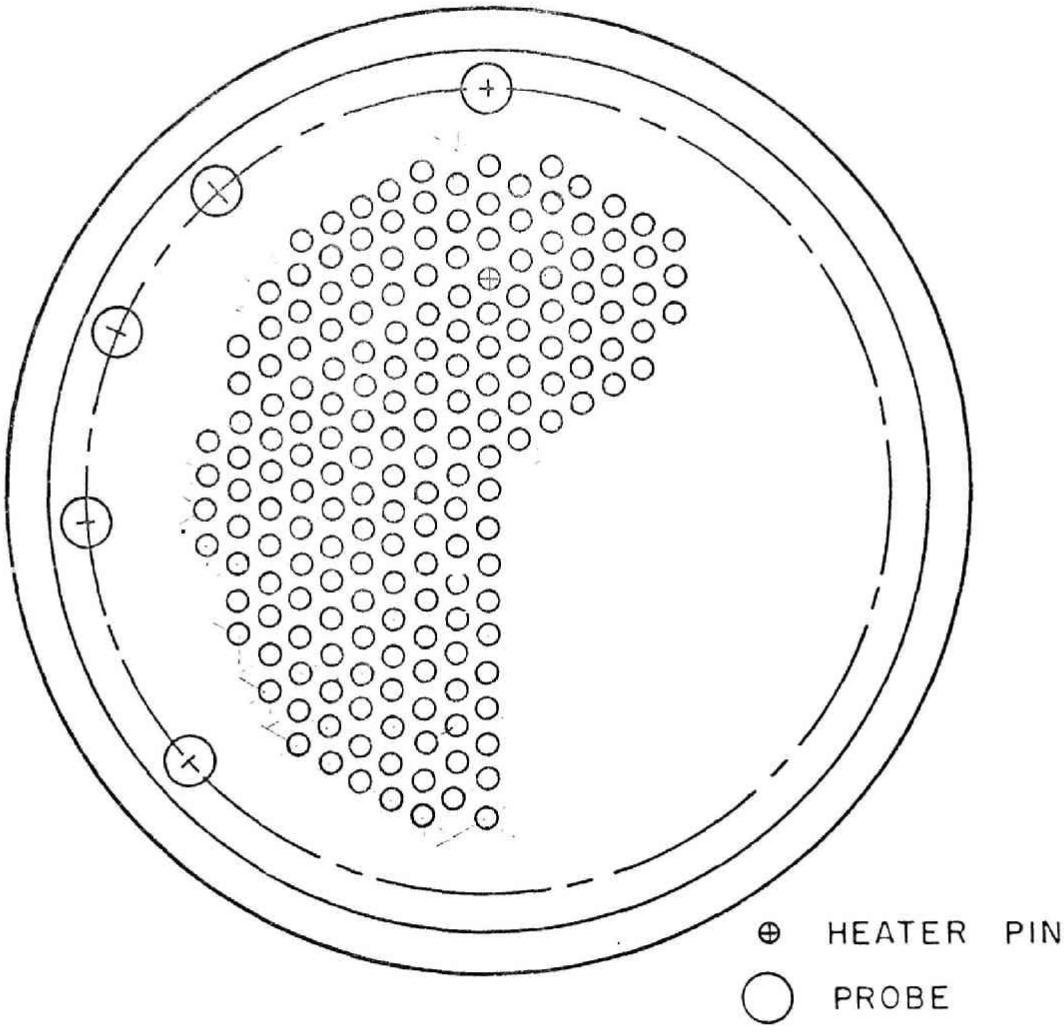

Fig. 35 Horizontal View of 184-Rod Bundle Arrangement

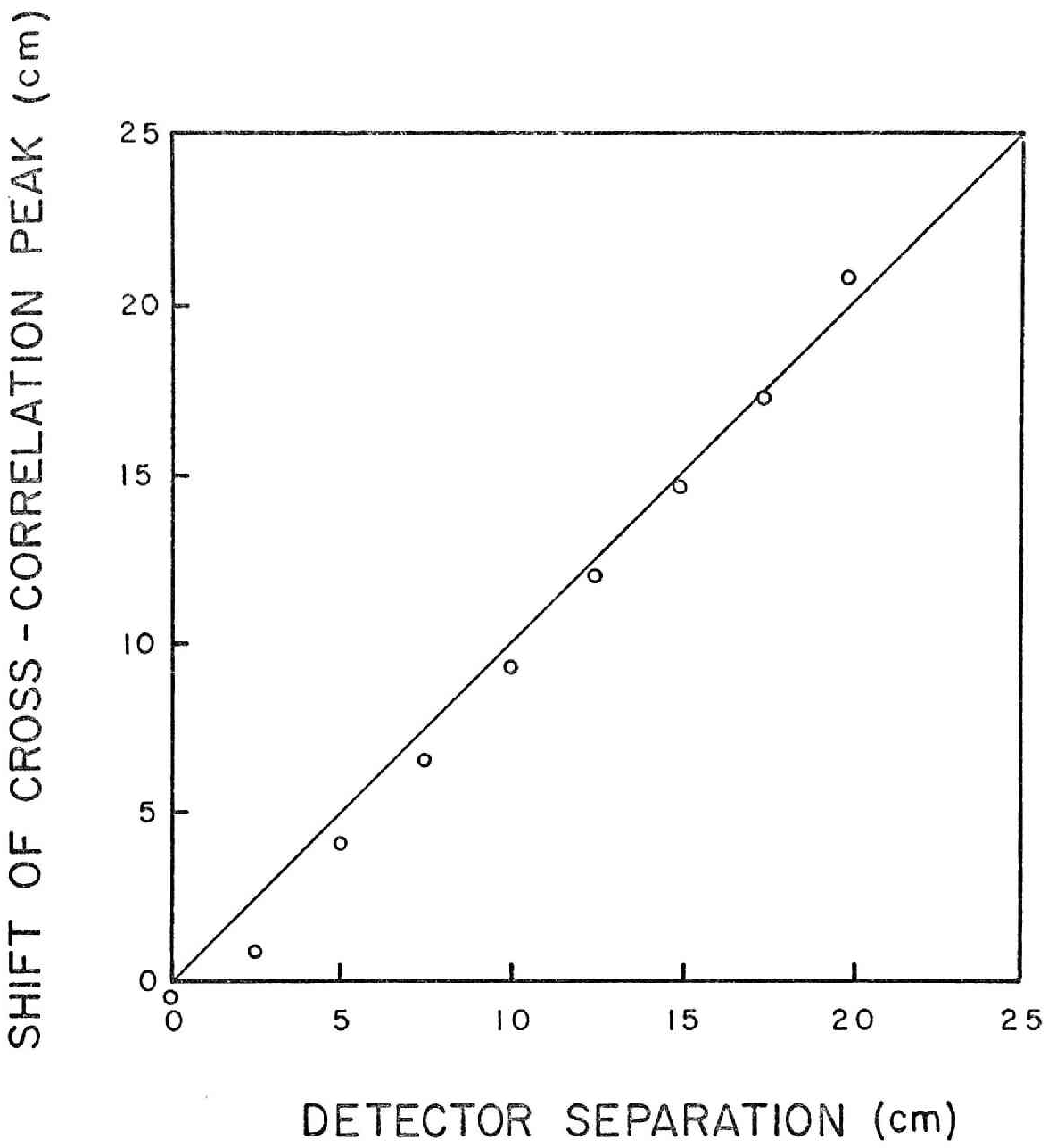

Fig. 36 Peak Locations of Cross-correlation Functions Measured with 184-Rod Bundle Arrangement by Horizontal Hydrophone Array at Level 0

Figure 37 compares the cross-correlation functions calculated by the ordinary and polarity coincidence computational modes. All the cross-correlation functions shown in the figure are based on 3810 sample pairs taken at level 10 by horizontal hydrophone array. Clearly at the detector location (0,4), both correlation functions agree well, giving well defined peaks at a lag time corresponding to the difference in distances from the heater to the hydrophone detectors (Figure 37(a)).

At the detector location (0,5), where the reflection effect is significant as previously discussed, results fail to agree (Figure 37(b)). The PCC was unable to produce a distinct peak, but produced a blunt, broad peak from which the assessment of a well defined difference in the distances was not possible. This exemplifies the weakness of the PCC mode when noise level is large. In the present case reflected waves are the superfluous noise.

In view of the poor performance of the PCC mode and the relatively easy accessibility of on-line real-time digital correlators, the use of ordinary cross-correlation mode is highly recommended for producing cross-correlation functions to be used for the detection of nucleate boiling sites by the triangulation technique.

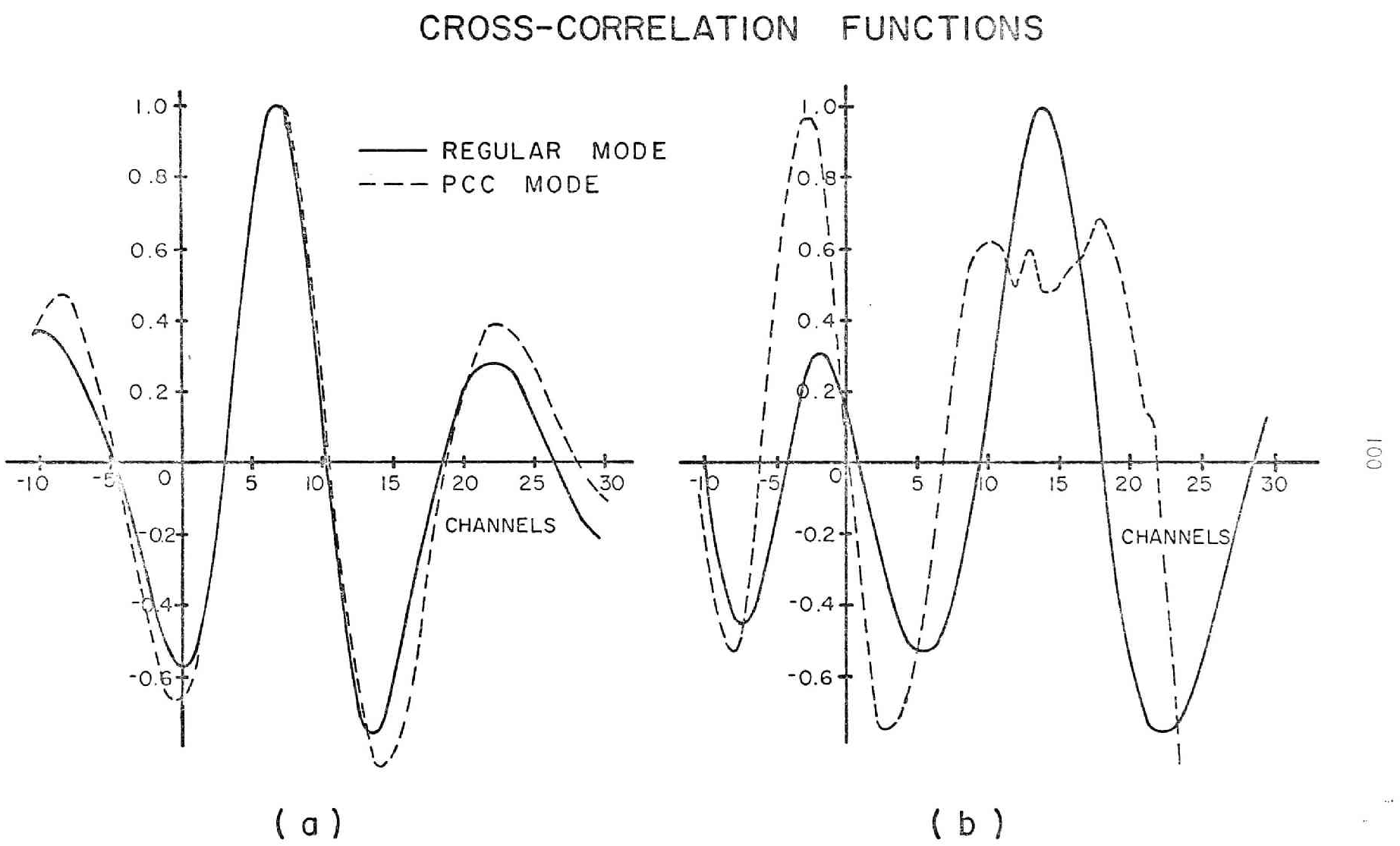

Fig. 37 Comparison of Cross-correlation Functions Computed by Regular and Polarity Coincidence Modes. (a) Hydrophone Array at Level 10, Position (0,4), (b) Hydrophone Array at Level 10, Location (0,5)

CHAPTER VII

CONCLUSIONS AND RECOMMENDATIONS

General Remarks

Characteristics of acoustic noise produced by nucleate boiling in water enclosed in a steel tank have been studied experimentally. The boiling was produced on a segment of zircalloy tube that was directly heated by applying low voltage, high current A. C. electric power. The boiling acoustic signals were detected by hydrophone(s) suspended in the tank water. They were analyzed in spectral densities and in cross-correlation functions. Spectral densities provided noise signatures of boiling acoustic fluctuations in the frequency range up to 50 kHz. By means of cross-correlation functions, triangulation of the boiling sites were performed.

The primary objective of the present investigation was to obtain fundamental information on the properties of boiling acoustic noise found in reactor-like systems with direct interest of applying the noise analysis technique to unambiguously detect and locate the boiling in such systems. This objective is of great significance from the viewpoint of reactor safety. Early detection of anomalous coolant boiling, especially in LMFBR's, is essential for the safe and economic production of energy. In the next section conclusions drawn from the present investigation are itemized.

Conclusions

1. Spectral peaks were found in low frequency range (below 5 kHz). These coincided with calculated resonance peaks of the system. Cross-correlation studies showed that the signals in this low frequency range were indeed due to the resonance of the fluid contained in finite geometry. This phenomenon was reported by many investigators, and there has been an assertion that the frequency peaks are at least partly due to the resonance of the containment vessel [39]. This was verified experimentally for the first time by the cross-correlation technique.
2. The use of boiling acoustic signals in the frequency range in which no appreciably large resonance peaks exist will lead to successful triangulation of the boiling site.
3. By triangulating boiling acoustic signals detected by a pair of hydrophones, the boiling noise was found to emanate from the vicinity of heat transfer surface where nucleation sites exist.
4. Reflection of acoustic signals in the container presents annoying problems in triangulating the boiling sites. In some cases large peaks in cross-correlation functions appear in ranges larger than the separation distance of

the two detectors. These superfluous peaks are easily identified and can be removed for triangulation purposes. In other instances the superfluous and the "coherent" peaks interfere, presenting a more difficult situation.

Existence of superfluous peaks may be considered as an indication of the departure of the detector location with respect to the boiling site.

5. The singal duration time of the acoustic noise needed to locate the boiling sites was quite small. In the present investigation signal duration time of 20 to 50 m sec was sufficient to successfully identify the boiling site by the triangulation method. This time is much shorter than the anticipated reactor-trip delay time (from generation of the reactor trip signal until insertion of negative reactivity starts) of 0.25 sec [1]. The triangulation of the boiling site may be performed on-line during this period. Or it may be performed by post-incidence analysis if the signals are recorded.
6. Triangulation of boiling sites was little affected by the presence of metallic (aluminum) rods in water. The speed of sound did not seem to change very much, and no significant reflections from the rods were found.
7. Compared with regular cross-correlation method, the PCC method is inferior in producing well-defined cross-correlation peaks in a short duration of time. This is especially

so when the level of noise signals (reflected signals in the present case) in large.

8. It is expected that the use of 10 to 20 hydrophones surrounding the reactor core will successfully triangulate the boiling location in the core, or at least a region of the core in which the boiling took place, if not pinpoint the exact coolant channel.

Recommendations

It is felt that the following items need to be studied in future in order to establish the technique of detecting anomalous coolant boiling in power reactors.

1. Mode of bubble collapse is dependent on the sub-cooling of the liquid. Effect of temperature distribution of the coolant on the triangulation method needs further investigation. Use of taller facility than the present boiling water tank is required.

2. Reduction of the strength and the speed of acoustic signals through two-phase media needs to be studied. Void distribution patterns in various modes of coolant channel blockage need to be considered carefully in order to obtain information regarding the location of the boiling sites.

3. In the present triangulation studies only a limited frequency passband beyond the resonance range was used due to the instrumentation capability. This should be extended to

higher frequency range, since only in the high frequency range the acoustic boiling noise could be separated from the background noises.

4. Transmission characteristics of boiling acoustic noise through more realistic heterogeneous media should be studied. UO_2 rods, instead of presently used aluminum rods, need to be used. It is proposed that the use will be made of the University of Florida SPERT Assembly (UFSA) for this purpose.

5. Triangulation technique needs to be pursued in systems with coolant flow. Capability of blocking part of the coolant channel is a highly desirable feature of the experimental set-up. Systems similar to Failed Fuel Mockup (FFM) loop at the Oak Ridge National Laboratory [87] should provide an excellent facility.

6. Instrumentation and data processing for the triangulation purposes must be investigated together with the characteristics of boiling acoustic noise. Method of statistical testing used in the field of pattern recognition must be incorporated to identify the anomaly.

7. Along with the item 6, other traiangulation technique besides the use of cross-correlation functions of the noise signals detected by two sensors may be found more useful. In particular, when strong reflections are present, use of multi-sensor correlation method should be pursued.

REFERENCES

1. J.B. van Erp, D.R. MacFarlane and H.K. Fauske, "Protection against Local Core Accidents in Liquid Metal Fast Breeder Reactors," Nuclear Engineering and Design, 15 (4), 441-457 (1971).

2. J.A. Thie, "Reactor Noise," Rowman and Littlefield, Inc., New York, N.Y. (1963).

3. R.E. Uhrig, "Random Noise Techniques in Nuclear Reactor Systems," The Ronald Press Company, New York, N.Y. (1970).

4. T.J. Marciniak, L.J. Habegger and H. Greenspan, "Summary Review of Neutronic Noise Techniques for Incipient Boiling Detection in Liquid Metal Fast Breeder Reactors," ANL-7652 (1970).

5. L.R. Boyd, "Ion Chamber Can Detect Nucleate Boiling," Nucleonics, 17 (3), 96 (1959).

6. A.L. Colomb and F.T. Binford, "The Detection of Boiling in a Water-cooled Reactor," ORNL-TM-274 (1962).

7. T.M. Sims and W.H. Tabor, "Report on Fuel-Plate Melting at the Oak Ridge Research Reactor, July 1, 1963," ORNL-TM-627 (1964).

8. W.H. Tabor and S.S. Hurt, III, "Oak Ridge Research Reactor Quarterly Report, April, May, and June of 1965," ORNL-TM-1290 (1965).

9. D.N. Fry, D.P. Roux, C.W. Ricker, S.E. Stephenson, S.H. Hanauer and J.R. Trinko, "Neutron-fluctuation Measurements at Oak Ridge National Laboratory," Neutron Noise, Waves and Pulse Propagation, AEC Symposium Series No. 9, 463-474 (1967).

10. M.A. Schultz, discussion to reference 9, p. 474.

11. E.L. Jordan,"Detection of in-Core Void Formation by Noise Analysis," Trans. Amer. Nucl. Soc., 9(1), 317 (1966).

12. R.F. Saxe, W.H. Sides, Jr. and R.G. Foster, Jr., "The Detection of Boiling in Nuclear Reactors," J. Nucl. Energy, 25, 139-153 (1971).

13. G. Zwingelstein, "Determination of Local Boiling in Light Water Reactors by Correlation of the Neutron Noise," CEA-R-3686 (1968).

14. V. Rajagopal, "Reactor-Noise Measurements on Saxton Reactor, "Noise Analysis in Nuclear Systems, AEC Symposium Series No. 4, 427-448 (1964).

15. V. Rajagopal and J.M. Gallagher, "Some Applications of Dynamic (Noise) Measurements in Pressurized Water Reactor Plants," Neutron Noise, Waves and Pulse Propagation, AEC Symposium Series No. 9, 487-501 (1967).

16. V. Rajagopal, "Dynamic Measurements in PWR Power Plants," Trans. Amer. Nucl. Soc., 10(1), 217(1967).

17. M. Izumi, et al. "Investigations on the Reactor Anomaly Diagnosis--Anomaly Detection by Reactor Noise Analysis," Pre-print, 1972 Annual Meeting of At. Energy Soc. Japan, D-20, 139 (1972).

18. J.C. Robinson and D.N. Fry, "Experimental Neutron Flux-to-Pressure Frequency Response for the Molten-Salt Reactor Experiment: Determination of Void Fraction in Fuel Salt," Nucl. Sci. and Eng., 42(3), 397-405 (1970).

19. D.N. Fry, R.C. Kryter and J.C. Robinson, "Investigation of Boiling Detection in the HFIR Using Out-of-Core Instrumentation," IEEE Trans., Nuclear Science, 18(1) 345-350(1971).

20. R.W. Albrecht, "The Use of Signal Coherence for Anomaly Detection in Nuclear Reactors," Nuclear Technology, 14, 208-217 (1972).

21. R.W. Albrecht, "The Detection of Small Voids in Nuclear Reactors by Coherence Methods," Trans. Am. Nucl. Soc., 15 (2), 924-925 (1972).

22. T. Nomura, S. Gotoh, and K. Yamaki, "Reactivity Measurements by the Two-detector Cross-correlation Method and Supercritical-reactor Noise Analysis," Neutron Noise, Waves and Pulse Propagation, AEC Symposium Series, No. 9, 217-246 (1967).

23. W. Seifritz, D. Stegemann, and W. Väth, "Two-detector Cross-correlation Experiments in the Fast-Thermal Argonaut Reactor (STARK)," Neutron Noise, Waves and Pulse Propagation, AEC Symposium series, No. 9, 195-216 (1967).

24. M.J. Dunn and M.J. Ohanian, "Boiling Detection in the 20 to 50 Kilohertz Frequency Range," Paper presented at the IAEA Symposium on Nuclear Power Plants Control and Instrumentation, Prague, 22-26, January 1973, IAEA/SM-168/E6, 1973.

25. J.M. Hogan and L.R. Boyd, "Joint Bettis-KAPL Nucleate Boiling Experiment," WAPD-168 (1957).

26. L.R. Boyd and R.L. Cummerow, "Sound Produced by Nucleate Boiling," KAPL-M-LRB-1 (1955).

27. R.F. Saxe, "Acoustic Characteristics of the Oak Ridge Research Reactor," Neutron Noise, Waves and Pulse Propagation, AEC Symposium Series No. 9, 475-485 (1967).

28. R.F. Saxe, "The Detection of Boiling in Nuclear Reactors," IEEE Trans., Nuclear Science, 18(1) 337-339 (1971).

29. T.T. Anderson and F.H. Just, "Acoustic Boiling Detection in Fast Breeder Reactors," paper presented at the ASM Materials Engineering Congress, Philadelphia, Pa., October 13-16, 1969.

30. L.C. James, "Experiments on Noise as an Aid to Reactor and Plant Operation," Nuclear Engineering, 10(104), 18-22 (1965).

31. F.R. Farmer, "Safety Assessment of Fast Sodium-Cooled Reactors in the United Kingdom," Nuclear Safety, 11(4), 283-288.

32. C.D. Swanson, "European Liquid Metal Cooled Breeder Reactor Instrumentation--A Trip Summary," HEDL-SA-170 (1971).

33. C.F. DePrisco, H. Kartluke, N. Maropis and W.B. Tarpley, "Ultrasonic Detection of Incipient Boiling and Cavitation," NYO-10010 (1962).

34. C.A. Mossman, "Incipient Boiling Detector," Nuclear Safety, 5(4) 372 (1964).

35. H. Kartluke, R.P. Wichner and H.W. Hoffman, "An Acoustic Instrument for Measuring Subcooling in Boiling Systems," ORNL-P-1678 (1965).

36. Aeroprojects, Inc., "Applications of Ultrasonic Energy: Ultrasonic Instrumentation for Nuclear Applications," NYO-3622-1 (1966), also see other bimonthly reports, NYO-3622-5, -6, and -7.

37. J.A. Bonnet, Jr. and R.K. Osborn, "On the Use of Acoustic Waves in Nuclear Power Reactors to Determine Average Void Fractions," Nucl. Sci. Eng., 43(1), 1(1971).

38. J.A. Bonnet, Jr. and R.K. Osborn, "Incipient Boiling Detection in Sodium-cooled Fast Reactors," Trans. Am. Nucl. Soc., 14(1), 309-310 (1971).

39. T.T. Anderson, T.P. Mulcahey, and C. Hsu, "Survey and Status Report on Application of Acoustic-Boiling-Detection Techniques to Liquid-Metal-Cooled Reactors," ANL-7469,(1970).

40. Lord Rayleigh, "On the Pressure Developed in a Liquid During the Collapse of a Spherical Cavity," Philosophical Magazine, 34, 94-98 (1917).

41. M.F.M. Osborne, "The Shock Produced by a Collapsing Cavity in Water," Trans. Am. Soc. Mech. Eng., 69(3), 253-266 (1947).

42. M.S. Plesset, "The Dynamics of Cavitation Bubbles," J. of Appl. Mech., 16(3), 277-282 (1949).

43. R.T. Knapp and A. Hollander, "Laboratory Investigations of the Mechanism of Cavitation," Trans. Am. Soc. Mech. Eng., 70, 419-435 (1948).

44. L.W. Florschuetz and B.T. Chao, "On the Mechanics of Vapor Bubble Collapse," Trans. Am. Soc. Mech. Eng., J. Heat Transfer, 87, 209 (1965).

45. H.K. Forster and N. Zuber,"Growth of a Vapor Bubble in a Superheated Liquid," J. Appl. Phys., 25(4), 474-478 (1954).

46. M.S. Plesset and S.A. Zwick, "The Growth of Vapor Bubbles in Superheated Liquids," J. Appl. Phys., 25(4), 493-500 (1954).

47. P. Dergarabedian, Paper No. 53-SA-10, Heat Transfer and Fluid Mech. Inst., June 1953.

48. M. Minnaert, "On Musical Air-Bubbles and the Sounds of Running Water," Phil. Mag. XVI, Ser. 7, 235-248 (1933).

49. J. Bree, "Theoretical Investigation into the Generation of Acoustic Noise by Nucleate Boiling," TRG Report 549 (1963).

50. M. Strasberg, "Gas Bubbles as Sources of Sound in Liquids," J. Acoust. Soc. Amer., 28 (1) 20-26 (1956).

51. V.I. Il'ichev and V.P. Lesonvskii, "On the Noise Spectra Associated with Hydrodynamic Cavitation," Sov. Phys. Acoustics 9, 25 (1963).

52. L.D. Meier, "Acoustical Investigation on Nucleate Boiling," Master's Thesis, University of Arizona, (1970).

53. R.R. Matthews and K.J. Henry, "Location and Repair of the DFR Leak," Nuclear Engineering, 13, 840-844 (1968).

54. Rural Cooperation Power Association, "Elk River Reactor Monthly Operating Report, No. 73, November 1968," COO-651-68 (1968).

55. R.J. Cash, L.R. Sweetin, "Locating Failed Fuel Subassemblies by Ultrasonic Triangulation of Released Fission Gas," Trans. Am. Nucl. Soc., 14(1), 305-306 (1971).

56. R.G. Liptai, et al., "Acoustic Emission," ASTM Special Technical Publication 505, American Society for Testing and Materials (1972).

57. R.E. Uhrig, "State of the Art of Noise Analysis in Water Reactors," Paper presented at the National Topical Meeting, Water Reactor Safety, March 26-28, 1973.

58. E.R. Reinhart and W.D. Jolly, "The EEI-TVA Acoustic Emission Program Results," Paper presented at the National Topical Meeting, Water Reactor Safety, March 26-28, 1973.

59. R. Gopal and C.J. Ross, "Acoustic Emission Monitoring Systems for Primary System Surveillance," paper presented at the National Topical Meeting, Water Reactor Safety, March 26-28, 1973.

60. N.O. Cross, L.L. Loushin and J.L. Thompson, "Acoustic Emission Testing of Pressure Vessels for Petroleum Refineries and Chemical Plants," Acoustic Emission, ASTM STP 505, Amer. Soc. for Testing Materials, 270-296 (1972).

61. V.M. Albers, ed., "Underwater Sound," Dowden, Hutchinson and Ross, Inc., Stroudsburg, Pennsylvania, (1972).

62. D.A. Gilbrech and R.C. Binder, "Portable Instrument for Locating Noise Sources in Mechanical Equipment," J. Acoust. Soc. Am, 30 (9), 842-846 (1958).

63. J.A. Thie, "Reactor-Noise Monitoring for Malfunctions," Reactor Technology, 14(4), 354-365 (Winter 1971-1972).

64. L.M. Jiji and J.A. Clark, "Bubble Boundary Layer and Temperature Profiles for Forced Convection Boiling in Channel Flow," J. Heat Transfer, 86, 50-58 (1964).

65. R.L. Ashley, et al., "SRE Fuel Element Damage, Final Report," NAA-SR-4488 (suppl) (1961).

66. P.G. Bentley, "The Sensitivity of Blockage Detection in P.F.R. by Coolant Temperature Monitoring," TRG Report 1156(R) (1966).

67. I. Tsunoda et al., "Development of Reactor Diagnostic Technology(3)," Pre-print, 1972 Fall Meeting Reactor Phys. & Engng., D-37, At. Energy Soc. Japan (1972).

68. W. Seifritz, "Special Thermocouple for Temperature Measurements in Liquid Metal Media," Atomkernenergie, 17(1), 72(1971).

69. Hideaki Nishihara, O. Takahashi and N. Shirafuji, "Gamma Heating Effect on Thermocouples Used for Temperature Fluctuation Measurement in Two-Phase Flow," Atomkernenergie, 20(2), 159 (1972).

70. M.J. Dunn, "Boiling Detection in the 20-50 Kilohertz Range," Master's Thesis, University of Florida (1972).

71. P.M. Morse, "Vibration and Sound," 2nd ed., McGraw-Hill Book Company, Inc., New York, N.Y., (1948).

72. R.L. Randall, "Transit Time Flowmeter Employing Noise Analysis Techniques, Part I. Water Loop Test," AI-AEC-12802, Instruments (1969).

73. J.S. Bendat, "Principles and Applications of Random Noise Theory," John Wiley & Sons, Inc., New York, N.Y., (1958).

74. Y.W. Lee, "Statistical Theory of Communication," John Wiley & Sons, Inc., New York, N.Y. (1960).

75. J.S. Bendat and A.G. Piersol, "Measurement and Analysis of Random Data," John Wiley & Sons, Inc., New York, N.Y. (1966).

76. H. Ekre, "Polarity Coincidence Correlation Detection of a Weak Noise Source," IEEE Trans. Info. Theory, IT-9, 18(1963).

77. P.M. Schultheiss and F.B. Tuteur, "Optimum and Suboptimum Detection of Directional Gaussian Signals in an Isotropic Gaussian Noise Field, Part II: Degradation of Detectability Due to Clipping," IEEE Trans. Military Electronics, MIL-9, 208(1965).

78. M. Kanefsky, "Detection of Weak Signals with Polarity Coincidence Arrays," IEEE Trans. Info. Theory, IT-12, 260 (1966).

79. M.C. Cheng, "The Clipping Loss in Correlation Detectors for Arbitrary Input Signal-to-Noise Ratios," IEEE Trans. Info. Theory, IT-14, 382 (1968).

80. J.B. Thomas and T.R. Williams, "On the Detection of Signals in Nonstationary Noise by Product Arrays," J. Acous. Soc. Amer., 31, 453(1959).

81. S.S. Wolff, J.B. Thomas, and T.R. Williams, "The Polarity-Coincidence Correlator: A Nonparametric Detection Device," IEEE Trans. Info. Theory, IT-8, 5(1962).

82. S.S. Wolff and J.L. Gastworth, "Robust Two-Input Correlators," J. Acous. Soc. Amer., 41, 1212(1967).

83. International Business Machine Corporation, "1130 Scientific Subroutine Package (1130-CM-02X), Programmer's Manual," International Business Machine Corporation, White Plains, N.Y. (1968).

84. V.A. Del Grosso and C.W. Mader, "Speed of Sound in Pure Water," J. Acoust. Soc. Amer. 52(5, Part 2), 1442-1446 (1972).

85. F.G. Friedlander, "Sound Pulses," Cambridge University Press (1958).

86. J.B. Keller and H.B. Keller, "Determinations of Reflected and Transmitted Fields by Geometrical Optics," J. Opt. Soc. Amer., 40, 48-52(1950).

87. A. G. Grindell, R. E. MacPherson, "Final System Design of the Failed Fuel Mockup (FFM) of the Liquid-Metal Fast Breeder Reactor," ORNL-TM-3656 (1972).

APPENDIX I

COMPUTER PROGRAMS FOR PROCESSING CROSS-CORRELATION FUNCTIONS

Computer programs written for processing cross-correlation functions on the IBM-1800/AD-80 hybrid computer are listed in this appendix. They contain the main program, subprogram CROSS for computing cross-correlation functions, subprogram FIGR for plotting cross-correlation functions, and subprogram NOISE for plotting the original traces of the data.

```
*IOCS(CARD,TYPEWRITER,PLOTTER,DISK)
* NONPROCESS PROGRAM
* ONE WORD INTEGERS
C
C       THIS PROGRAM READS IN M SETS OF 2*N DATA POINTS (N/CHANNEL
C       *2 CHANNELS) THOUGH A-D CONVERTER AND STORES THEM IN
C       DISK.  THEY ARE CROSS-CORRELATED SET BY SET, AND AVERAGED
C       BEFORE PLOTTED.
C
C           A = STORAGE LOCATIONS OF CHANNEL A DATA (FED THROUGH
C               EVEN-NUMBERED TERMINATIONS OF THE AD-80 PATCH
C               BOARD).
C           B = STORAGE LOCATIONS OF CHANNEL B DATA (FED THROUGH
C               ODD-NUMBERED TERMINATIONS OF THE AD-80 PATCH
C               BOARD).
C           DATA = STORAGE LOCATIONS OF CHANNEL A AND CHANNEL
C               B DATA.
C           L = NUMBER OF LAGS (.LE.30)
C           M = NUMBER OF DATA SETS (.LE. 100)
C           N = NUMBER OF DATA POINTS/CHANNEL/SET (.LE. 127)
C                 ****************************************
C           IPLOT =-1     PLOT RAW DATA.
C                  0,1    DO NOT PLOT RAW DATA.
C                  1      PLOT CORR FUN ON PREVIOUS.FIGURE.
C           IPOL   = 0     CALCULATE REGULAR CORRELATION FUNCTION.
C                  1      CALCULATE POLARITY CORRELATION.
C           IRUN   = 0     NO RUN (NO MORE DATA).
C                  1      CORR FIGURE NORMALIZED TO THIS RUN.
C                  2      CORR FIGURE NORMALIZED NOT TO THIS RUN.
C                 ****************************************
C
      INTEGER A(127),B(127),DATA(254)
      DIMENSION R(30),S(30),RR(30),SS(30),FF(2)
      COMMON A,B,FF,IMAX,JMAX,L,N,R,S,IPOL,IPLOT,AVERA,AVERB
      DEFINE FILE 5(100,254,U,NXX)
C
C      CALL PLOT CHECKS THE PLOTTER PEN POSITION.
C
      CALL FPLOT (2,0.,0.)
C
   18 FORMAT(6I4)
  100 READ (2,18) IRUN,L,M,N,IPLOT,IPOL
      IF (IRUN) 99,99,101
  101 CONTINUE
      N2=N*2
      FM=M
C
C      CALL OPER SWITCHES THE ANALOG COMPUTER TO OPER POSITION.
C      AMPLITUDE OF THE ANALOG SIGNALS SHOULD BE .LT. 100 VOLTS.
C
      CALL OPER
C
      PAUSE 001
C
```

```
      DO 1 INDEX = 1, M
      CALL ANLQK (DATA,N2)
    1 WRITE (5'INDEX) DATA
      DO 32 I=1,L
      RR(I)=0.
   32 SS(I)=0.
C
      DO 22 INDEX = 1, M
      READ (5'INDEX) DATA
      DO 2 I = 1, N
      J = N2 - 2*I + 1
      B(I)=DATA(J)
    2 A(I)=DATA(J+1)
C
      CALL CROSS
      DO 3 I=1,L
      RR(I)=RR(I)+R(I)
    3 SS(I)=SS(I)+S(I)
22 CONTINUE
C
      DO 42 I=1,L
      R(I)=RR(I)/FM
   42 S(I)=SS(I)/FM
      RMAX=R(1)
      DO 201 I=1,L
      IF (RMAX-R(I)) 200,200,201
  200 RMAX=R(I)
      IMAX=I
  201 CONTINUE
      SMAX=S(1)
      DO 301 I=1,L
      IF (SMAX-S(I)) 300,300,301
  300 SMAX=S(I)
      JMAX=I
  301 CONTINUE
      FACTR=RMAX
      IF (RMAX-SMAX) 400,401,401
  400 FACTR=SMAX
  401 CONTINUE
      WRITE (1,16) IMAX,JMAX,FACTR
   16 FORMAT (1H //6HIMAX =,I3,8H, JMAX =,I3,9H, FACTR =,F12.4)
      FF(IRUN)=FACTR
      CALL FIGR
      IF (IPLOT) 95,96,96
   95 CALL NOISE
   96 GO TO 100
   99 CALL LOGFF
      CALL EXIT
      END
```

```
*ONE WORD INTEGERS
      SUBROUTINE CROSS
      INTEGER A(127),B(127)
      DIMENSION R(30),S(30),FF(2)
      COMMON A,B,FF,IMAX,JMAX,L,N,R,S,IPOL,IPLOT,AVERA,AVERB
C        CALCULATE AVERAGES OF SERIES A AND B
      FN=N
      AVERA=0.0
      AVERB=0.0
      IF(N-L)50,50,100
   50 R(1)=0.0
      S(1)=0.0
      RETURN
  100 DO 110 I=1,N
      AVERA=AVERA+A(I)
  110 AVERB=AVERB+B(I)
      AVERA=AVERA/FN
      AVERB=AVERB/FN
C        CALCULATE CROSSCOVARIANCES OF SERIES A AND B
C        IF IPOL = 1, DO POLARITY CORRELATION.
      IF (IPOL) 111,111,131
  111 CONTINUE
      DO 130 J=1,L
      NJ=N-J+1
      SUMR=0.0
      SUMS=0.0
      DO 120 I=1,NJ
      IJ=I+J-1
      SUMR=SUMR+(A(I)-AVERA)*(B(IJ)-AVERB)
  120 SUMS=SUMS+(A(IJ)-AVERA)*(B(I)-AVERB)
      FNJ=NJ
      R(J)=SUMR/FNJ
  130 S(J)=SUMS/FNJ
      RETURN
  131 DO 150 J=1,L
      NJ=N-J+1
      SUMR=0.0
      SUMS=0.0
      DO 141 I=1,NJ
      IJ=I+J-1
      IF (A(I)-AVERA) 133,133,132
  132 F=1.0
      GO TO 134
  133 F=-1.0
  134 CONTINUE
      IF (B(IJ)-AVERB) 135,135,136
  135 F=-F
  136 CONTINUE
      SUMR=SUMR+F
      IF (A(IJ)-AVERA) 138,138,137
  137 G=1.0
      GO TO 139
  138 G=-1.0
  139 CONTINUE
      IF (B(I)-AVERB) 140,140,141
```

```
140  G=-G
141  SUMS=SUMS+G
     FNJ=NJ
     R(J)=SUMR/FNJ
150  S(J)=SUMS/FNJ
     RETURN
     END
```

```
*ONE WORD INTEGERS
      SUBROUTINE FIGR
      INTEGER A(127),B(127)
      DIMENSION R(30),S(30),FF(2)
      COMMON A,B,FF,IMAX,JMAX,L,N,R,S,IPOL,IPLOT,AVERA,AVERB
    4 FORMAT (I3)
    5 FORMAT (F4.1)
   13 FORMAT (' CORRELATION FUNCTION')
   14 FORMAT ('                                        ')
   15 FORMAT ('CHANNELS')
   26 FORMAT (F12.4)
      READ (2,14)
      WRITE (1,14)
      SX=12./2.54/30.
      SY=10./2.54
      DY=0.2001
      IF (IPLOT) 16,16,17
   16 CALL SCALF (SX, SY, -30., 0.)
      CALL FGRID (0,-30.,0.,5.,12)
      CALL FGRID (1,0.,0.,0.2,5)
      CALL FGRID (3,0.,0.,0.2,5)
      XD=.37/SX
      X = -30.
      Y = -.25/SY
      DEL = 5.
      EP = 0.01
      DO 10 I=1,13
      IF (ABS(X) - EP) 9,9,7
    7 CALL FCHAR (X-XD, Y, .15, .15, 0.)
      GO TO 77
    9 CALL FCHAR(-.55/SX,Y,.15,.15,0.)
   77 IX=X
      WRITE (7,4) IX
      X = X + DEL
   10 CONTINUE
      CALL FCHAR (32.,Y,.11,.1,0.)
      WRITE (7,15)
      X = -0.7/SX
      Y = -1.0005
      DEL = DY
      XD = .075/SY
      DO 20 I=1, 11
      IF (ABS(Y) - EP) 19, 11, 11
   11 CALL FCHAR (X,Y-XD,.15, .15, 0.)
      WRITE (7,5) Y
   19 Y = Y + DEL
   20 CONTINUE
      GO TO 18
   17 CALL SCALF (SX, SY,  50., 0.)
   18 CONTINUE
      X=0.5
      Y = S(1)/FF(1)
      CALL FPLOT(-2,X,Y)
      DO 40 I=1, 30
      X=1.5-I
```

```
      Y=S(I)/FF(1)
      CALL FPLOT (0, X, Y)
40    CONTINUE
      CALL FPLOT(-1,X,Y)
      X=0.5
      Y = R(1)/FF(1)
      CALL FPLOT(-2,X,Y)
      DO 50 I=1,30
      X=I-0.5
      Y=R(I)/FF(1)
      CALL FPLOT (0, X, Y)
50    CONTINUE
      IF (IPLOT) 51,51,52
51    CALL FCHAR (-1.7/SX, 1.15,.17, .24, 0.)
      WRITE (7,13)
      CALL FCHAR ( 5.,-1.1, .1, .1, 0.)
      WRITE (7,14)
      CALL FCHAR (5.,-1.2,.1,.1,0.)
      WRITE (7,26) FF(1)
52    CALL FPLOT (1,50.,0.)
      RETURN
      END
```

```
* ONE WORD INTEGERS
      SUBROUTINE NOISE
      INTEGER A(127),B(127)
      DIMENSION R(30),S(30),FF(2)
      COMMON A,B,FF,IMAX,JMAX,L,N,R,S,IPOL,IPLOT,AVERA,AVERB
  301 FORMAT('A                ')
  302 FORMAT('B                ')
      CALL SCALF (1.,1.,0.,0.)
      CALL FPLOT(1,0.,-2.)
      CALL FPLOT(2,6.35,-2.)
      CALL FPLOT(1,6.35, 2.)
      CALL FPLOT(2,0.,2.)
      CALL FPLOT(1,0.,2.)
      F=1000.
      X=0.
      Y=(A(1)-AVERA)/F+2.
      CALL FPLOT(-2,X,Y)
      DO 400 I=1,127
      X=I/20.-.05
      Y=(A(I)-AVERA)/F+2.
      CALL FPLOT(0,X,Y)
  400 CONTINUE
      CALL FPLOT(-1,X,Y)
      X=0.025
      Y=(B(1)-AVERB)/F-2.
      CALL FPLOT(-2,X,Y)
      DO 500 I=1,127
      X=I/20.-0.025
      Y=(B(I)-AVERB)/F-2.
      CALL FPLOT(0,X,Y)
  500 CONTINUE
      CALL FCHAR(.5,3.8,.15,.18,0.)
      WRITE(7,301)
      CALL FCHAR(.5,-.2,.15,.18,0.)
      WRITE(7, 302)
      CALL FPLOT(1,15.,0.)
      RETURN
      END
```

APPENDIX II

CROSS-CORRELATION FUNCTIONS

Results of cross-correlation functions calculated by the hybrid computer are included in this appendix. The cross-correlation functions are normalized to unity in the range of time lag shown in the figures. Labelling of the figures has the following meanings.

First line - detector positions

Numbers in parentheses mean horizontal position number for single rod experiments (see Figure 17). The vertical level is designated by L = (height in cm from the standard level of the heater element middle point).

Second line - heater power

P = (nominal wattage measured by the wattmeter).

Third line - temperature

T = (degrees centigrade of the bulk water).

Fourth line - frequency passband

F = (lower and upper cut-off frequencies in kHz).

Fifth line - data size

M = (this number multiplied by 127 equals the number of processed data pairs).

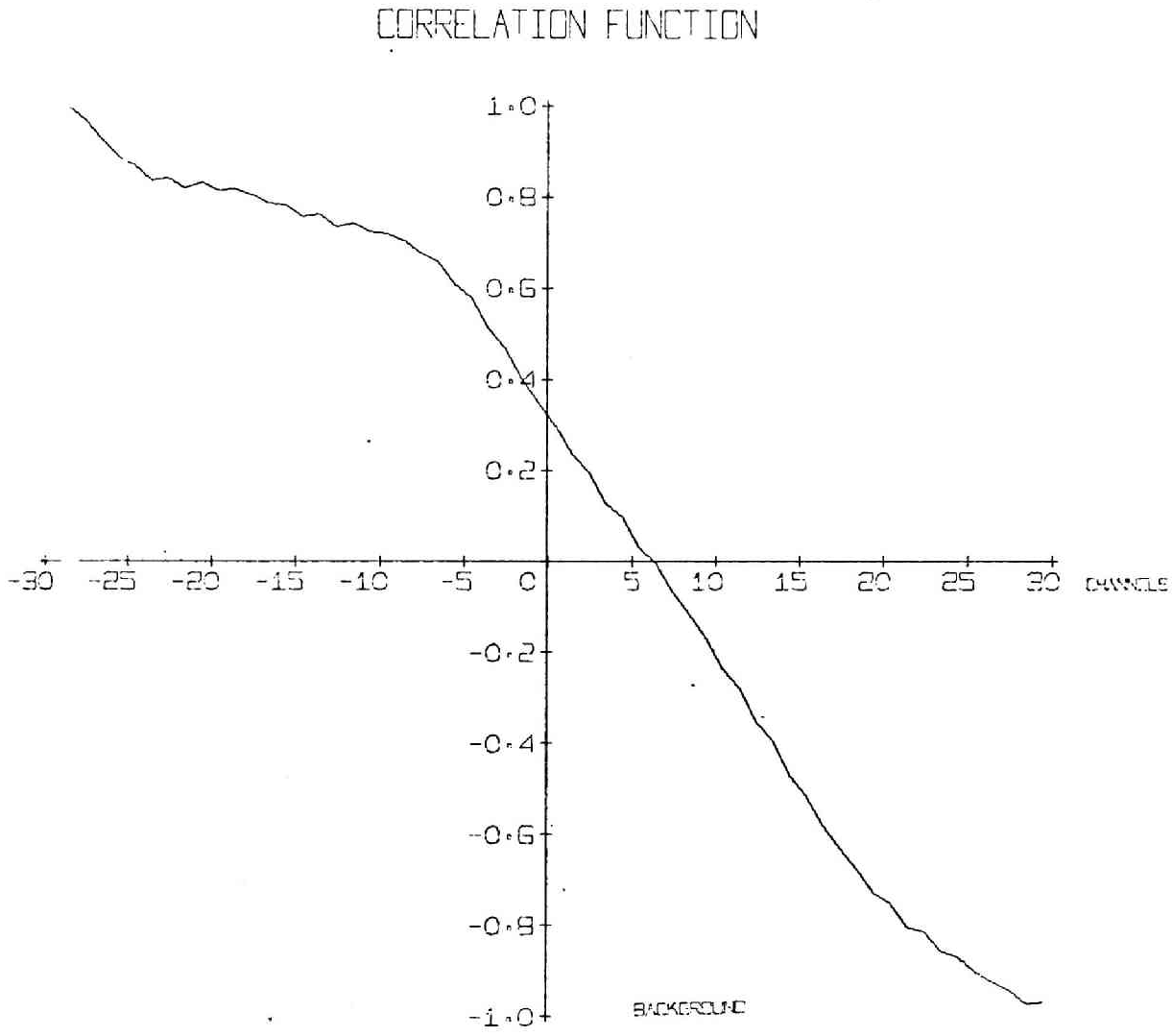

Fig. 38 Cross-correlation Function Output - I

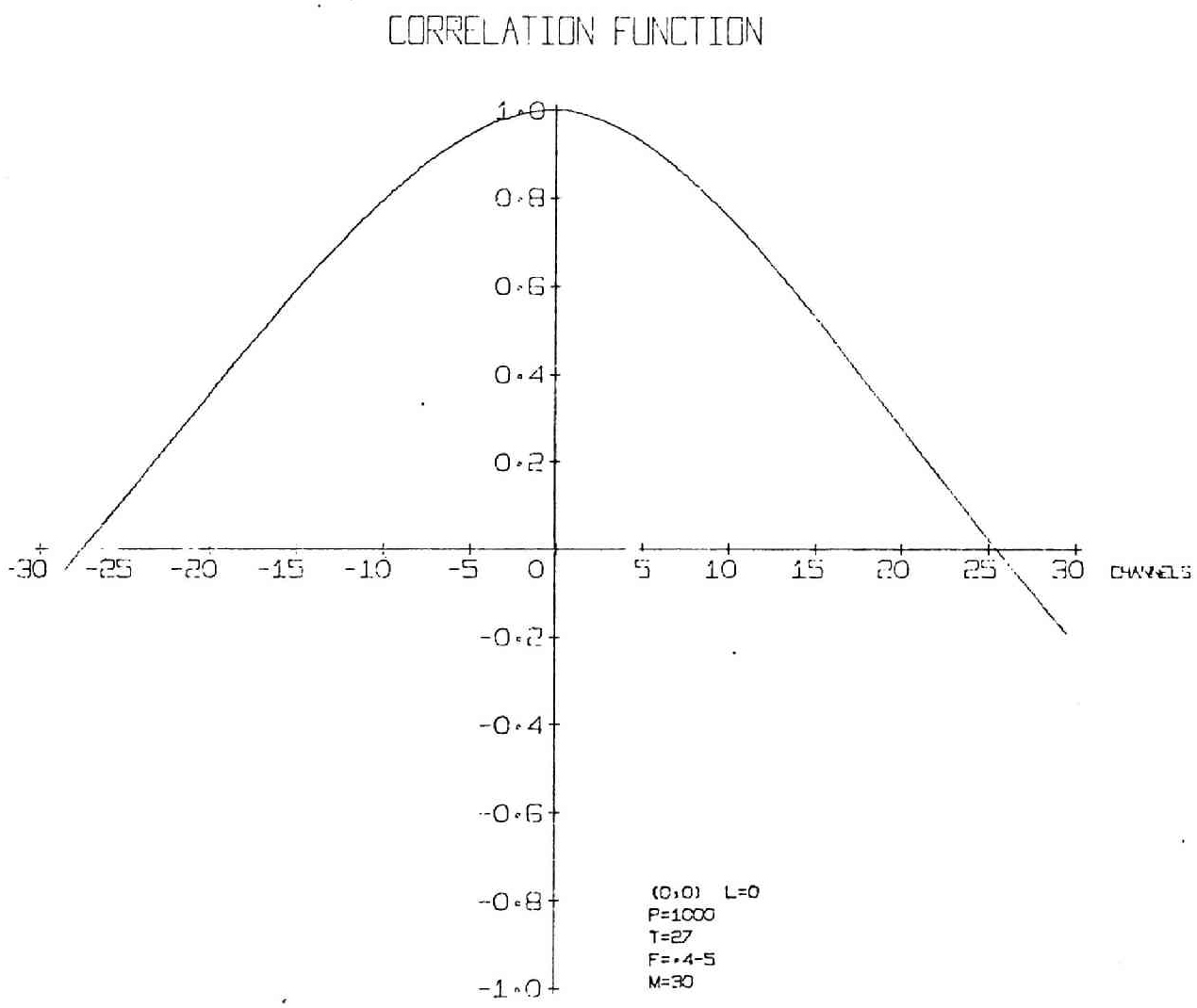

Fig. 39 Cross-correlation Function Output - 2

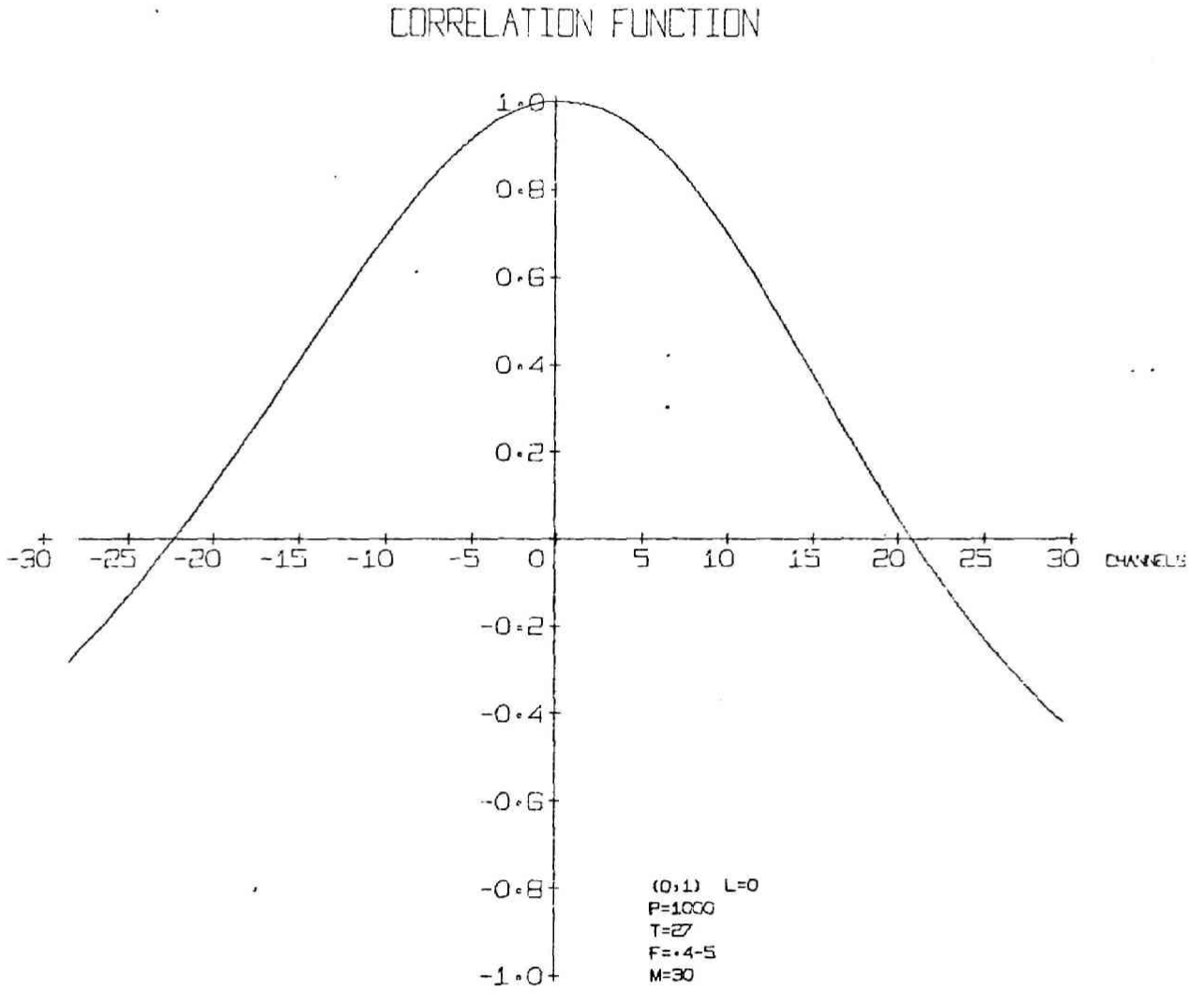

Fig. 40 Cross-correlation Function Output - 3

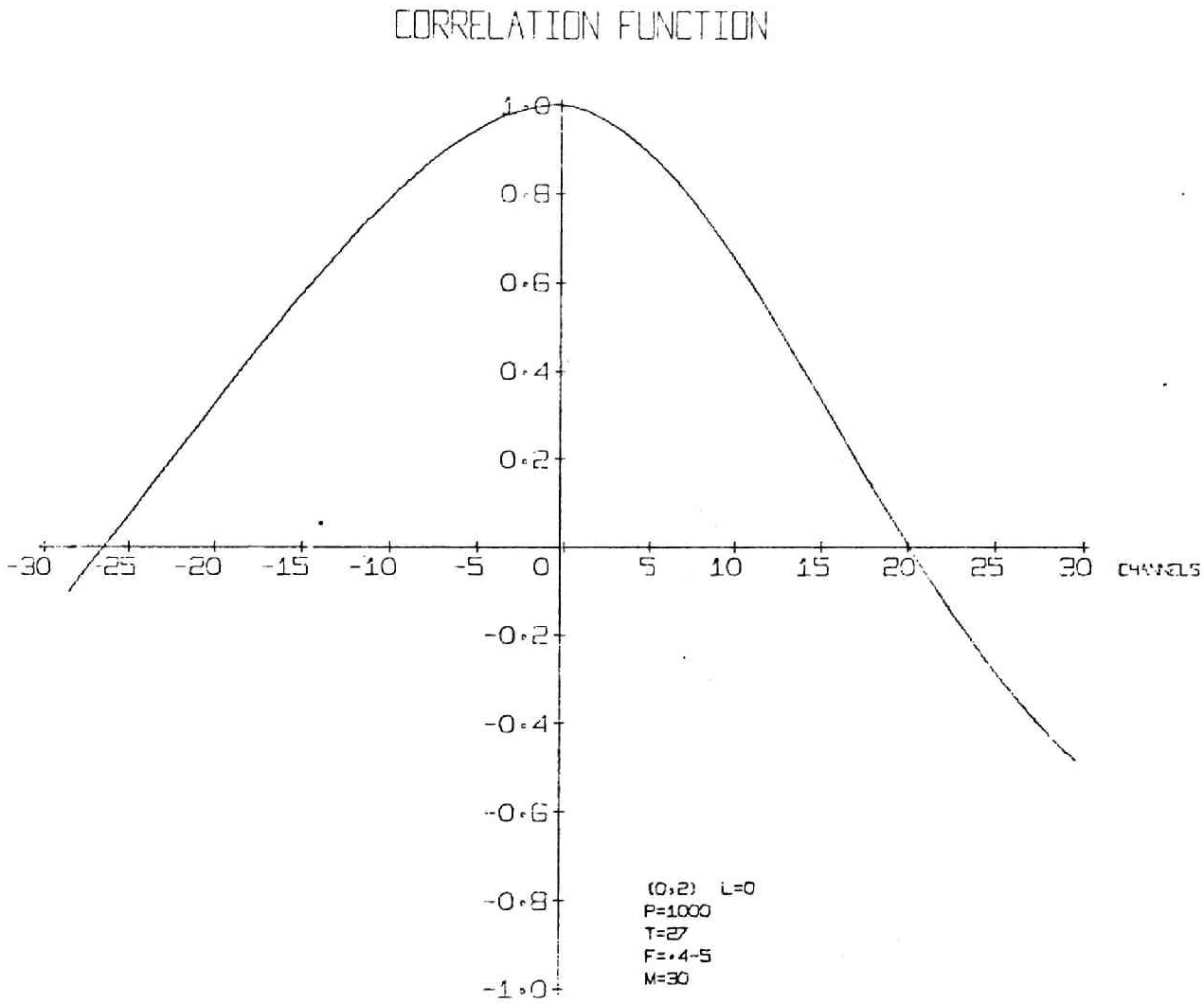

Fig. 41 Cross-correlation Function Output - 4

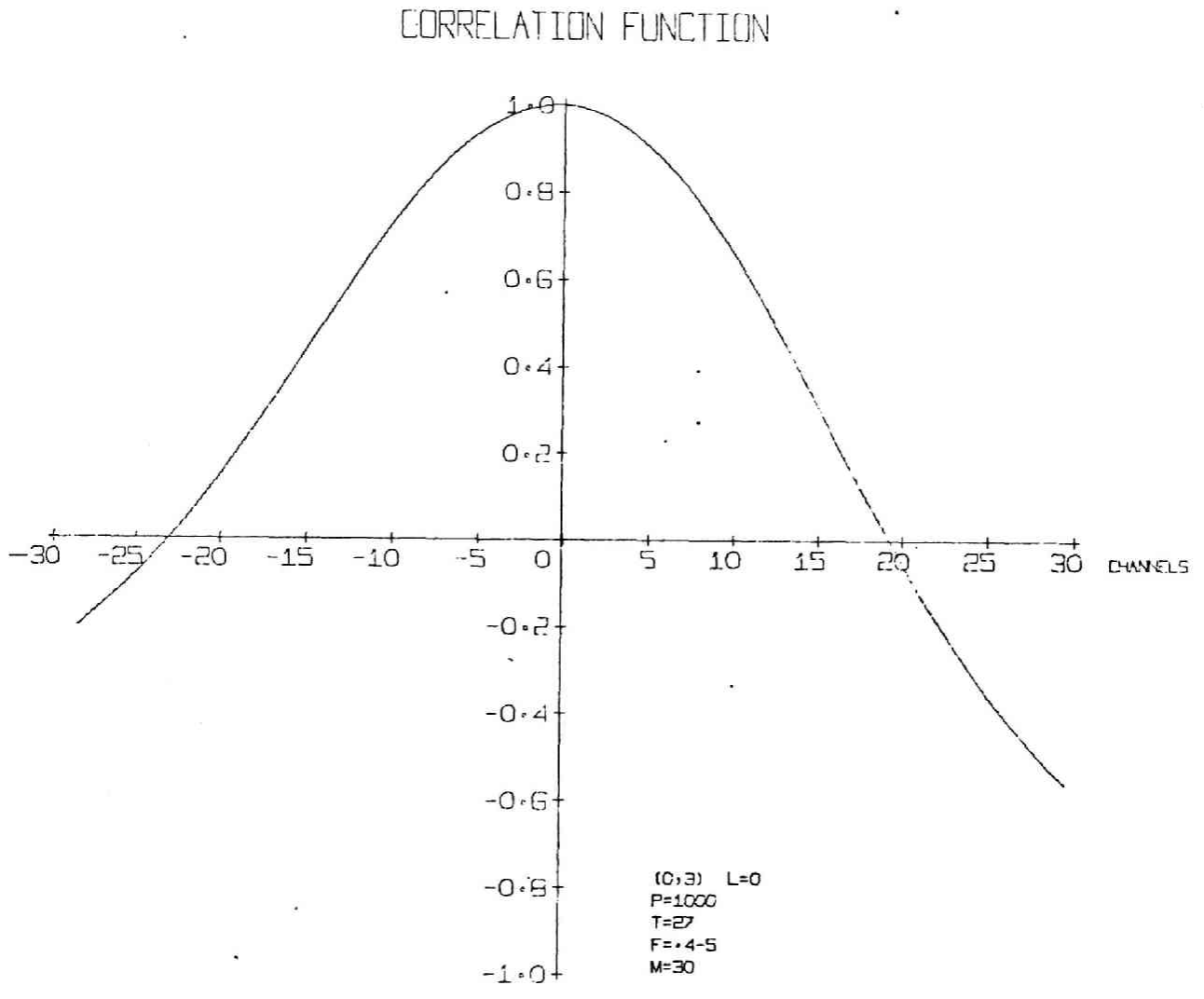

Fig. 42 Cross-correlation Function Output - 5

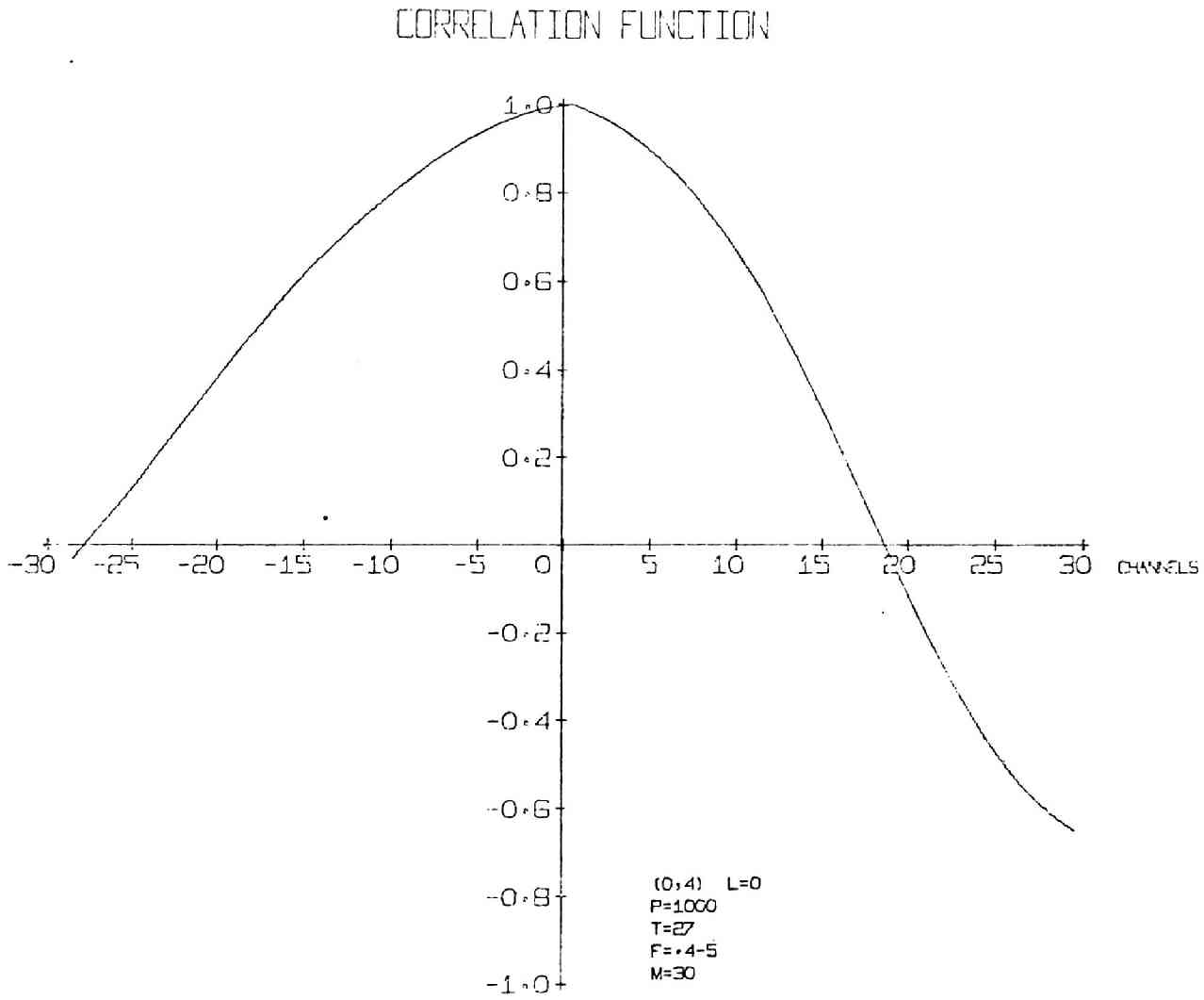

Fig. 43 Cross-correlation Function Output - 6

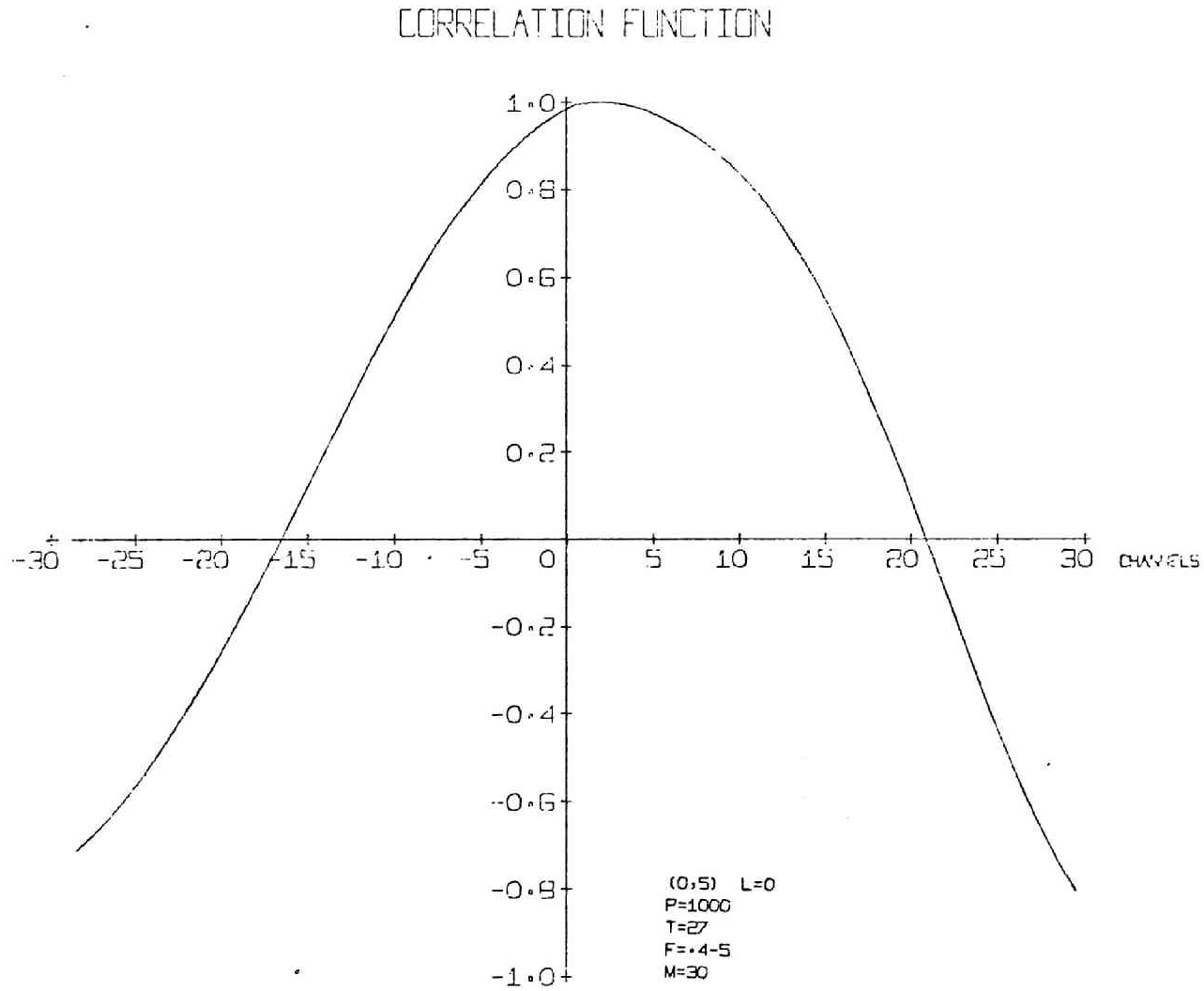

Fig. 44 Cross-correlation Function Output - 7

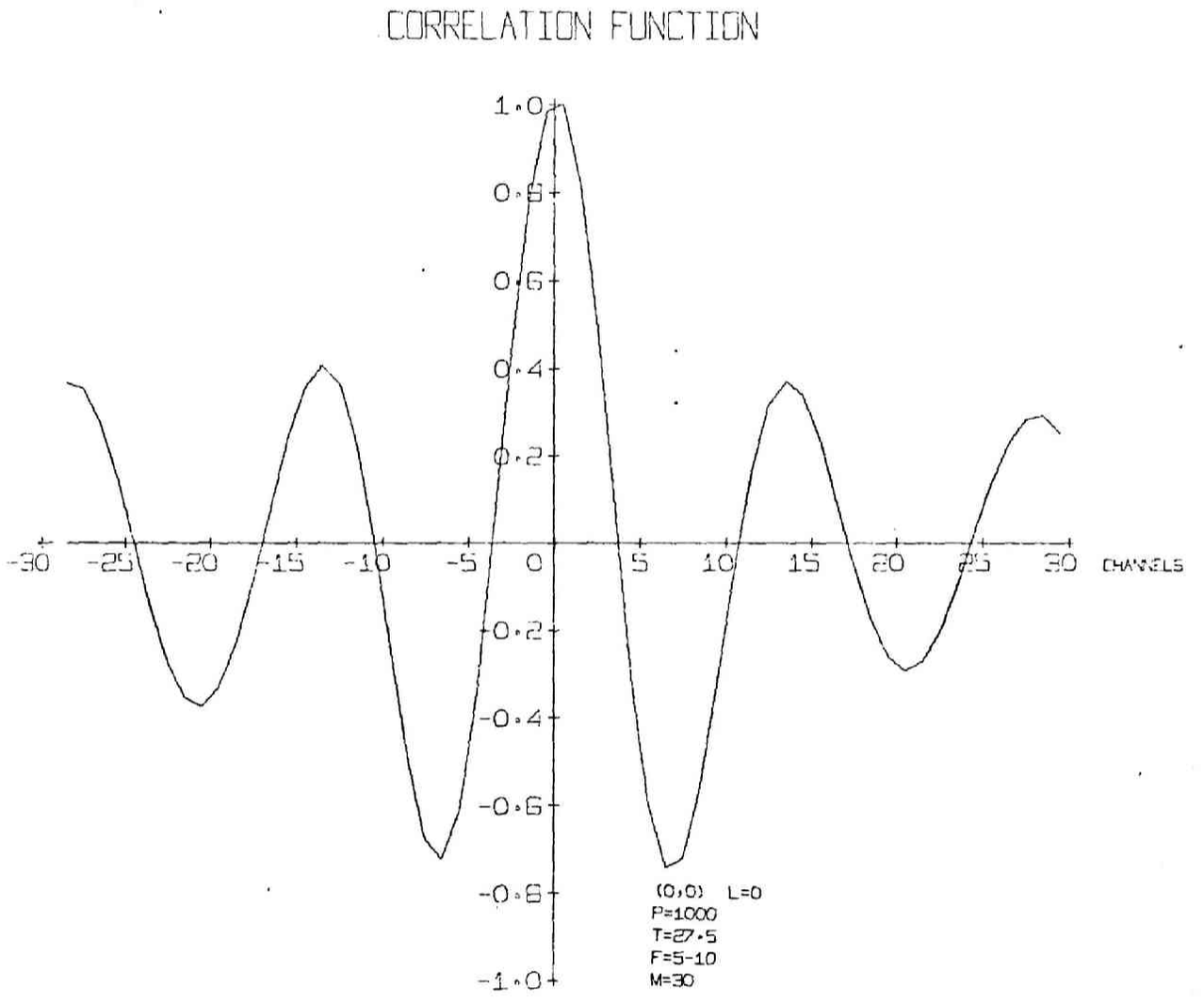

Fig. 45 Cross-correlation Function Output - 8

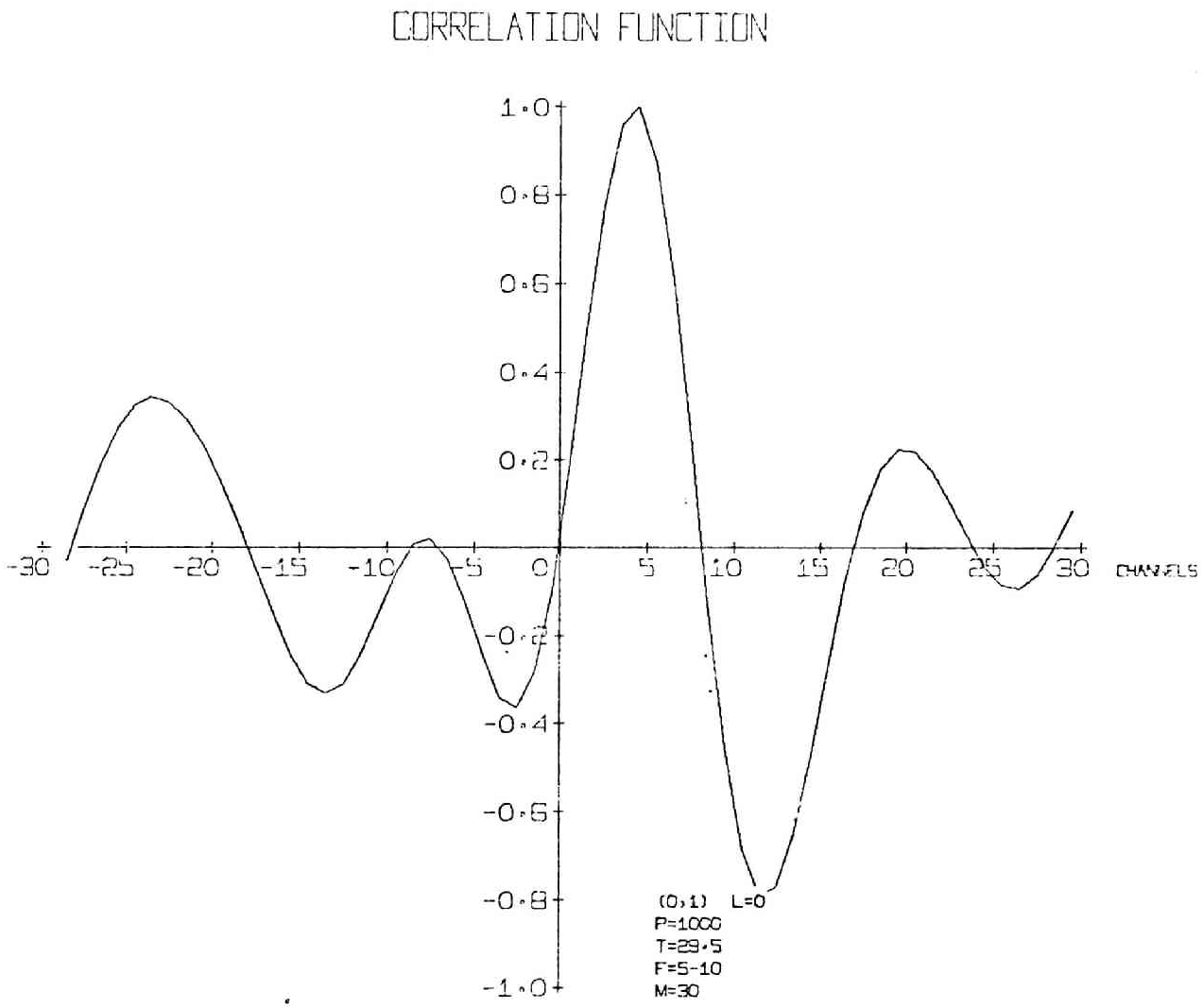

Fig. 46 Cross-correlation Function Output - 9

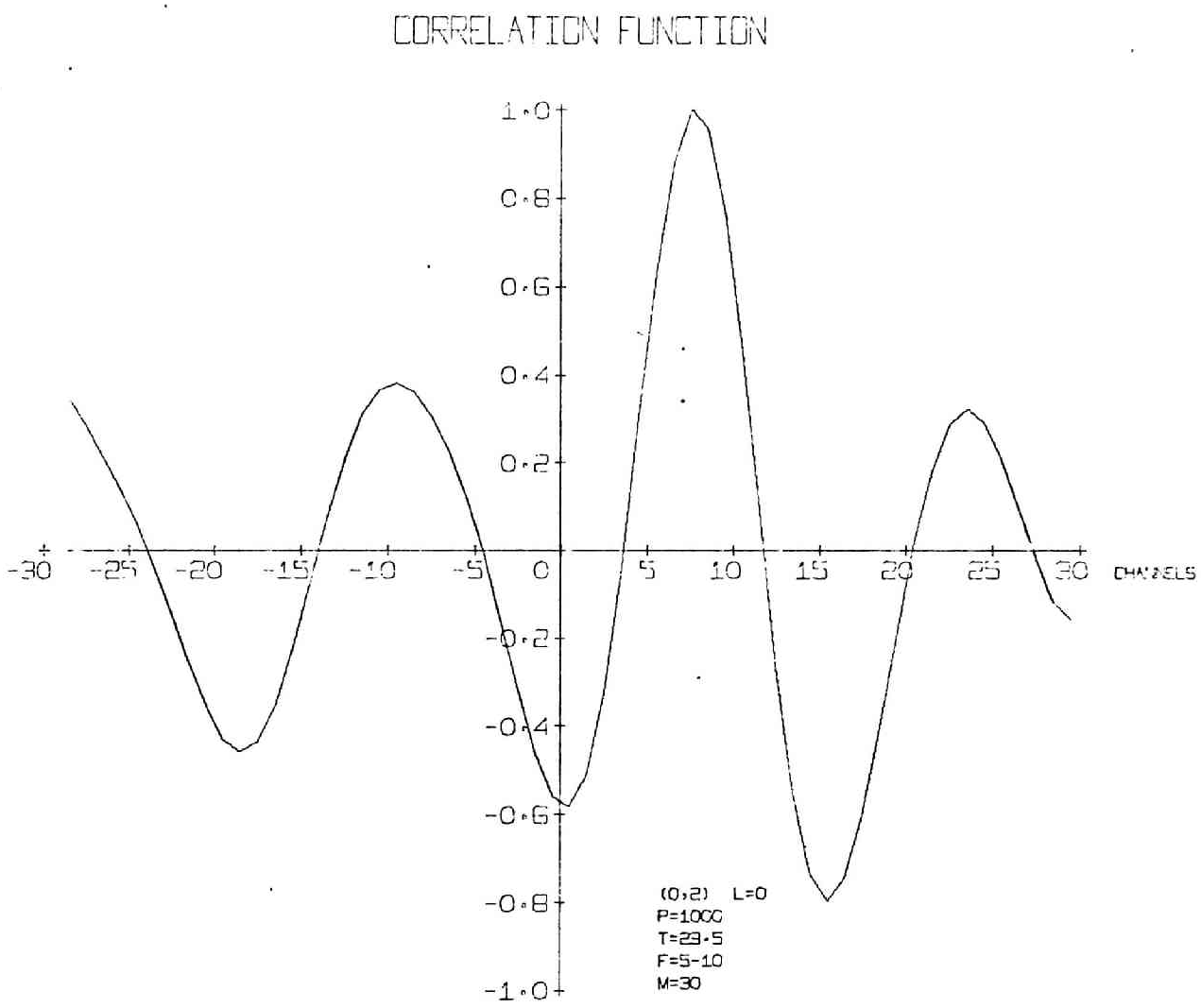

Fig. 47 Cross-correlation Function Output - 10

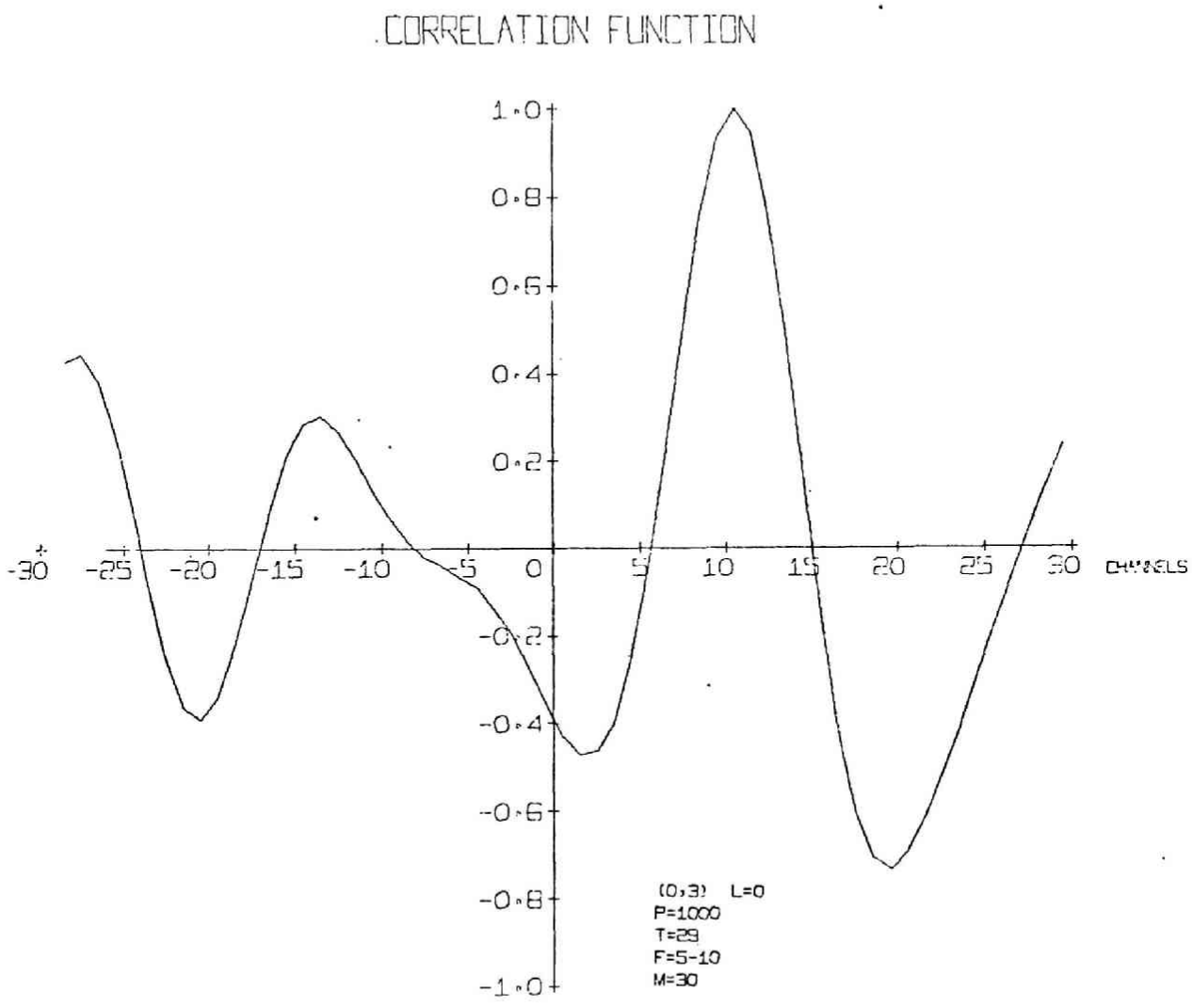

Fig. 48 Cross-correlation Function Output - II

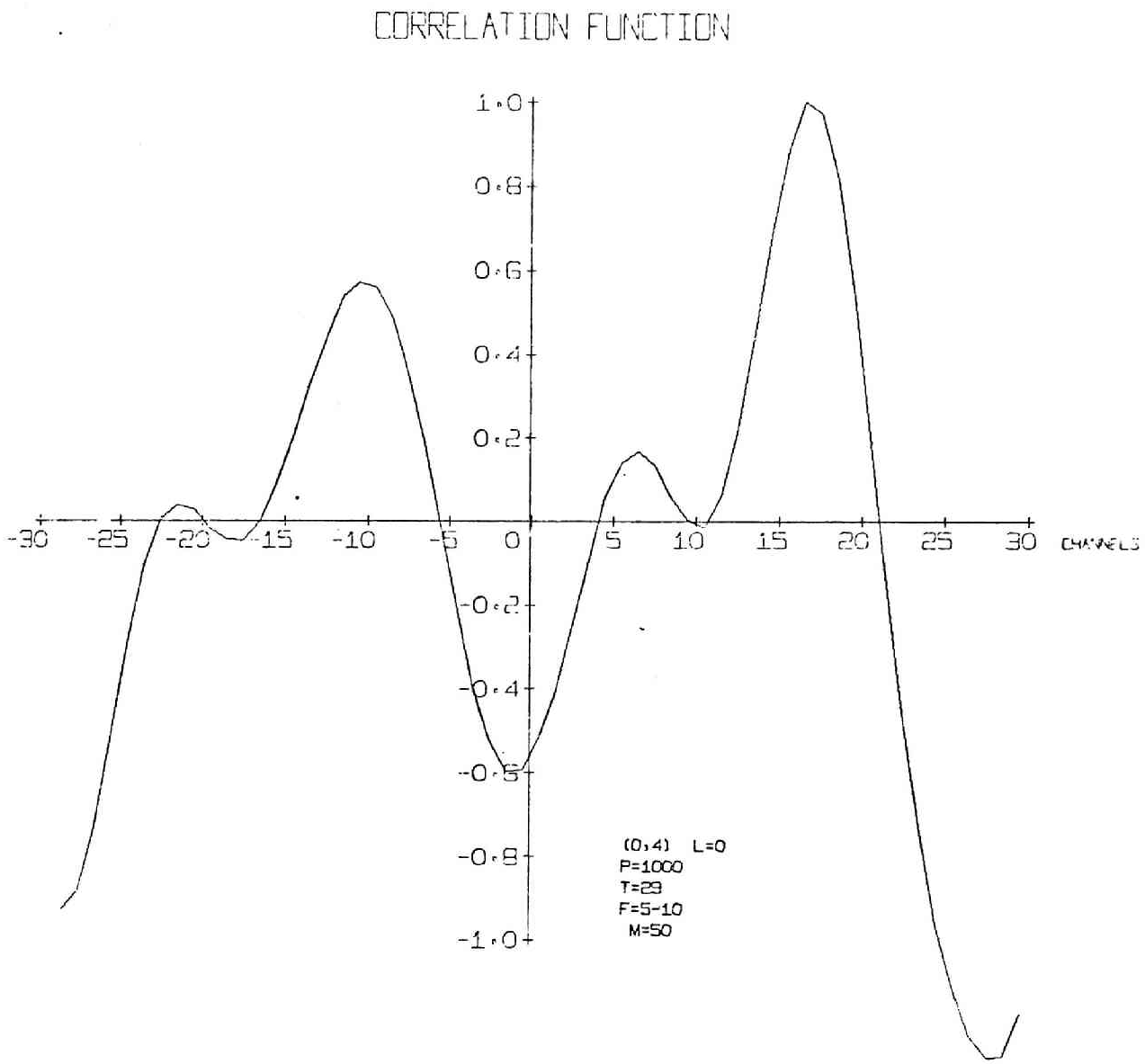

Fig. 49 Cross-correlation Function Output - 12

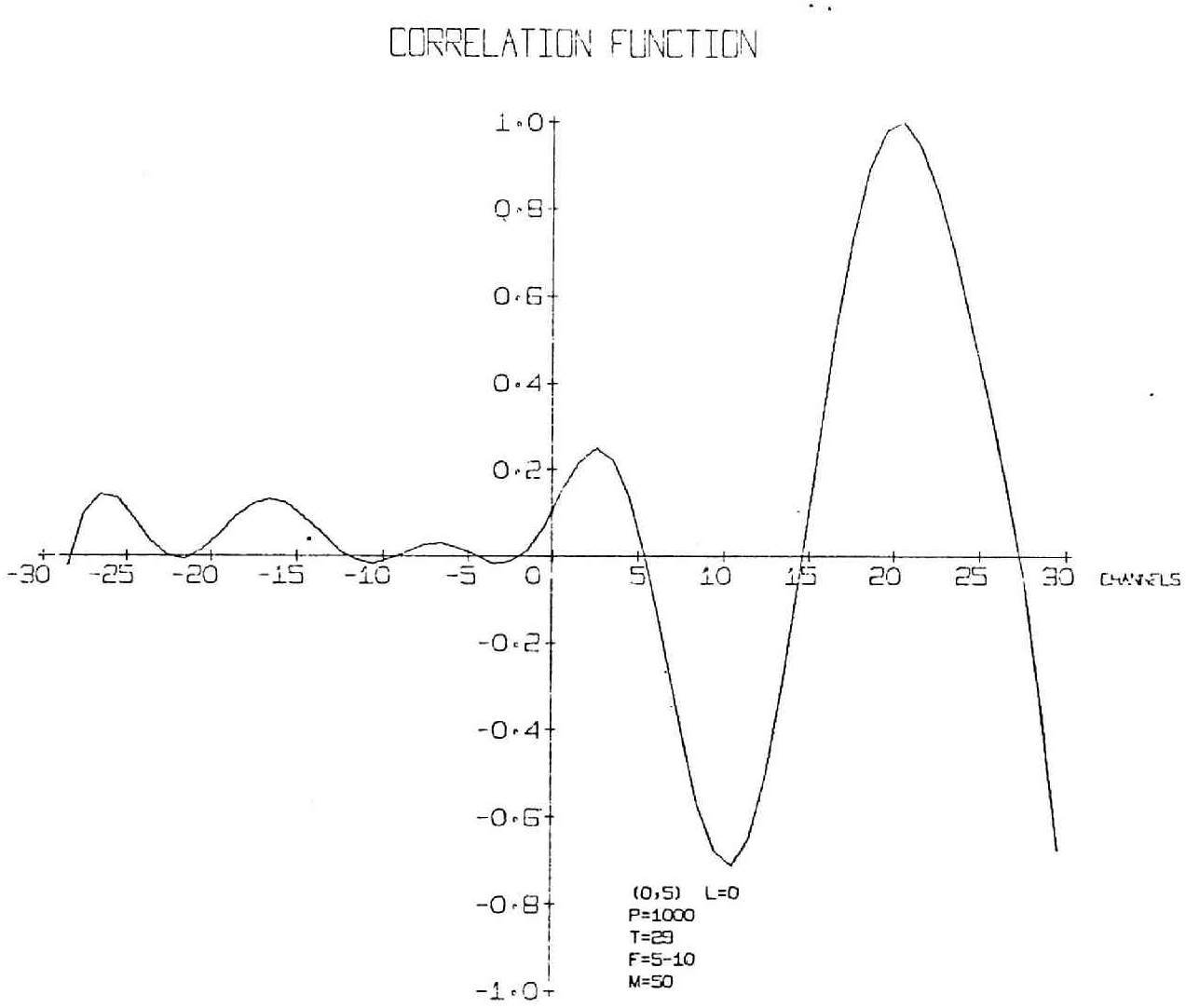

Fig. 50 Cross-correlation Function Output - 13

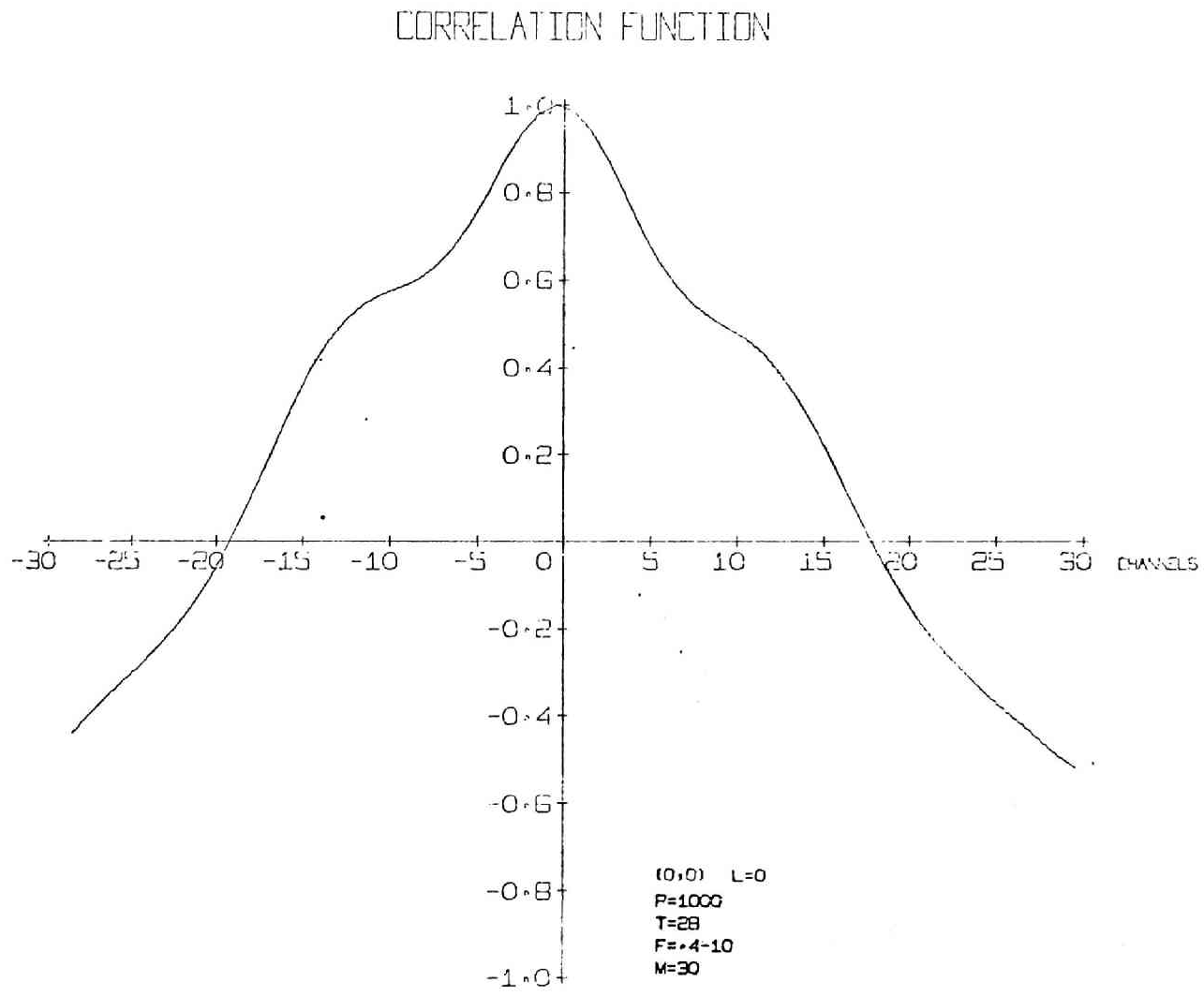

Fig. 51 Cross-correlation Function Output - 14

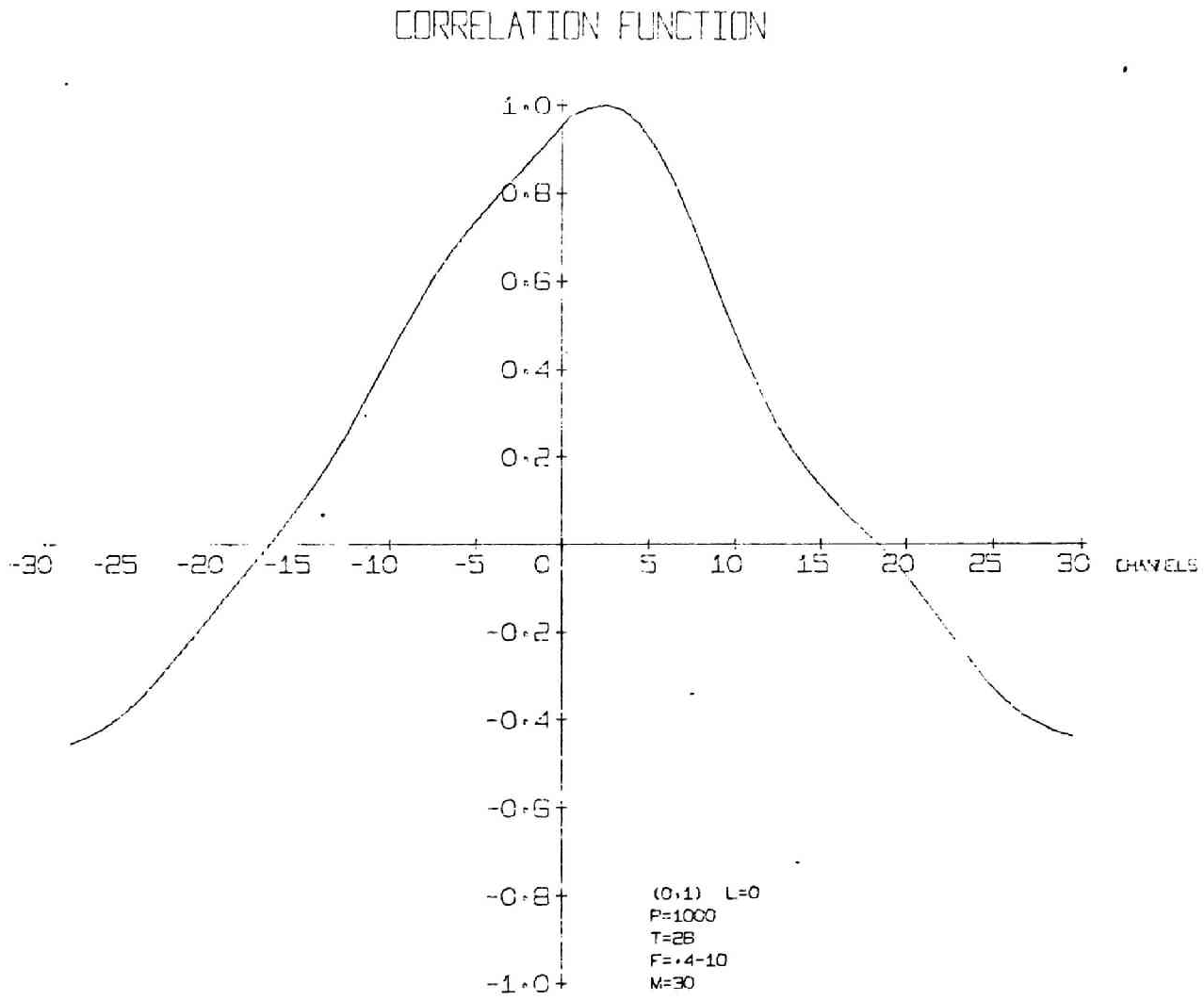

Fig. 52 Cross-correlation Function Output - 15

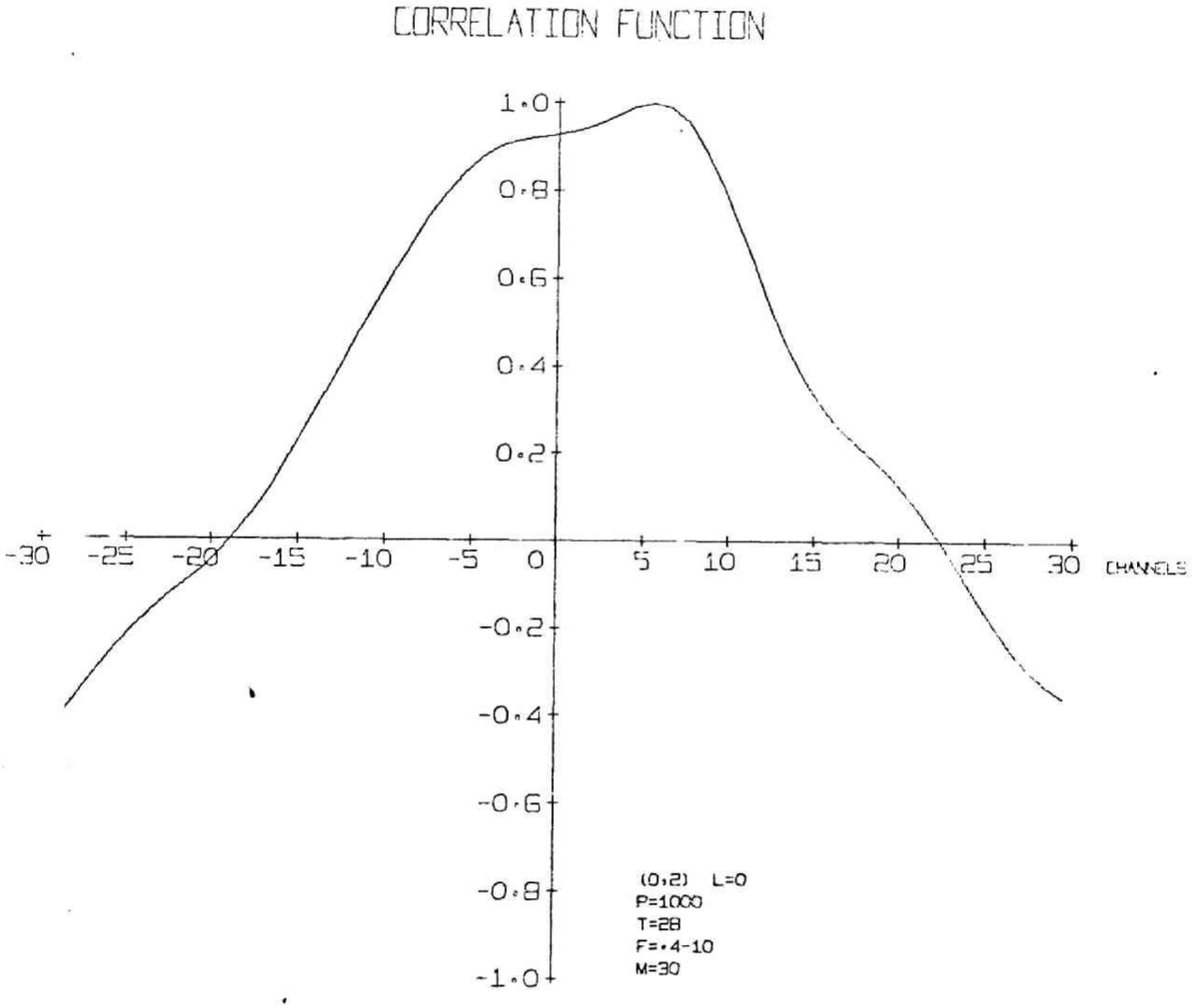

Fig. 53 Cross-correlation Function Output - 16

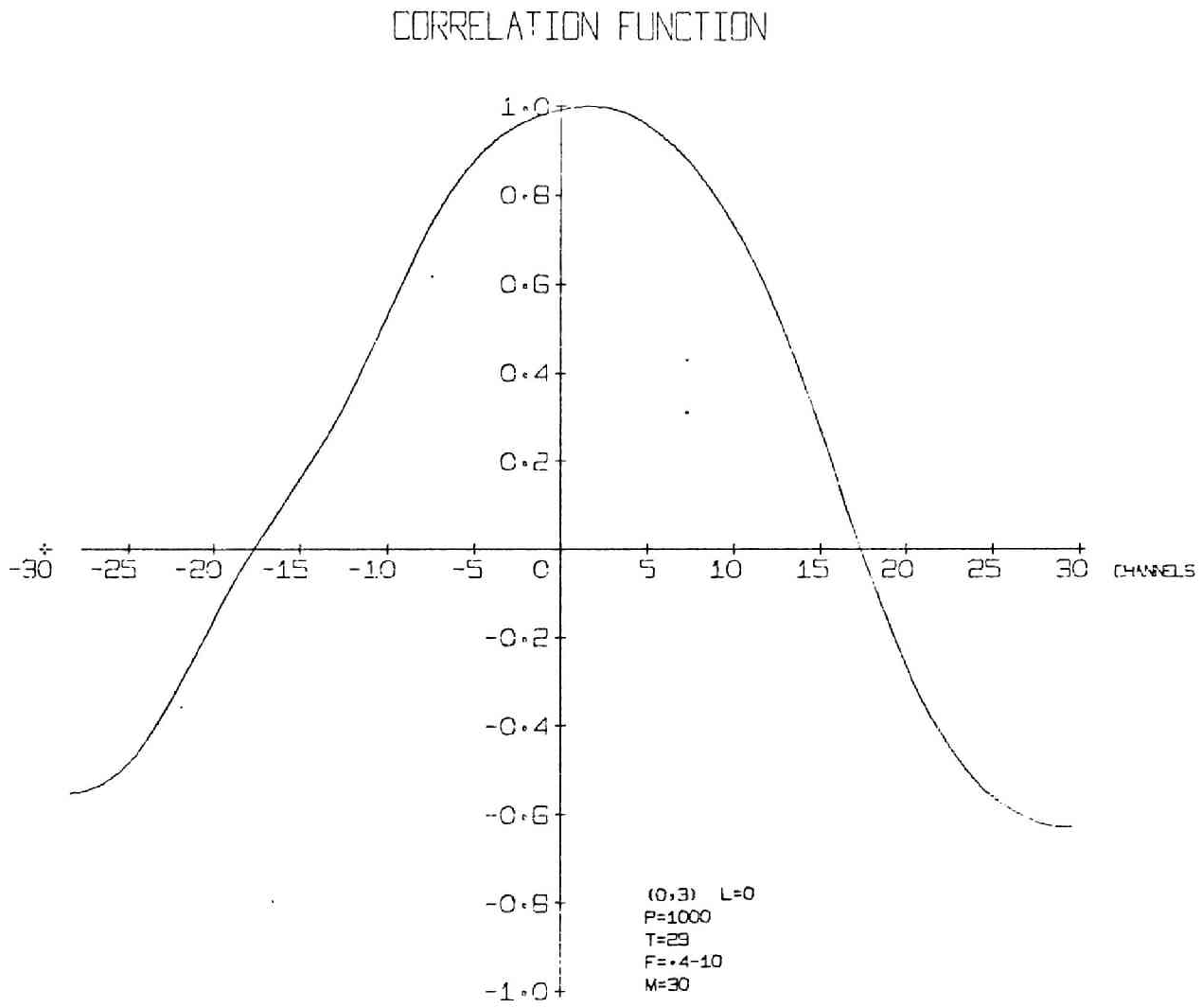

Fig. 54 Cross-correlation Function Output - 17

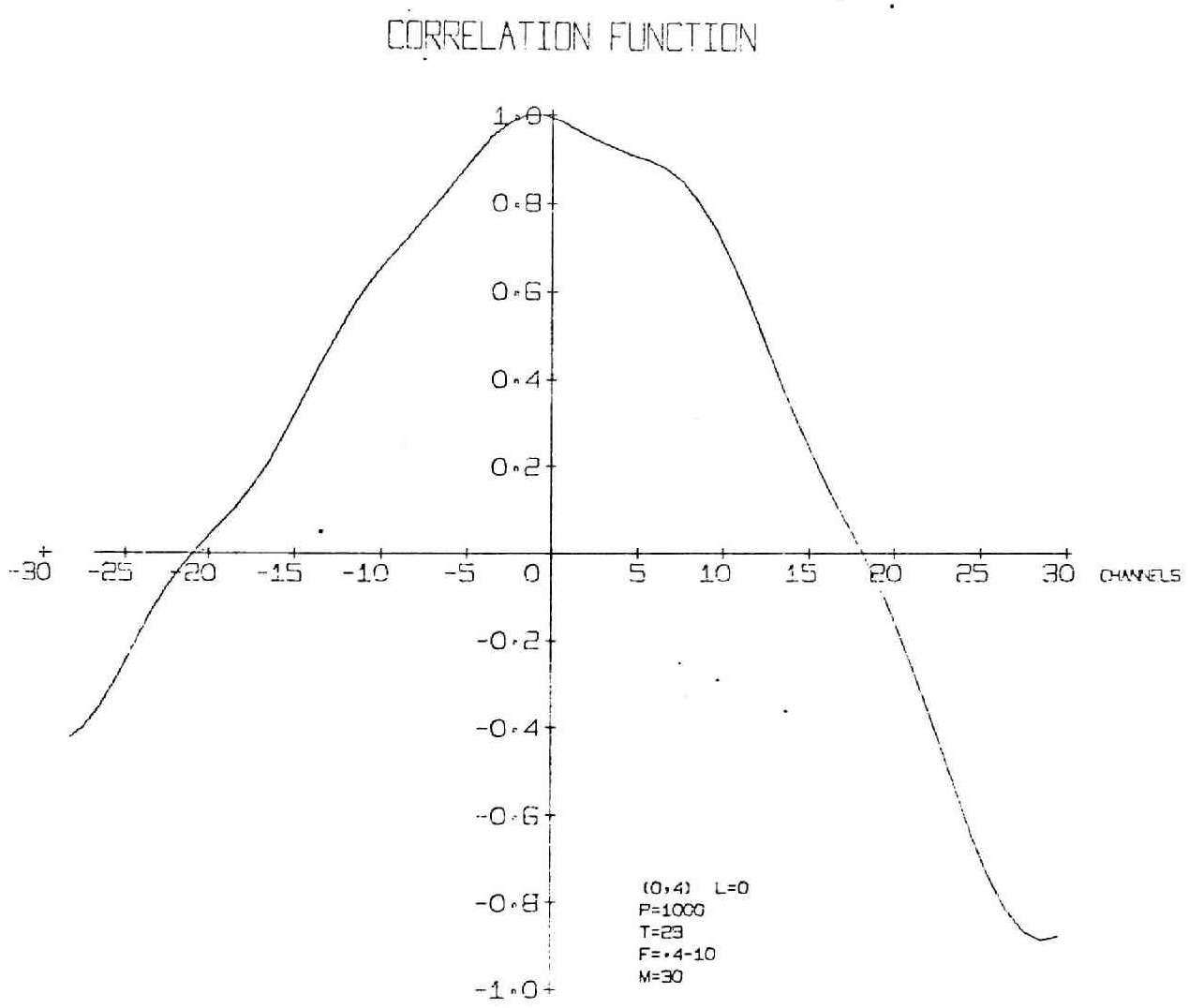

Fig. 55 Cross-correlation Function Output - 18

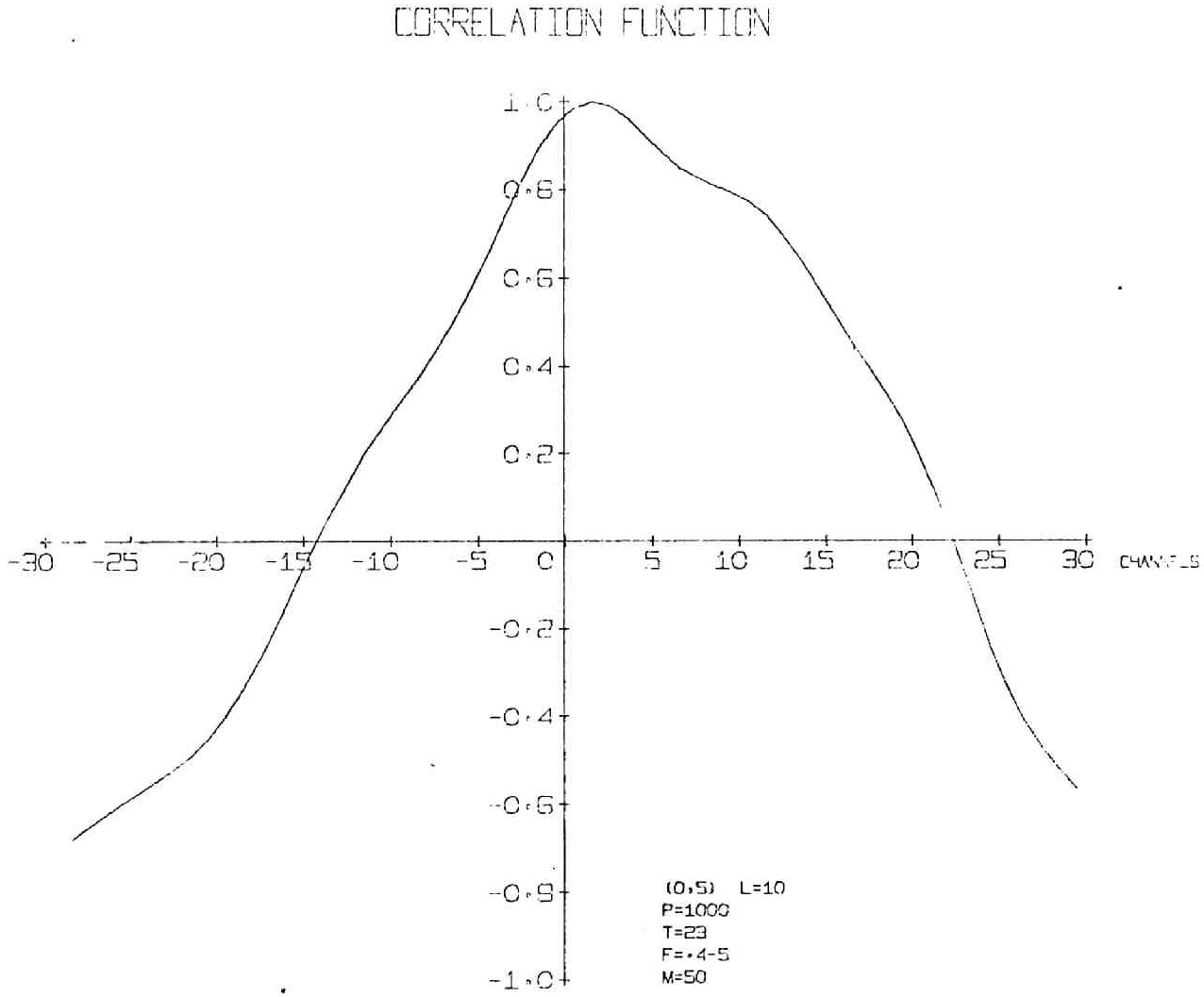

Fig. 56 Cross-correlation Function Output - 19

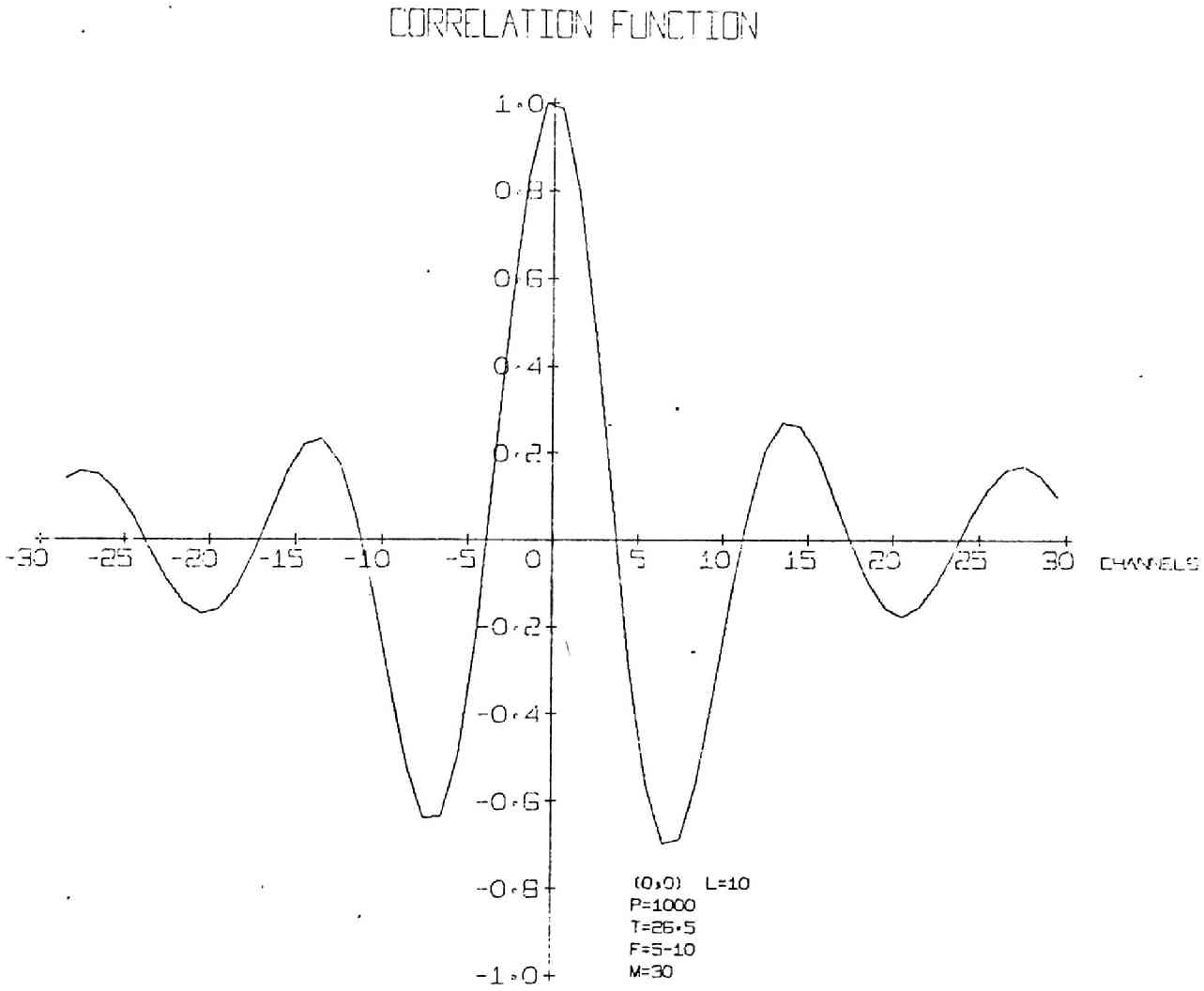

Fig. 57 Cross-correlation Function Output - 20

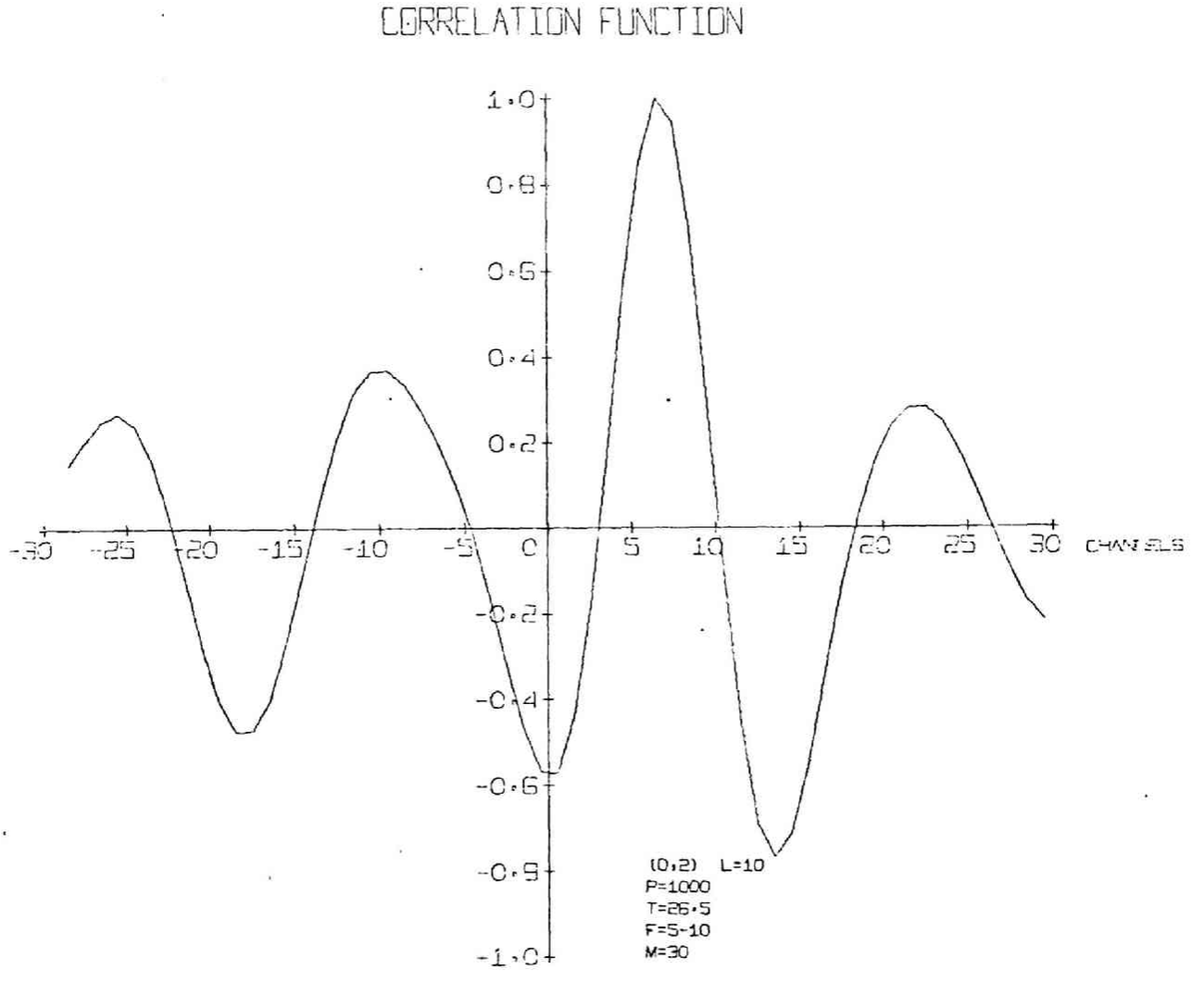

Fig. 58 Cross-correlation Function Output - 21

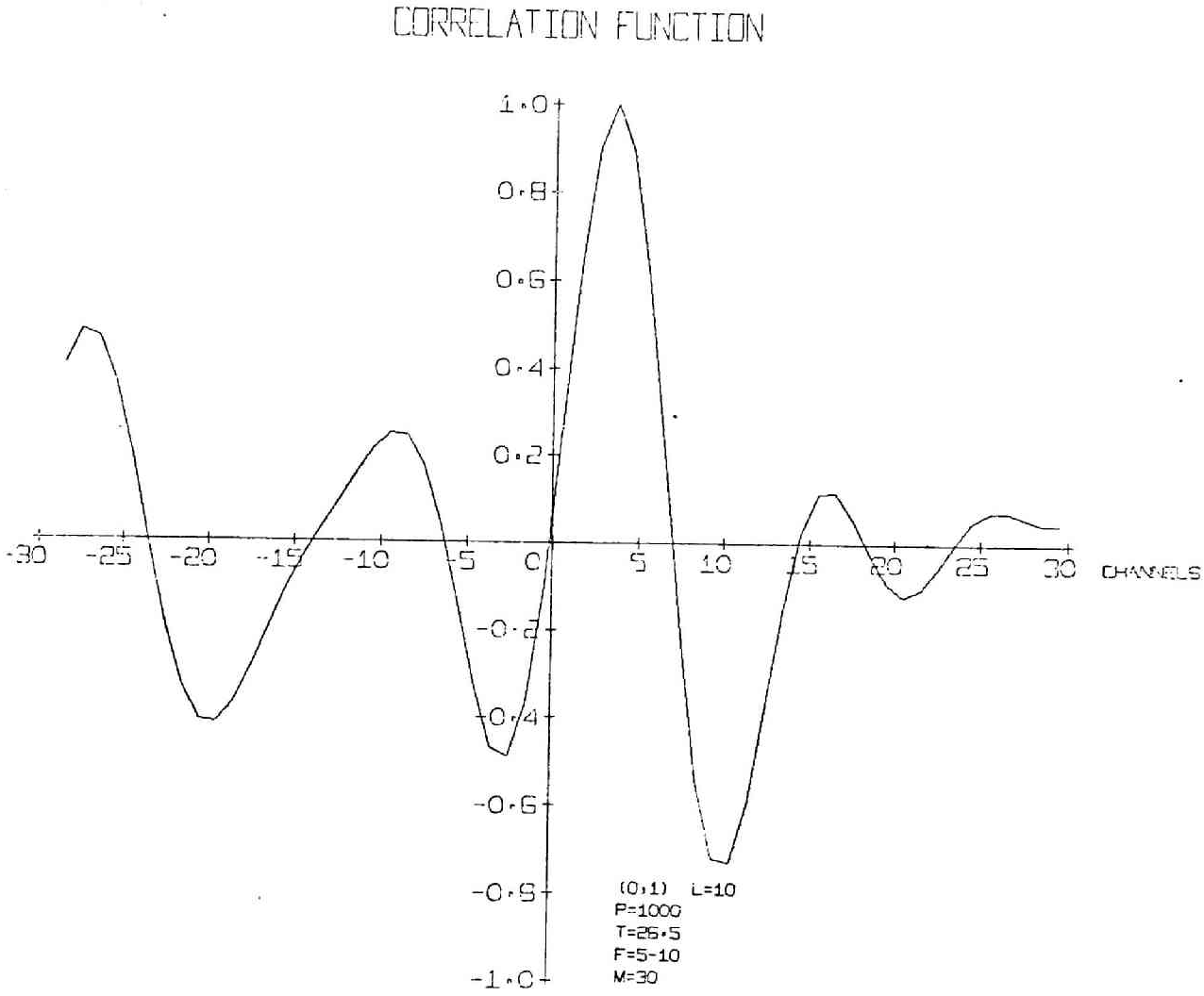

Fig. 59 Cross-correlation Function Output - 22

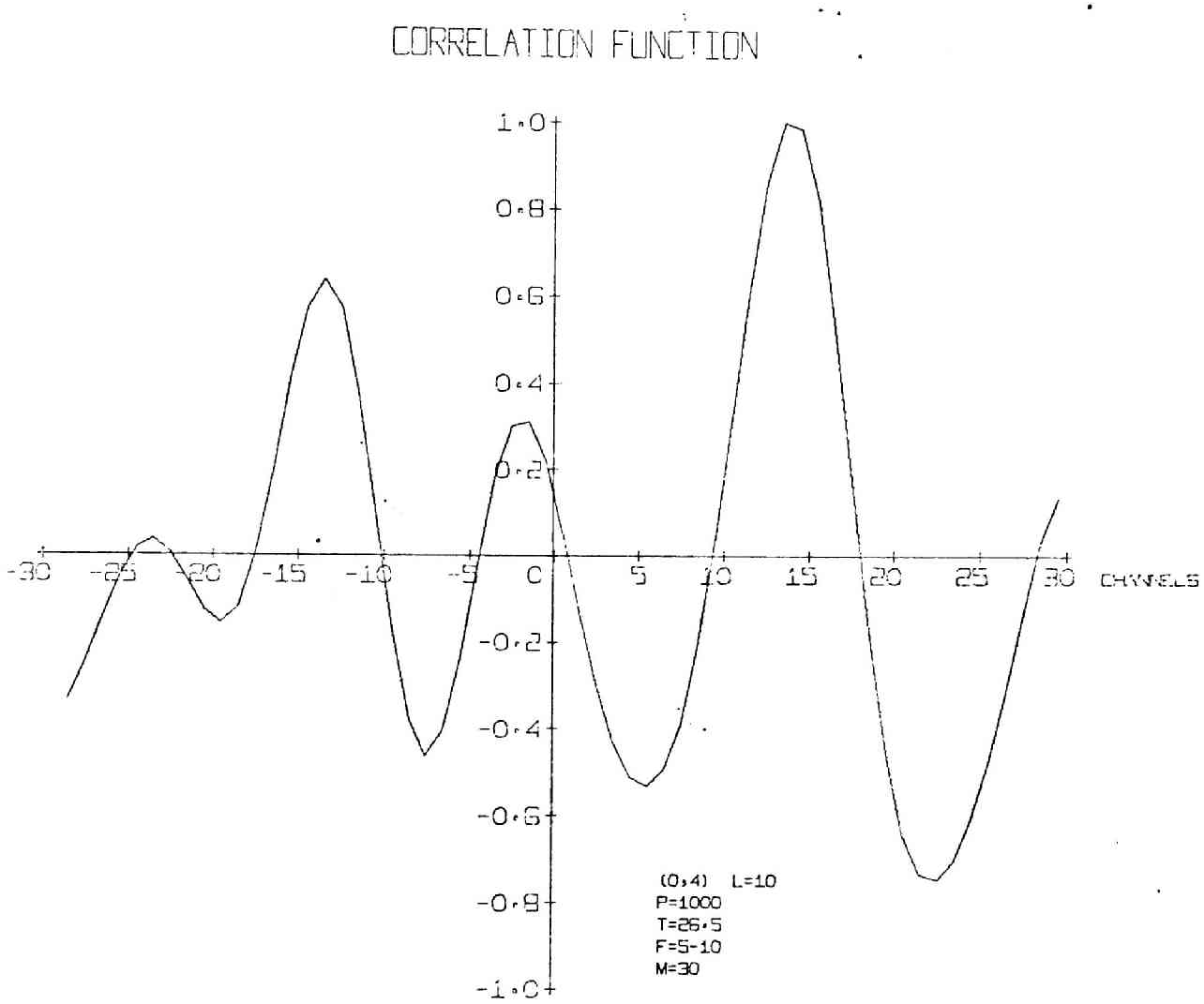

Fig. 60 Cross-correlation Function Output - 23

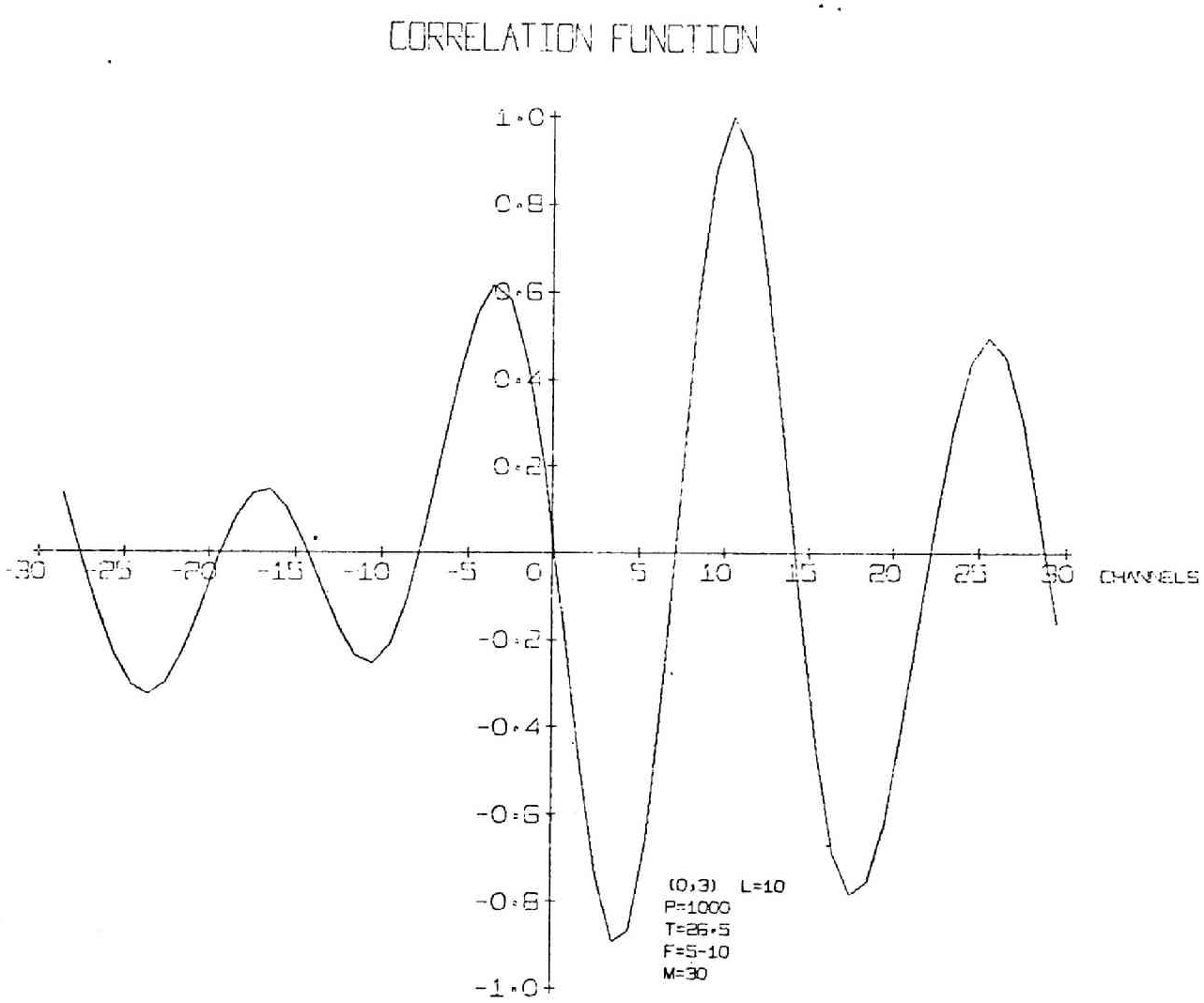

Fig. 61 Cross-correlation Function Output - 24

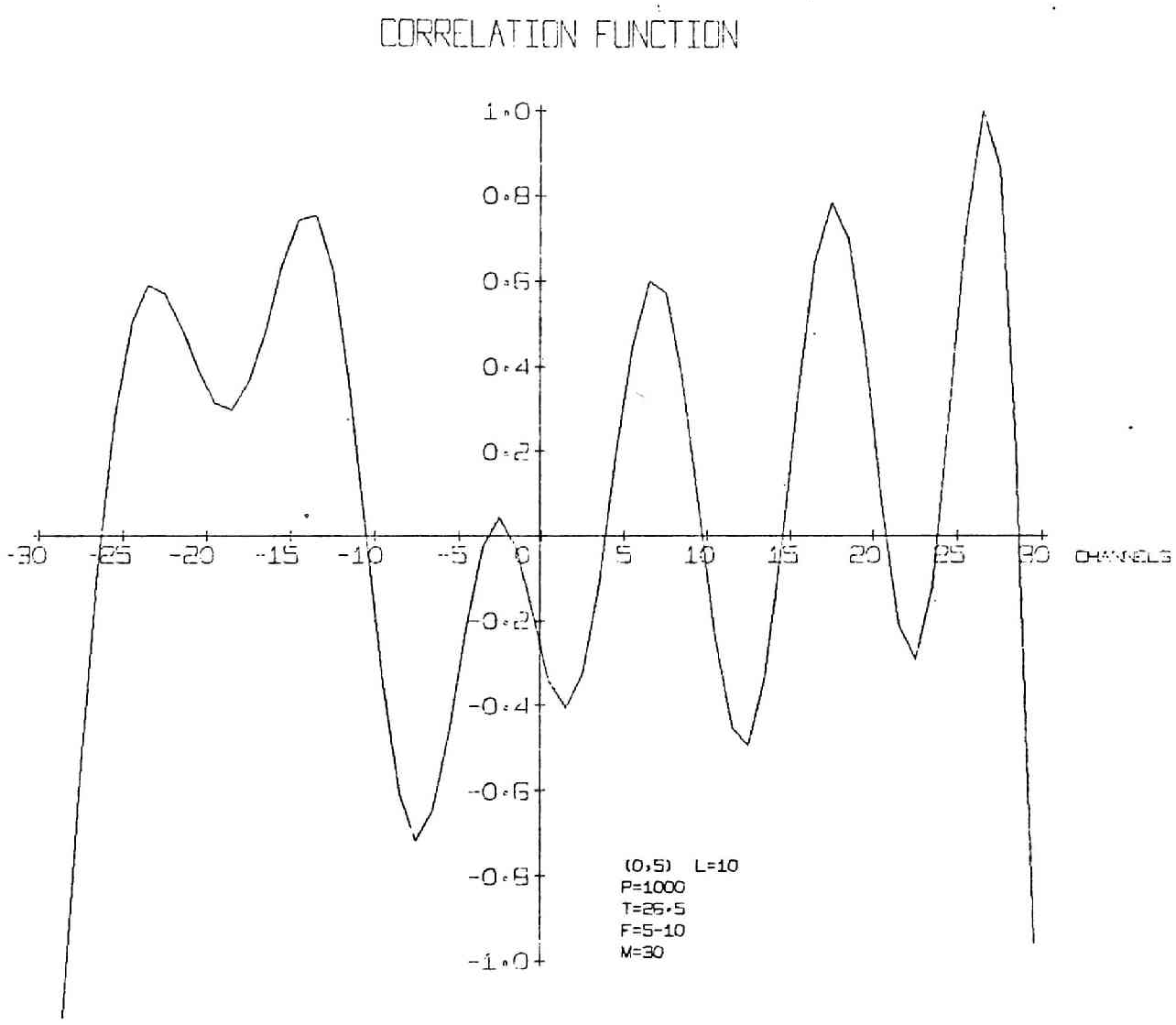

Fig. 62 Cross-correlation Function Output - 25

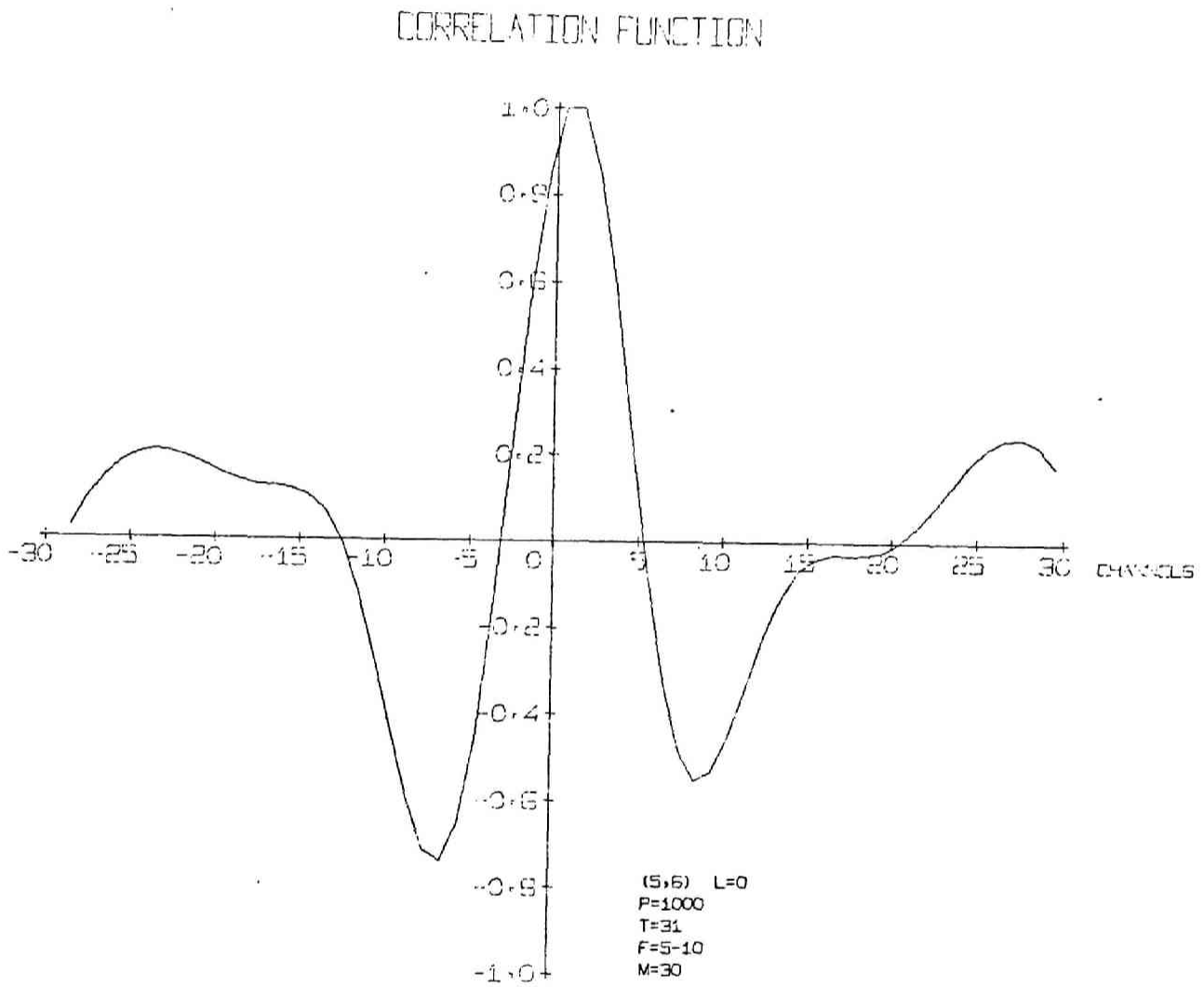

Fig. 63 Cross-correlation Function Output - 26

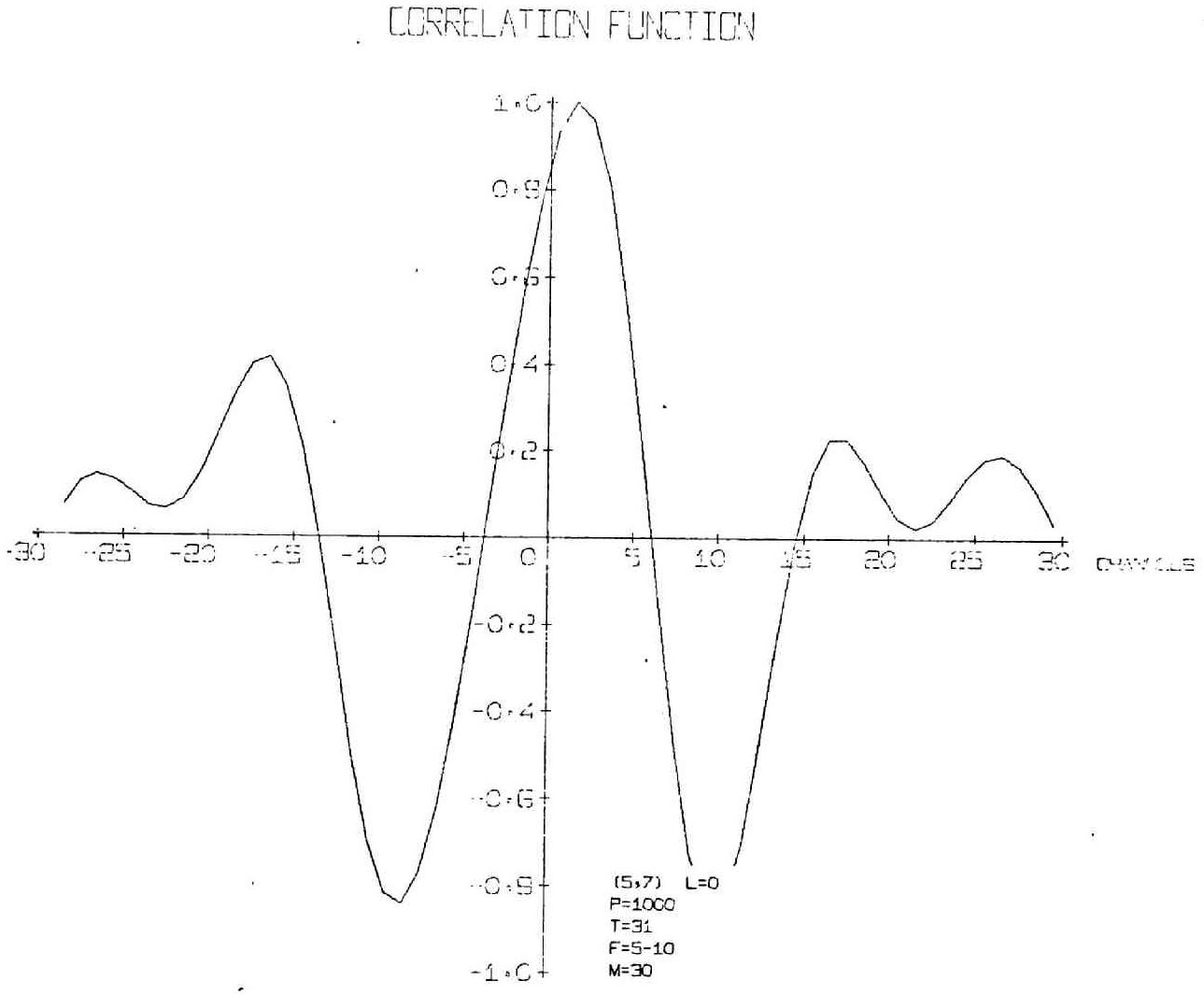

Fig. 64 Cross-correlation Function Output - 27

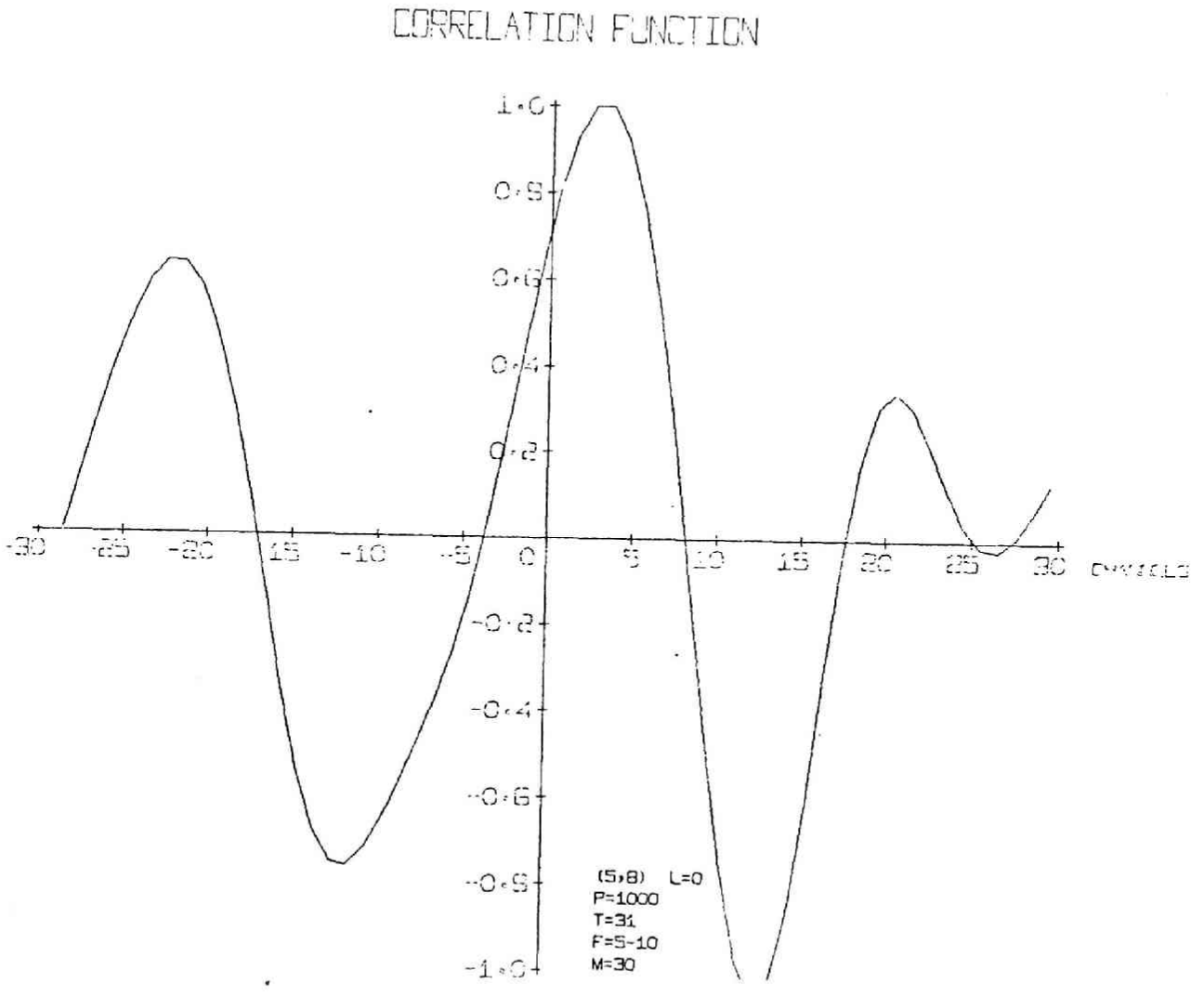

Fig. 65 Cross-correlation Function Output - 28

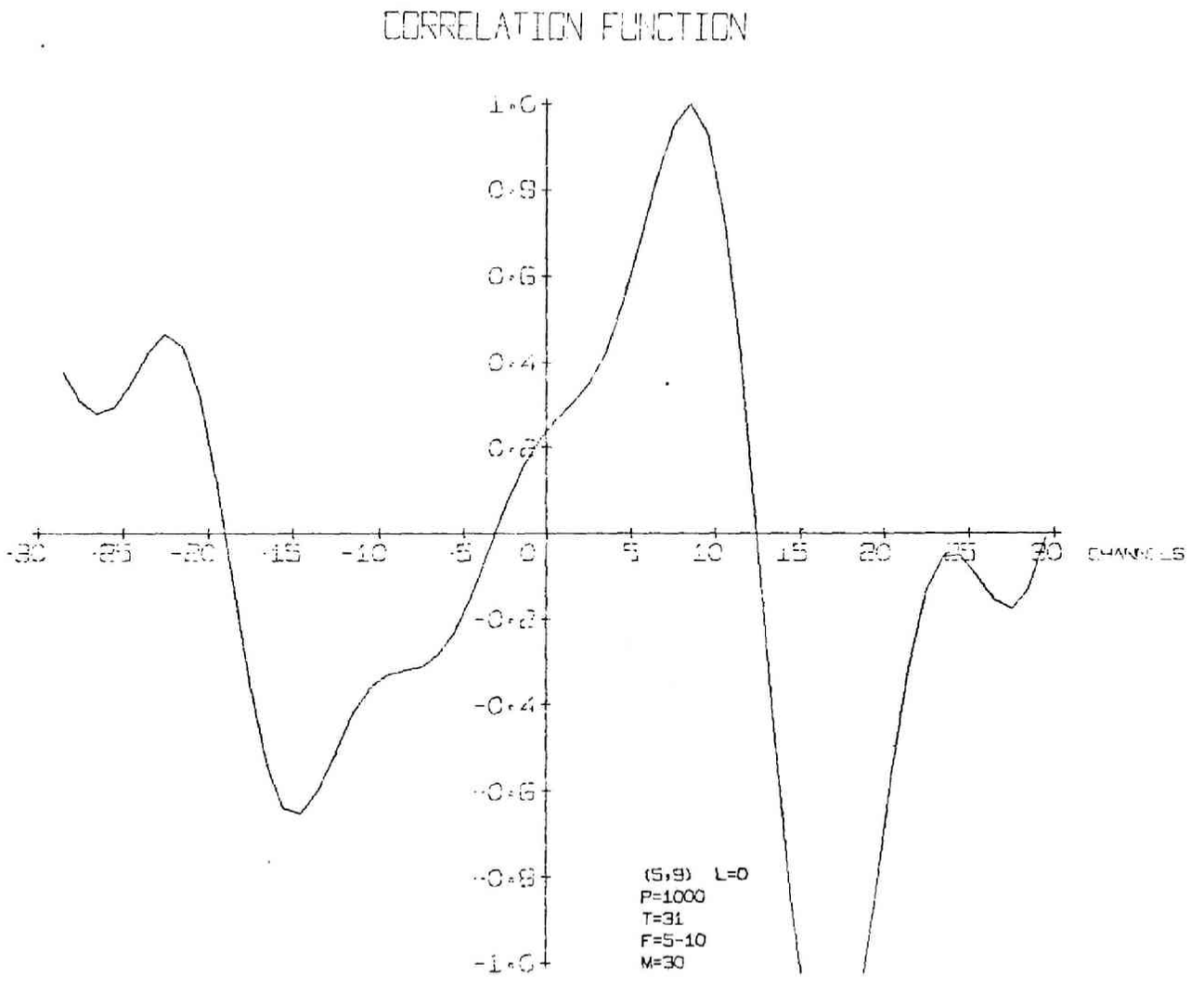

Fig. 66 Cross-correlation Function Output - 29

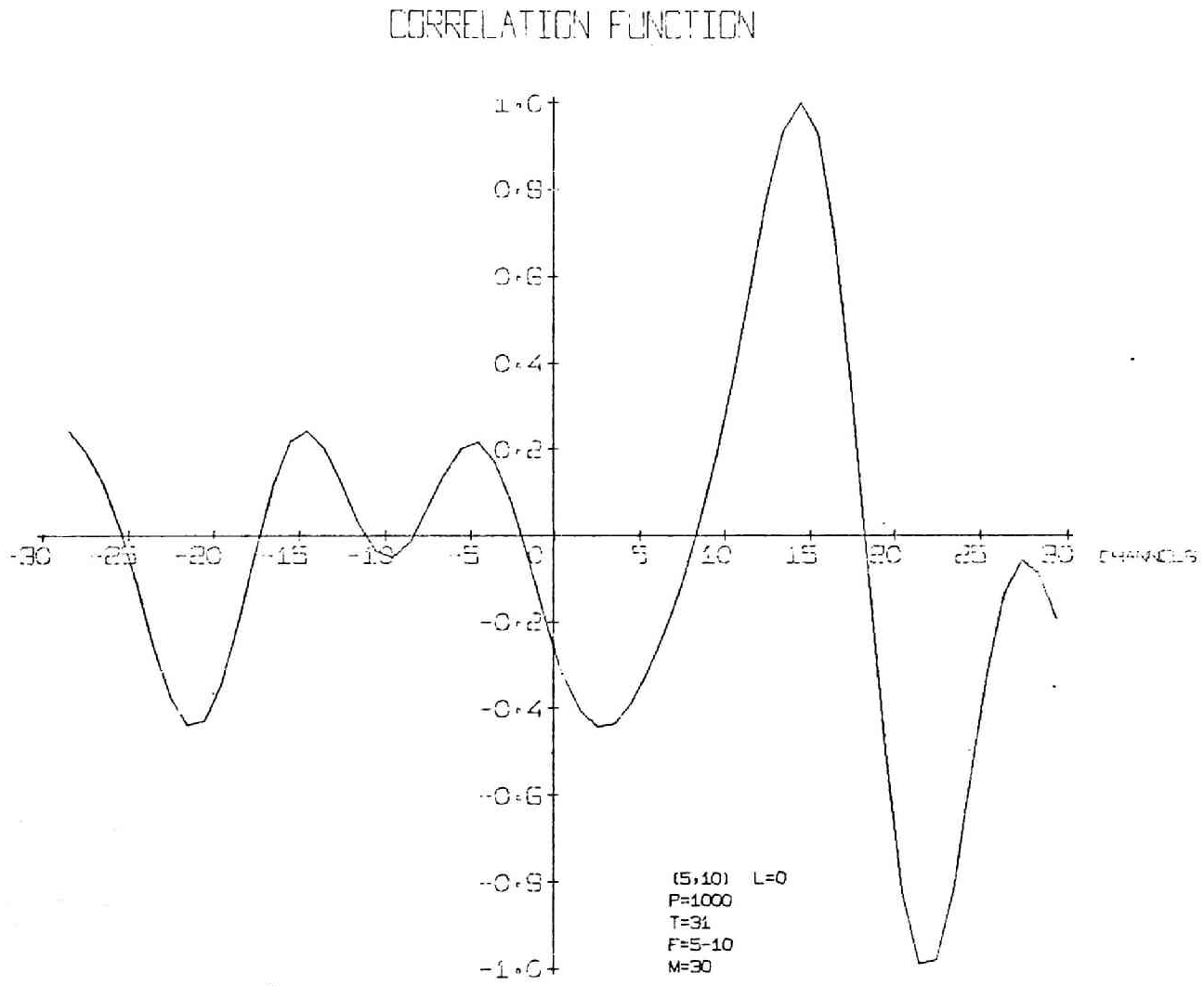

Fig. 67 Cross-correlation Function Output - 30

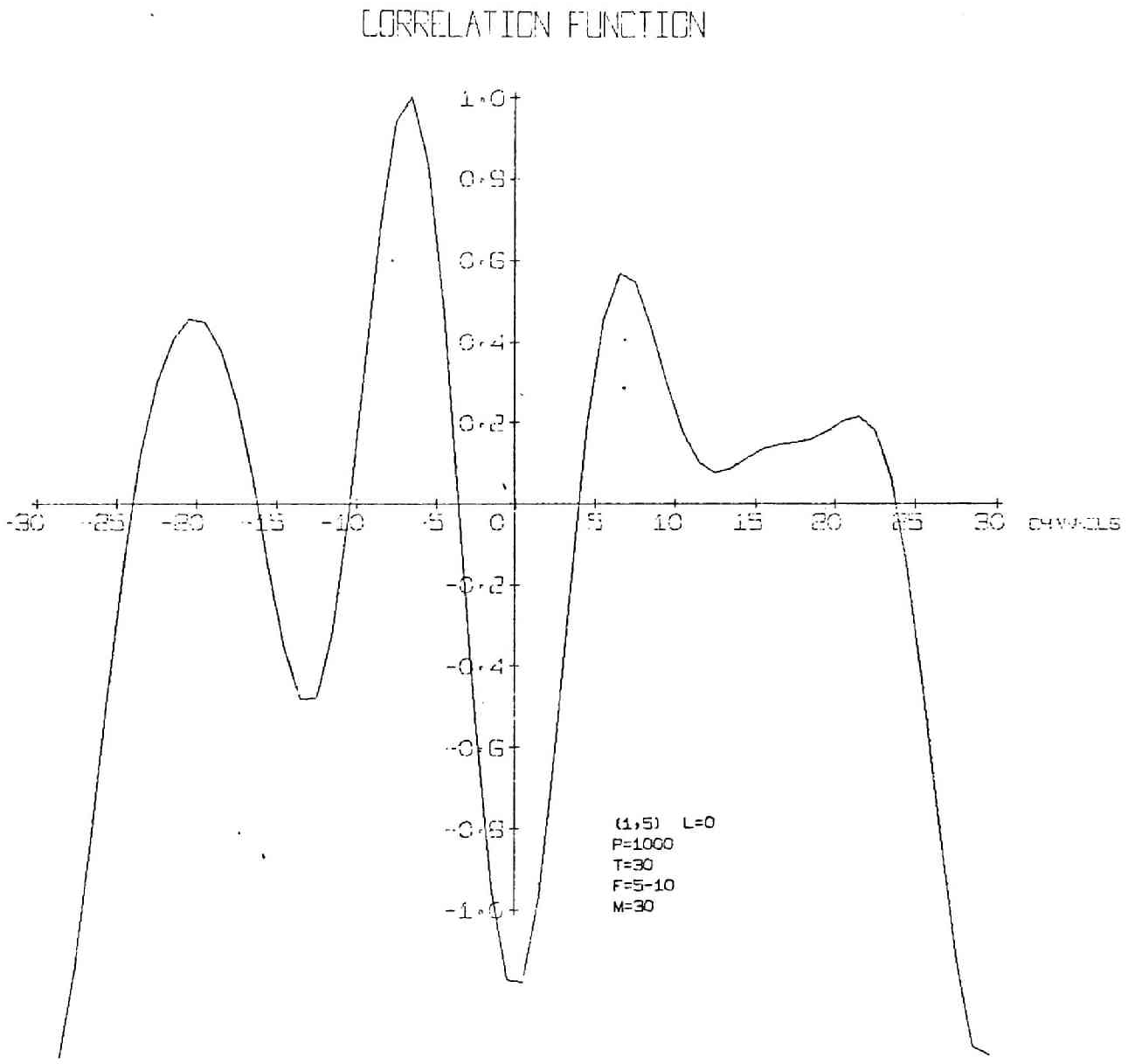

Fig. 68 Cross-correlation Function Output - 31

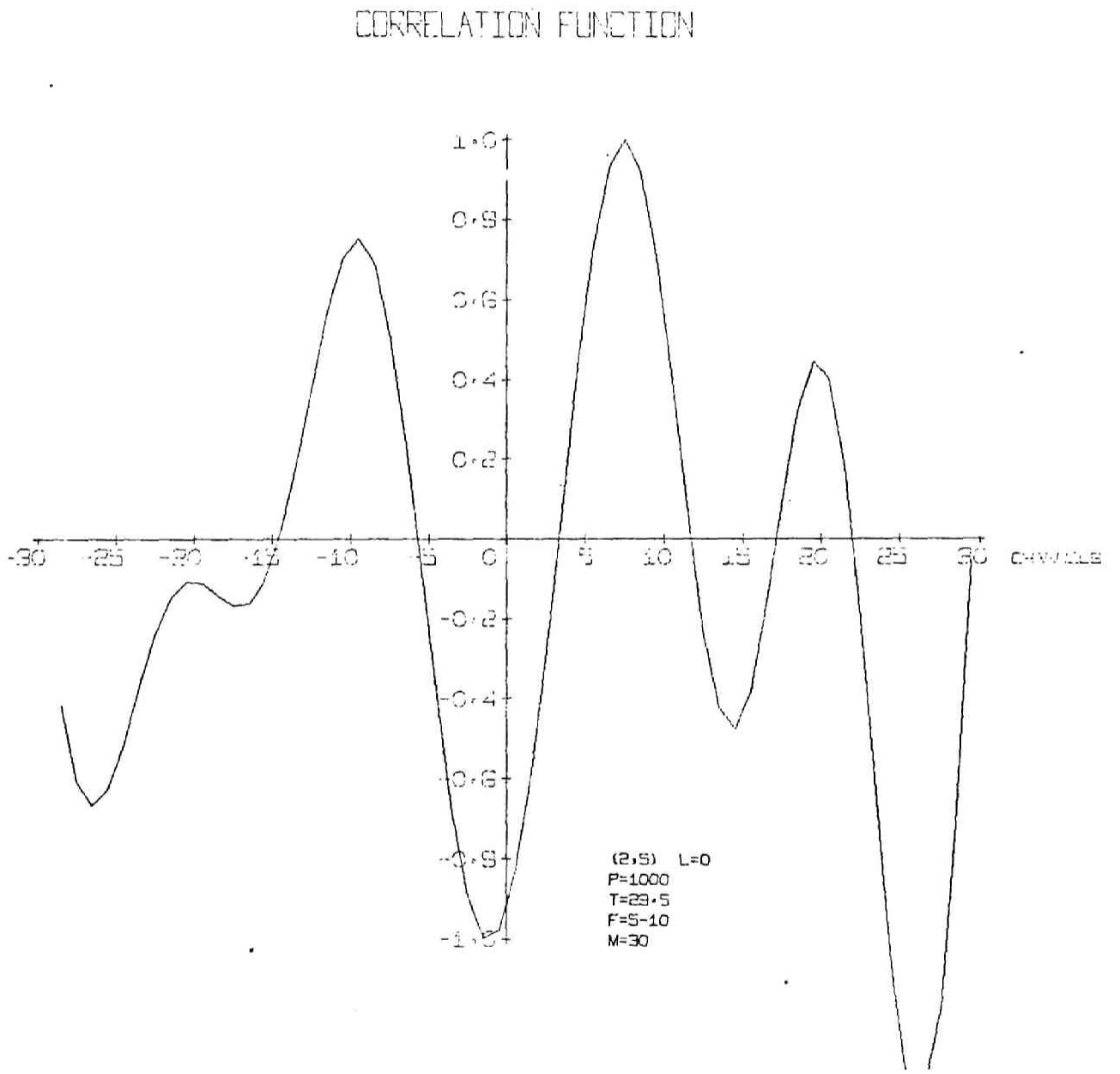

Fig. 69 Cross-correlation Function Output - 32

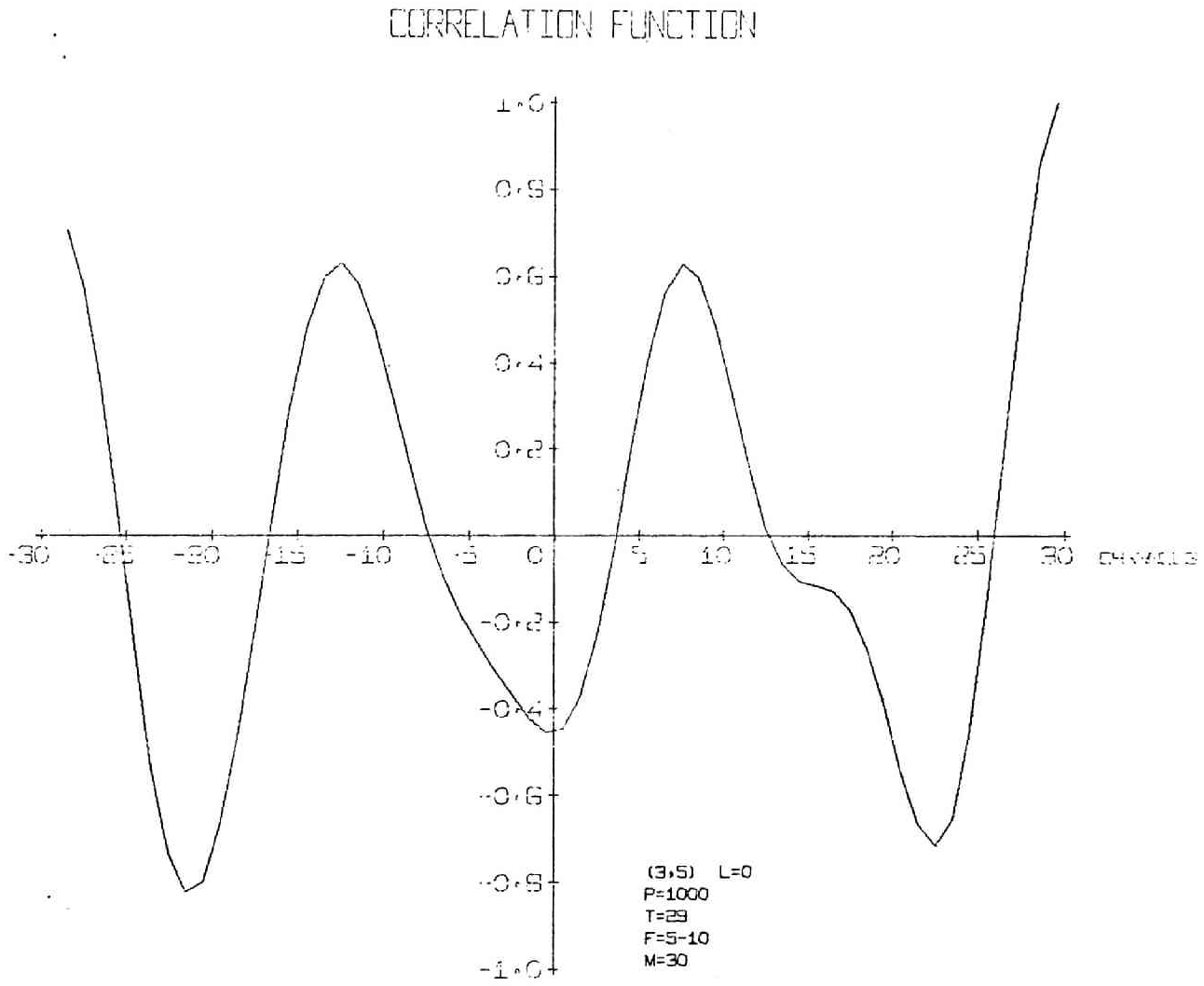

Fig. 70 Cross-correlation Function Output - 33

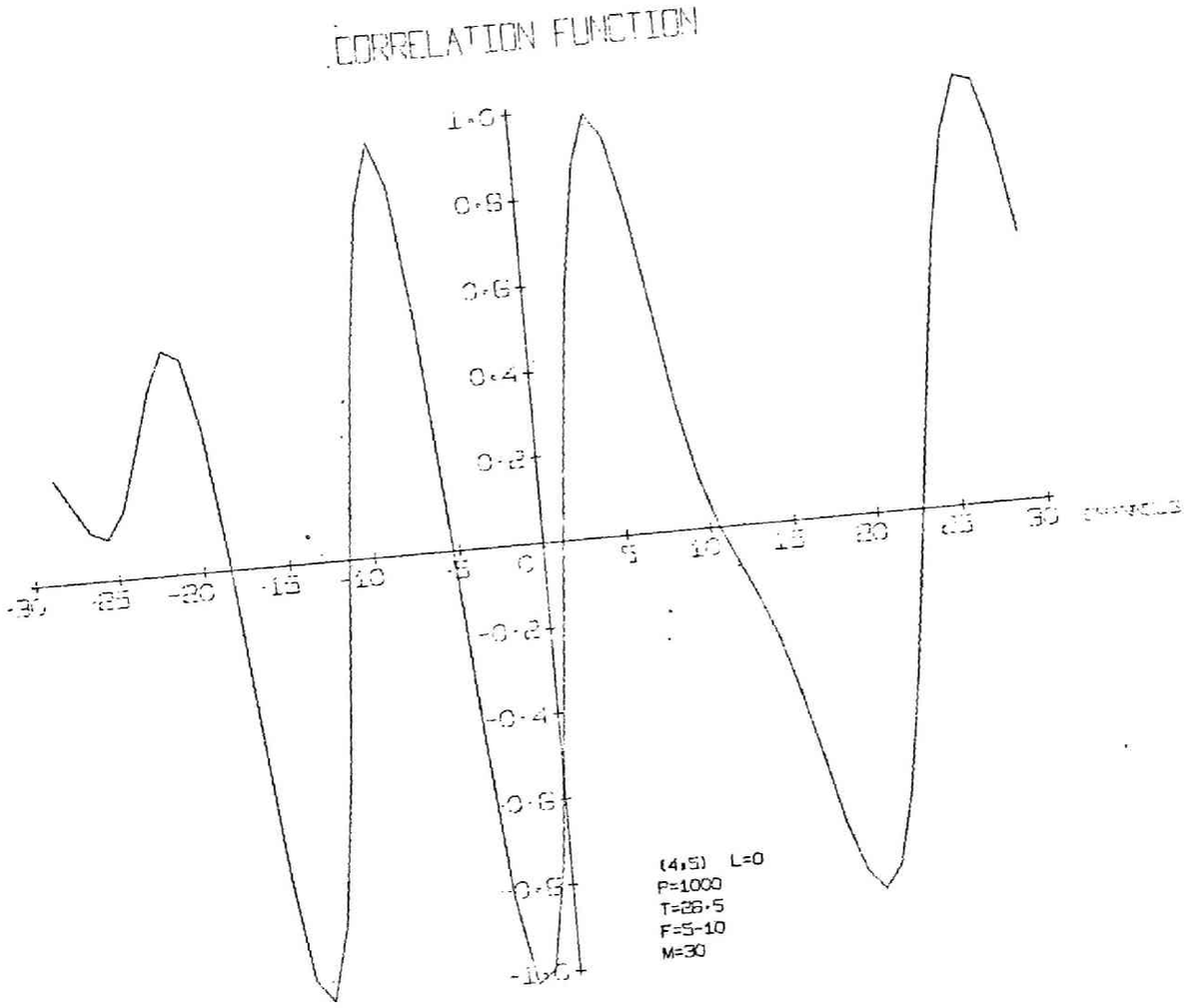

Fig. 71 Cross-correlation Function Output - 34

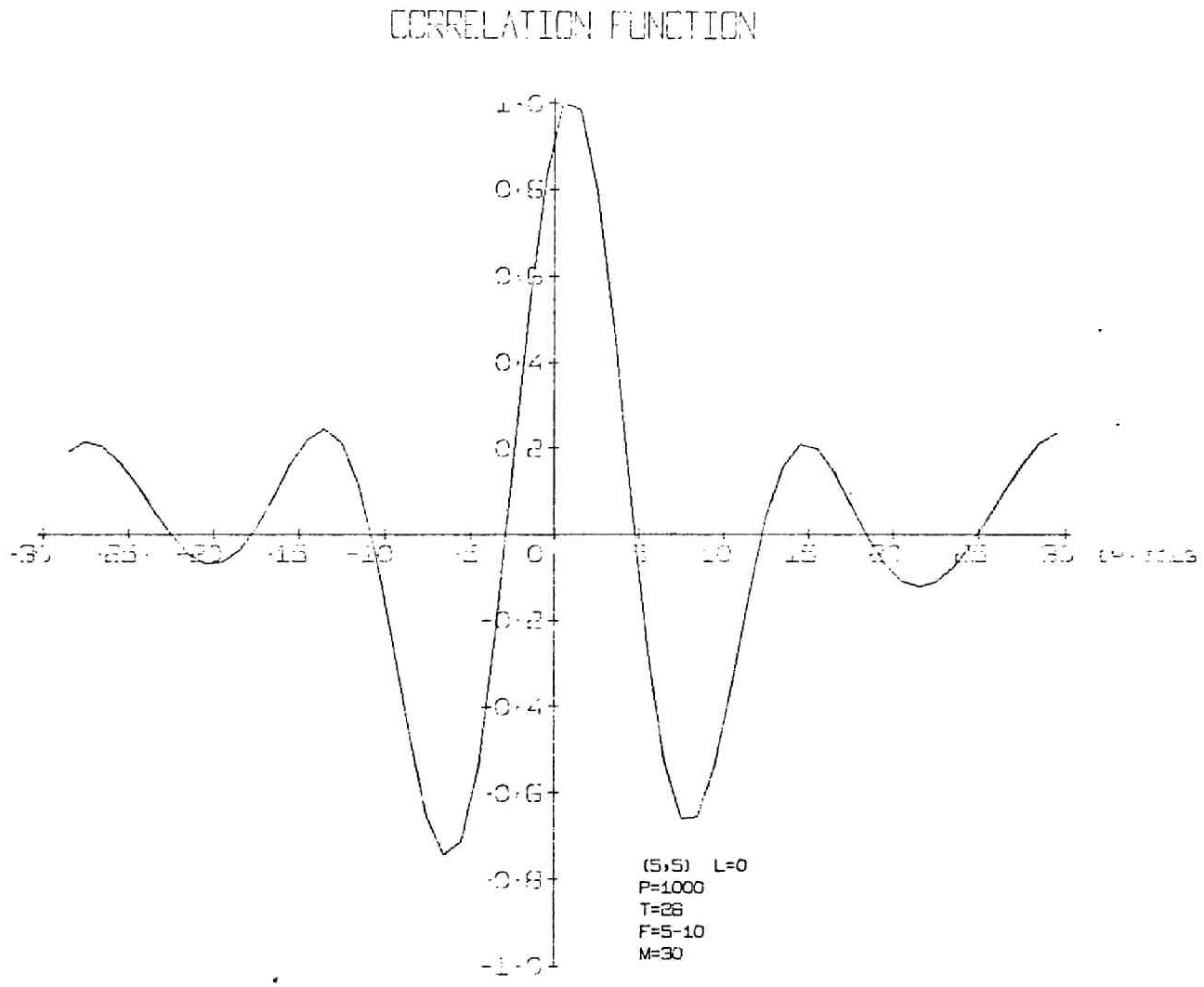

Fig. 72 Cross-correlation Function Output - 35

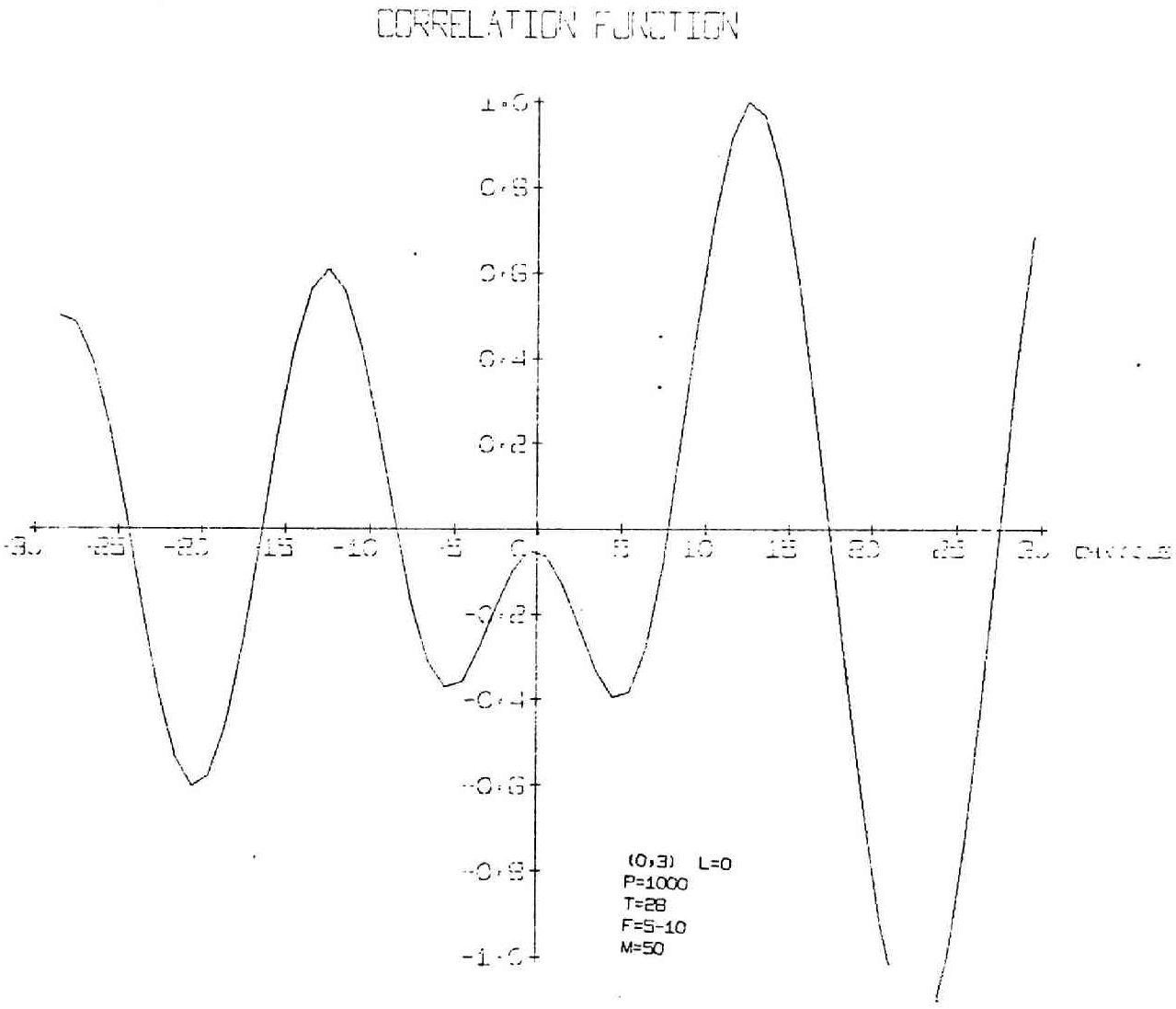

Fig. 73 Cross-correlation Function Output - 36

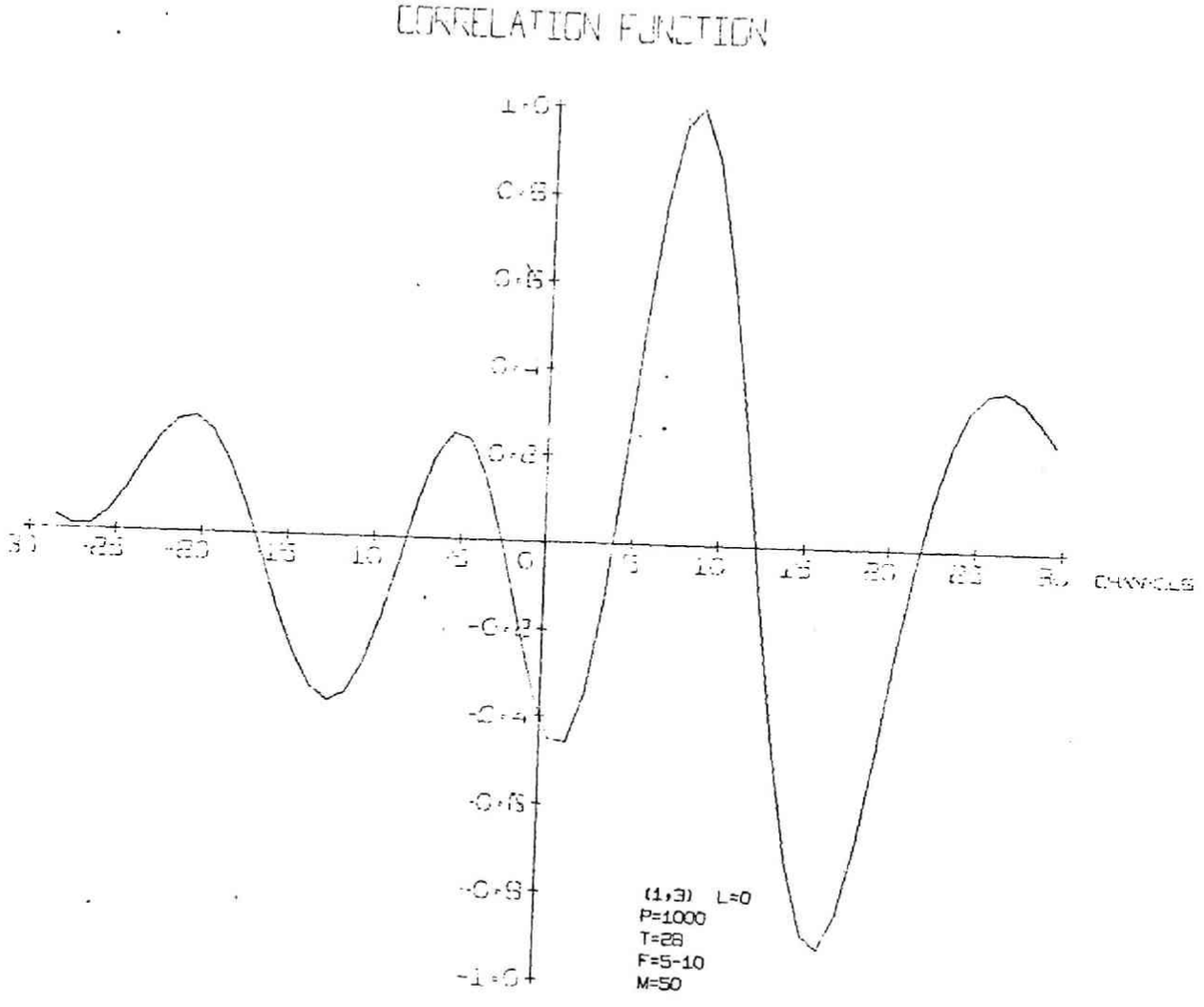

Fig. 74 Cross-correlation Function Output - 37

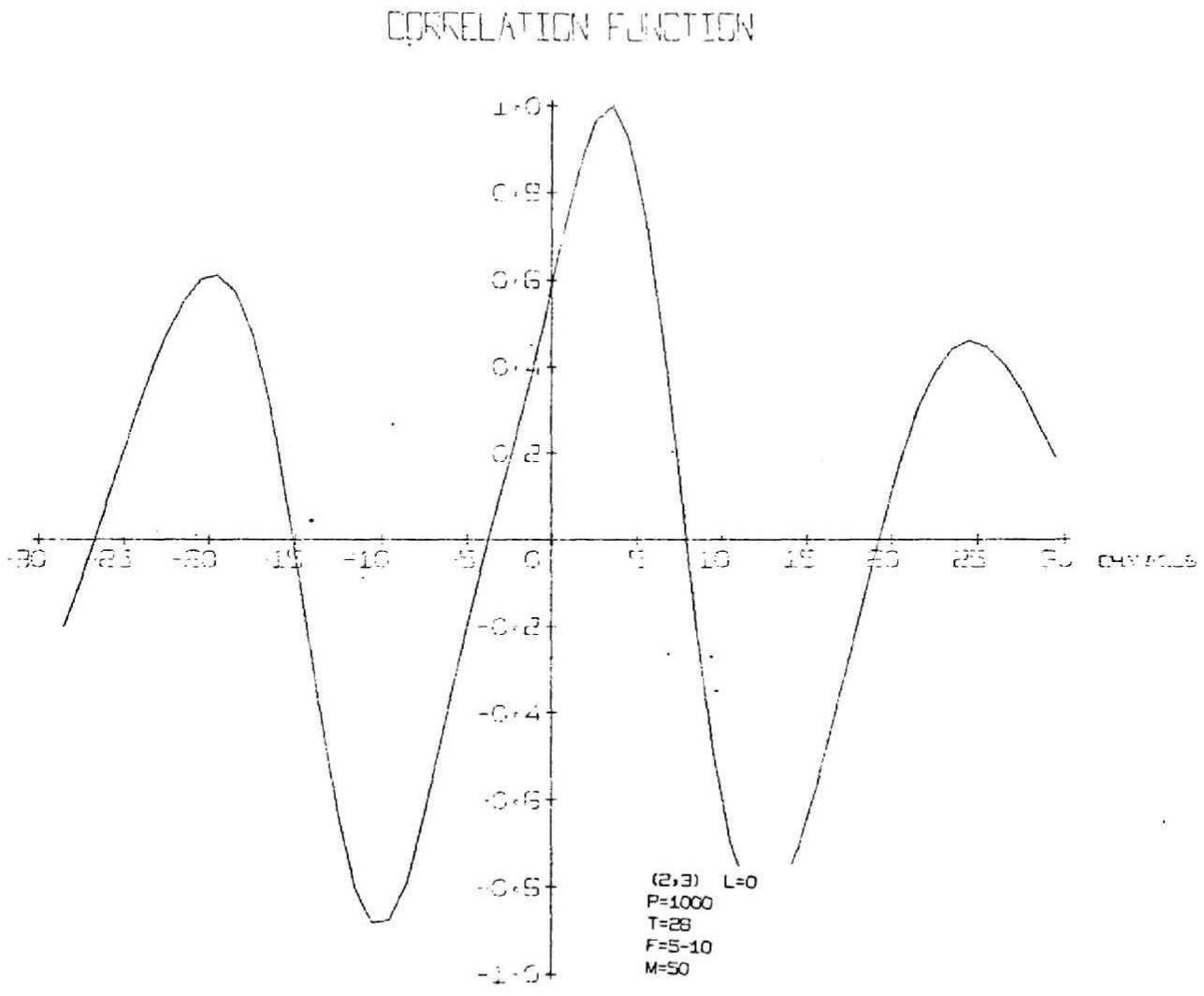

Fig. 75 Cross-correlation Function Output - 38

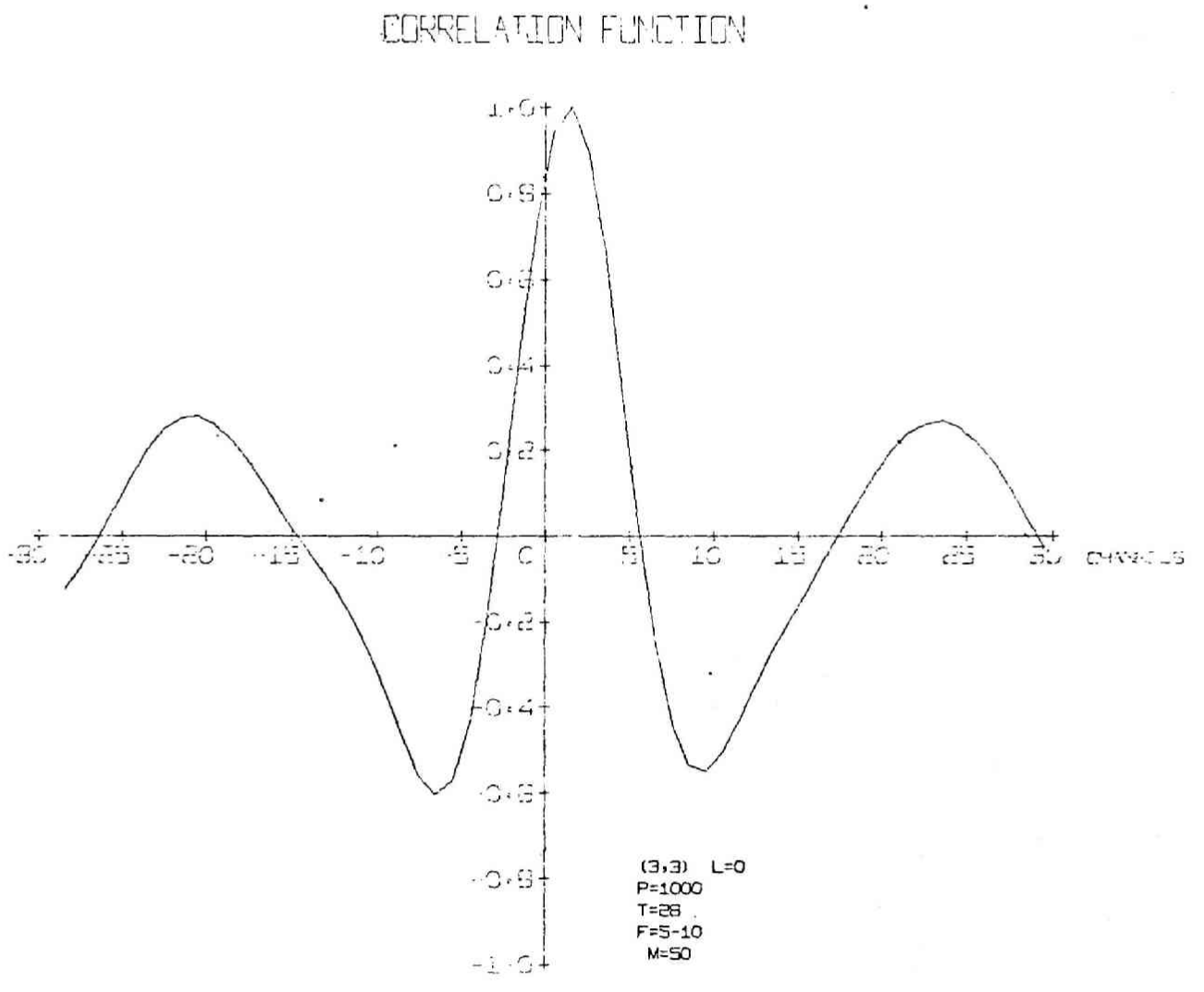

Fig. 76 Cross-correlation Function Output - 39

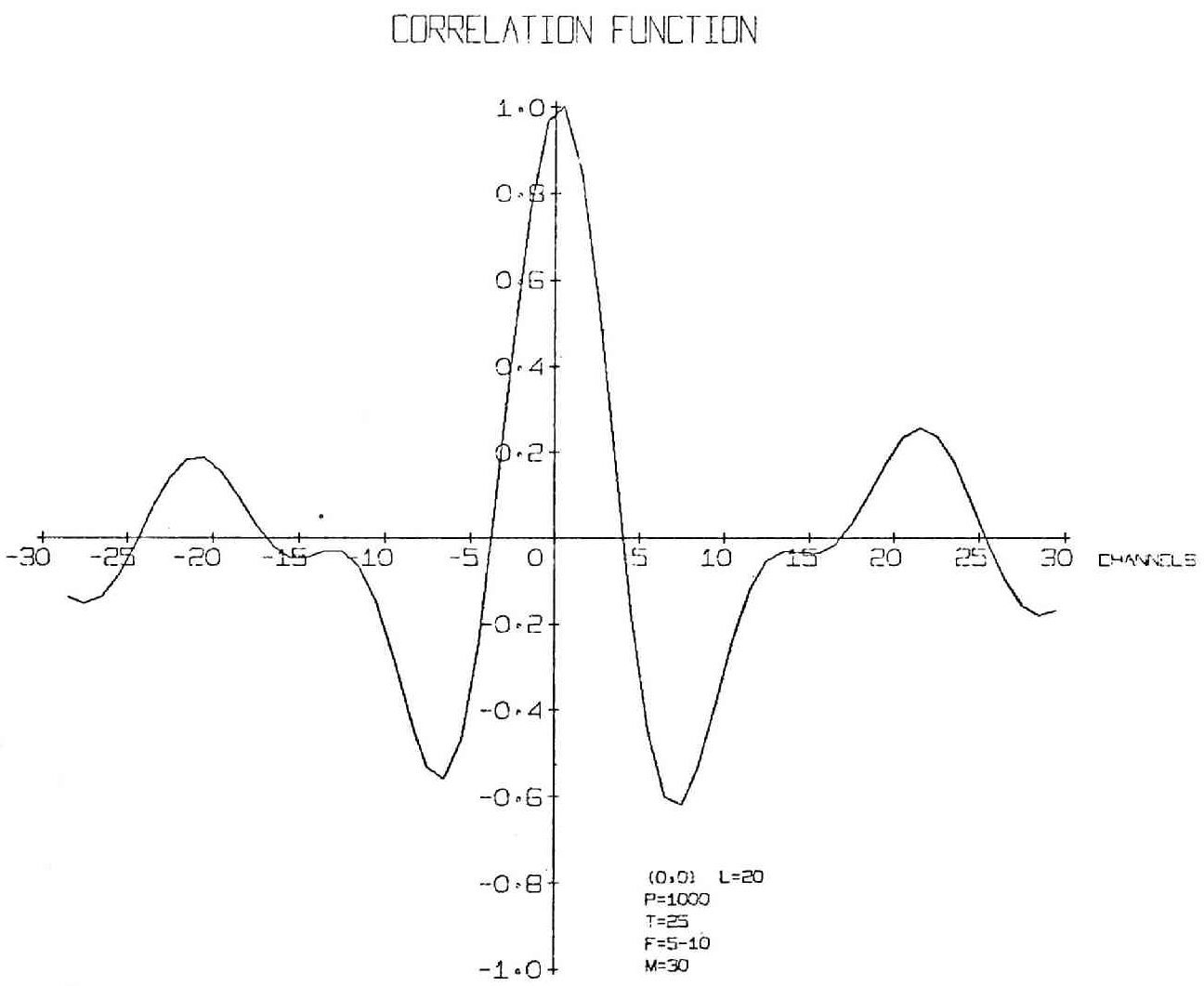

Fig. 77 Cross-correlation Function Output - 40

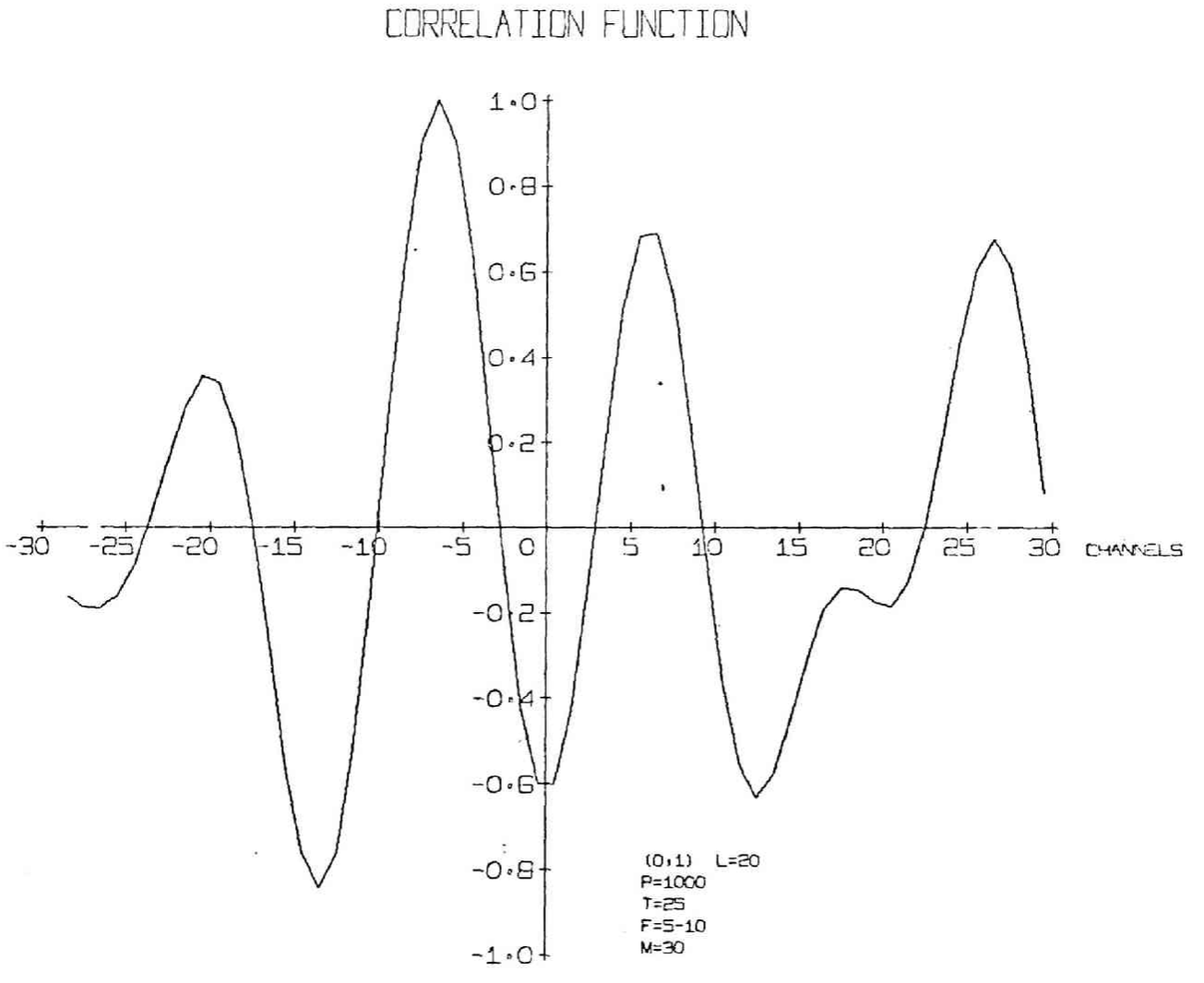

Fig. 78 Cross-correlation Function Output - 41

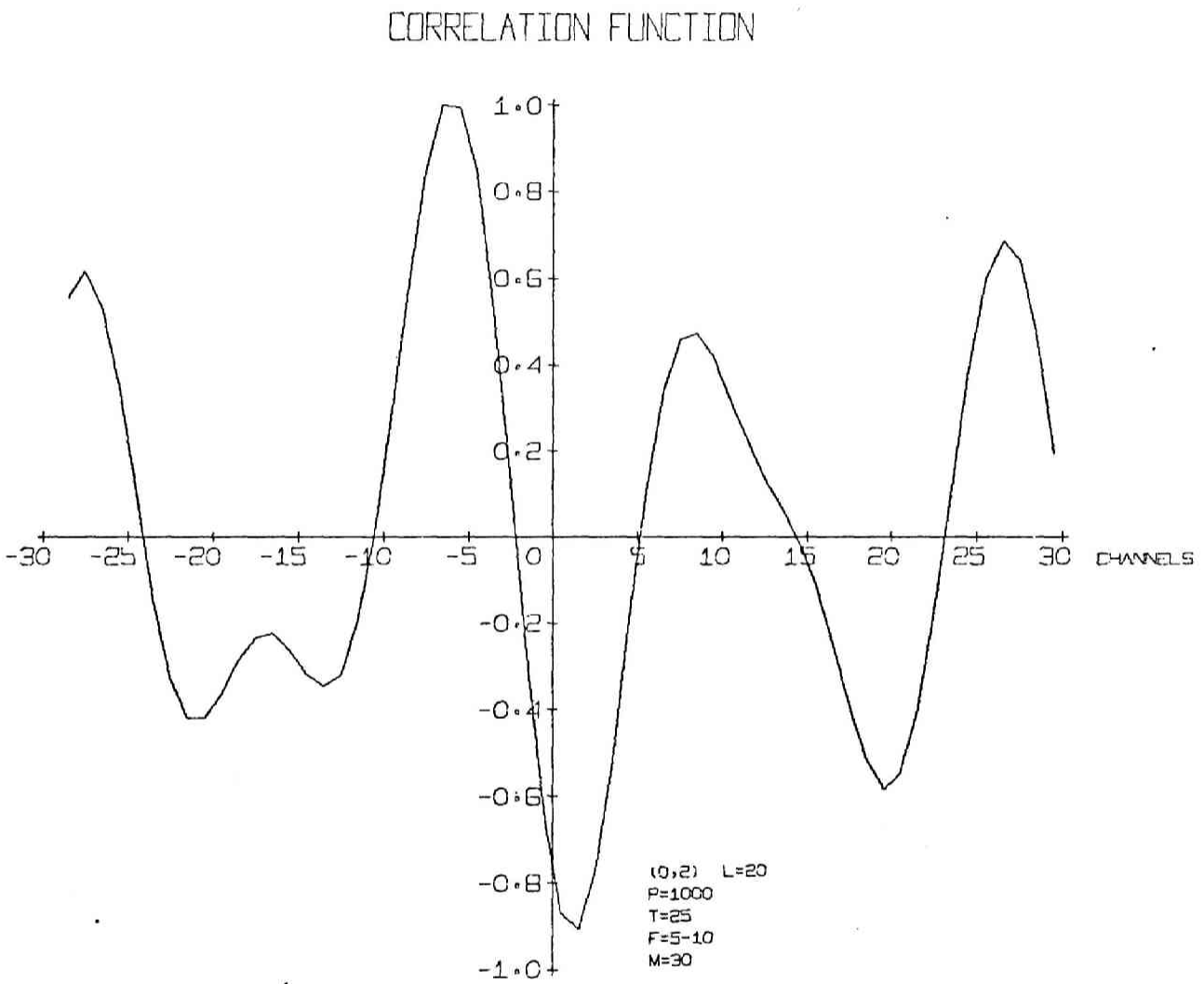

Fig. 79 Cross-correlation Function Output - 42

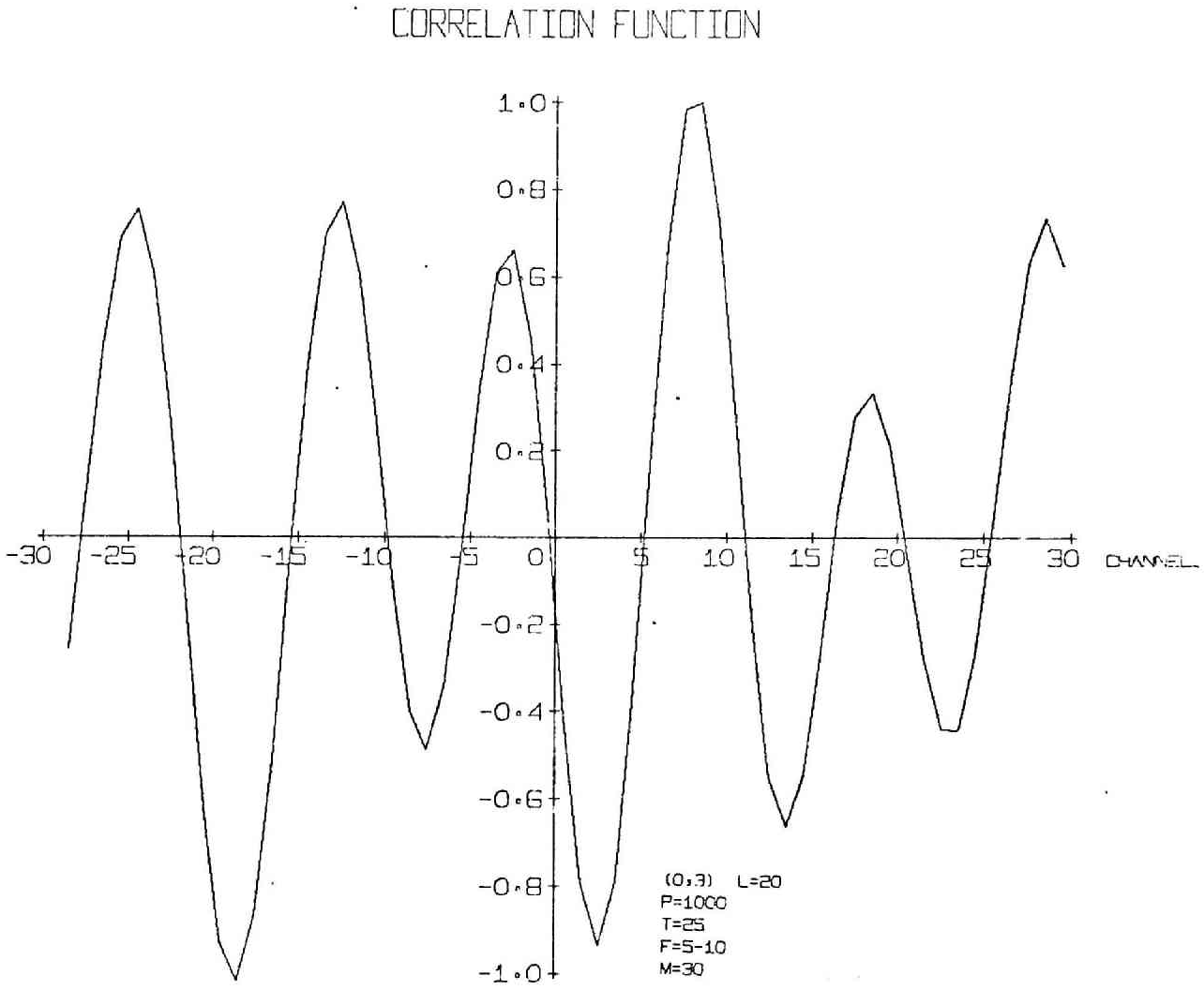

Fig. 80 Cross-correlation Function Output - 43

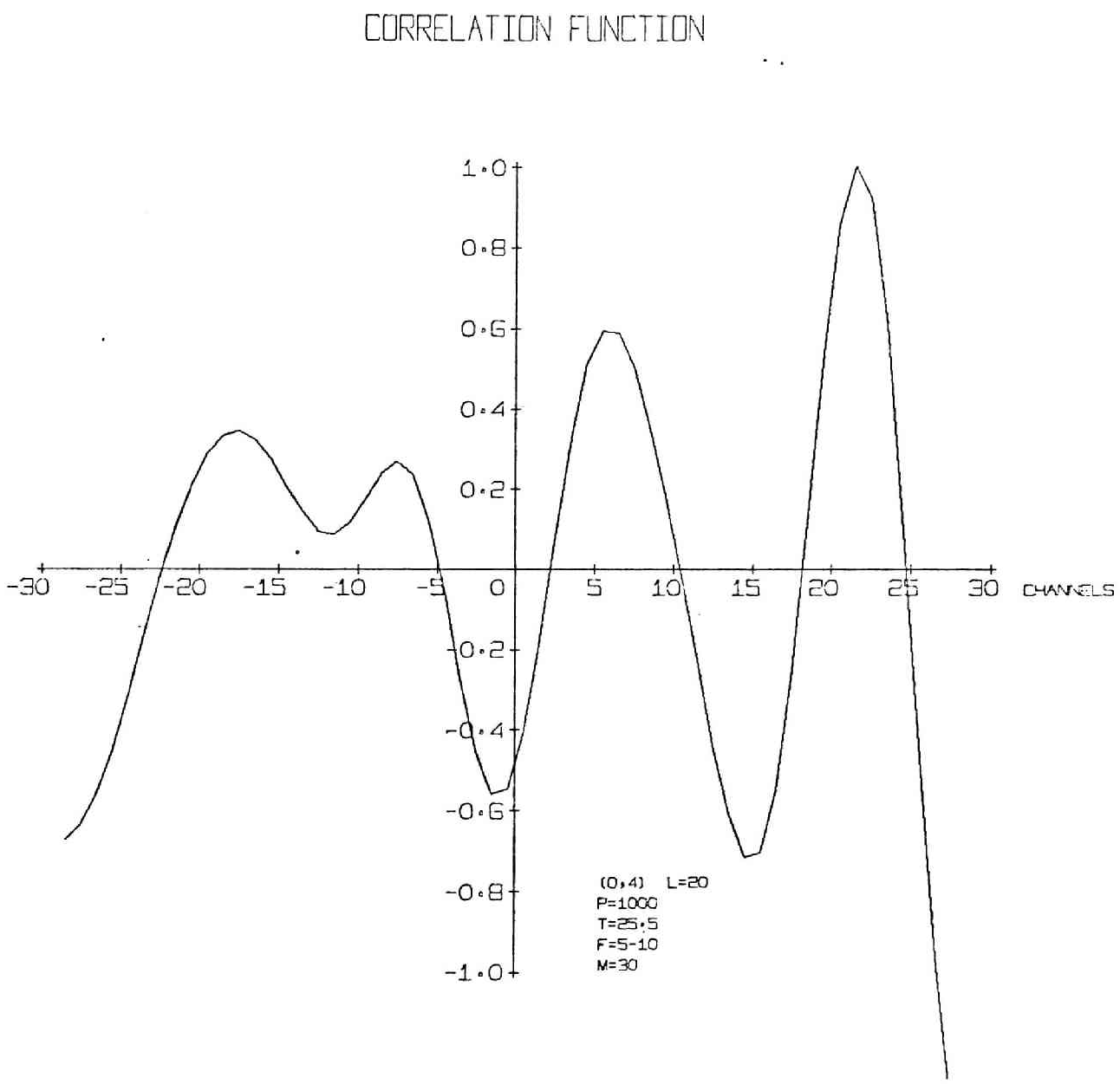

Fig. 81 Cross-correlation Function Output - 44

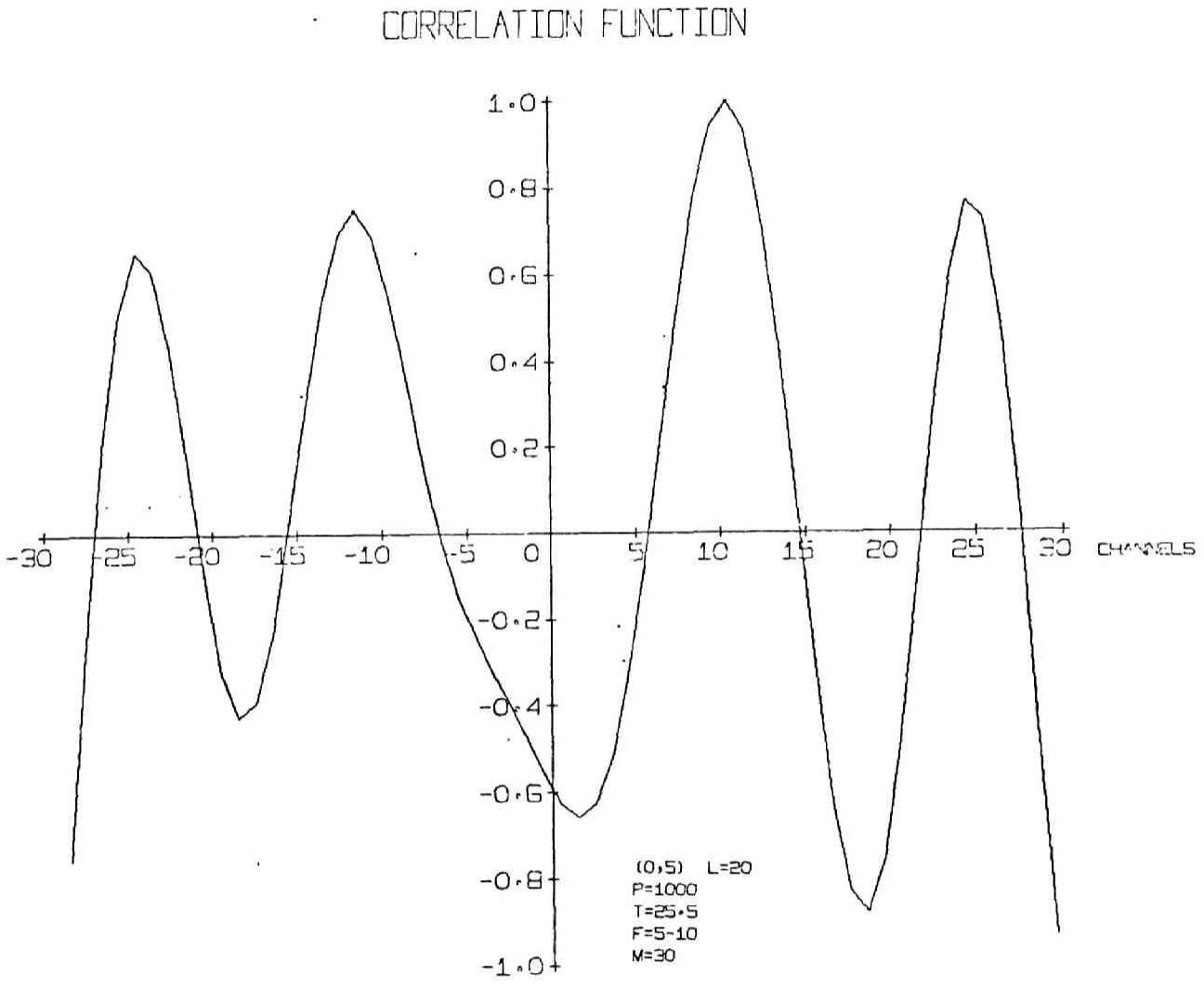

Fig. 82 Cross-correlation Function Output - 45

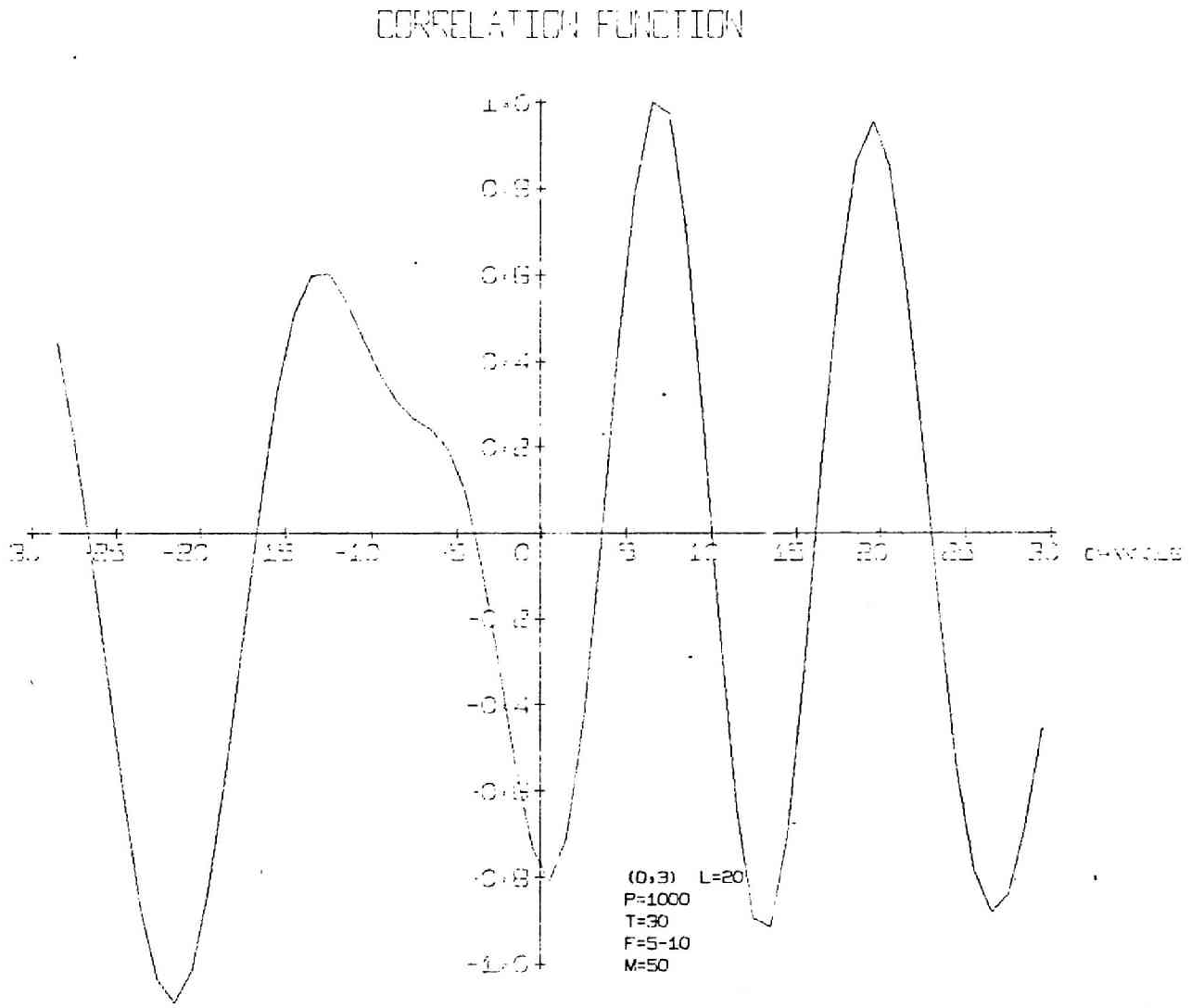

Fig. 83 Cross-correlation Function Output - 46

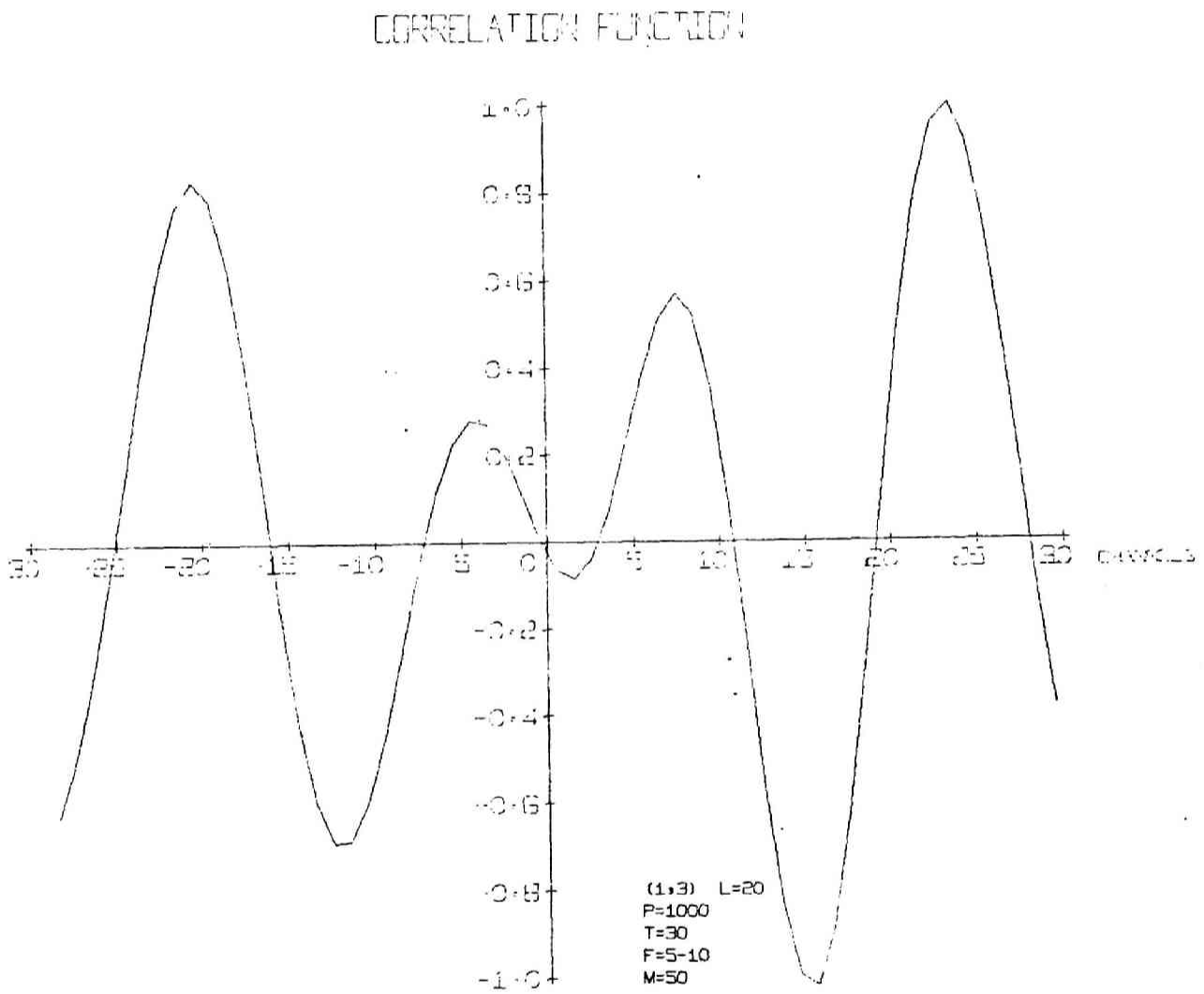

Fig. 84 Cross-correlation Function Output - 47

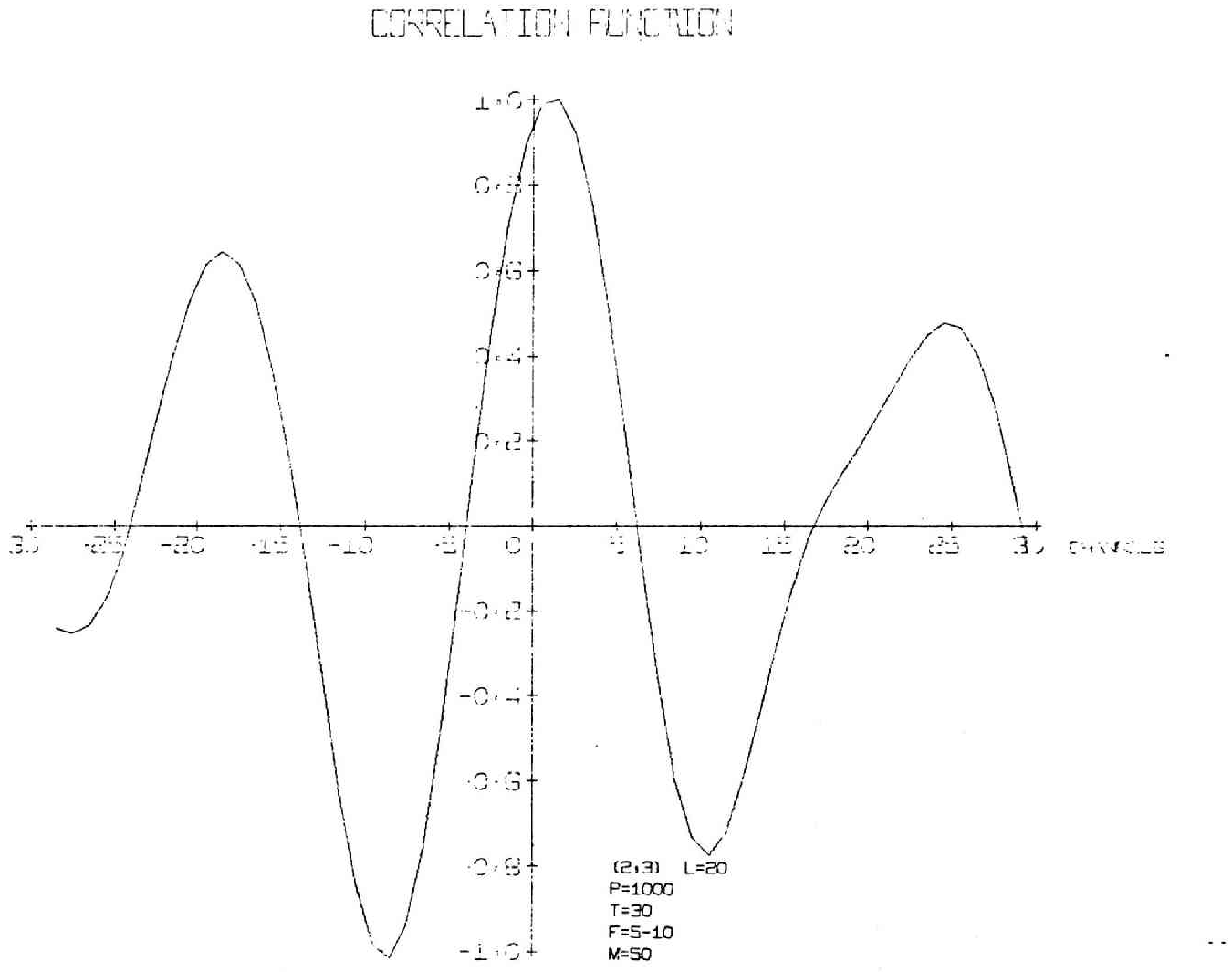

Fig. 85 Cross-correlation Function Output - 48

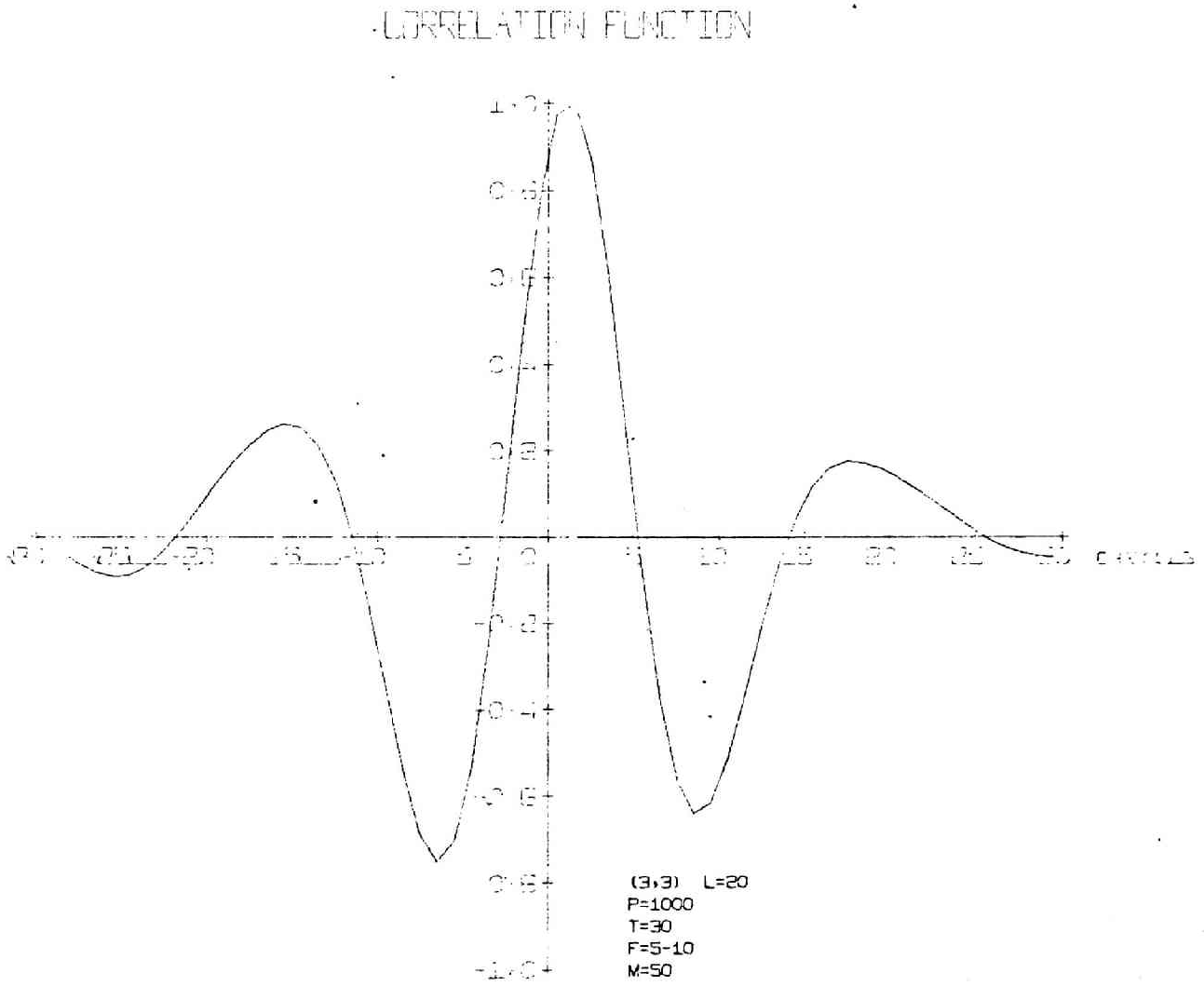

Fig. 86 Cross-correlation Function Output - 49

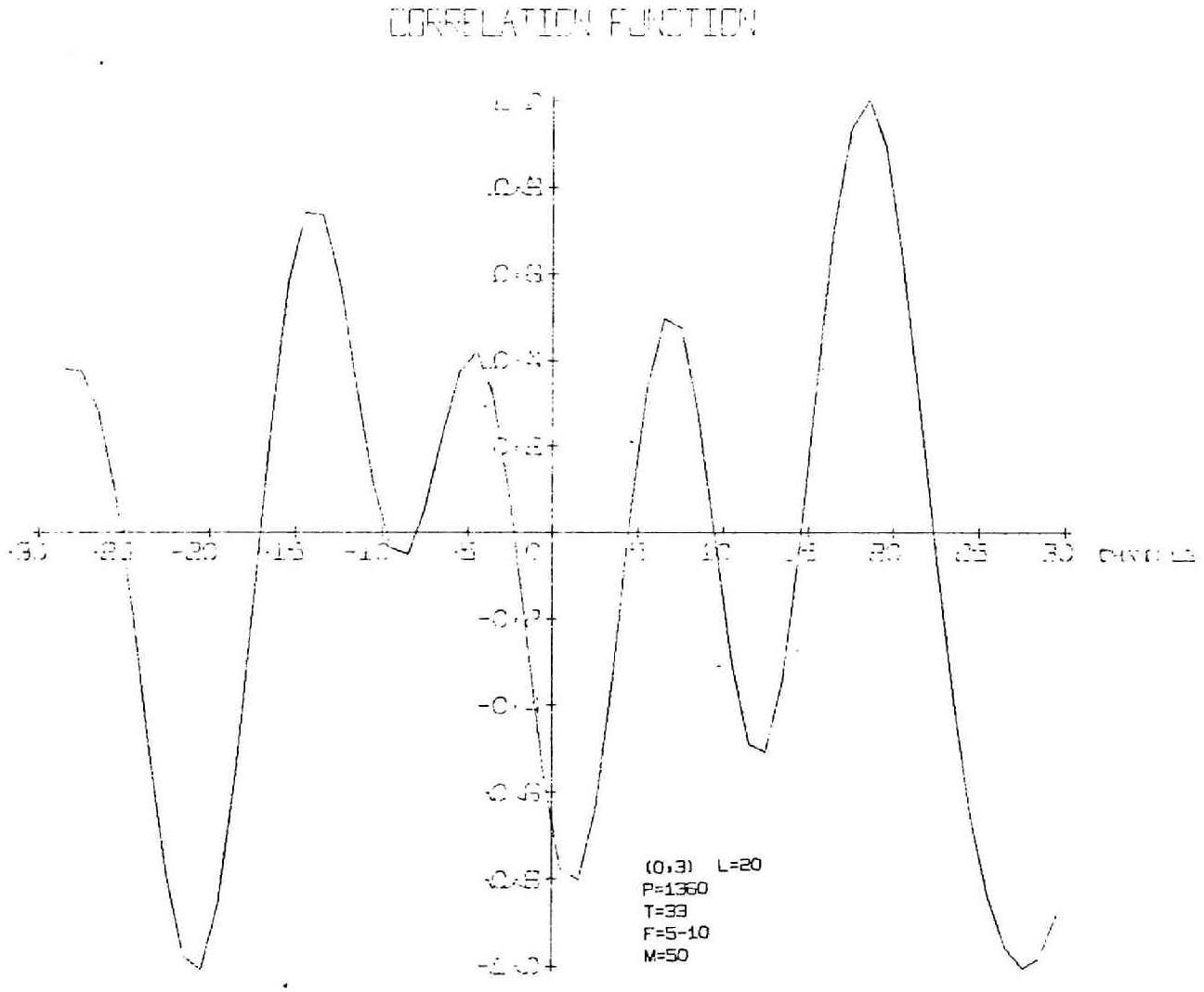

Fig. 87 Cross-correlation Function Output - 50

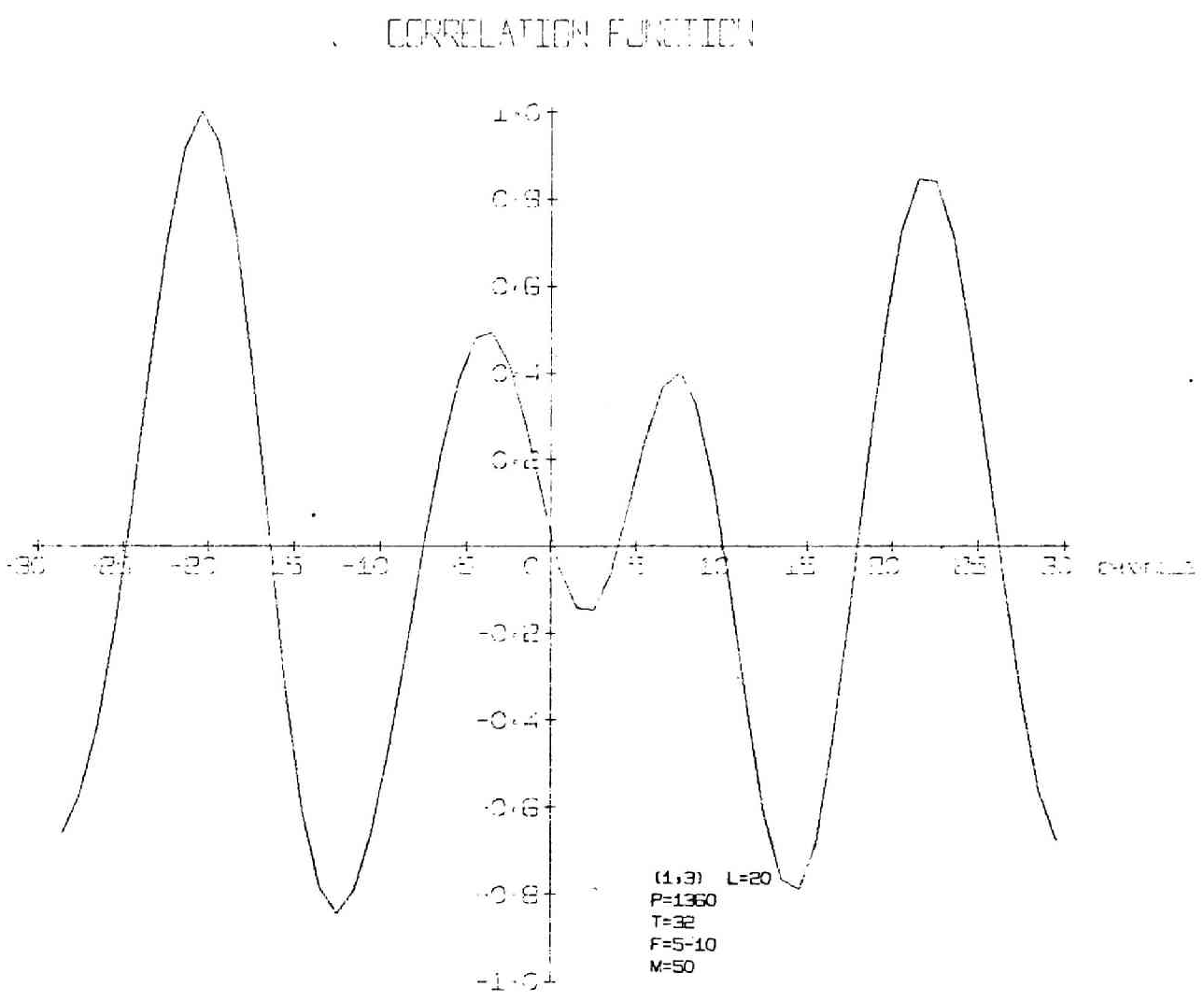

Fig. 88 Cross-correlation Function Output - 51

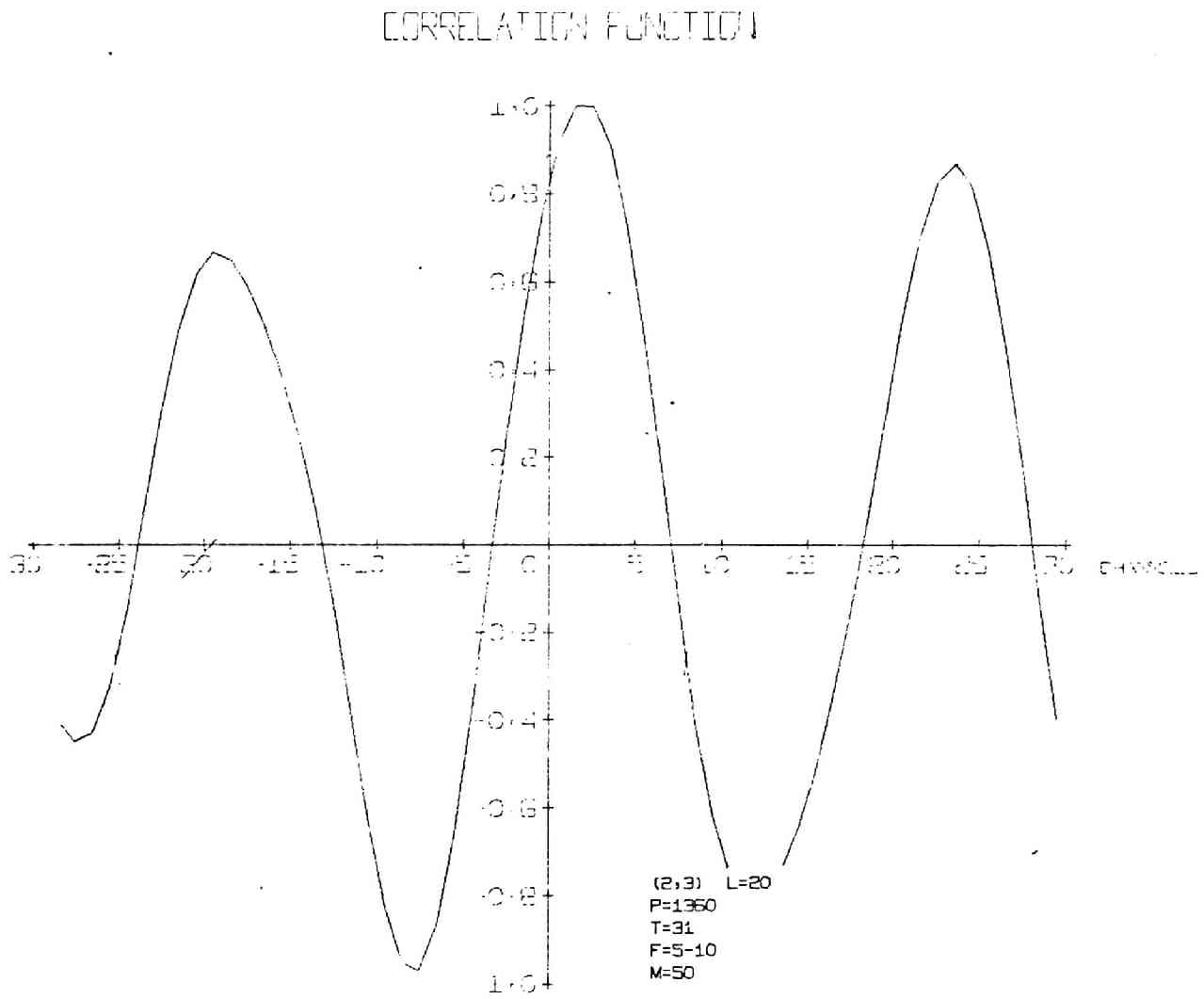

Fig. 89 Cross-correlation Function Output - 52

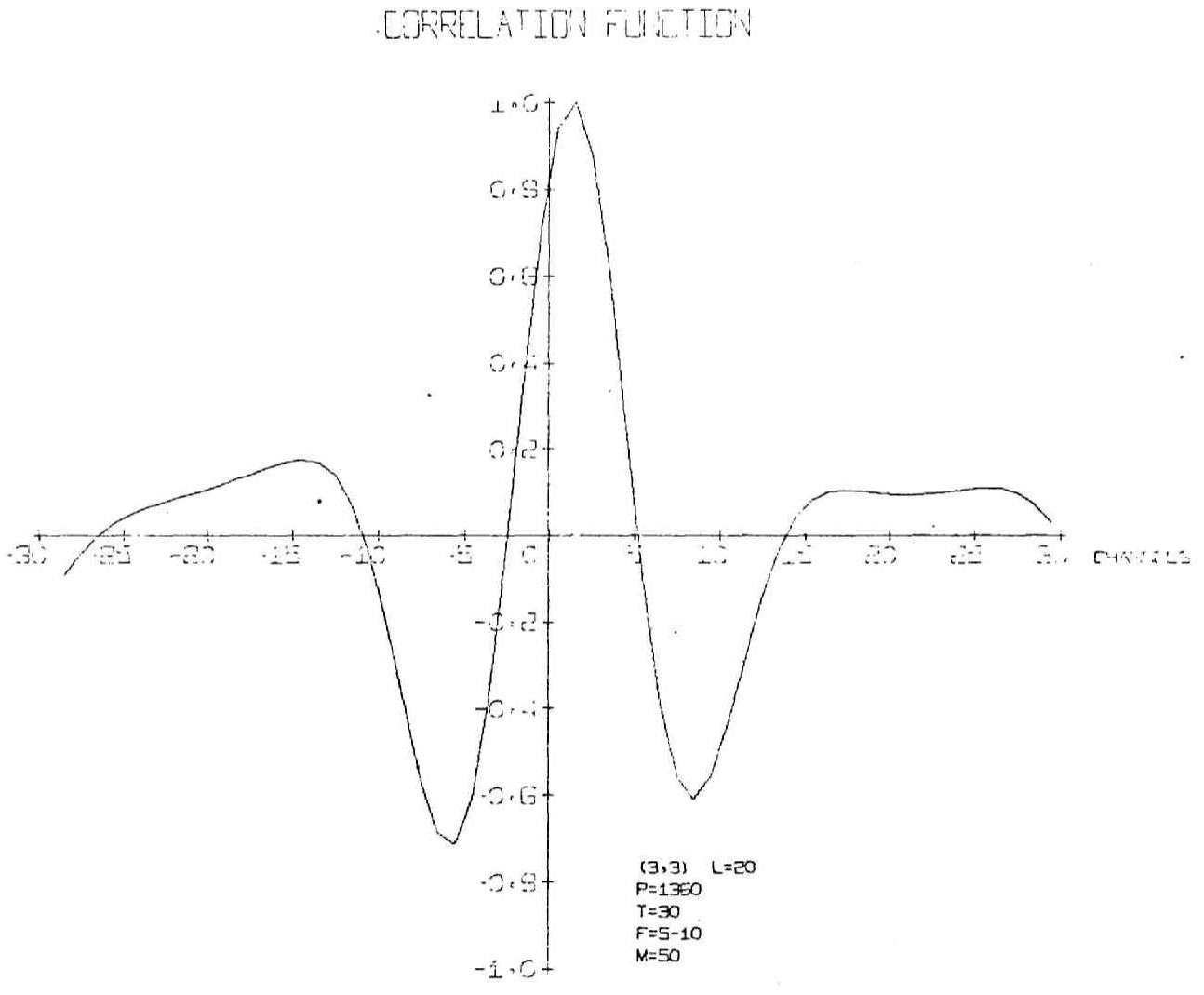

Fig. 90 Cross-correlation Function Output - 53

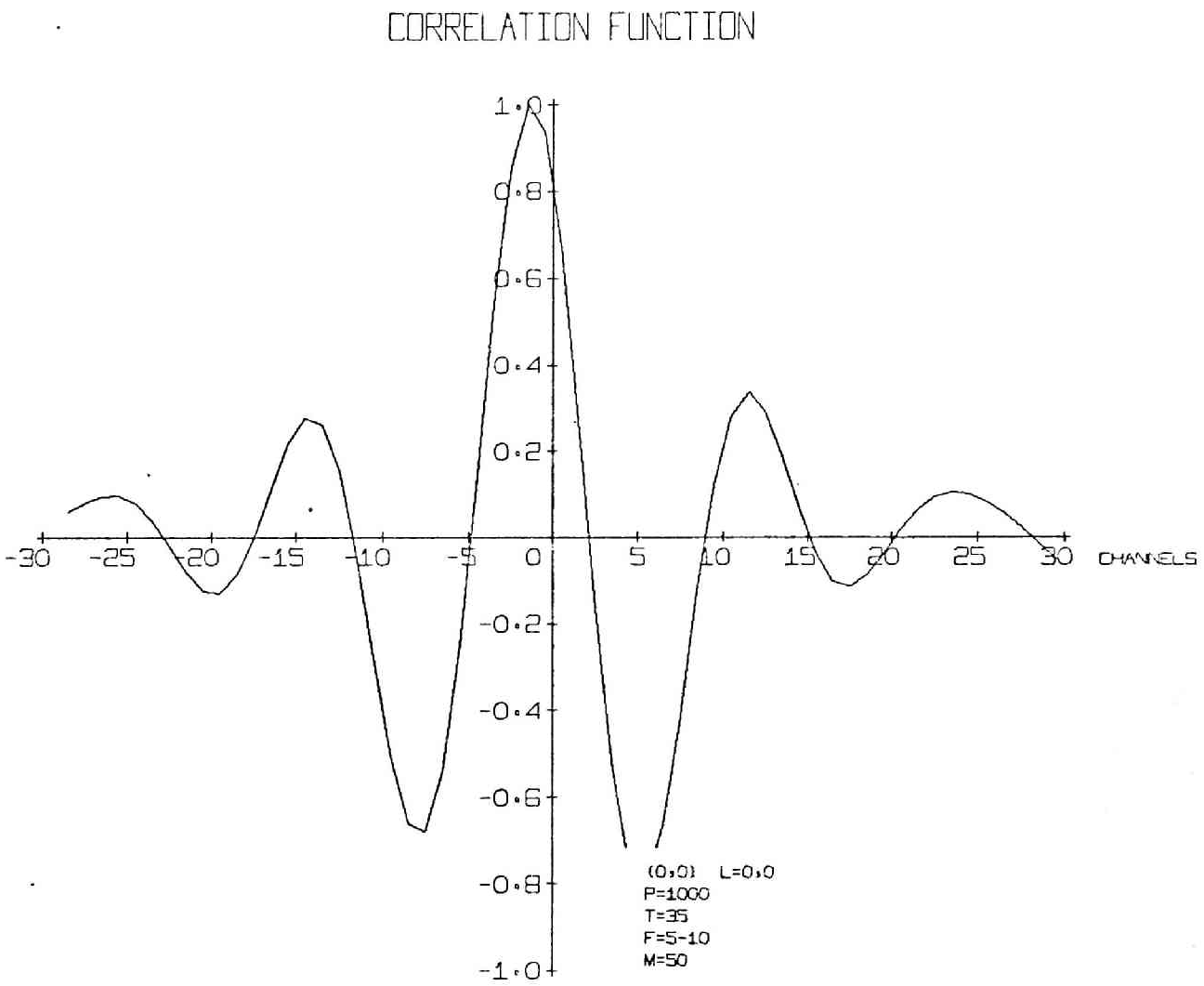

Fig. 91 Cross-correlation Function Output - 54

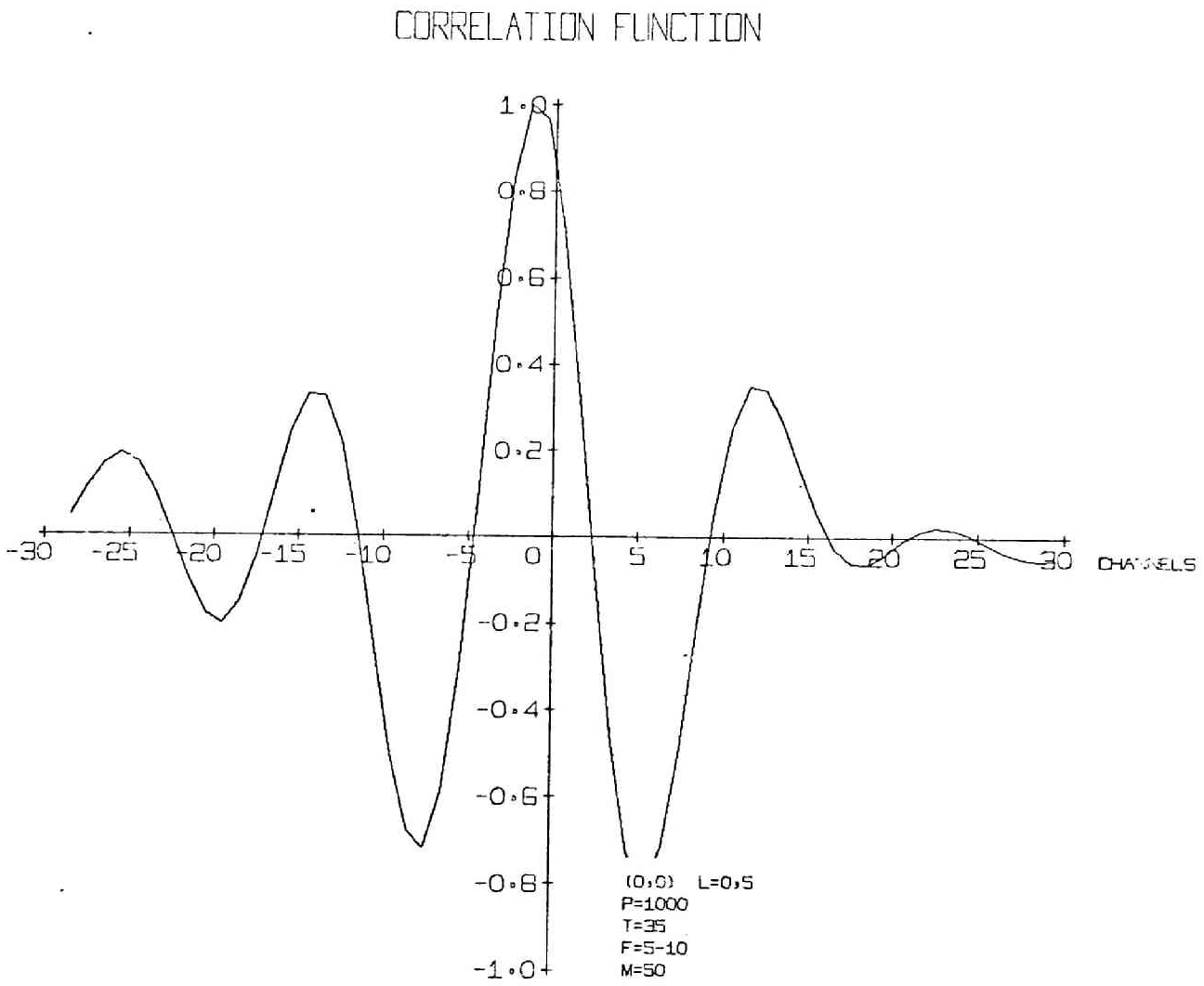

Fig. 92 Cross-correlation Function Output - 55

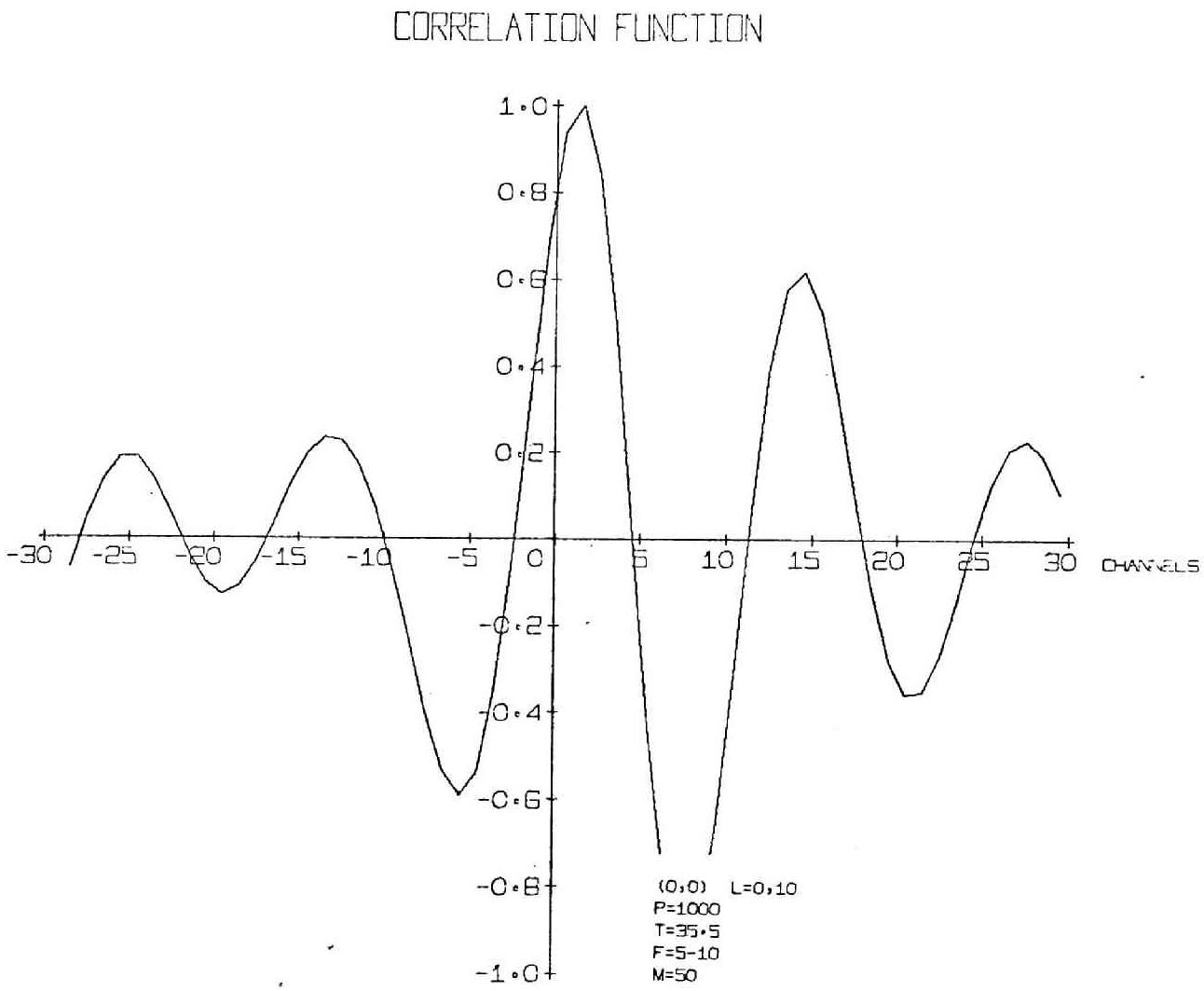

Fig. 93 Cross-correlation Function Output - 56

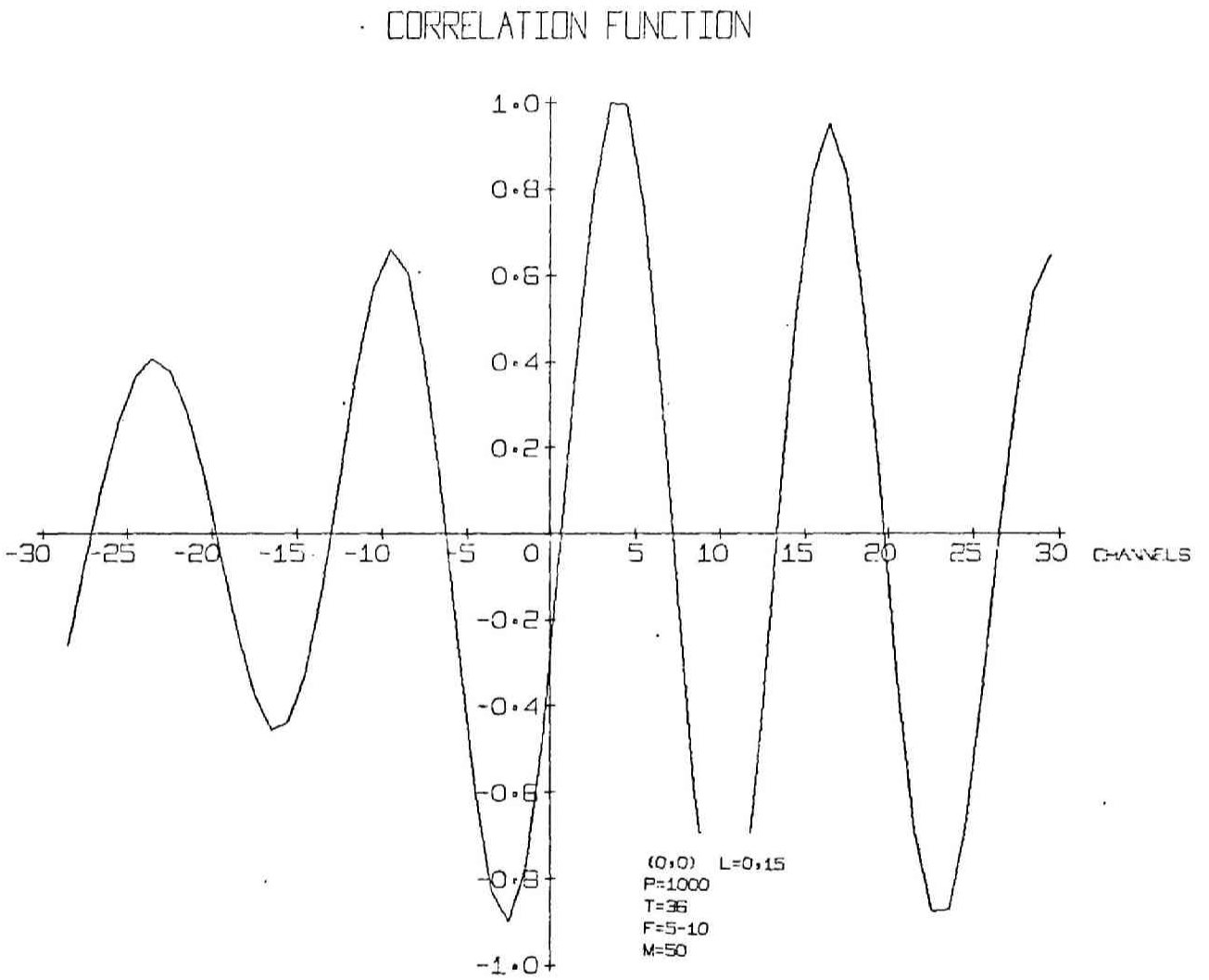

Fig. 94 Cross-correlation Function Output - 57

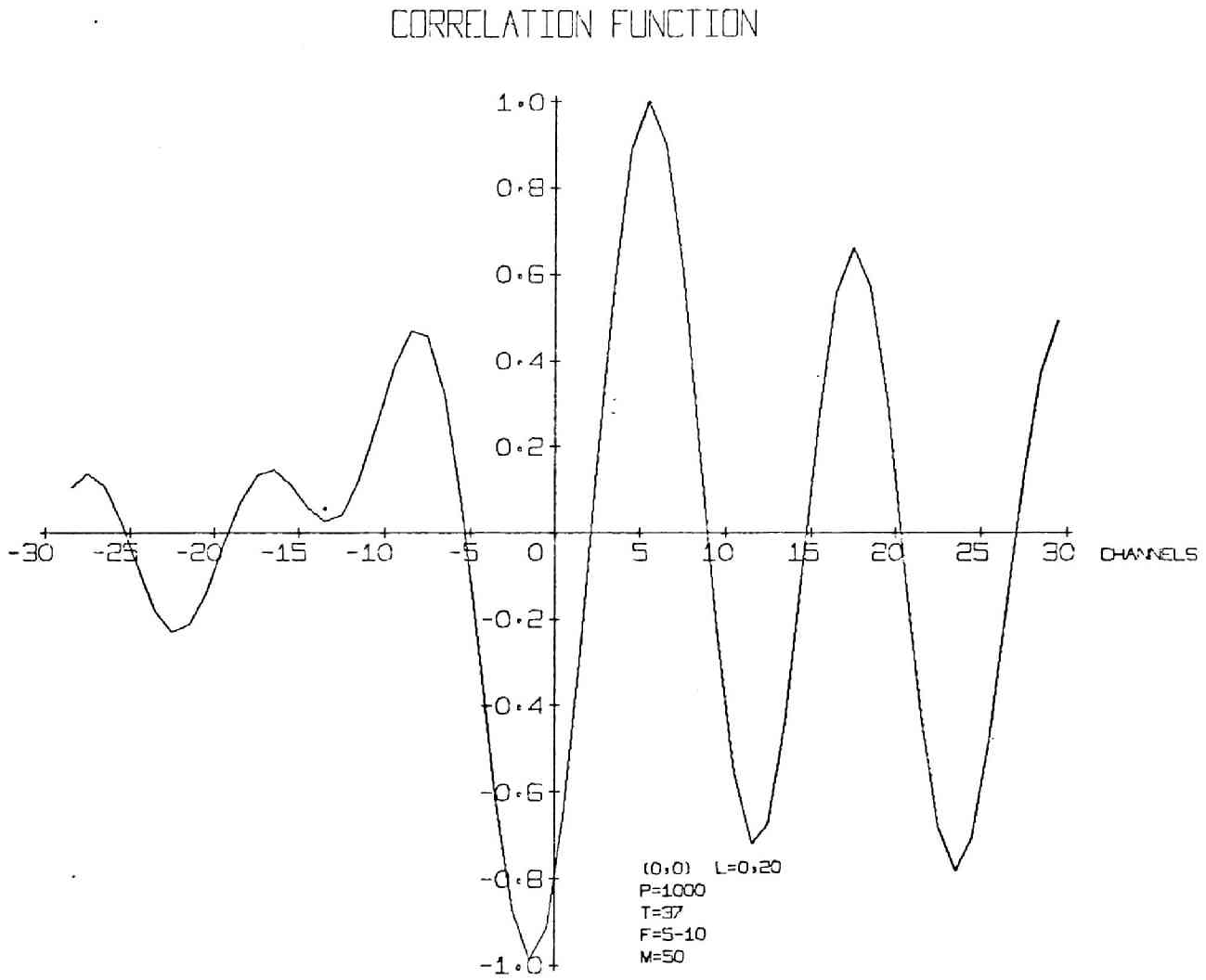

Fig. 95 Cross-correlation Function Output - 58

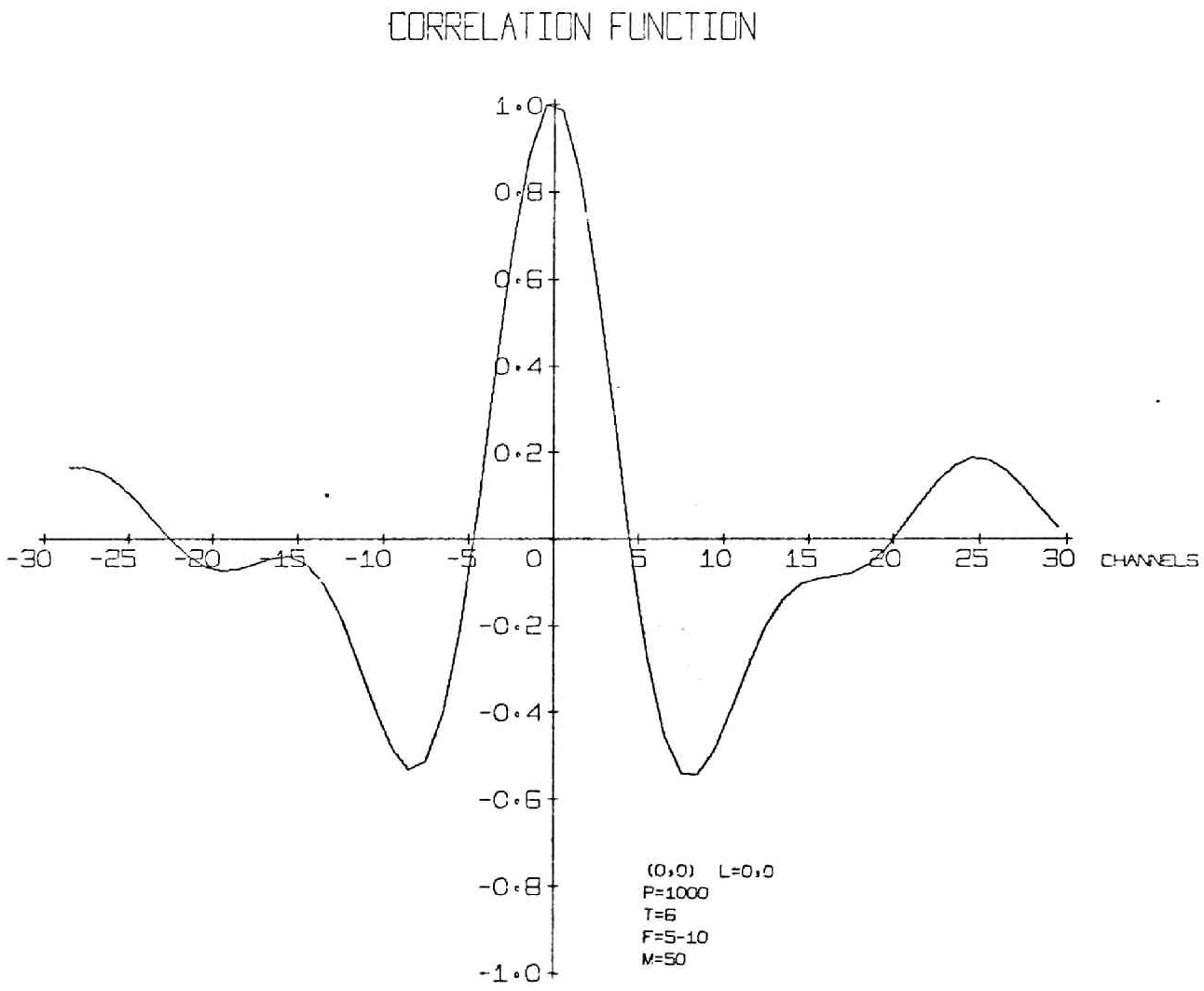

Fig. 96 Cross-correlation Function Output - 59

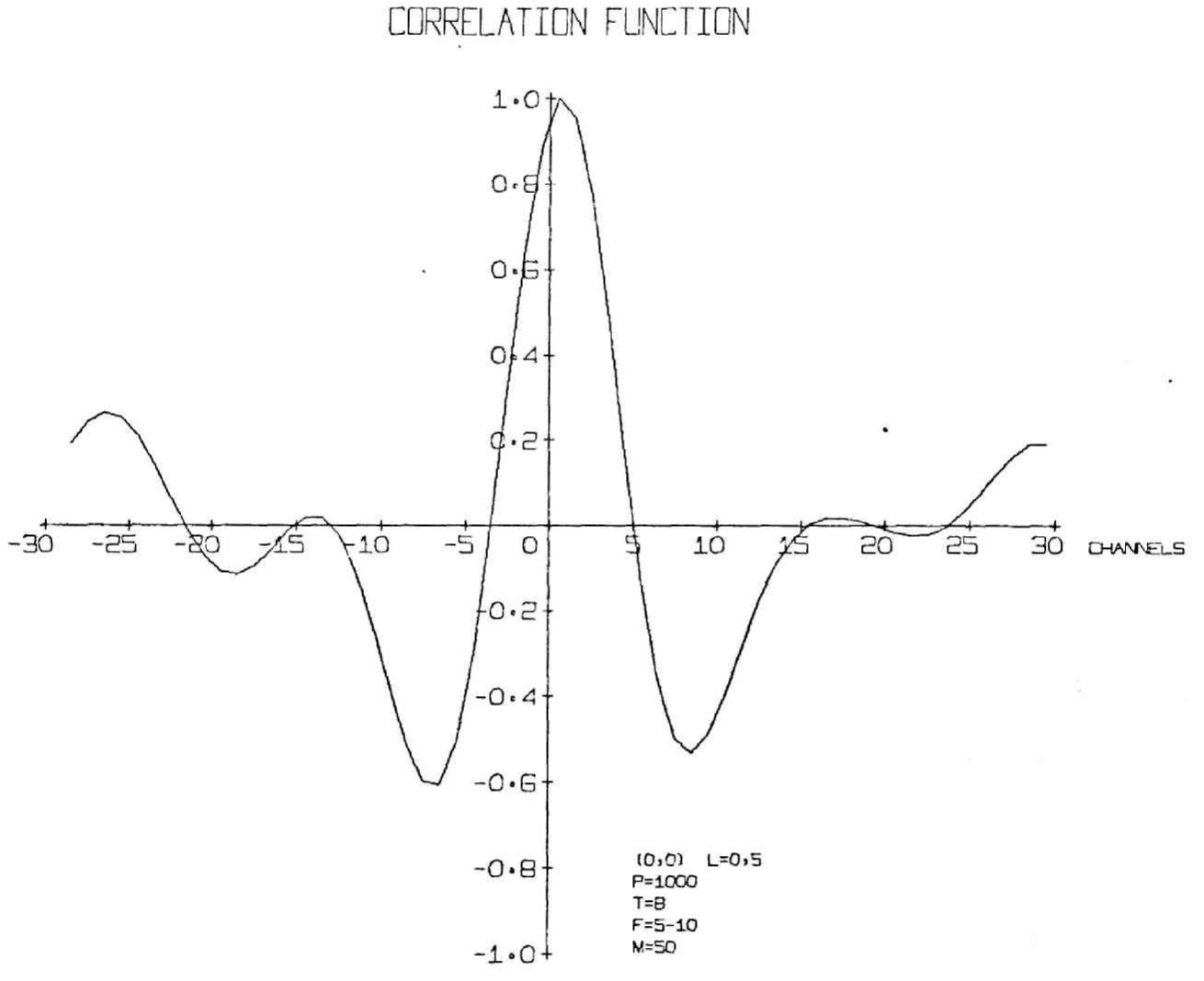

Fig. 97 Cross-correlation Function Output - 60

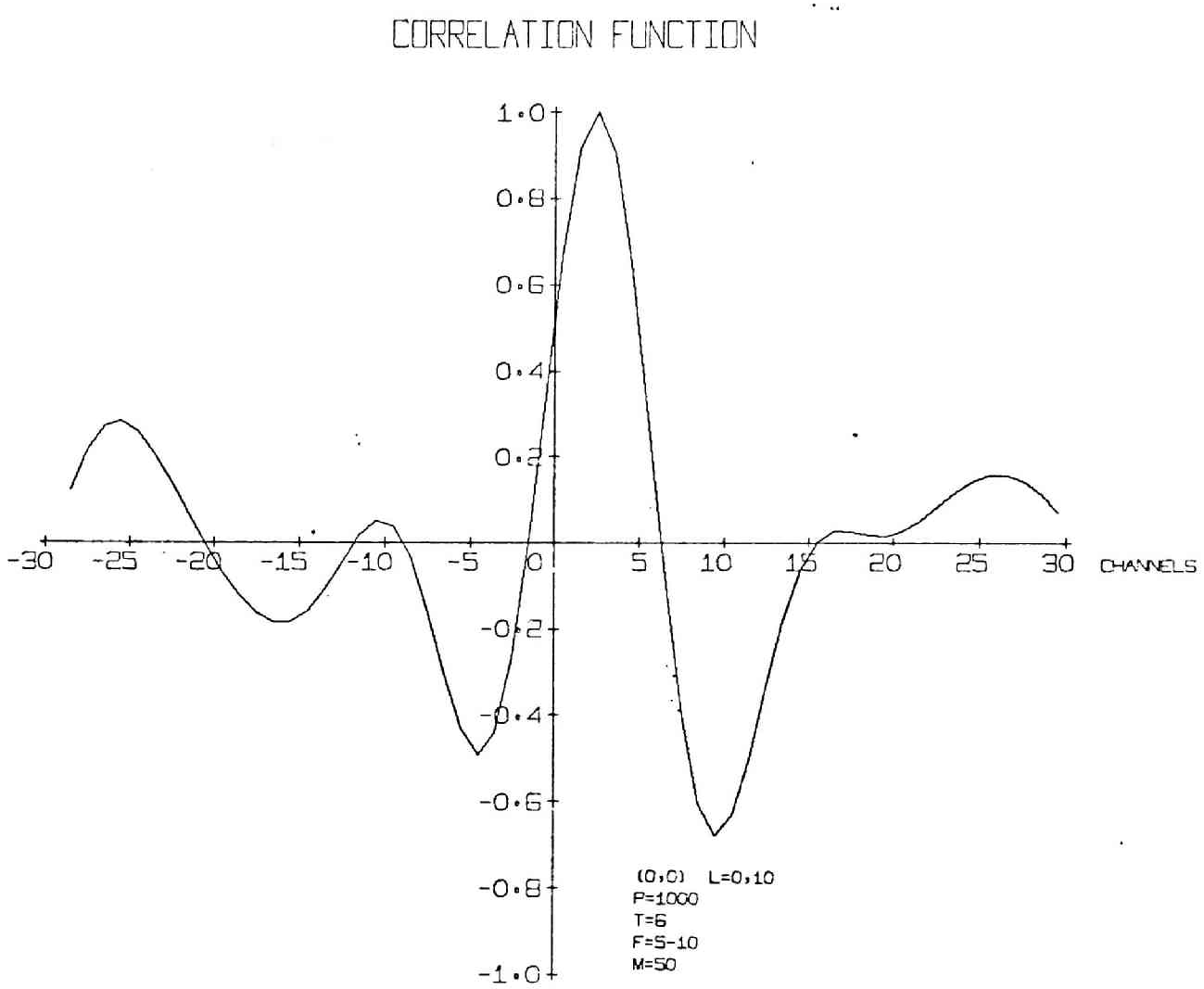

Fig. 98 Cross-correlation Function Output - 61

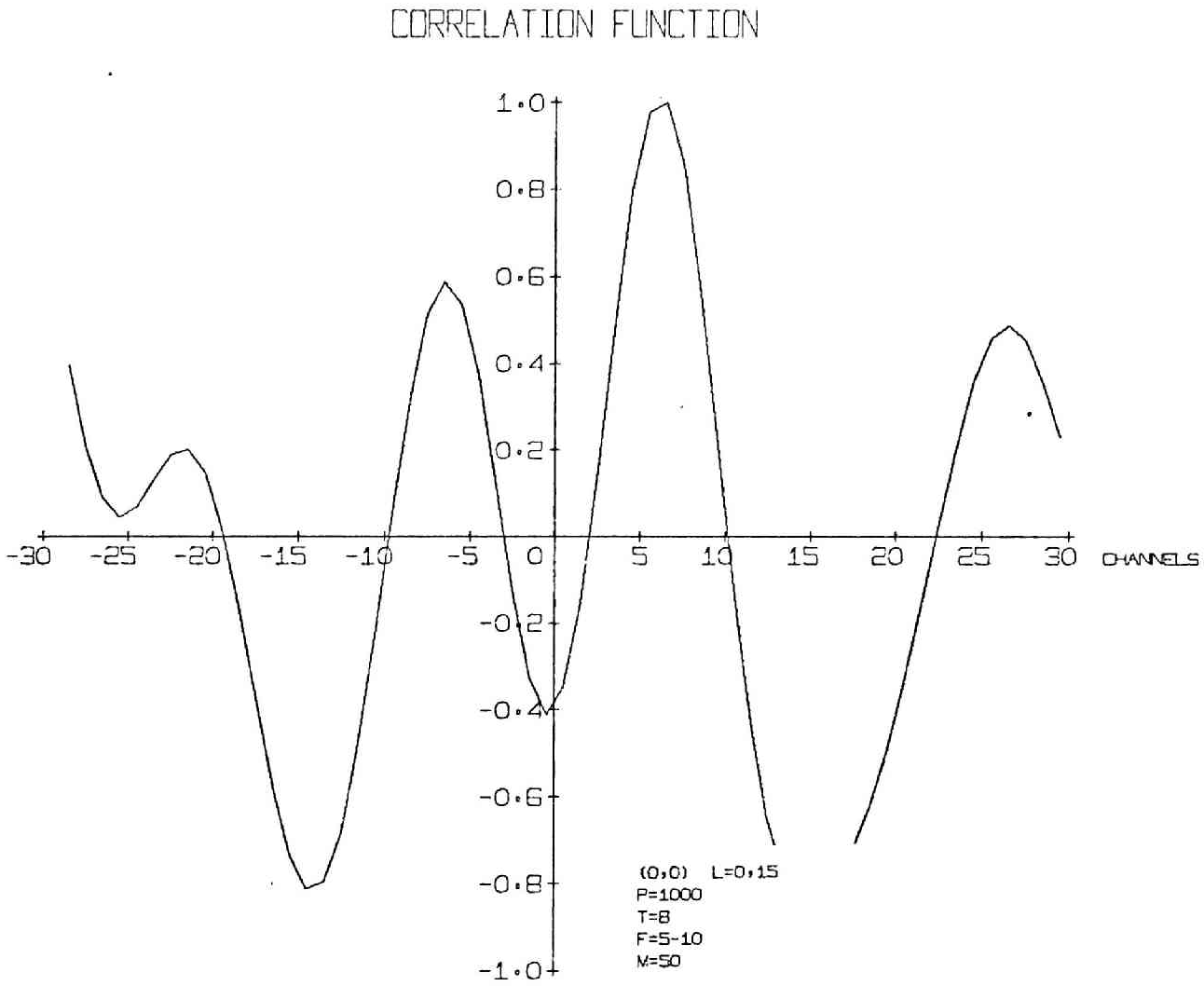

Fig. 99 Cross-correlation Function Output - 62

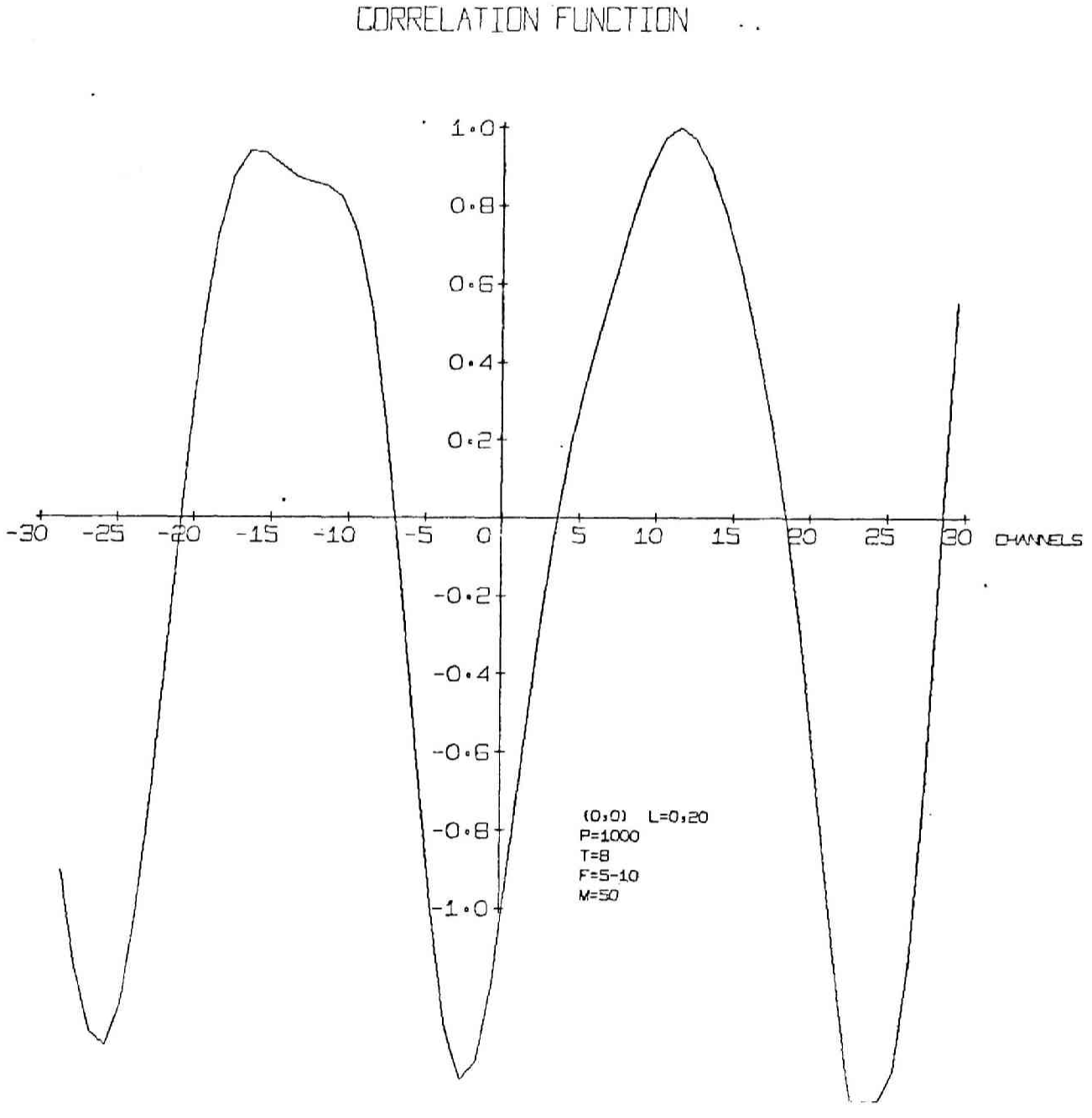

Fig. 100 Cross-correlation Function Output - 63

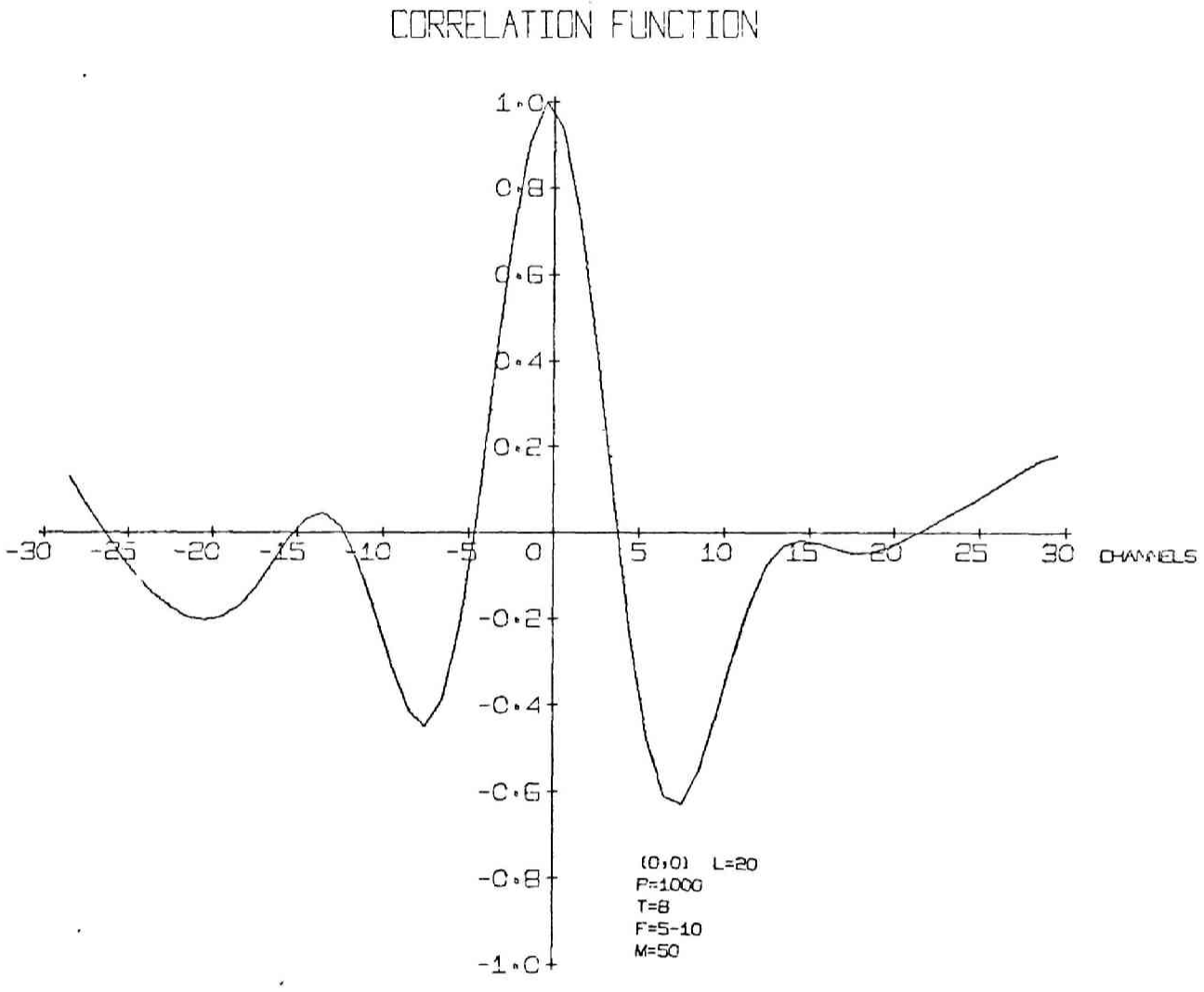

Fig. 101 Cross-correlation Function Output - 64

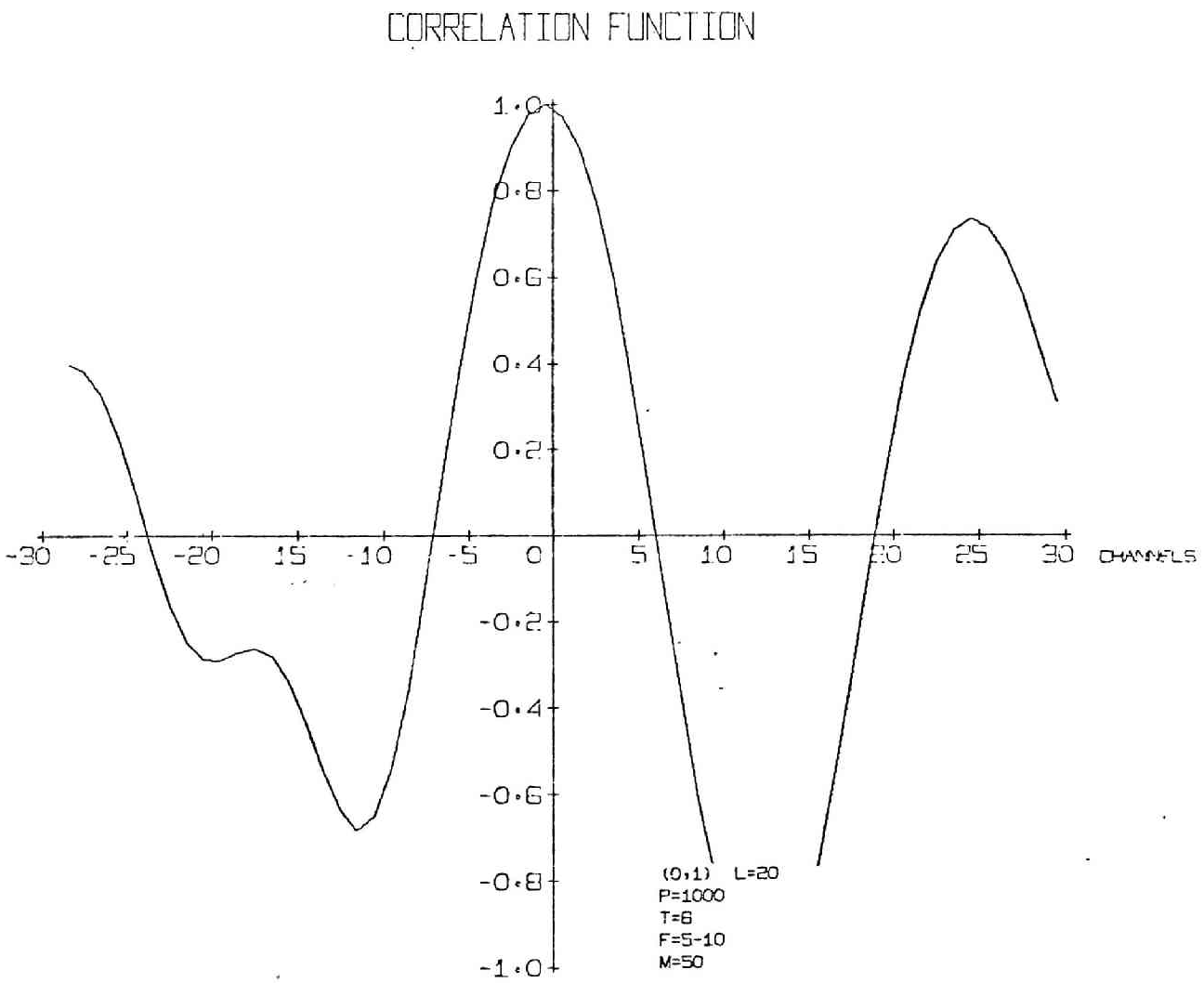

Fig. 102 Cross-correlation Function Output - 65

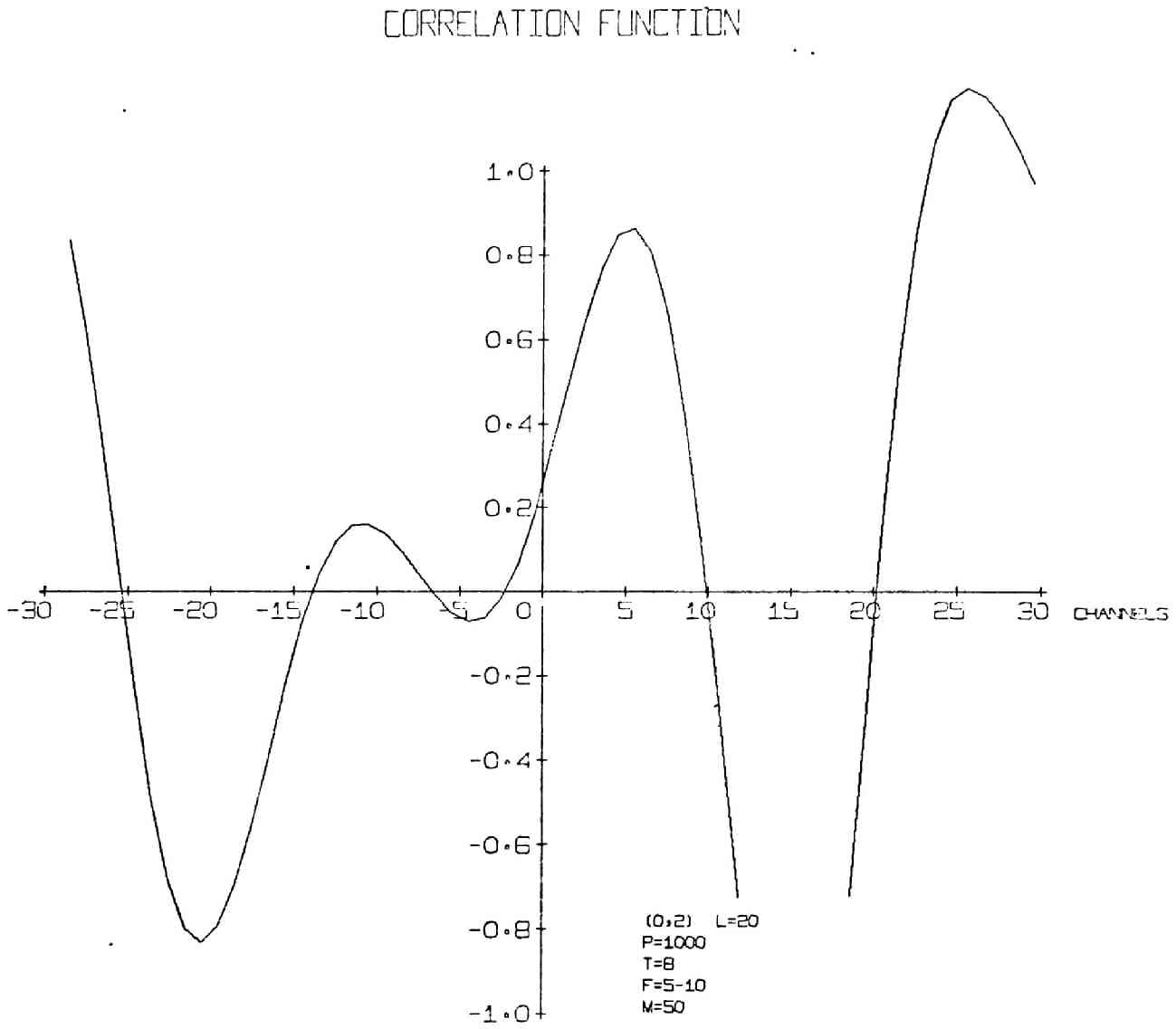

Fig. 103 Cross-correlation Function Output - 66

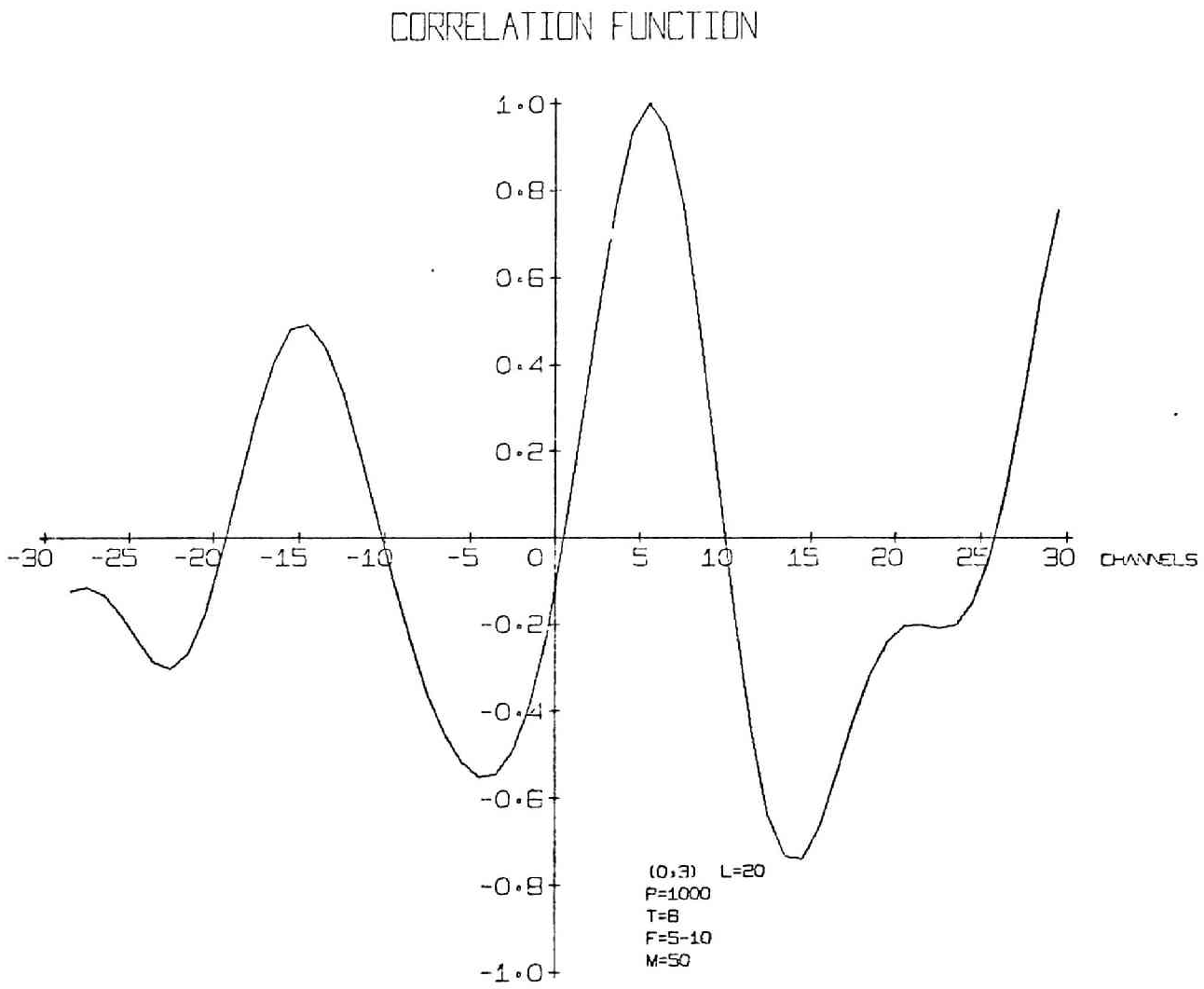

Fig. 104 Cross-correlation Function Output - 67

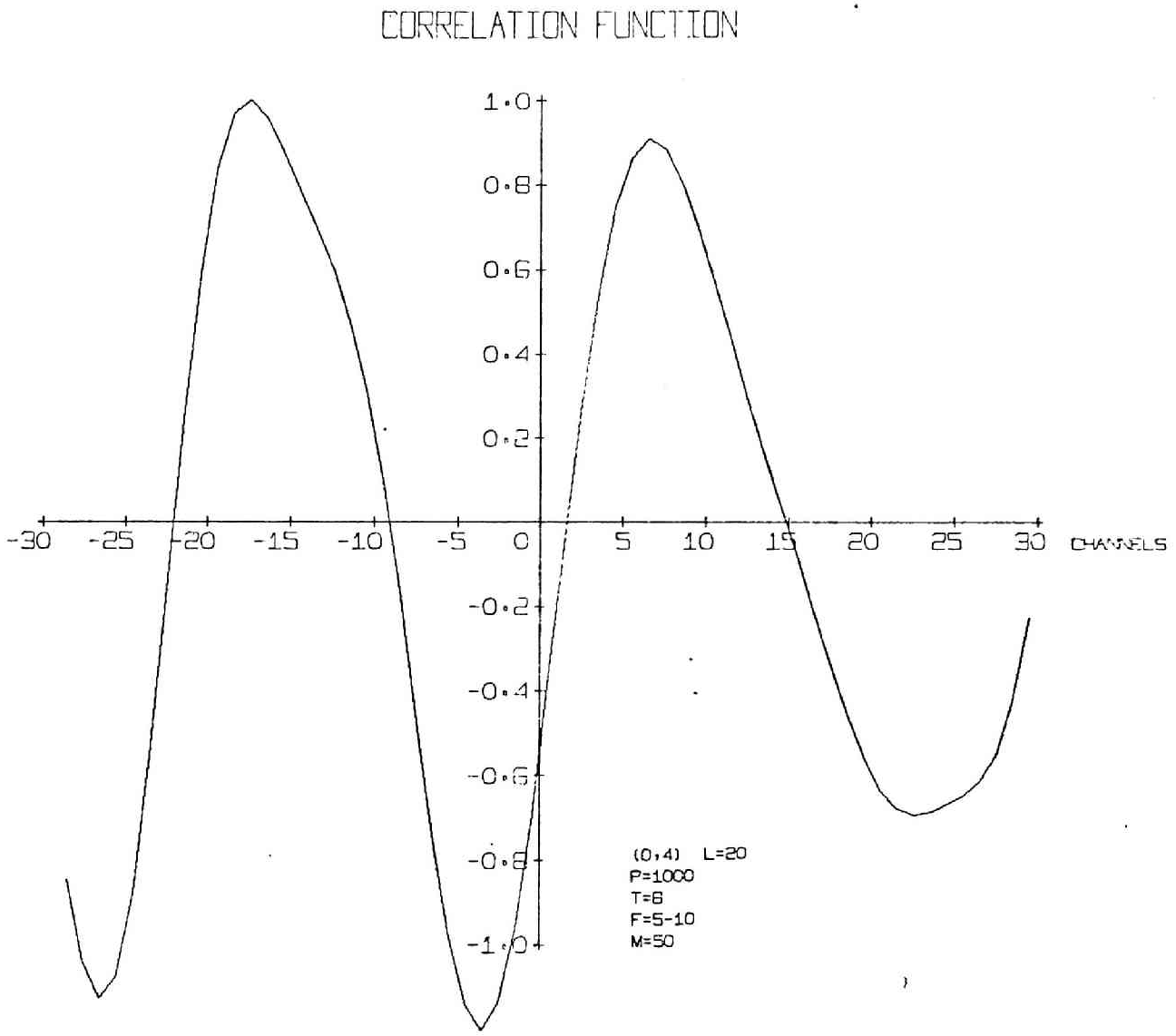

Fig. 105 Cross-correlation Function Output - 68

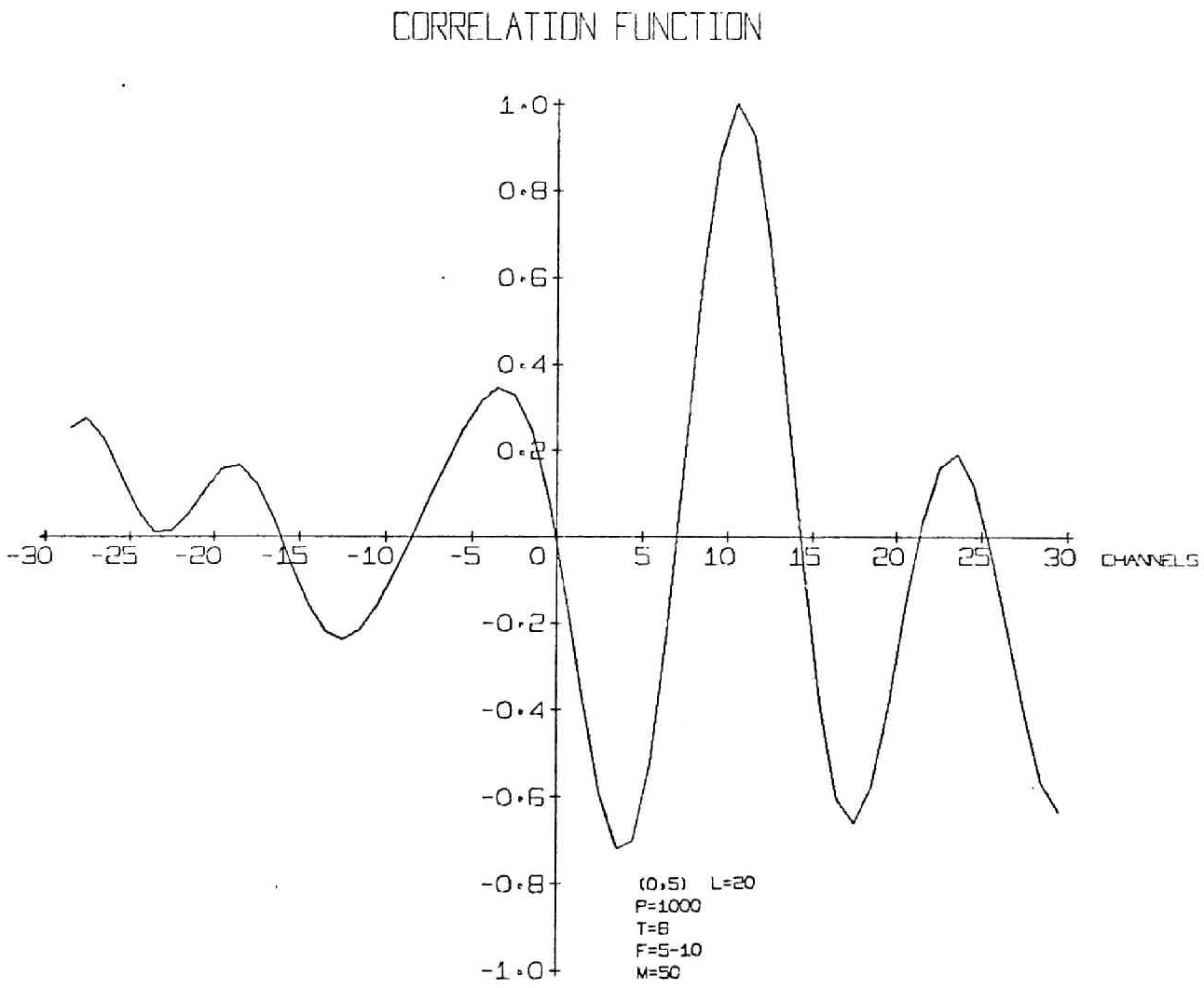

Fig. 106 Cross-correlation Function Output - 69

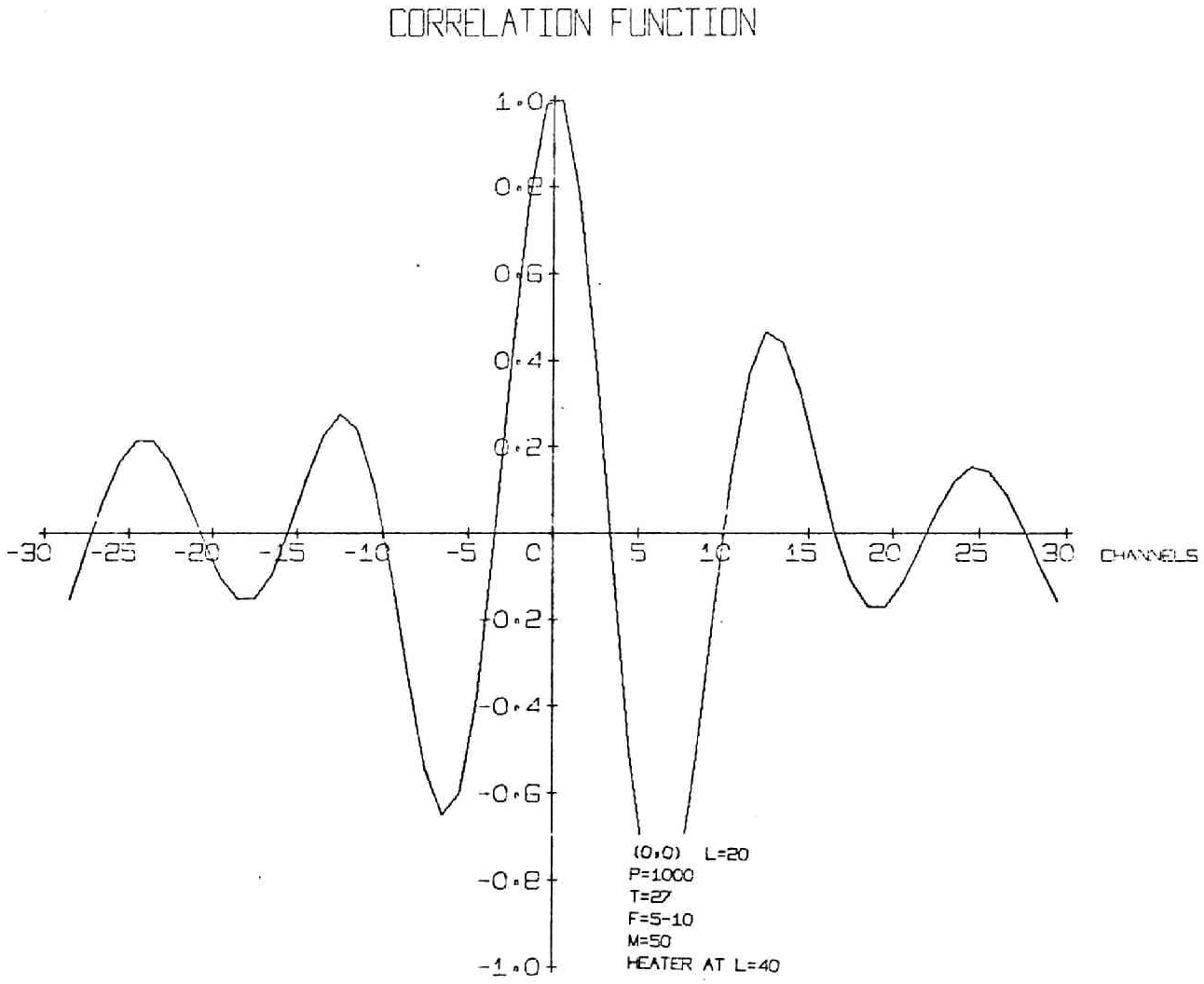

Fig. 107 Cross-correlation Function Output - 70

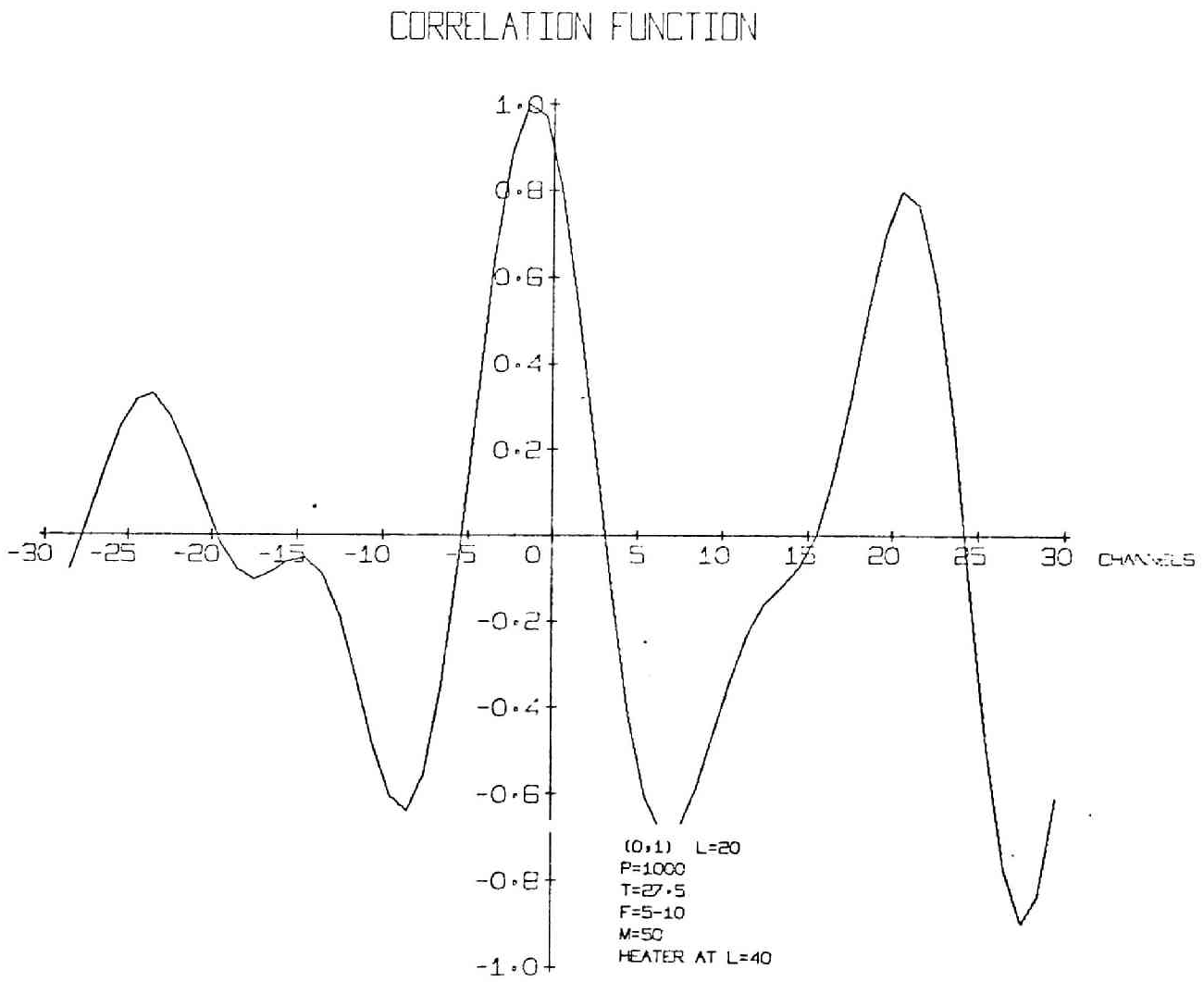

Fig. 108 Cross-correlation Function Output - 71

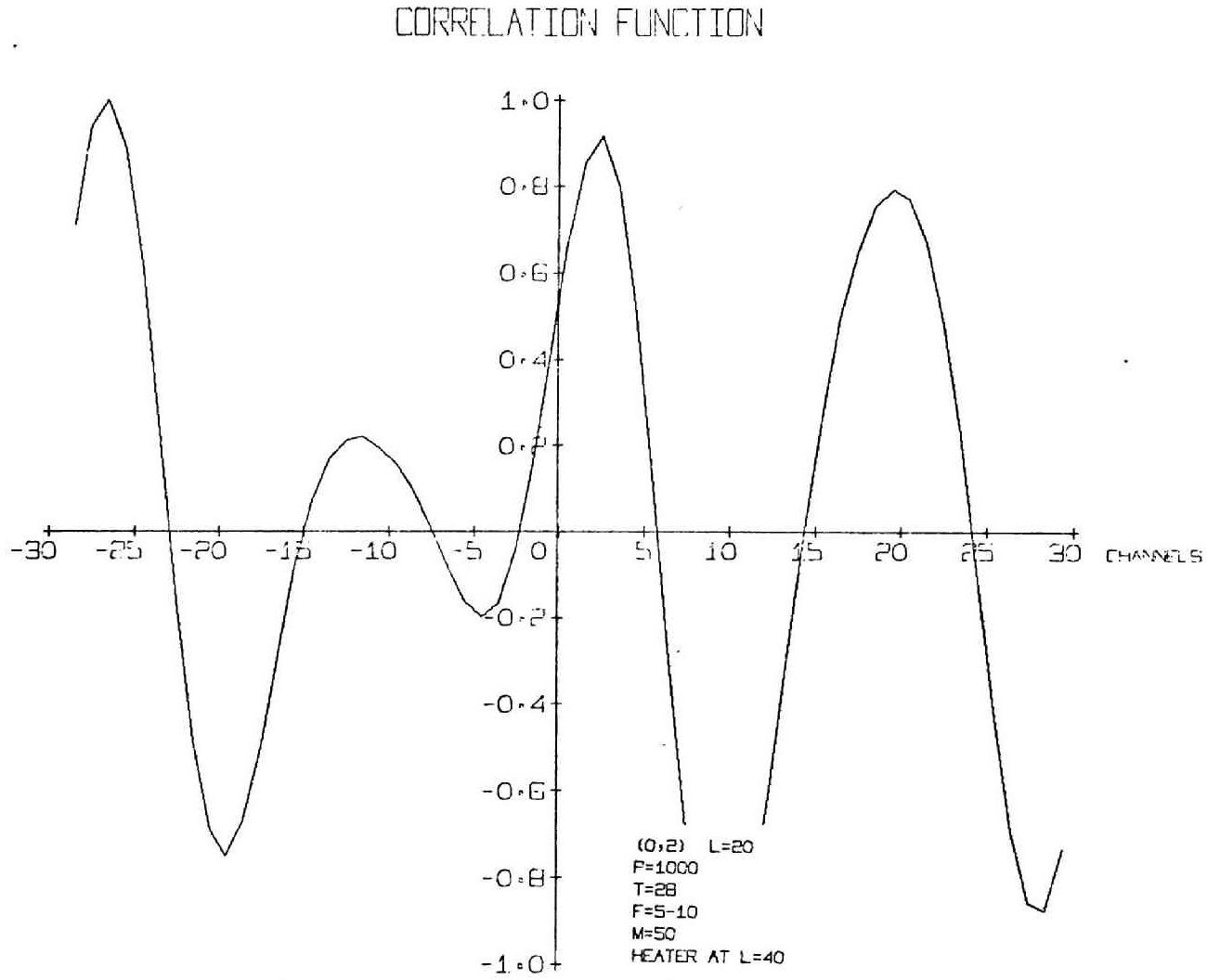

Fig.109 Cross-correlation Function Output - 72

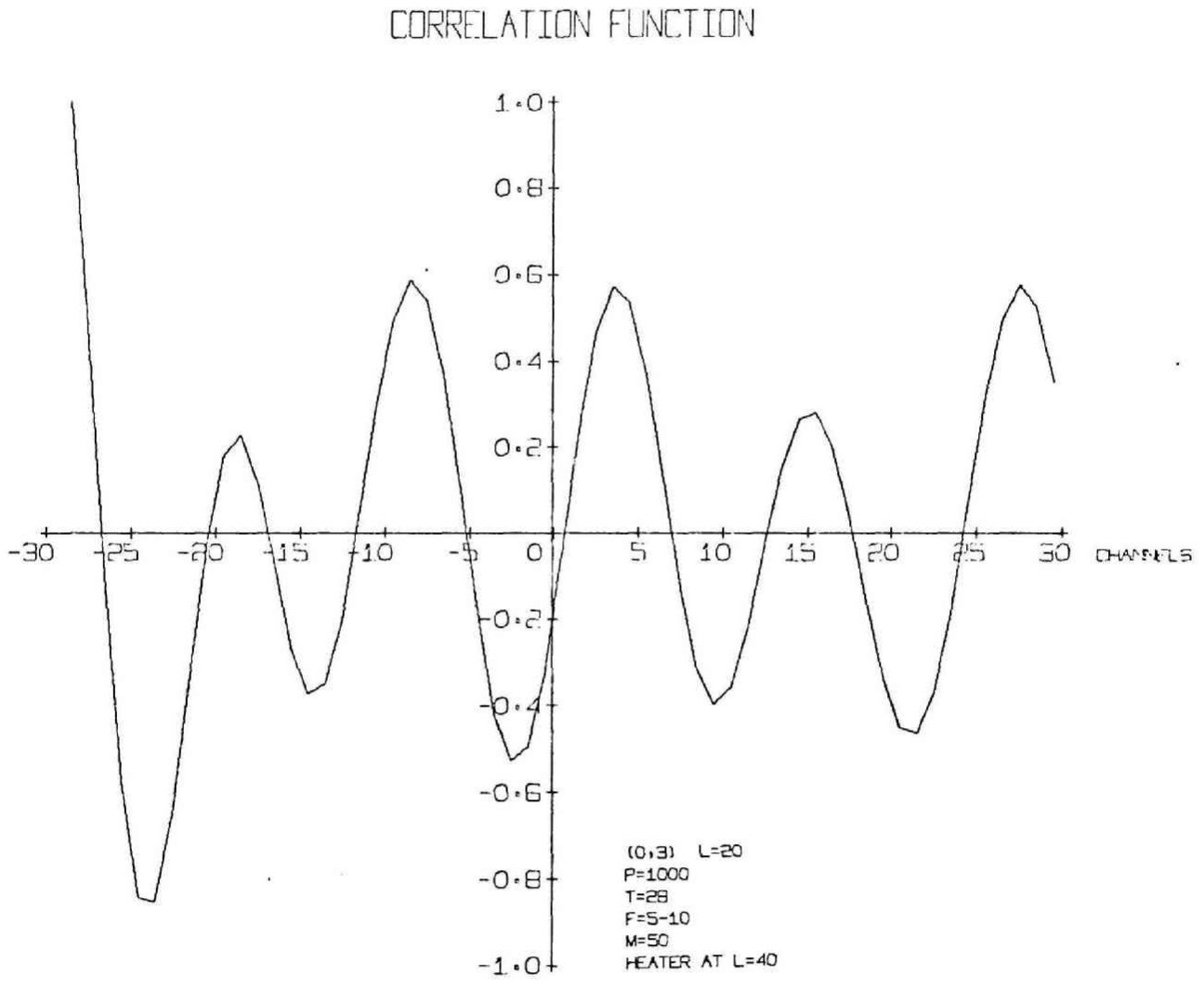

Fig. 110 Cross-correlation Function Output - 73

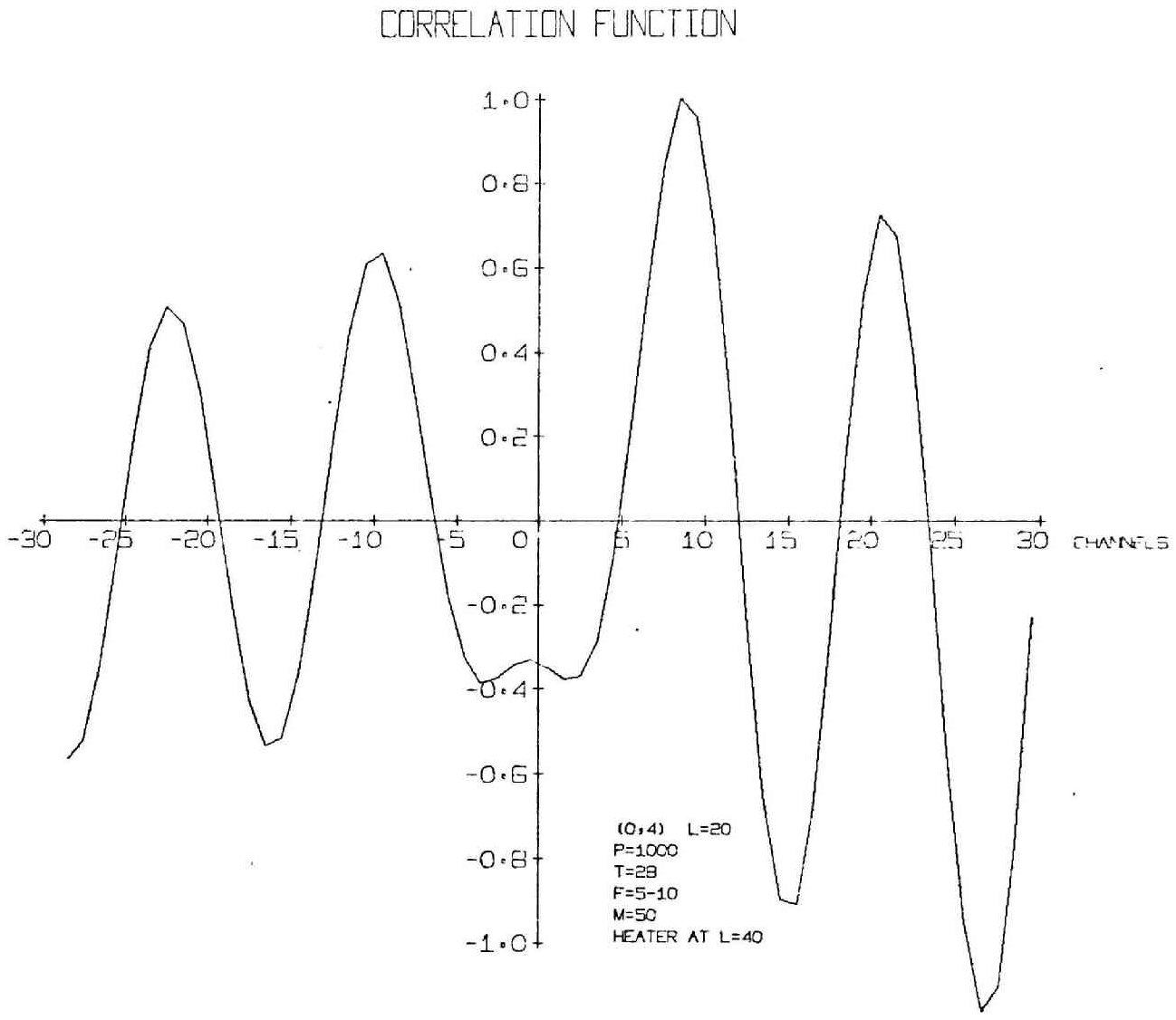

Fig. III Cross-correlation Function Output - 74

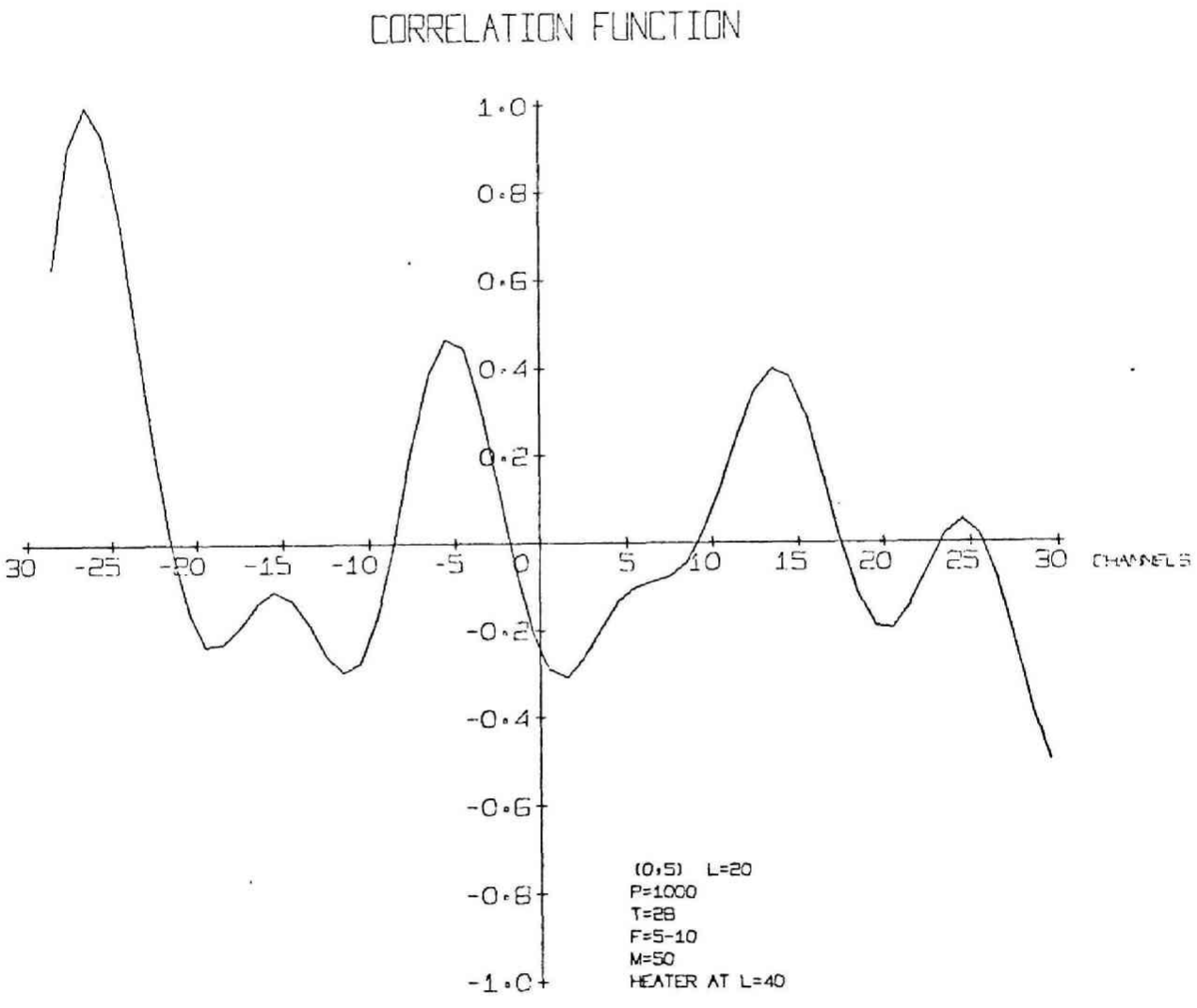

Fig. 112 Cross-correlation Function Output - 75

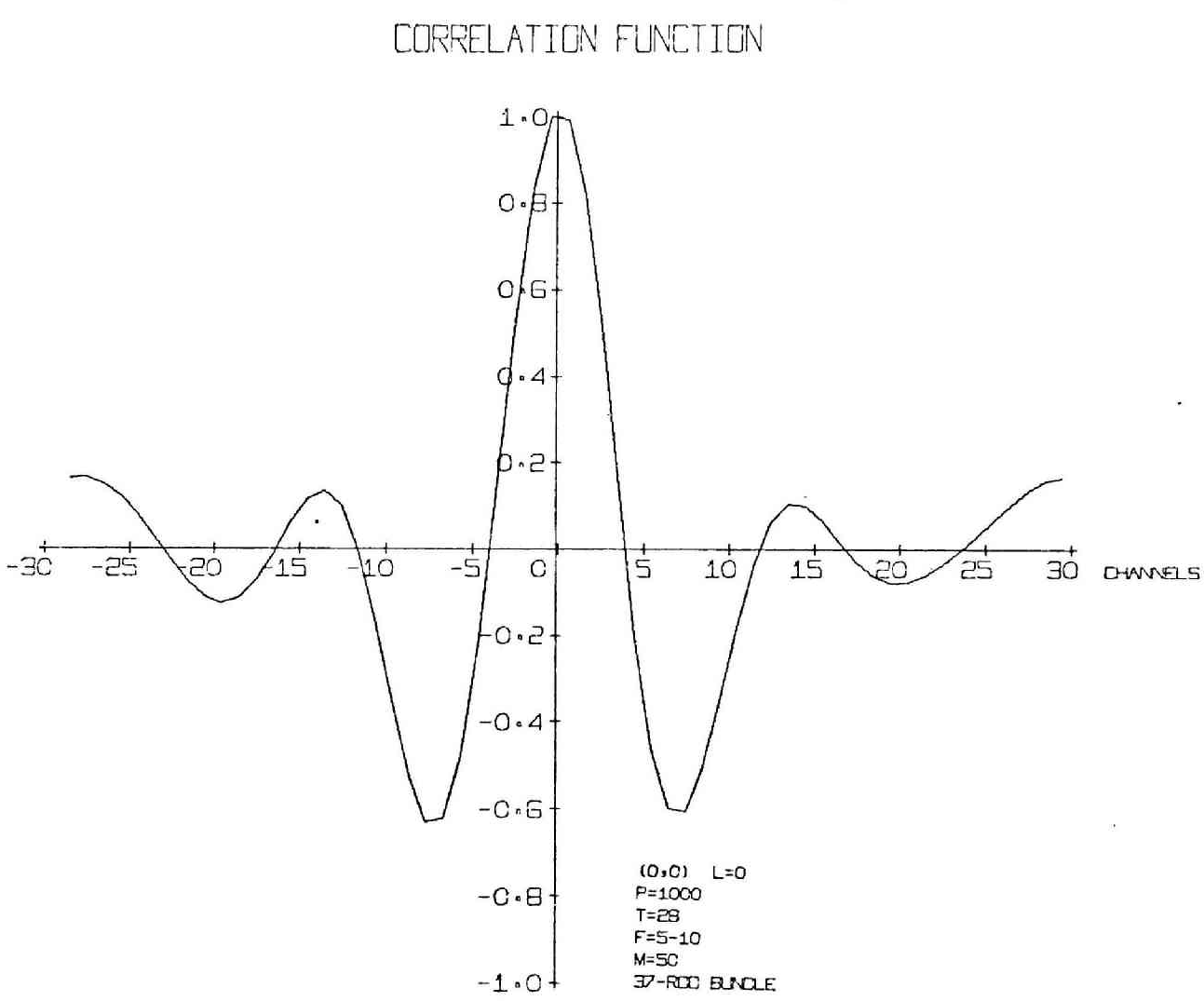

Fig. 113 Cross-correlation Function Output - 76

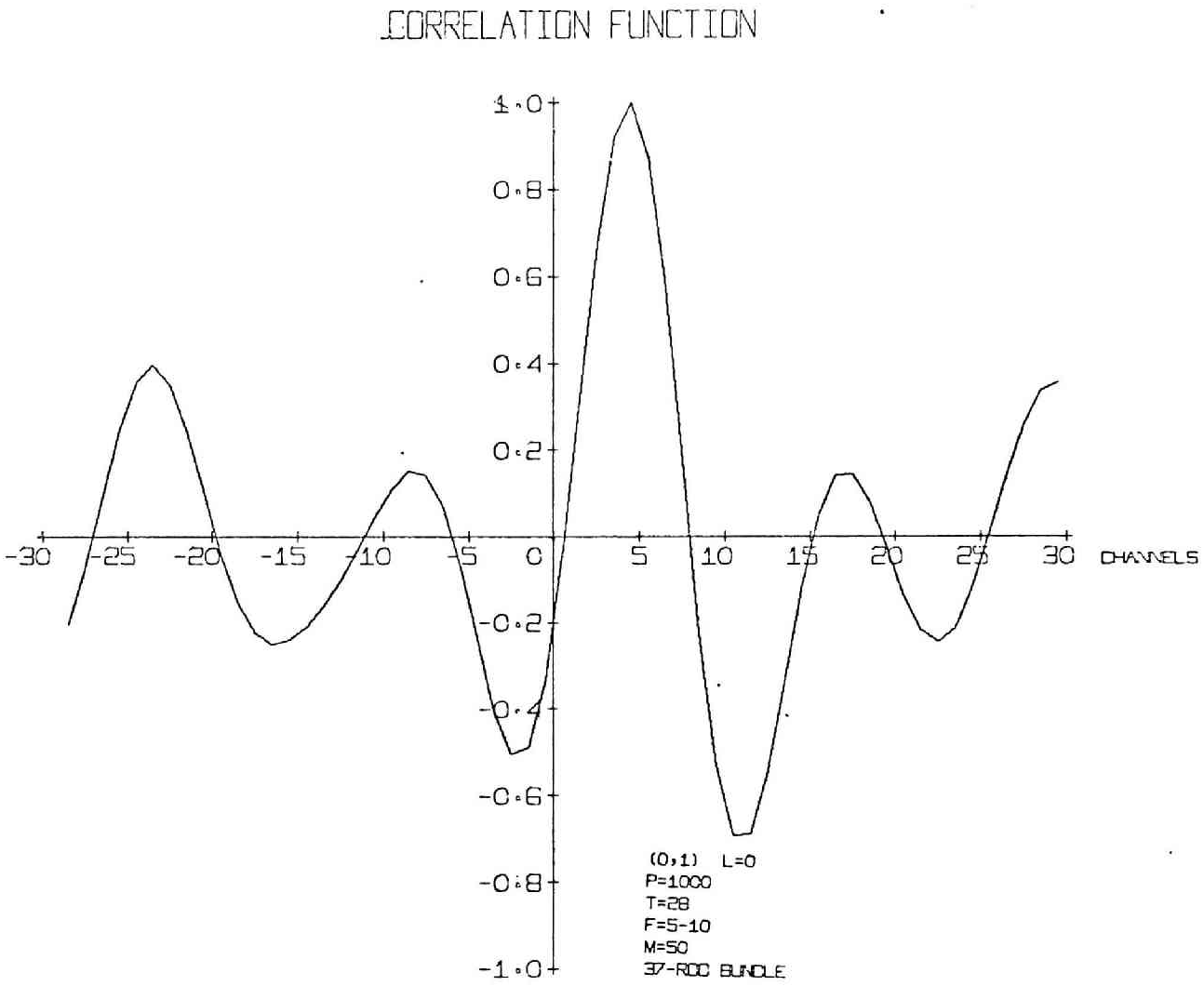

Fig. 114 Cross-correlation Function Output - 77

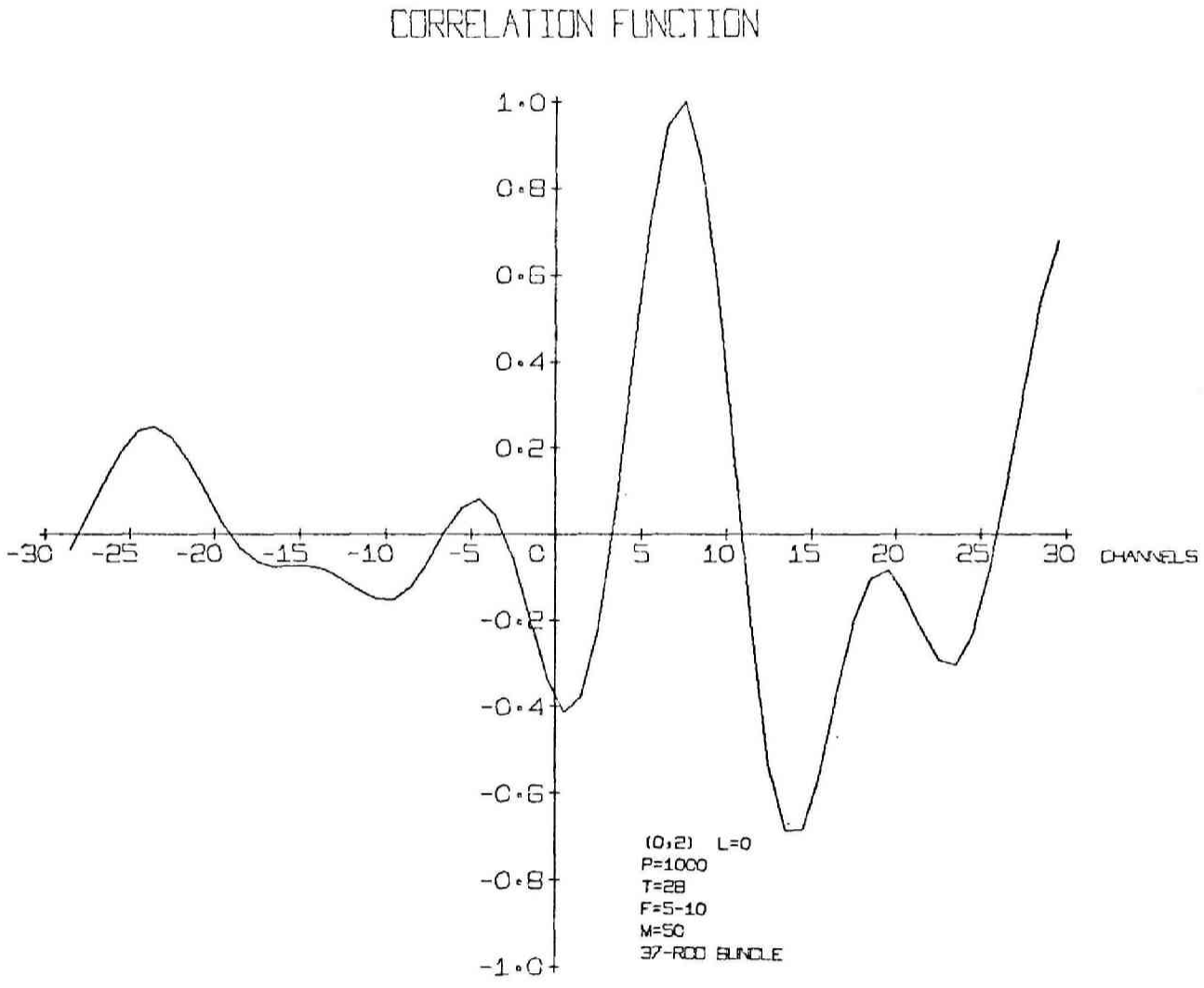

Fig. 115 Cross-correlation Function Output - 78

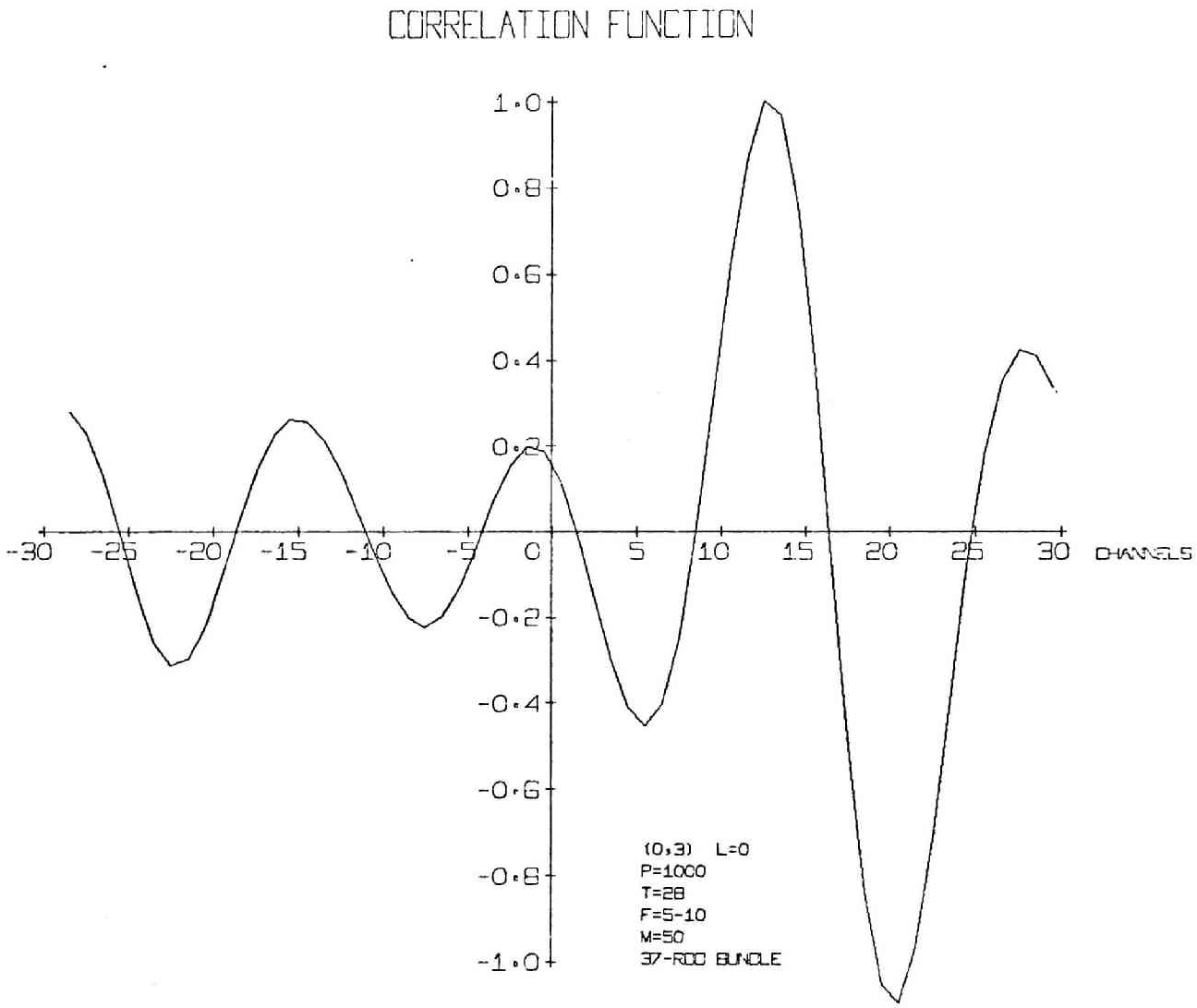

Fig. 116 Cross-correlation Function Output - 79

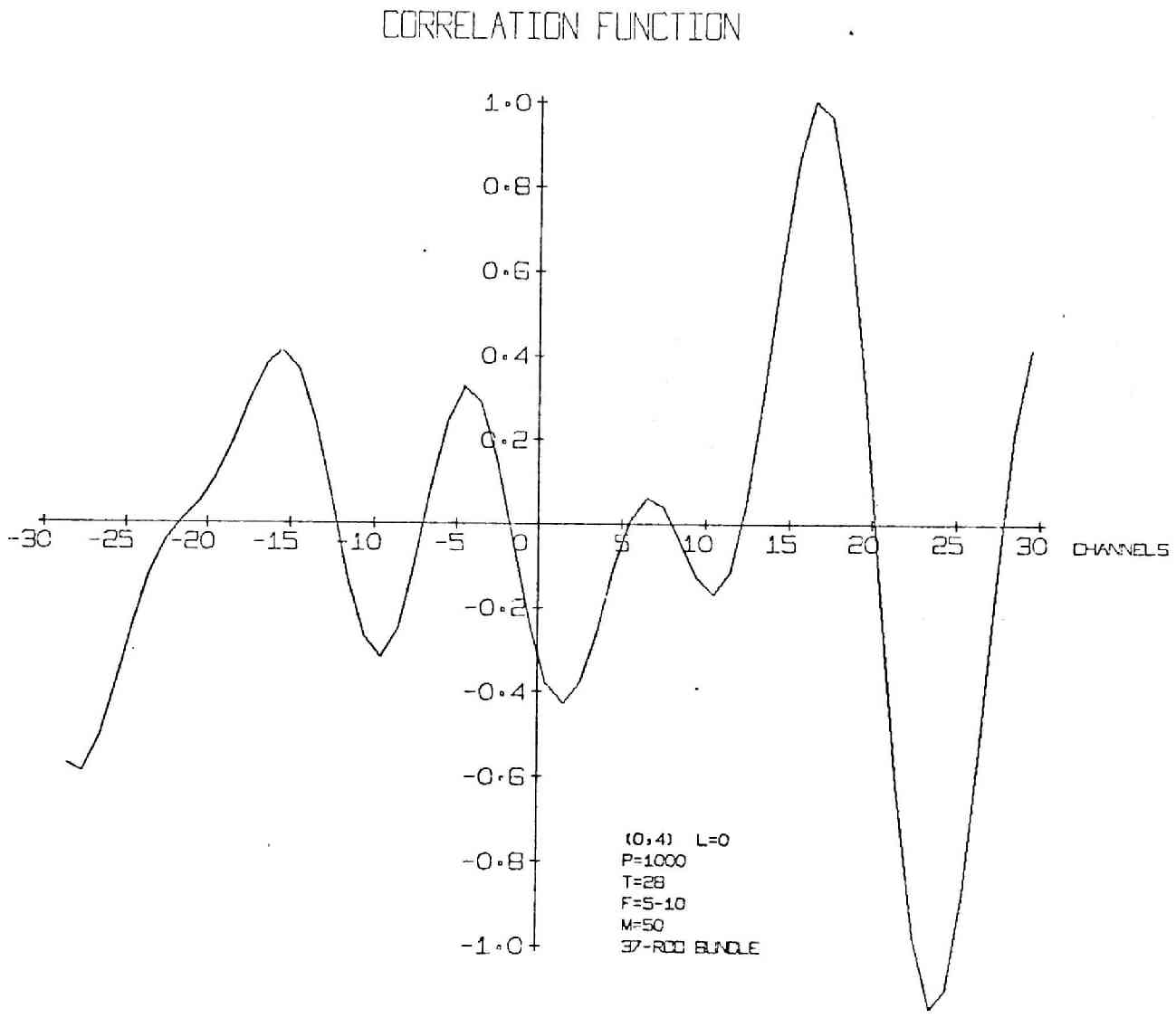

Fig. 117 Cross-correlation Function Output - 80

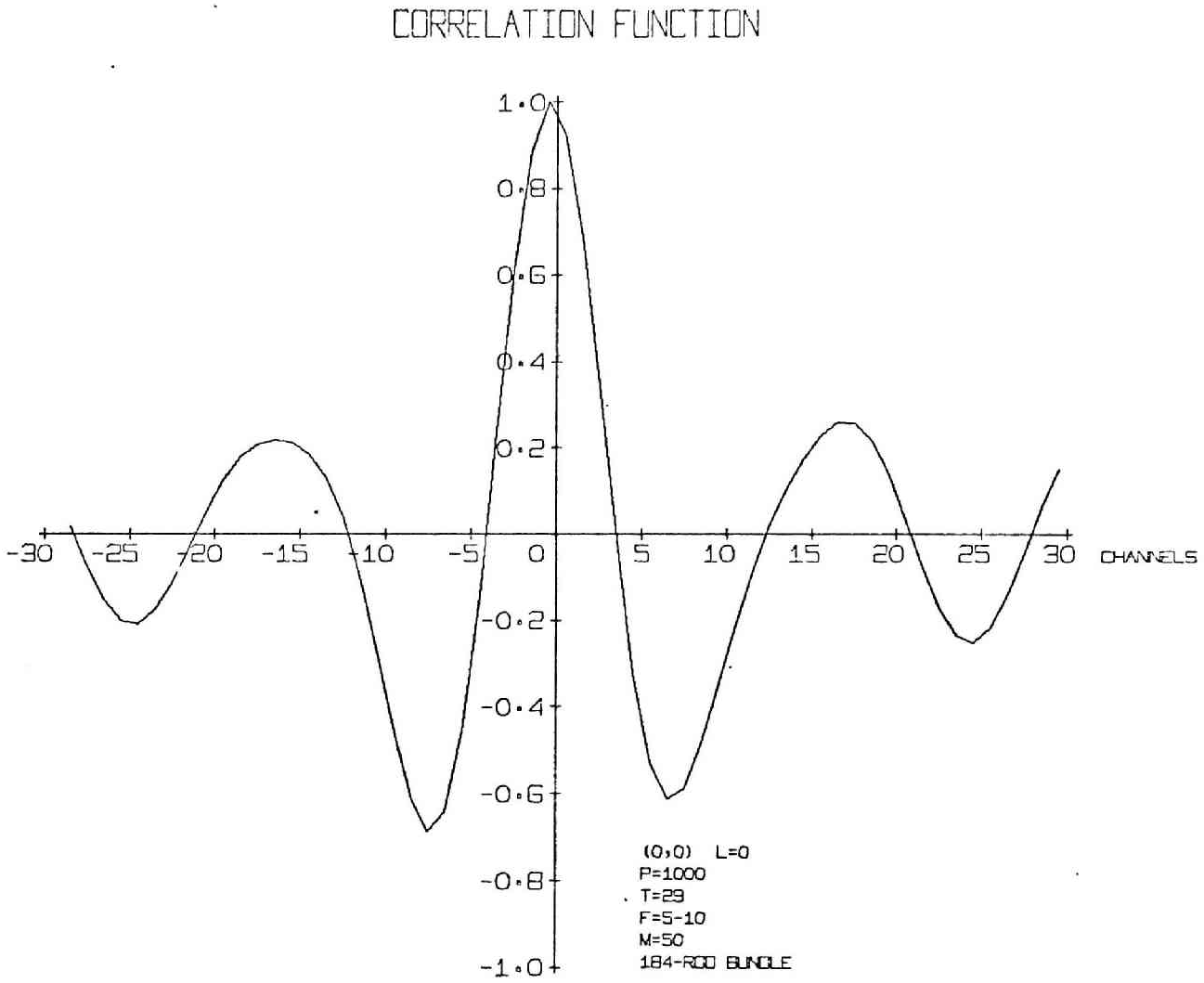

Fig. 118 Cross-correlation Function Output -81

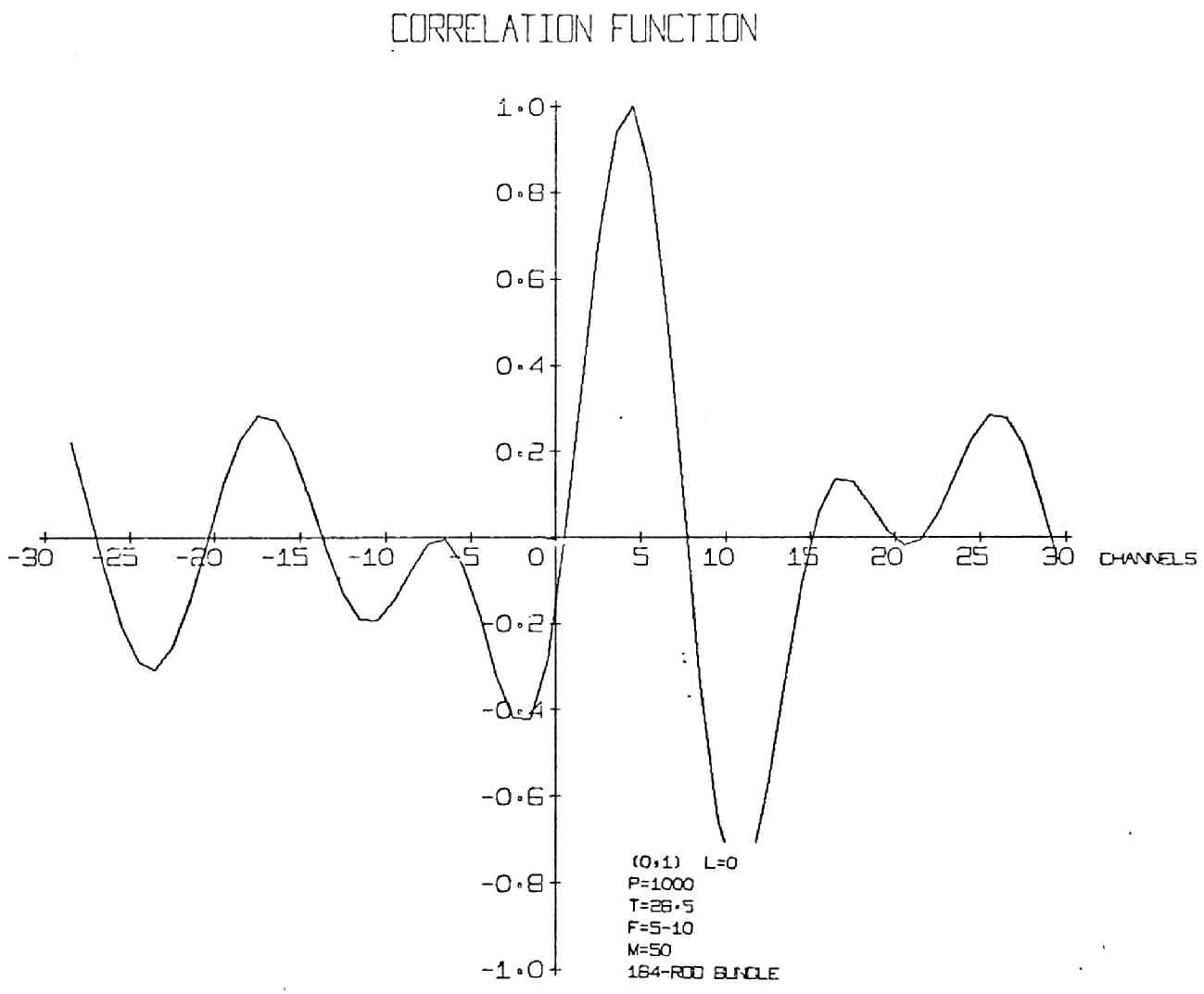

Fig. 119 Cross-correlation Function Output - 82

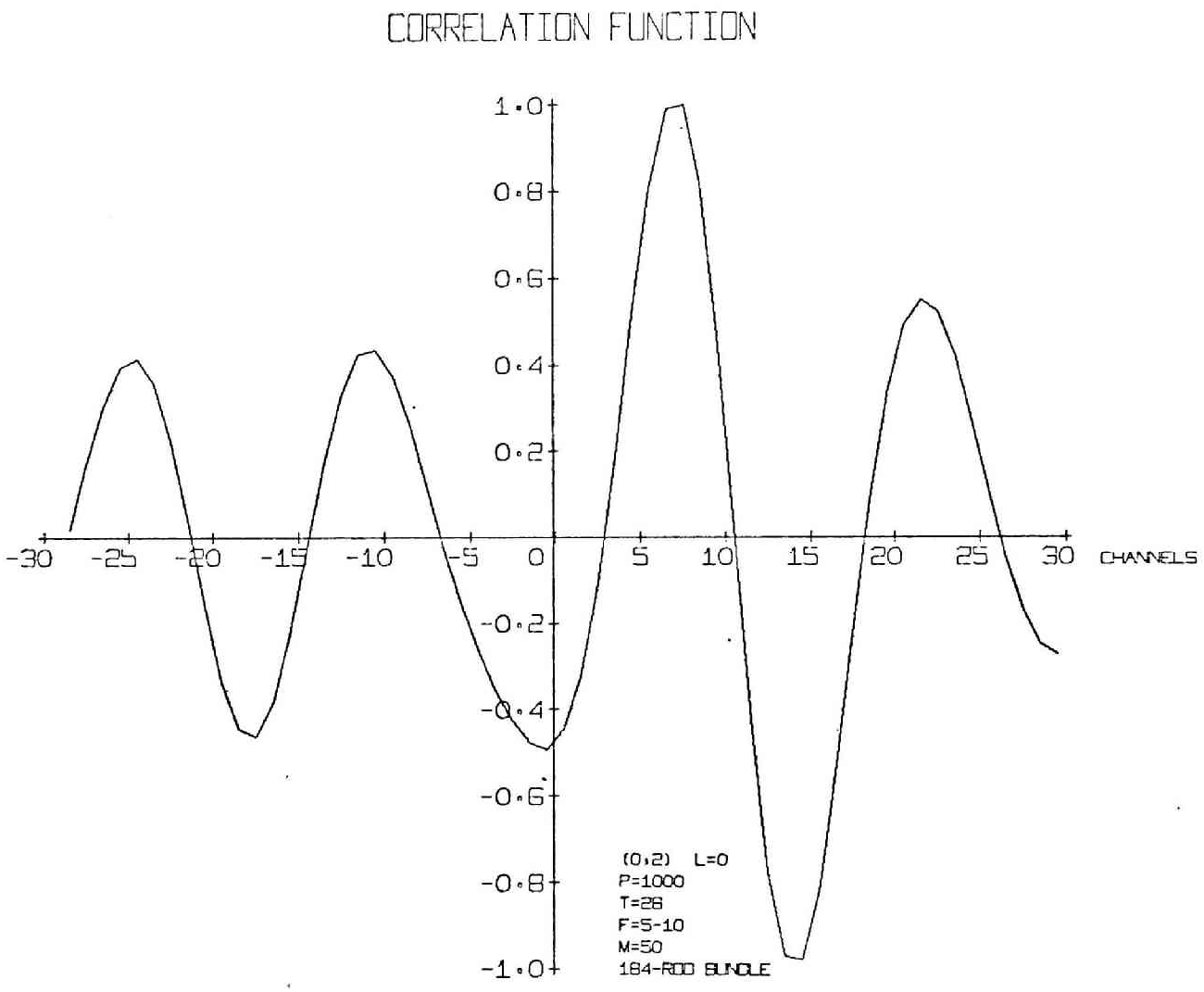

Fig. 120 Cross-correlation Function Output - 83

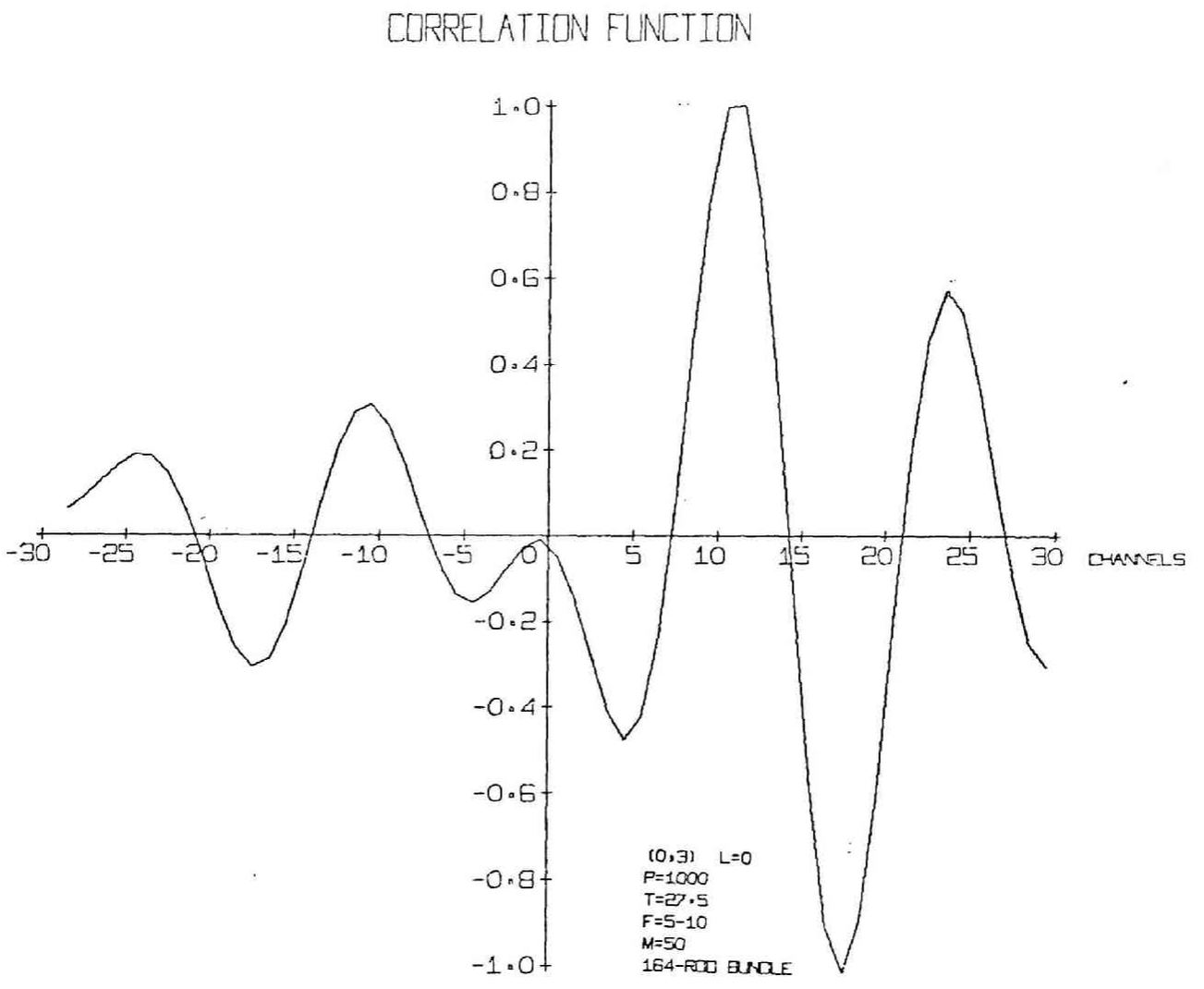

Fig. 121 Cross-correlation Function Output - 84

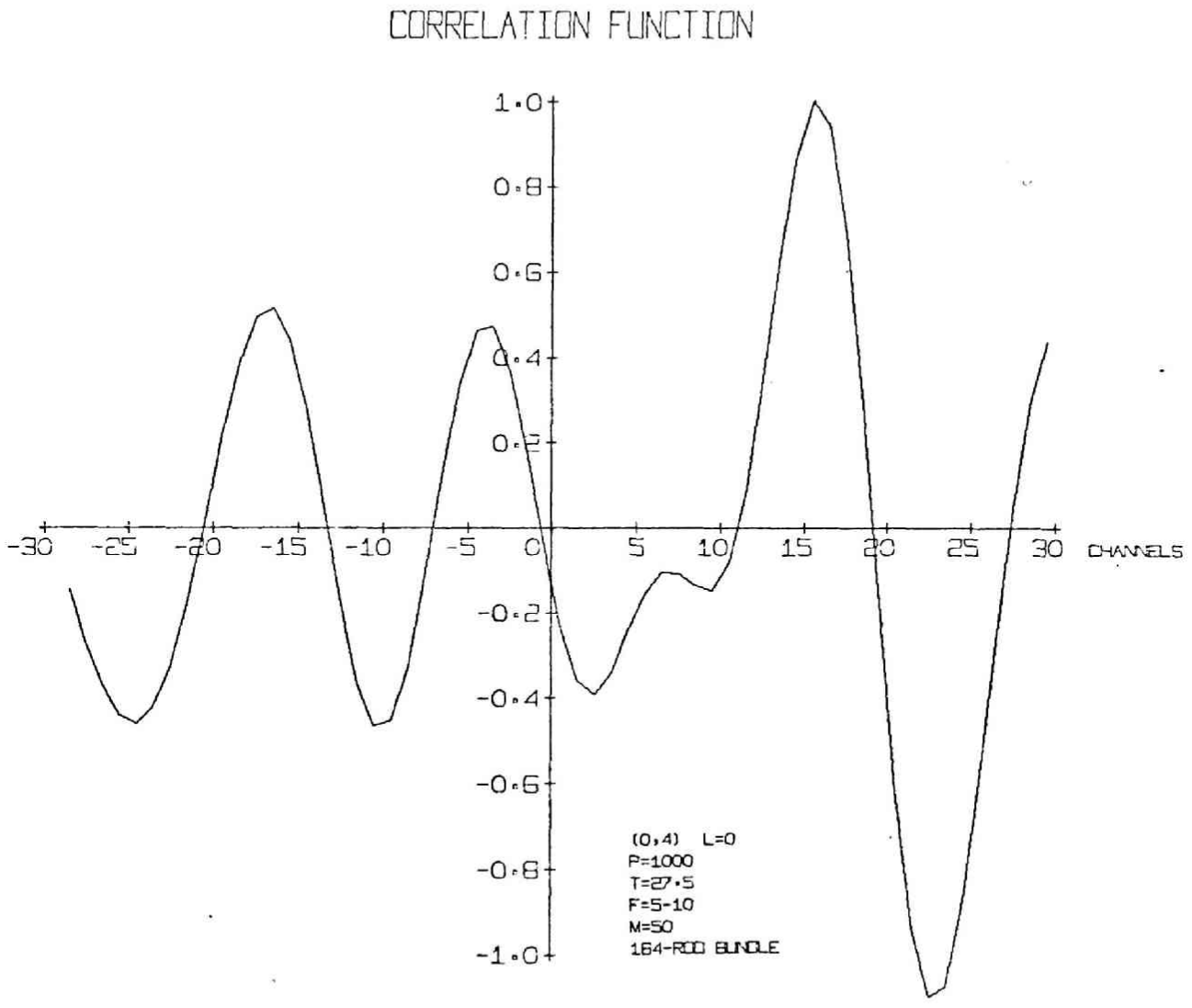

Fig. 122 Cross-correlation Function Output - 85

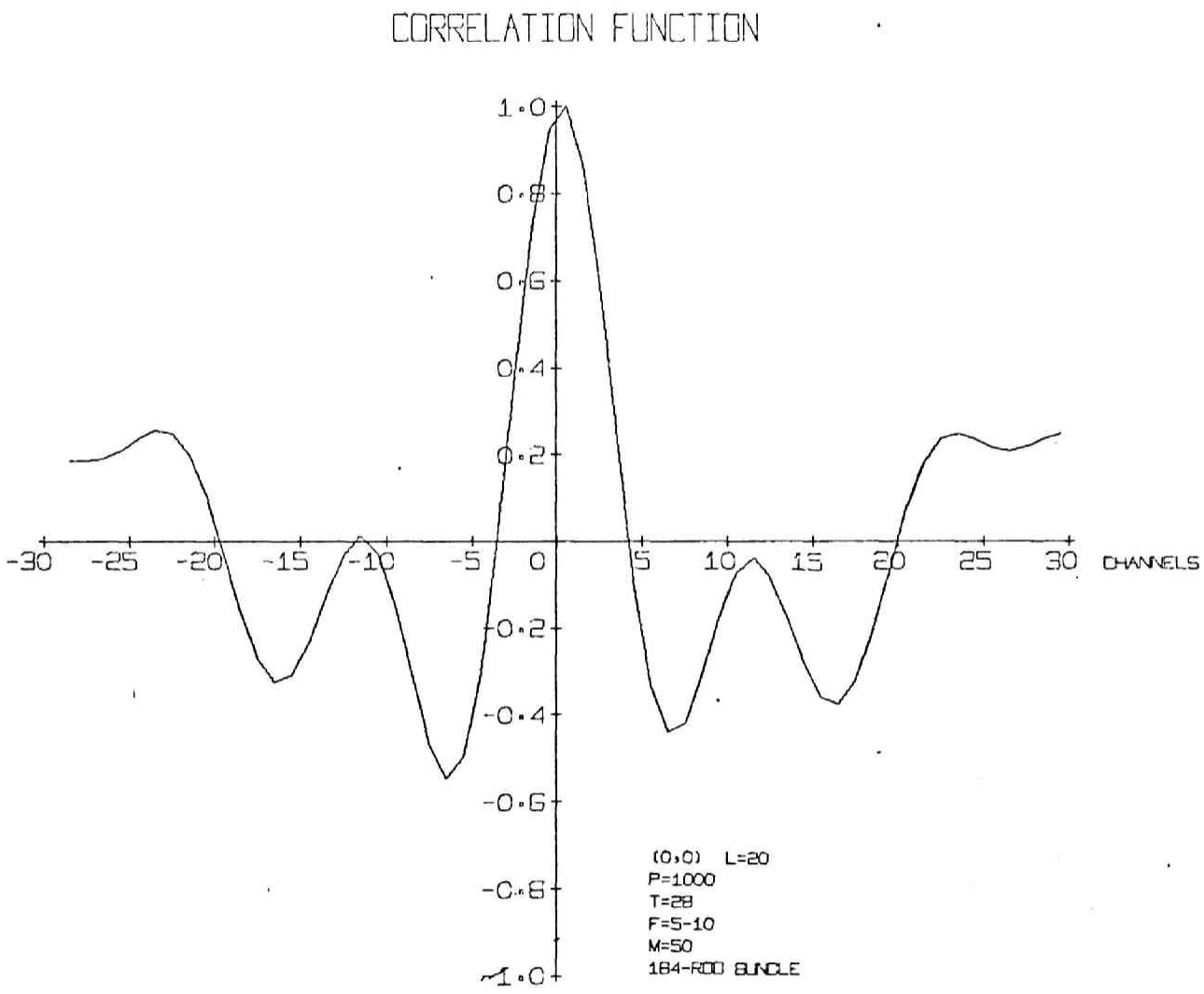

Fig. 123 Cross-correlation Function Output - 86

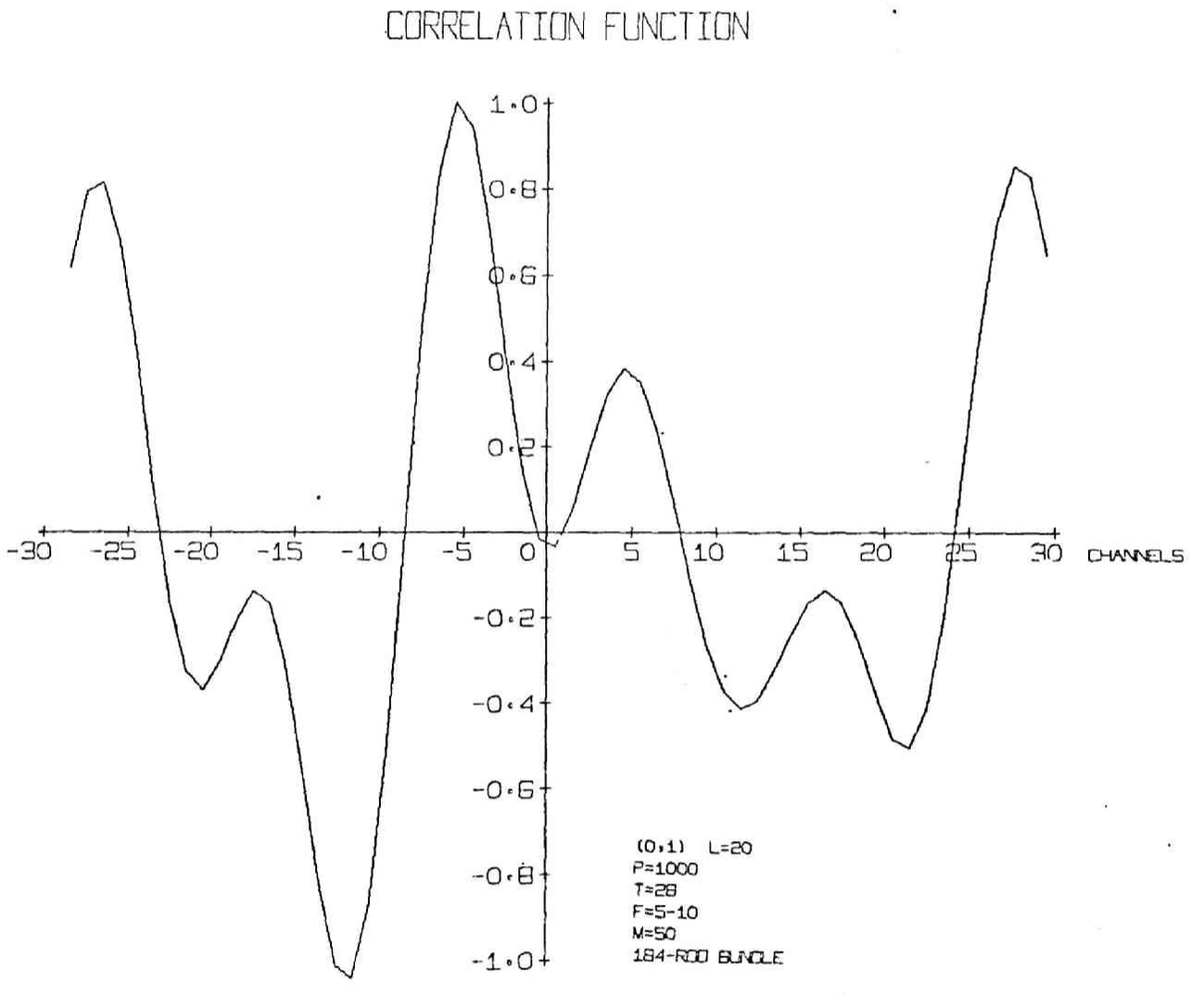

Fig. 124 Cross-correlation Function Output - 87

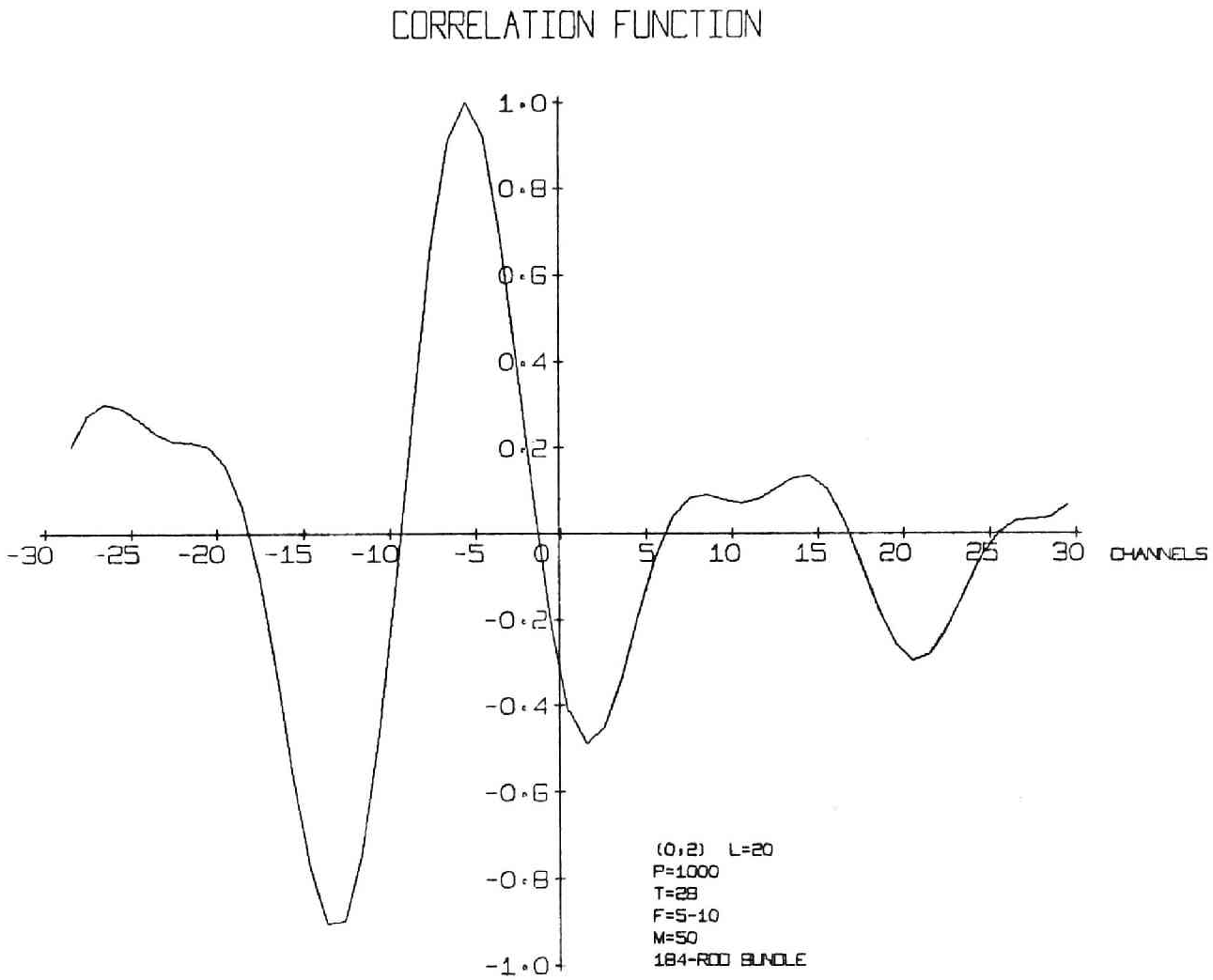

Fig. 125 Cross-correlation Function Output - 88

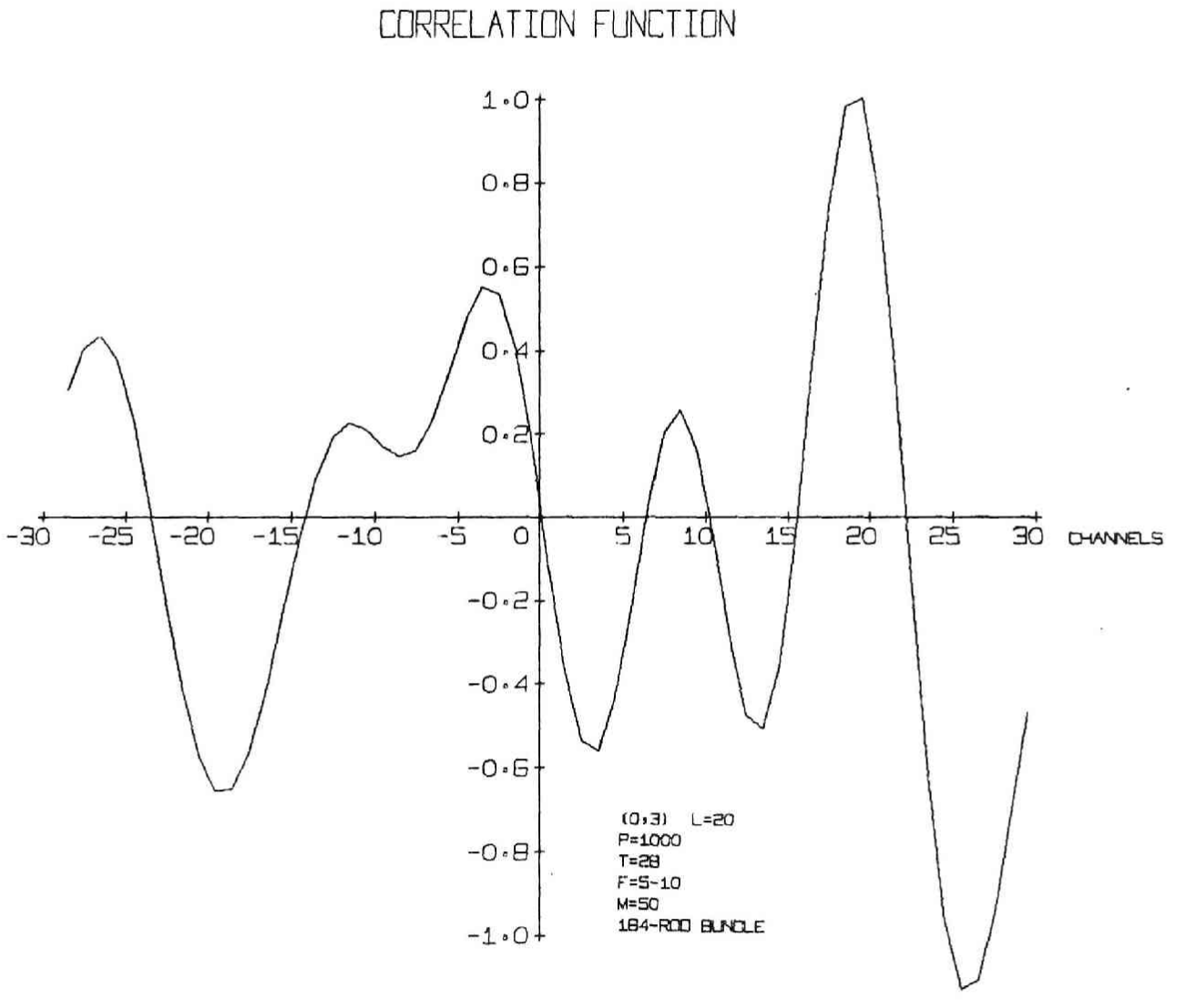

Fig. 126 Cross-correlation Function Output - 89

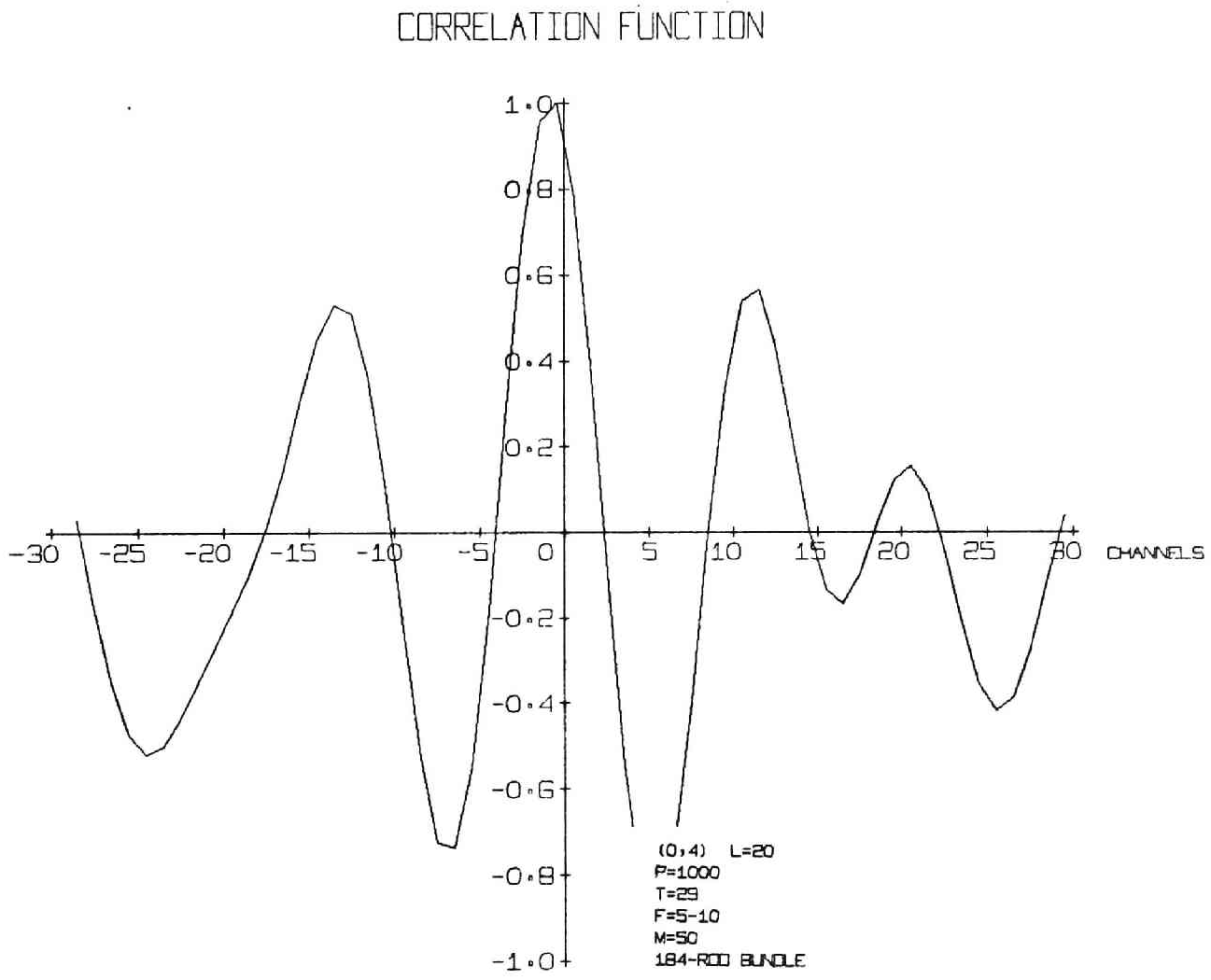

Fig. 127 Cross-correlation Function Output - 90

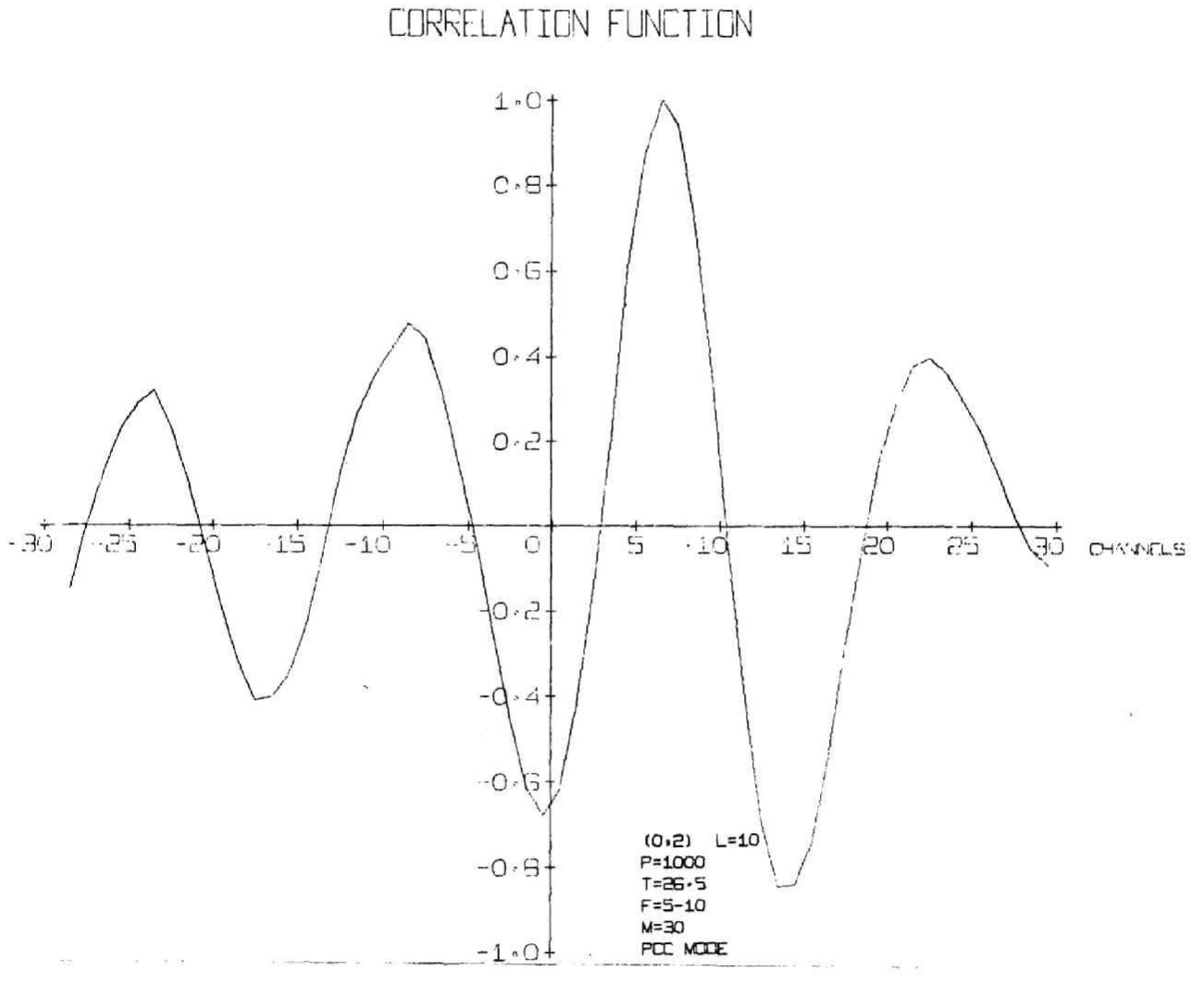

Fig. 128 Cross-correlation Function Output - 91

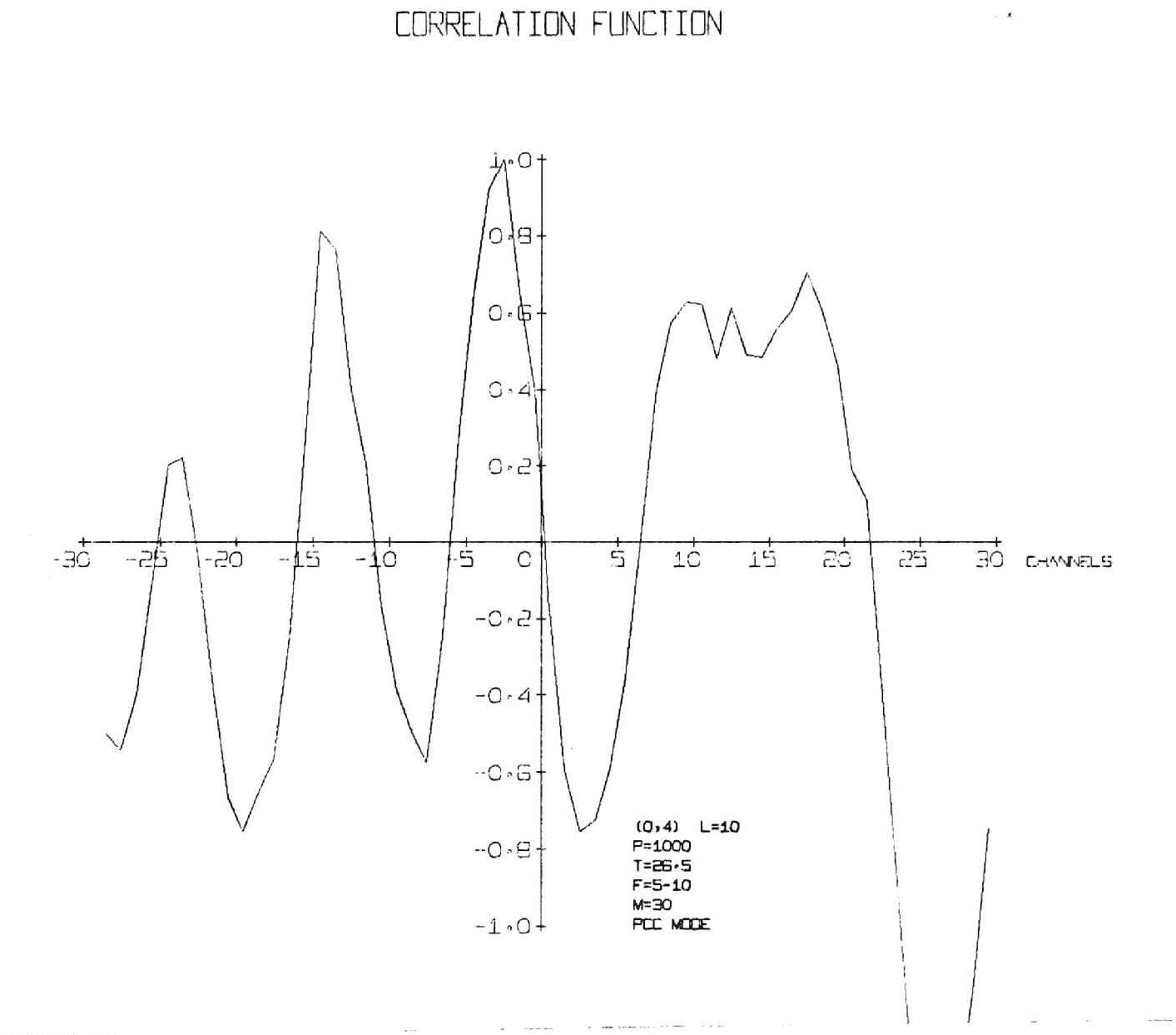

Fig. 129 Cross-correlation Function Output - 92

APPENDIX III

COMPUTER PROGRAMS FOR REFLECTION STUDIES

Two computer programs for studying acoustic reflections are listed in this appendix. One is to obtain ray-wavefront patterns of the direct and reflected waves. The other calculates the divergence factor. Subprogram MIRR is used with both of the programs.

```
*ONE WORD INTEGERS
C         THIS CODE COMPUTES THE WAVE FRONT OF A SPHERICAL ACOUSTIC
C         PLUSE REFLECTED INSIDE AN INFINITE CYLINDER
      REAL L
      COMMON R,PI
      PI = 3.141592
C         READ IN PARAMETERS
    1 FORMAT (8F8.5,2I5)
    2 READ (2,1) R,X0,Y0,C,DT,DA,T0,TMAX,IRAY,IPLOT
      IF (X0**2.+Y0**2.) 3,99,3
C         R = RADIUS OF CYLINDER
C         X0,Y0 = INITIAL SOURCE LOCATION
C         X,Y = WAVE FRONT LOCATION AT T
C         L = DISTANCE OF TRAVEL
C         C = SOUND VELOCIT
C         T = TIME
C         T0 = INITIAL TIME
C         DT = TIME INCREMENT
C         TMAX = MAXIMUM TRAVEL TIME
C         A = ANGLE FROM THE X-AXIS
C         DA = ANGULAR INCREMENT
C
C         IRAY = 0  DRAW WAVE FRONTS
C              = 1  DRAW EMANATING RAYS
C         IPLOT = 0  PROCEED PLOTTING PAPER
C               = 1  ROLL BACK PLOTTING PAPER
C
C         LENGTH IS IN CM, AND TIME IS IN MICRO-SECOND
C
C         NEXT STATEMENTS DRAW THE CROSS-SECTION OF THE CYLINDER
    3 CONTINUE
      SX=0.1
      SY=0.1
      DAN=2.*PI/1500.
      CALL SCALF(SX,SY,-R,0.)
      X=-R
      Y=0.
      CALL FPLOT(-2,X,Y)
      DO 5 I=1,1500
      A=DAN*I
      X=-R*COS(A)
      Y=R*SIN(A)
    5 CALL FPLOT(0,X,Y)
      CALL FPLOT(-1,X,Y)
      CALL FPLOT(-2,X0,Y0)
      CALL POINT(0)
      CALL FPLOT( 1,X0,Y0)
C         SET INITIAL VALUES
      T=T0
      L=C*T
      A=0.
   20 CONTINUE
      AS=A
      XS=X0
      YS=Y0
```

```
C          FIND THE WAVE FRONT (X,Y)
   25  X=XS+L*COS(AS)
       Y=YS+L*SIN(AS)
C          CHECK IF (X,Y) IS INSIDE THE CYLINDER
       IF (X**2.+Y**2.-R**2.) 30,30,40
   30  CONTINUE
       CALL FPLOT(-2,X,Y)
       GO TO 50
   40  CONTINUE
C          FIND MIRROR IMAGE SOURCE POINT (X1,Y1)
       CALL MIRR(XS,YS,AS,GAMMA,X1,Y1,A1,D,SS)
       XS=X1
       YS=Y1
       AS=A1
       GO TO 25
   50  CONTINUE
       IF (IRAY) 51,51,72
   51  A=A+DA
       IF (A-2.*PI) 60,70,70
   60  GO TO 20
   70  IF (IRAY) 71,71,90
   71  A=0.0
       CALL FPLOT( 1,X,Y)
   72  T=T+DT
       IF (T-TMAX) 80,80,85
   80  L=C*T
       GO TO 20
   85  IF (IRAY) 90,90,86
   86  T=T0
       L=C*T
       CALL FPLOT( 1,X,Y)
     GO TO 51
   90  CONTINUE
       IF (IPLOT) 91,91,92
   91  CALL FPLOT(1, 50.,0.)
       GO TO 2
   92  CALL FPLOT(1,-25.,0.)
       GO TO 2
   99  CALL LOGFF
       CALL EXIT
  100  STOP
  110  END
```

```
*ONE WORD INTEGERS
C         THIS CODE COMPUTES THE DIVERGENCE FACTOR OF THE DIRECT
C         AND REFLECTED WAVES INSIDE AN INFINITE CYLINDER DUE TO
C         SPHERICAL ACOUSTIC SOURCE
C         DOUBLE REFLECTION NOT INCLUDED IN THIS DECK
      REAL L,LL
      COMMON R,PI
     PI = 3.141592
C         READ IN PARAMETERS
    1 FORMAT (5F8.5,I5)
    2 READ (2,1) R,X0,Y0,DA,DL,IDIV
      IF (X0**2.+Y0**2.) 3,99,3
C         R = RADIUS OF CYLINDER
C         X0,Y0 = INITIAL SOURCE LOCATION
C         X,Y = WAVE FRONT LOCATION
C         L = DISTANCE OF TRAVEL
C         LL = DISTANCE FROM WALL TOSOURCE
C         A = ANGLE FROM THE X-AXIS
C         DA = ANGULAR INCREMENT
C         DF = DIVERGENCE FACTOR
C         IDIV = 0  DIRECT WAVE
C              = 1  REFLECTED WAVE
C
C         DIVERGENCE FACTOR NORMALIZED TO UNITY ON THE NEARESTWALL
C
C         NEXT STATEMENTS DRAW THE CROSS-SECTION OF THE CYLINDER
    3 CONTINUE
      SX=0.1
      SY=0.1
      DAN=2.*PI/1500.
      CALL SCALF(SX,SY,-R,0.)
      X=-R
      Y=0.
      CALL FPLOT(-2,X,Y)
      DO 5 I=1,1500
      A=DAN*I
      X=-R*COS(A)
      Y=R*SIN(A)
    5 CALL FPLOT(0,X,Y)
      CALL FPLOT(-1,X,Y)
      CALL FPLOT(-2,X0,Y0)
      CALL POINT(0)
      CALL FPLOT( 1,X0,Y0)
C         READ DIVERGENCE FACTOR
    6 READ (2,7) DF
    7 FORMAT (F10.5)
      IF (DF) 8,8,10
    8 CALL FPLOT(1 ,50.,0.)
      GO TO 2
   10 A=0.
C         FIND DISTANCE TO WALL FROM SOURCE, LL
   11 CALL MIRR(X0,Y0,A,GAMMA,X1,Y1,A1,D,SS)
      LL=SS/2./COS(GAMMA)
C         FIND DIVERGENCE FACTOR ON THE WALL
      DFW=(R-D)/LL
```

```
C         IF GIVEN DF IS LESS THAN DFW, THERE IS NO LOCATION FOR
C         THIS DF FOR THE PRESENT INCIDENT ANGLE A
      IF (DF-DFW) 70,20,20
   20 CONTINUE
C       REFLECTED OR DIRECT WAVE
      IF (IDIV) 30,30,40
   30 CONTINUE
C         CALCULATE L FOR DIRECT WAVE
      L=(R-D)/DF
      X=X0+L*COS(A)
      Y=Y0+L*SIN(A)
      GO TO 60
   40 CONTINUE
C         FIND L FOR REFLECTED WAVE
      L=LL
   41 P=LL/L
      PR=(R-D)/L/SQRT(1.-2.*LL*(1.-P)/(R*COS(GAMMA)))/P
      IF (PR-DF) 45,50,50
   45 L=L+DL
      GO TO 41
   50 X=X1+L*COS(A1)
      Y=Y1+L*SIN(A1)
      GO TO 60
      IF (X**2.+Y**2.-R**2.) 51,60,60
   51 CALL FPLOT(1,X,Y)
      GO TO 70
   60 CALL FPLOT (-2,X,Y)
   70 A=A+DA
      IF (A-2.*PI) 11,11,80
   80 CALL FPLOT(1,X,Y)
      GO TO 6
   99 CALL LOGFF
      CALL EXIT
  100 STOP
  101 END
```

```
*ONE WORD INTEGERS .
      SUBROUTINE MIRR  (X0,Y0,A,GAMMA,X1,Y1,A1,D,SS)
      COMMON R,PI
C        THIS SUBROUTINE CALCULATES THE MIRROR IMAGE SOURCE
C        POINT (X1,Y1), THE ANGLE OF THE REFLECTED RAY A1 AND
C        THE ANGLE OF REFLECTION GAMMA FROM THE ORIGINAL
C        SOURCE AT (X0,Y0), EMANATING AT AN ANGLE A
C        NOTE ABS(GAMMA).LE.PI/2., HENCE COS(GAMMA).GE.0.
      D=SQRT(X0**2.+Y0**2.)
      IF (X0) 10,20,10
   10 RATIO=Y0/X0
      BETA=ATAN(RATIO)
      GO TO 30
   20 IF (Y0) 21,21,22.
   21 BETA =-PI/2.
      GO TO 30
   22 BETA=PI/2.
   30 CONTINUE
      SG=SIN(A-BETA)*D/R
      CG=SQRT(1.-SG**2.)
      TG=SG/CG
      GAMMA=ATAN(TG)
      THETA=A-GAMMA
      SS=2.*(R-D*COS(THETA-BETA))
      A1=PI+A-2.*GAMMA
      X1=X0+SS*COS(THETA)
      Y1=Y0+SS*SIN(THETA)
      RETURN
      END
```